

Fluorine and the Environment

Atmospheric Chemistry,
Emissions, & Lithosphere

EDITED BY

Alain Tressaud

ADVANCES IN FLUORINE SCIENCE 1

Fluorine and the Environment

Atmospheric Chemistry, Emissions, & Lithosphere

ASSOCIATE EDITORS

B. Ameduri, *Research Director, CNRS, Montpellier, France*

P. Atkins, *Director of Environmental Affairs, Alcoa Inc., New York, USA*

G. Haufe, *Muenster University, Germany*

J. Knowles, *UCL, London, UK*

T. Nakajima, *Aichi Institute of Technology, Toyota, Japan*

M. Pontié, *Laboratory of Environmental Sciences, Angers, France*

R. Syvret, *Research Associate, Air Products, Allentown, PA, USA*

S. Tavener, *York University, UK*

J. Winfield, *Glasgow University, UK*

Fluorine and the Environment

Atmospheric Chemistry, Emissions, & Lithosphere

Volume 1

Edited by

Alain Tressaud

Research Director CNRS,

ICMCB-CNRS

University of Bordeaux I

Pessac Cedex,

France



ELSEVIER

Amsterdam ● Boston ● Heidelberg ● London ● Oxford ● Paris
● San Diego ● San Francisco ● Singapore ● Sydney ● Tokyo

Elsevier
Radarweg 29, PO Box 211, 1000 AE Amsterdam, The Netherlands
The Boulevard, Langford Lane, Kidlington, Oxford OX5 1GB, UK

First edition 2006

Copyright © 2006 Elsevier B.V. All rights reserved

No part of this publication may be reproduced, stored in a retrieval system or transmitted in any form or by any means electronic, mechanical, photocopying, recording or otherwise without the prior written permission of the Publisher.

Permissions may be sought directly from Elsevier's Science & Technology Rights Department in Oxford, UK: phone (+44) (0) 1865 843830; fax (+44) (0) 1865 853333; email: permissions@elsevier.com. Alternatively, you can submit your request online by visiting the Elsevier web site at <http://elsevier.com/locate/permissions>, and selecting *Obtaining permission to use Elsevier material*.

Notice

No responsibility is assumed by the publisher for any injury and/or damage to persons or property as a matter of products liability, negligence or otherwise, or from any use or operation of any methods, products, instructions or ideas contained in the material herein. Because of rapid advances in the medical sciences, in particular, independent verification of diagnoses and drug dosages should be made.

Library of Congress Cataloging in Publication Data

A catalogue record for this book is available from the Library of Congress.

British Library Cataloguing in Publication Data

A catalogue record for this book is available from the British Library.

ISBN-13: 978-0-444-52811-7

ISBN-10: 0-444-52811-3

ISSN: 1872-0358

For information on all Elsevier publications
visit our website at books.elsevier.com

Printed and bound in Italy

06 07 08 09 10 10 9 8 7 6 5 4 3 2 1

Working together to grow
libraries in developing countries

www.elsevier.com | www.bookaid.org | www.sabre.org

ELSEVIER

BOOK AID
International

Sabre Foundation

CONTENTS

Contributors	vii
Preface	ix
Foreword	xi
Introduction	xv
1. Fluorine in the Atmosphere <i>Philippe Ricaud and Franck Lefèvre</i>	1
2. Evaluation and Selection of CFC Alternatives <i>Akira Sekiya, Masaaki Yamabe, Kazuaki Tokuhashi, Yasuo Hibino, Ryoichi Imasu and Hidekazu Okamoto</i>	33
3. Trifluoromethyl Sulphur Pentafluoride, SF ₅ CF ₃ : Atmospheric Chemistry and Its Environmental Importance via the Greenhouse Effect <i>Richard P. Tuckett</i>	89
4. Production of Second- or Third-Generation Fluorine-based Refrigerants from (Photo)-Dechlorination of Fluorocarbon Wastes <i>Hideo Nishiumi, Koichi Sato and Ryo Kato</i>	131
5. Volcanic Fluorine Emissions: Observations by Fourier Transform Infrared Spectroscopy <i>Georgina M. Sawyer and Clive Oppenheimer</i>	165
6. Fluorine and Coexisting Volatiles in the Geosphere: The Role in Japanese Volcanic Rocks <i>Katsuro Anazawa</i>	187
7. Fluorine Compounds in Gaseous Emissions from Industrial Sources: The Case of Ceramic Industries <i>Giuliana Bonvicini, Alberto Fregni and Carlo Palmonari</i>	225
8. Some Problems Relating to Fluorides in the Environment: Effects on Plants and Animals <i>Alan W. Davison and Leonard H. Weinstein</i>	251
Subject Index	299

This page intentionally left blank

CONTRIBUTORS

Katsuro Anazawa	187
Giuliana Bonvicini	225
Alan W. Davison	251
Alberto Fregni	225
Yasuo Hibino	33
Ryoichi Imasu	33
Ryo Kato	131
Franck Lefèvre	1
Hideo Nishiumi	131
Hidekazu Okamoto	33
Clive Oppenheimer	165
Carlo Palmonari	225
Philippe Ricaud	1
Koichi Sato	131
Georgina M. Sawyer	165
Akira Sekiya	33
Kazuaki Tokuhashi	33
Richard P. Tuckett	89
Leonard H. Weinstein	251
Masaaki Yamabe	33

This page intentionally left blank

PREFACE

Here is the first volume of a new series of books: *Advances in Fluorine Science*, in which research results of fluorine-related fields will be presented in a topical way. Such a series aims to cover a much broader scope than conventional organic or inorganic chemistry, and to reach beyond chemistry towards important disciplines in which fluorine and fluoride compounds have a decisive impact. I am thinking of the frontiers of fluorine with biology, physics, environmental sciences, health, earth sciences, materials sciences, new technologies and, why not, cosmochemistry or archaeology. It appears to me that this aspect has been more or less neglected during these last decades. (*Throughout the series both terms 'fluorine' and 'fluoride' will be equally used, the former being used in most cases as the element and not as difluorine gas*).

The individual volumes of *Advances in Fluorine Science* will be thematic, addressing comprehensively both the science and applications in transdisciplinary areas, e.g. *Fluorine & the Environment*, *Fluorine & Health*, *Fluorine & Life Sciences*, *Fluorine & New Technologies & Materials*, *Fluorine & Energy*, etc. One of the reasons to choose this original viewpoint comes from the observation that the different scientific communities are often unaware of each other, for instance on one side the chemistry community – and in our case Fluorine scientists – and on the other side environmental sciences, medicine, and renewable energy communities. I do hope that such a series will allow both sides to be brought closer together.

The contents of each volume are carefully chosen in the forum of the Board of Associate Editors, who collectively represent most of the relevant areas covered in the series, in order to present each area of interest in a balanced way.

It was recently stated that fluorine chemistry is experiencing a renaissance, because of the outstanding properties attached to this element which can be met in many occasions of our life, e.g. bioceramics and dental restoratives, cooking ware, tooth pastes, cardiovascular or ophthalmologic surgery, new gases less harmful for our environment, protection of our cultural heritage, archeometrics, materials for new or alternative energies, optics and micro-electronics, etc. Although the benefits of fluorine compounds for our society are evident in many fields, the drawbacks caused to our environment by some of these products should not be underestimated. But this dual aspect should promote among the

groups dealing with fluorine and fluoride products a great challenge for finding solutions to overcome all these problems. While I realize this project is an ambitious one, I follow the scientist Alan Kay, who once said *The best way to predict the future is to invent it.*

I would like to thank heartily Profs. Emeriti Paul Hagenmuller, University Bordeaux¹ and Neil Bartlett University of California at Berkeley for their constant support and encouragements during many decades. Many thanks are due also to the members of the “Fluorine group” of ICMCB for their dynamism and good harmony.

I should not forget the personal help and everyday thoughtfulness of my wife Vivian and my whole family.

Alain Tressaud
Pessac, March 2006

FOREWORD

Fluorides and fluorine chemistry have important impact on many aspects of modern life. Most are aware of Teflon coatings in cooking utensils, the impact of chlorofluorocarbons on the ozone layer, the beneficial influence of fluoride on dental caries, and the utility of substituting F for H in making pharmaceuticals such as fluorouracil. But generally there is less awareness of the impact, real or potential, that fluorine chemistry can have on improving our environment, saving energy via new synthetic approaches, making more potent and longer-lasting batteries, and improving nuclear-reactor technology. These are some of the issues to be addressed in this series of volumes.

Apart from the proton, the fluorine atom binds to more elements than any other atom. This is because the chemical bonds that the F-ligand makes with other atoms are intrinsically strong. The small size and closed-shell electron configuration of the bound fluorine ligand account for these properties. Indeed, the close proximity and mutual repulsion of the valence electrons in the small F_2 molecule cause it to be weakly bound. This (contrasting with the strong double bond in O_2) gives fluorides a high thermodynamic stability, relative to oxides. In addition, the high effective nuclear charge and smallness of bound F, make it the most electronegative of ligands. So, we find that except for helium and neon, fluorine is known to bind to all of the elements. Moreover, fluorine often excites the highest oxidation state attainable in an element. Only in cases where the univalence of the F-ligand demands high coordination (and strong ligand–ligand repulsion) does oxygen surpass fluorine in that respect (as in the nonexistence of the octafluorides of xenon or osmium, contrasting with the known tetroxides of those elements).

Fluorides at the high oxidation-state limit are frequently at or near their coordination limit for that element, and this bestows high volatility on the fluorides of many metals such as TiF_4 , MoF_6 , WF_6 , and the hexafluorides of the platinum metals. These can be convenient sources of the metals. Other volatile fluorides such as the halogen fluorides and noble-gas fluorides can be more easily used as fluorinating agents than fluorine itself. Krypton difluoride is even more potent as an oxidizer than F_2 itself.

Often the closed-shell electron configuration of bound F lends chemical and physical inertness to coordinatively saturated molecules. Examples are fluoro-

carbons and sulfur fluorides such as SF₆ and CF₄. These kinetically inert, and therefore easily used gases, can be used in plasmas as the source of F atoms, to provide fluoro-coatings for surfaces. But, because they are 'greenhouse gases' their containment and disposal have to be carefully managed. Although inertness often bestows highly beneficial long-lasting properties (as for example in poly-fluorocarbon containers and Teflon coatings in cookware), we also see the harmful impact of such inertness in the large greenhouse-gas effects of chloro-fluorocarbons, and molecules like SF₆ and CF₃SF₅. Understanding how to maximize the advantages and minimize the adverse effects of such inert materials is at the heart of some of the topics covered in these volumes. Fluorocarbon-based molecules remain the most promising substitutes for the banned chlorofluorocarbons, and the synthesis of labile refrigerant substitutes for them is still an active area of synthetic endeavor. But important environmental impact is not confined to inert fluorides. The labile fluorides also pose their own problems. Environmental issues therefore will constitute an important aspect of this series.

Many fluorides are not inert. The high thermodynamic stability of the HF molecule often renders fluorides unstable with respect to hydrolysis; and if the element to which the F is bound is in a high oxidation state, then this HF can be accompanied by oxygen, ozone, or other oxidation products. Because HF causes severe tissue damage and corrodes glass and other materials, the handling and containment of fluorides require knowledge and care. Even though there are hazards associated with it, the solvent properties of liquid anhydrous HF (aHF) are so favorable, especially in carrying out fluorinations below room temperature, that it is likely to play a much larger role in clean efficient (green) chemistry than hitherto.

Hydrolysis of fluorides also frequently results in substitution of OH groups for F. Since OH is not greatly different in size from F, structural properties of partially hydrolyzed fluorides are often akin to those of the parent fluoride, even though there may be important physical and chemical differences. An instance of that is the well-known impact of F substitution for OH in apatite; fluoroapatite in teeth bestowing resistance to dental caries.

Another substitution of importance is that of F for H, especially in organic materials. The small F-ligand is able to take the place of H in organic molecules without this change having much steric effect. Such a substitution with positron emitter ¹⁸F in biologically active molecules, can, via positron emission tomography, be of value in medical and other biological studies. But ordinary F for H substitution has already (e.g. fluorouracil) provided useful pharmaceuticals. Because of the high electronegativity of F compared with H, however, the chemical impact of the substitution is usually profound. Synthetic strategies, for the specific substitution of certain H by F, represent an important branch of fluorine chemistry. That will have representation in this series.

There is little doubt that fluorides could provide the means for efficient high-power reversible electrical energy storage. The high electronegativity, lightness in weight, and small anion size, combine to make F^- a desirable component of any battery system. Primary batteries based on carbon fluorides and lithium are already in common use. A long-lived reversible counterpart is an achievable goal for fluorine chemists, especially in the exploitation of lamellar materials such as modified graphites into which either fluorine or lithium can be intercalated. It is also becoming clear that as the global demands for energy grow, and greenhouse-gas effects also increase, we must use energy more efficiently and also depend more on nuclear energy. Molten fluoride reactors may well have a role in that energy production.

But other solid-state fluorides are also having greater roles in our high-tech products. Here the tight binding of the F-ligand valence electrons again has importance. Ligand to metal charge transfer requires much energy in most fluorides, and as a consequence those bands are shifted well into the ultraviolet region. Fluoride glasses and other solid fluorides owe their favorable optical properties to this high electronegativity of fluorine, and have many applications in lasers, optical fibres, waveguides, and optical amplifiers.

Here I have skimmed over the broad terrain that these volumes will cover. In what I am sure will be a highly diverse set of authoritative articles, I am certain there will be an admirable depth of coverage, that will bring out the multitude of properties that spring from the fluorine ligand.

Neil Bartlett,
Orinda, California, February 2006

This page intentionally left blank

INTRODUCTION TO ***“FLUORINE AND THE ENVIRONMENT”***

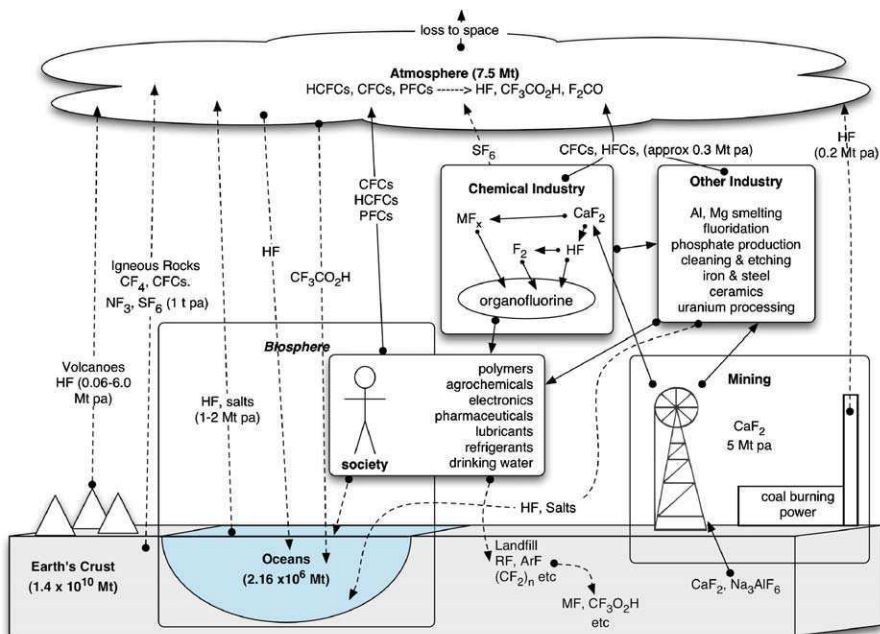
Fluorine is the 12th and one of the most reactive elements in the periodic table. With an abundance of 0.65‰ in the Earth's crust, it is found in more than 300 minerals and is widely distributed in the biosphere (flora and fauna). With its small size, weight and closed-shell electron configuration, it is used extensively for instance in the ceramics, pharmaceutical/health, energy storage and various other industries. Among the latter, the production of the chlorofluorocarbon (CFC) gases from the 1930s was for a long time seen as a highly useful application, used as refrigerant agents, sprays and insulation materials, until it was shown by Molina and Rowland in 1974 that the photochemical breakdown of the CFC gases would give rise to highly reactive Cl and ClO species which destroy ozone by catalytic reactions. (It should be noted that the F atoms which are produced are quickly converted to HF by reactions with H₂O and thus do not participate in ozone-destroying reactions.) The originally proposed catalytic cycle by Molina and Rowland especially affects ozone above about 30 km. The report, in 1985, by Joe Farman and colleagues from the British Antarctic Survey of a major ozone loss at high southern latitudes during springtime – the so-called “ozone hole” – came as a total surprise since it happened at 12–22 km altitude, where normally maximum ozone concentrations did occur. In addition, the location was farthest away from the northern hemisphere regions where the atmospheric input of CFCs took place. Although not predicted, intensive research showed that the ozone hole was caused by catalytic reactions, involving Cl, ClO and Cl₂O₂ as catalysts. These catalysts are promoted by reactions of HCl and ClONO₂ on or in particles in the lower stratosphere, to produce Cl₂ and HNO₃. The particles consist of water, sulfuric and nitric acid, in super-cooled liquid or solid states. Cold temperatures promote such reactions. Photolysis of Cl₂ quickly leads to Cl atoms when sunlight returns to the Antarctic lower stratosphere after the long polar night. Similar, but less effective, ozone-destroying reactions take place in Arctic regions in years when the lower stratosphere is sufficiently cold. However, this occurs less frequently over the Arctic than over the Antarctic. It should be noted that ozone destruction can also take place by photolysis of bromo-chloro-fluoro

carbons, in which case also Br and BrO catalysts are produced, which, molecule by molecule, are two orders of magnitude more efficient in destroying ozone than the chlorine radicals. The “opening” of the “ozone hole” in the altitude region of 12–22 km, at exactly the altitude regions where normally maximum ozone concentrations are found, is probably the greatest surprise in the history of atmospheric chemistry, indicating that intensive research is needed regarding the environmental consequences of the use of halogens, including fluorine-containing chemicals. In this regard not only effects on ozone but also the climatic consequences of the input of halogen-containing industrial chemicals should be taken into account. With atmospheric lifetimes of about 45 and 100 years, the global warming potential (GWP) of the CFC gases at 100 year horizons are 5,000 and 10,000, the climate warming produced by the injection of 1 kg of the CFCs compared to 1 kg of CO₂. With lifetimes often of the order of several thousands of years, several fluorine-containing organic gases can have GWPs of many thousands of years, the largest being SF₆ (GWP ≈ 22,000) and SF₅CF₃ (GWP ≈ 17,500). Their atmospheric loadings are still rather low, 40 pptv for CF₄ and still less than 1 pptv for SF₅CF₃ (1 pptv = 10⁻¹² mole/mole), but with a large growth rate of 6% per year.

Since 1996, the production of CFCs and their Br-containing analogues is no longer allowed and are being replaced by H-containing analogues which are largely removed in the troposphere by reaction with OH, the “detergent of the atmosphere,” giving them a much reduced lifetime in the atmosphere with corresponding reductions in effects on stratospheric ozone. The worldwide ban of the CFCs and several other ozone-destroying halogenated chemicals is considered to be a success story in global environmental protection. We have, however, been very lucky. If the chemical industry had developed organic bromine components instead of the CFCs, or alternatively, if chlorine chemistry would have run more like that of bromine, then, without any preparedness, we would have been faced with a catastrophic ozone hole everywhere and at all seasons during the early 1970s, before atmospheric chemists had developed the necessary knowledge to identify the problem and the appropriate techniques for the necessary critical atmospheric measurements. Noting that nobody had given any thought to the atmospheric consequences of the releases of Cl and Br before 1974. I can only conclude that mankind has been very lucky.

The ignorance about the atmospheric effects of the CFC gases until the mid-1970s, at a time when their abundances were rapidly rising is a lesson which should be for ever heeded. Here I have concentrated on the atmospheric effects. Impacts on other compartments of the environments should likewise be topics of research to prevent major environmental impacts. Such research will greatly profit from interdisciplinary research, which will be facilitated by the book series on fluorine and the many possible products containing F.

Fluorine fluxes and reservoirs in the atmosphere and on the Earth can be illustrated by the following scheme, kindly provided by S. Tavener and J. Clark from a forthcoming chapter of this series.



The fluorosphere: A schematic representation of fluorine reservoirs and flux on the Earth, with approximate volumes. (Reproduced with permission from S. Tavener and J. Clark – “Fluorine: Friend or Foe? A Green Chemist’s Perspective,” to appear in Advances in Fluorine Science series, 2006.

Prof. Paul J. Crutzen
Mainz, March 2006

This page intentionally left blank

CHAPTER 1

Fluorine in the Atmosphere

Philippe Ricaud^{1,*} and Franck Lefèvre²

¹*Laboratoire d'Aérologie, Observatoire de Midi-Pyrénées, Université Paul Sabatier, 14, Avenue Edouard Belin, 31400 Toulouse, France*

²*Service d'Aéronomie, Université Pierre et Marie Curie, Institut Pierre Simon Laplace, Tour 45, Couloir 45-46, 3^e et 4^e étages (boîte 102), 4 place Jussieu, 75252 Paris Cedex 05, France*

Contents

1. Introduction	2
2. Sources and sinks	3
3. Chemical impacts	7
3.1. Chemistry of stratospheric fluorine	7
3.2. Chemistry of stratospheric chlorine	15
3.3. Links with stratospheric bromine chemistry	17
3.4. Chlorine–bromine reactions in an “Ozone Hole” configuration	18
4. Radiative impacts	20
5. Measurements	22
6. Trends and scenarios	26
References	30

Abstract

Scientific evidence, accumulated over more than two decades of study by the international research community, has shown that human-produced halocarbons are responsible for the observed depletions of the ozone layer. Fluorine-containing chlorofluorocarbons (CFCs) and halons are sufficiently long-lived so as to reach the stratosphere where they are photodissociated to release chlorine, bromine, and fluorine atoms. Although chlorine and bromine have been proven to be main responsible for the destruction of the ozone layer in the polar regions, fluorine by itself does not contribute to ozone depletion. Fluorine atoms released from the photodissociation of fluorine-bearing sources are quickly sequestered into carbonyl compounds and subsequently into the ultimate hydrogen fluoride, which is very stable in the stratosphere. The primary interest in monitoring inorganic fluorine (defined as F_y) in the atmosphere is as a surrogate of the amounts of its precursors, mainly the CFCs and hydrochlorofluorocarbons, involved in ozone depletion by chlorine. Fluorinated halocarbons and other gases such as perfluorocarbons or sulfur hexafluoride (SF₆) are also extremely potent greenhouse gases for which the current trends must be monitored and future scenarios of growth must be evaluated.

*Corresponding author.

E-mail: philippe.ricaud@aero.obs-mip.fr

1. INTRODUCTION

Ozone levels in the atmosphere undergo normal seasonal variations, but recent levels of ozone loss over the poles and lower latitudes could not be explained by natural variability alone. Man-made chlorofluorocarbon (CFC) compounds were developed in the early 1930s for a variety of industrial and commercial applications, but it was not until the 1970s that these and other chlorine-containing substances were suspected of having the potential to destroy atmospheric ozone. In 1985, a team of British researchers first reported unusually low ozone levels over Halley Bay, Antarctica, which were caused by chemical reactions with chlorine and nitrogen compounds [1]. Research was initiated that found CFCs to be largely responsible for the anomalously low levels during the polar springtime. This polar ozone depletion at lower stratospheric altitudes is what has been termed as the “ozone hole.” The primary concern over ozone depletion is the potential impacts on human health and ecosystems due to increased UV exposure. Increase in skin cancer and cataracts in human populations are expected in a higher UV environment. Lower yields of certain cash crops may result owing to increased UV-B stress. Higher UV-B levels in the upper ocean layer may inhibit phytoplankton activities, which can impact the entire marine ecosystem. In addition to direct biological consequences, indirect effects may arise through changes in atmospheric chemistry. Increased UV-B will alter photochemical reaction rates in the lower atmosphere that are important in the production of surface layer ozone and urban smog.

Concern over these potential effects has prompted the international community to enact policies aimed at reducing the production of ozone-depleting chemicals. An important event in the history of international ozone policy was the Montreal Protocol on Substances That Deplete the Ozone Layer (1987), which called for the phase-out and reduction of certain substances over a multiyear time frame. Discoveries of more extensive ozone loss and rapid formulation of replacement substances for chlorine-containing compounds have led to refinements of the original protocol. Updates set forth at London (1990) and Copenhagen (1992) have called for accelerated phase-out and replacement schedules.

The Montreal Protocol on Substances That Deplete the Ozone Layer is a landmark international agreement designed to protect the stratospheric ozone layer. The treaty was originally signed in 1987 and substantially amended in 1990 and 1992. The Montreal Protocol stipulates that the production and consumption of compounds that deplete ozone in the stratosphere – CFCs, halons, carbon tetrachloride, and methyl chloroform – are to be phased out by 2000 (2005 for methyl chloroform). Methyl bromide, an ozone-depleting compound used extensively in agricultural applications, is set to be phased out internationally by 2010. In December 2005, it was decided at the Montreal Conference to extend the commitments of the Kyoto Protocol beyond 2012. The framework for the Montreal Protocol was based on the Vienna Convention for the Protection of the Ozone

Layer (1985), a non-binding agreement that outlined states' responsibilities for protecting human health and the environment against the adverse effects of ozone depletion.

The CFCs are entirely of anthropogenic origin, and have found use as foam-blowing agents, as refrigerants, and as solvents. These compounds are quite stable in the atmosphere and have lifetimes of between 50 and 500 years or even more. These long lifetimes, coupled with their strong infrared absorption capacity, also make the CFCs significant greenhouse gases. Although the CFCs make up the greatest fraction of the halogen burden in the atmosphere, a number of other compounds must also be considered when compiling an atmospheric halogen burden. Hydrofluorocarbons (HFCs), hydrochlorofluorocarbons (HCFCs) together with perfluorocarbons (PFCs) are currently being developed as replacements for the CFCs, and some of these compounds are already in use and have been detected in the atmosphere. Halons, which are fully halogenated compounds containing bromine, have been manufactured as fire suppressants. In addition, some natural sources of halogen exist in the form of partially halogenated methane and ethane. HCl is also an important contributor to the tropospheric chlorine budget, with a wide variety of natural and anthropogenic sources.

In parallel, the Kyoto Protocol (1997) is actually under discussion as an amendment to the United Nations Framework Convention on Climate Change (UNFCCC). Countries that ratify this protocol commit to reduce their emissions of carbon dioxide and five other greenhouse gases, among them CFCs and HCFCs, or engage in emission trading if they maintain or increase emissions of these gases. The objective of the protocol is the stabilization of greenhouse gas concentrations in the atmosphere at a level that would prevent dangerous anthropogenic interference with the climate system. Indeed, the Intergovernmental Panel on Climate Change (IPCC) has predicted an average global rise in temperature of 1.4 to 5.8°C between 1990 and 2100. Some current estimates indicate that even if successfully and completely implemented, the Kyoto Protocol will have some difficulties in providing a significant reduction in temperature.

The present chapter deals with atmospheric fluorine by studying sources and sinks of halogen compounds. It then presents the chemical and radiative impacts of these compounds on the Earth's atmosphere. Measurement networks and platforms are presented. Finally, present and future halogen trends are quantified based upon different emission scenarios.

2. SOURCES AND SINKS

Halogens are found in the atmosphere in two general forms, organic and inorganic. The organic species are often referred to as "source gases," since these species are released at the Earth's surface (from a variety of sources, some

natural and some man-made). Destruction of the source gases in the atmosphere leads to the release of halogens, which are then partitioned into a number of inorganic forms through chemical reactions. The CFC, HCFC, and HFC are manufactured for use as refrigerants, foam-blowing agents, and solvents. The manufacture of CFCs is now banned due to their impact on stratospheric ozone levels, and HCFCs will progressively also be phased out of production. HFCs have been shown to be “ozone friendly” and are replacing their chlorine-containing analogues in industrial applications. Halons, bromine- and fluorine-containing organic compounds, have been used as fire-extinguishing compounds in the past. Their production is now banned owing to their harmful effects on stratospheric ozone. Examples include Halon-1301 (CF_3Br) and Halon-1211 (CF_2ClBr).

Following the initial proposals of the potential impacts of CFCs on stratospheric ozone, measurement programs were established to monitor the concentrations of organic halogen source gases in the atmosphere and to determine temporal and spatial trends in their abundances (Figs. 1 and 2). Thus a global data network is now available from which the budget of these halogen source gases can be assessed (see Section 5). The atmospheric abundances, trends, and lifetimes of the primary organic fluorine-containing species are listed in Table 1. All CFCs, HCFCs, and halons have purely anthropogenic sources. Chlorine source gases such as CH_3CCl_3 and CCl_4 are also entirely man-made, while CH_3Cl is the major contributor to the natural halogen burden.

Approximately 85% of the total amount of organic chlorine comes from compounds with solely anthropogenic sources. These anthropogenic compounds are

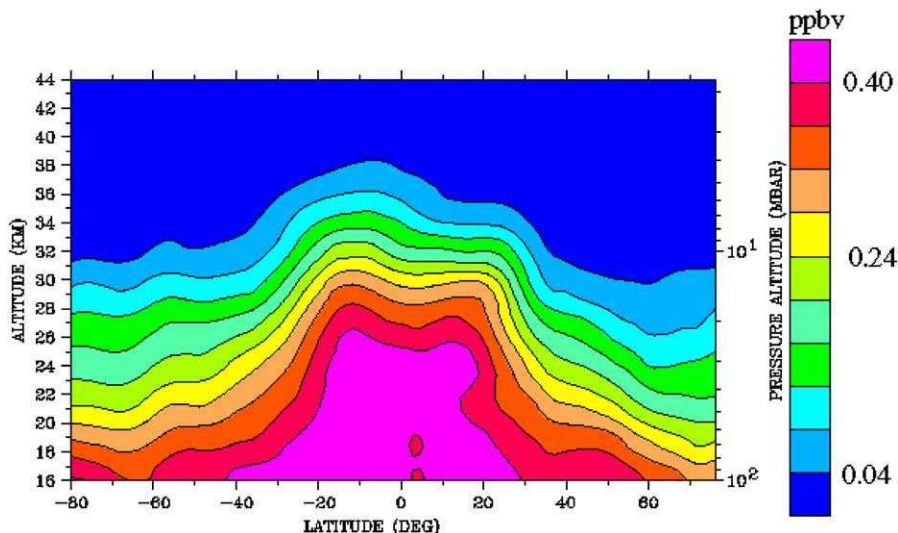


Fig. 1. Global latitude vs. height distribution of CCl_2F_2 (CFC-12), as measured by the CLAES instrument aboard the UARS satellite in March 1992.

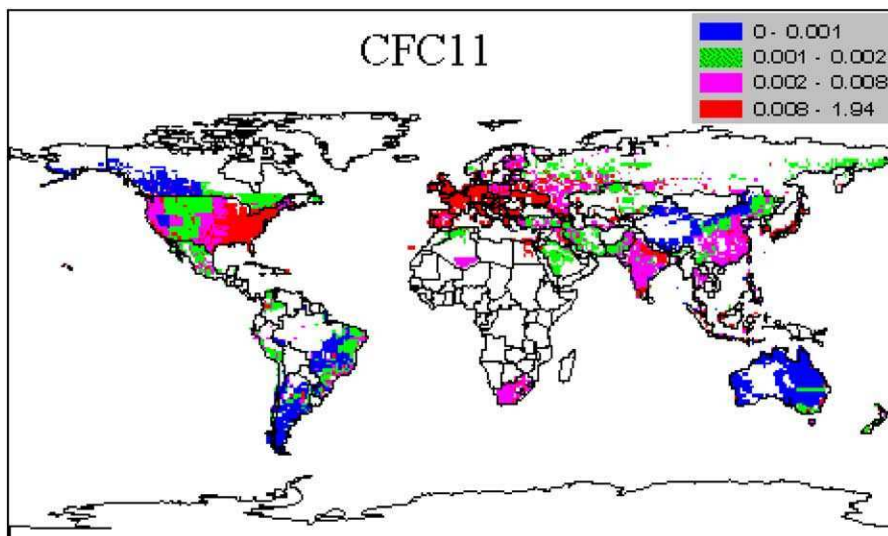


Fig. 2. Emission distribution of CCl_3F (CFC-11) based on McCulloch *et al.* [2]. Within countries in which the emissions have been distributed according to population figures. Data compiled by Jennifer Logan (Harvard University).

used primarily as refrigerants (CFCs-11, -12, and -114, HCFC-22), foam-blowing agents (HCFCs-142b, -141b, and -22, CFCs-11 and -12), solvents (CFC-113, HCFC-141b, methyl chloroform, carbon tetrachloride, chloroform, trichloroethylene, and perchloroethylene), and fire retardants (Halon-1211). Global production of CFC-11 and -12 began in the early 1960s (along with CCl_4) and increased rapidly through the mid-1970s. Maximum production happened in 1988 and decreased substantially since that time. Production of CFCs, methyl chloroform, carbon tetrachloride, and halons has been phased out and production of HCFC and HFC replacements has been phased in by developed countries as of 1996, as called for by the 1987 Montreal Protocol report and subsequent amendments on regulation of substances that deplete the ozone layer.

The main sources of atmospheric inorganic fluorine are the CFCs and HCFC-22 (Table 1). Therefore, the trends in atmospheric chlorine and fluorine levels are both tightly linked to the observed trends in these gases. Unlike chlorine, however, fluorine does not play a significant role in stratospheric ozone destruction because of the high stability of the reservoir species HF (see Section 3.1).

Ozone-depleting halogens in the troposphere continue to decrease. As of mid-2000, equivalent organic chlorine in the troposphere was nearly 5% below the peak value in 1992–1994. The recent rate of decrease is slightly less than in mid-1990s due to the reduced influence of methyl chloroform on this decline. In 2000, tropospheric mixing ratios of CFC-11 (Fig. 3) and -113 were decreasing faster than in 1996, and mixing ratios of CFC-12 were still increasing, but more slowly.

Table 1. Main organic sources for stratospheric fluorine chemistry and their associated lifetime, mixing ratio, and growth rate, as for 2000

Chemical formula	Common or industrial name	Mixing ratio (ppt)	Lifetime (year)	Growth rate (% per year)
<i>Major sources</i>				
CCl ₂ F ₂	CFC-12	543	100	0.42
CCl ₃ F	CFC-11	260	45	-0.41
CCl ₂ FCClF ₂	CFC-113	82	85	-0.43
CHClF ₂	HCFC-22	143	12	3.8
<i>Minor sources</i>				
CH ₂ FCF ₃	HFC-134a	14.6	14	27
CH ₃ CCl ₂ F	HCFC-141b	13	9.3	15
CH ₃ CClF ₂	HCFC-142b	12.5	17.9	9.4
CHF ₃	HFC-23	15.5	270	5.8
CHF ₂ CF ₃	HFC-125	1.4	29	22
CClF ₂ CClF ₂	CFC-114	17.2	300	-0.58
CBrClF ₂	H-1211	4.1	16	3.2
CBrF ₃	H-1301	2.9	65	2.8
CBrF ₂ CBrF ₂	H-2402	0.43	20	0.2
<i>Inert</i>				
CF ₄	FC-14	76	50,000	1
SF ₆	Sulfur hexafluoride	4.6	3200	4.5
CClF ₂ CF ₃	CFC-115	8.1	1700	0.20

Non-anthropogenic sources of CFCs, halons, carbon tetrachloride, methyl chloroform, and HCFCs are insignificant.

The substantial reduction in emissions of ozone-depleting substances during the 1990s that are inferred from measured atmospheric trends are consistent with controls on production and consumption in the fully amended and adjusted Montreal Protocol. The year 1999 is the first in which production and consumption of a class of ozone-depleting substances (CFCs) were restricted by all Parties to the Montreal Protocol. Atmospheric measurements are consistent with emissions derived from reported global production data for CFCs. Indeed, combined chlorine and bromine in the lower stratosphere (10–25 km), where most ozone loss occurs, leveled off around 1999. Bromine is included as an ozone-depleting chemical because although it is not as abundant as chlorine, it is 45 times more effective per atom in destroying stratospheric ozone. Earlier measurements showed that the peak of equivalent chlorine (chlorine plus 45 times bromine) had already occurred at the surface between mid-1992 and mid-1994 (Fig. 3).

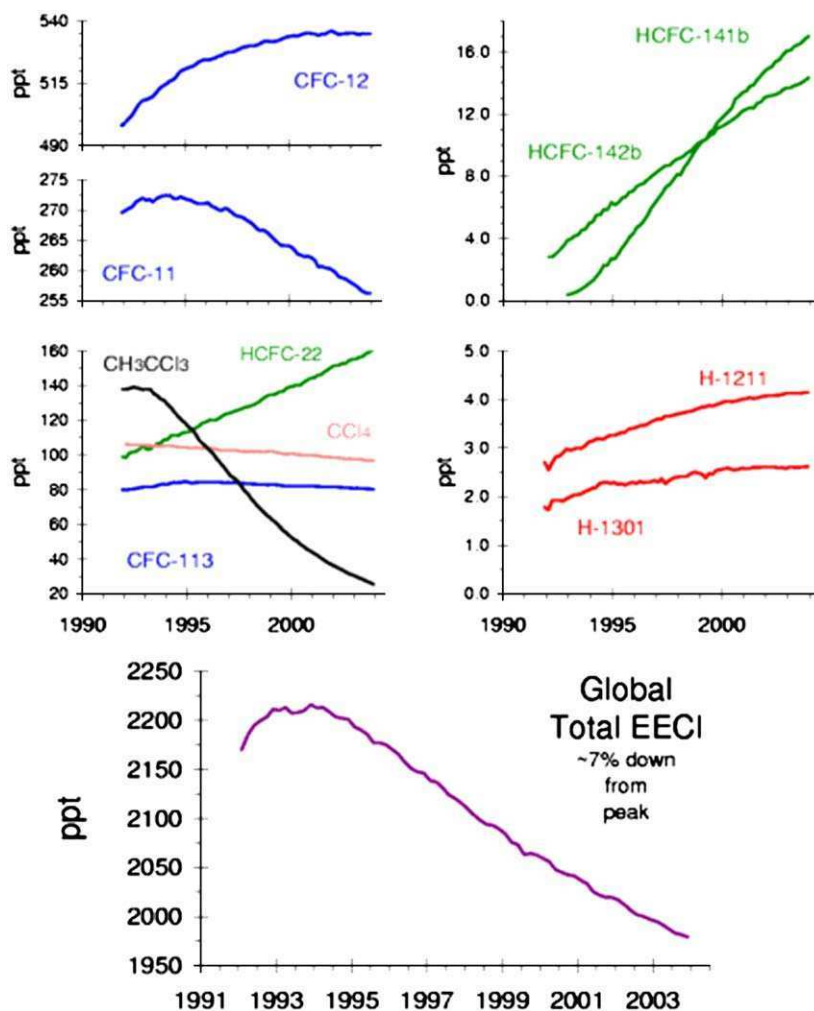


Fig. 3. Global trends in anthropogenic halocarbons (upper panels) and in equivalent chlorine (EECI = chlorine plus 45 times bromine).

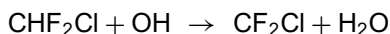
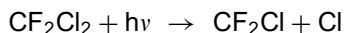
3. CHEMICAL IMPACTS

3.1. Chemistry of stratospheric fluorine

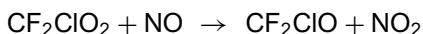
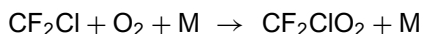
The release of fluorine from CFCs, HCFCs, and other fluorine-containing gases is believed to be analogous to the better-known CH_4 oxidation scheme. An important assumption made is that when CFCs break down in the stratosphere, the first bond that is broken is a carbon–chlorine bond, and the remaining C–Cl bonds

break before any C–F bonds do (based on consideration of the thermodynamics of the dissociation of halogen-substituted analogues of methyl radical [3,4]). In the case of HCFCs, the C–H bonds break first.

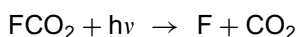
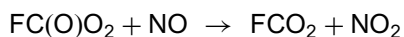
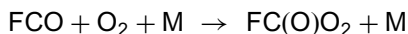
From this assumption, CFCs and HCFCs containing two fluorine atoms are first broken down to CF_2Cl . This is the case for the two most abundant fluorine-containing source gases, CF_2Cl_2 (CFC-12) and CHF_2Cl (HCFC-22):



CF_2Cl then undergoes the following chain of reactions:



Thus each molecule of CFC-12 breaks down to form one molecule of carbonyl fluoride, COF_2 . This species (Fig. 4) has a relatively long lifetime and is only slowly photolyzed. It is therefore an important fluorine temporary reservoir in the middle stratosphere. Measurements of COF_2 are still relatively sparse. Rinsland *et al.* [5] were the first to report a mixing ratio profile from the ATMOS space shuttle experiment. A recent update of the ATMOS spectra analysis is given by Irion *et al.* [6]. These measurements indicate that COF_2 forms relatively high in the stratosphere following the photolysis of CF_2Cl_2 . The general morphology of the vertical profile shows a peak of COF_2 at about 30 km at mid-latitudes, with a mixing ratio larger than 200 parts per trillion volume (pptv) in 1994, in good agreement with the balloon observations reported by Sen *et al.* [7]. In the tropics, the maximum abundance of COF_2 is found at a higher altitude, at about 40 km [8]. This may be simply understood in terms of stratospheric dynamics and the chemistry of the precursor CF_2Cl_2 . CFCs enter the stratosphere largely through upward motion in the tropics, where they are photolyzed weakly in the lower stratosphere because of the large overlying column of ozone. As altitude increases, the CFCs photodissociate and various breakdown products are formed. In the upper stratosphere, COF_2 is photolyzed more rapidly and releases two fluorine atoms F as follows:



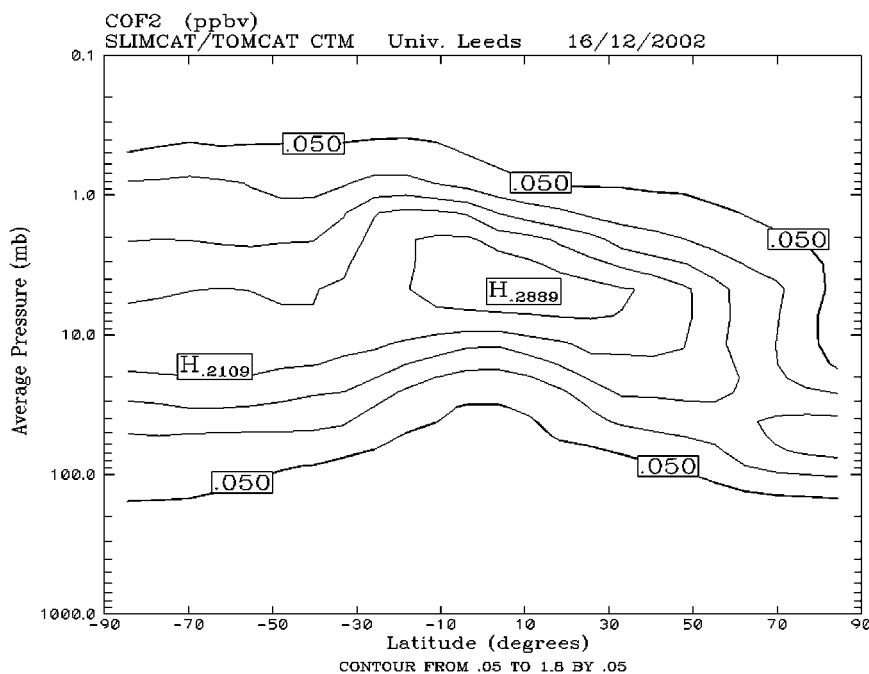


Fig. 4. Latitude vs. pressure distribution of COF₂ (ppbv) as calculated by the SLIMCAT 3D chemical-transport model for the December 2002 period (Courtesy M. Chipperfield, University of Leeds). Contour from 0.05 to 1.80 by 0.05 ppbv. H_{0.2889} means local high value of 0.2889 ppbv.

These processes explain the slow decrease in COF₂ observed above 30 km at mid-latitudes and above 40 km in the tropics. Numerical models indicate that mixing ratios larger than 50 pptv should persist into the mesosphere [4,9]. Note that the absolute abundance of COF₂ shows a time evolution that reflects the trend in man-made fluorine-bearing compounds. Zander *et al.* [8] report for instance a 67% increase in the burden of COF₂ in the middle and upper stratosphere between 1985 and 1992. The long-term monitoring of COF₂ at Jungfraujoch (46°N) also allowed Melen *et al.* [10] to identify a 4% per year increase in the COF₂ vertical column abundance between 1985 and 1995 (Fig. 5).

Because of its relatively long lifetime in the lower and middle stratosphere, COF₂ is an important temporary fluorine reservoir and contributes significantly to the column abundance of total inorganic fluorine (defined as $F_y = [\text{HF}] + 2[\text{COF}_2] + [\text{COFCl}]$) at all latitudes: long-term measurements performed from the ground at Jungfraujoch show that about 30% of F_y is in the form of COF₂ [12], whereas the model simulations performed by Chipperfield *et al.* [9] predict that over 50% may still be in this form in the tropics (Fig. 6).

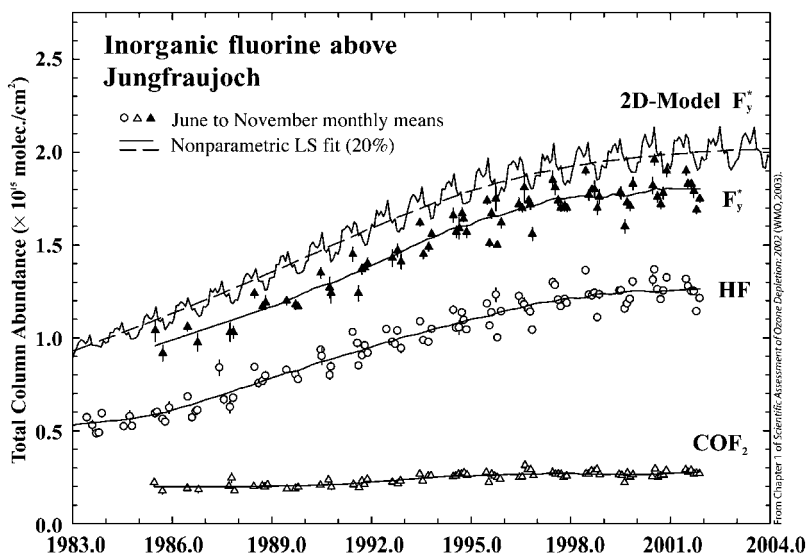
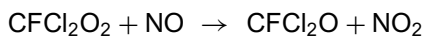
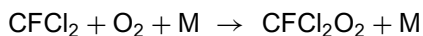
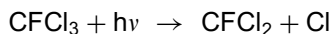
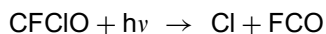


Fig. 5. Time series of monthly mean vertical column abundances of HF (open circles: update from Mahieu *et al.* [11]); COF_2 (open triangles: update from Melen *et al.* [10]); and their weighted sum, F_y^* (filled triangles; where $F_y^* = [\text{HF}] + 2[\text{COF}_2]$) derived from observations at the Jungfraujoch (46.5°N) between 1983 and 2001. The thick lines through the individual datasets represent nonparametric least-squares fits with 20% weighting. Also shown is column F_y^* above the Jungfraujoch calculated with a two-dimensional (2D) model [9]. The 10–12% high bias in the model calculations compared with the summer/fall observations is believed to arise in part from systematic uncertainties in the meridional transport of the 2D model. Taken from WMO [12].

CFCs with a single fluorine atom such as CFCl_3 (CFC-11), an important contributor to the fluorine input in the atmosphere, are initially broken down to CFCl_2 , which then undergoes a chain of reactions:



Thus, the photolysis of CFC-11 here leads to the formation of chlorofluoroformaldehyde, CFCIO. This temporary reservoir is photolyzed more rapidly than COF_2 and produces FCO:



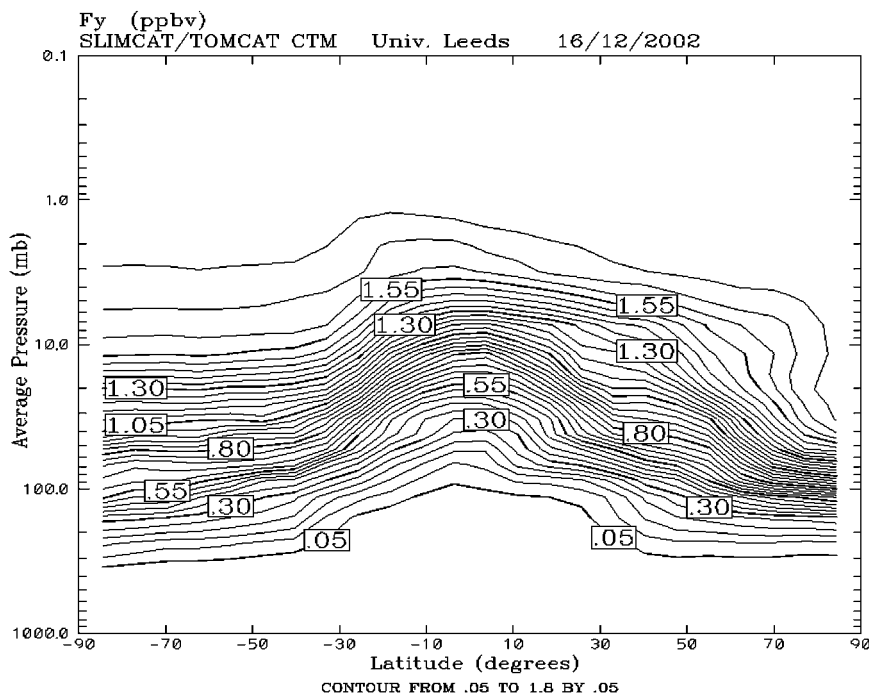


Fig. 6. Latitude vs. pressure distribution of total inorganic fluorine F_y (ppbv) as calculated by the SLIMCAT 3D chemical-transport model for the December 2002 period (Courtesy M. Chipperfield, University of Leeds). Contour from 0.05 to 1.80 by 0.05 ppbv.

which in turn releases fluorine atoms by the process already mentioned above. Because of its shorter lifetime, CFCIO is much less efficient than CF_2O for sequestering fluorine in the stratosphere. CFCIO has not been measured yet in the stratosphere but model calculations indicate that it is formed at a lower altitude than CF_2O , following the photolysis of $CFCl_3$, the CFC being photolyzed lower in the atmosphere. The peak mixing ratio is found at about 25 km at mid-latitudes. Models predict a slightly higher maximum in the tropics, at about 30 km [9], with a maximum mixing ratio on the order of 160 pptv in 2002 (see Fig. 7). Since CFCIO is also the most easily photolyzed fluorine-containing breakdown product, its abundance falls off rapidly with increasing altitude above the peak: CFCIO becomes more than one order of magnitude smaller than COF_2 5 km above its peak, at 30 km. From model calculations [9], the contribution of CFCIO to the column abundance of total inorganic chlorine is of the order of 10% at mid-latitudes.

In the middle and upper stratosphere, the free F atoms produced by the dissociation of the intermediate reservoirs COF_2 and CFCIO mostly react with O_2

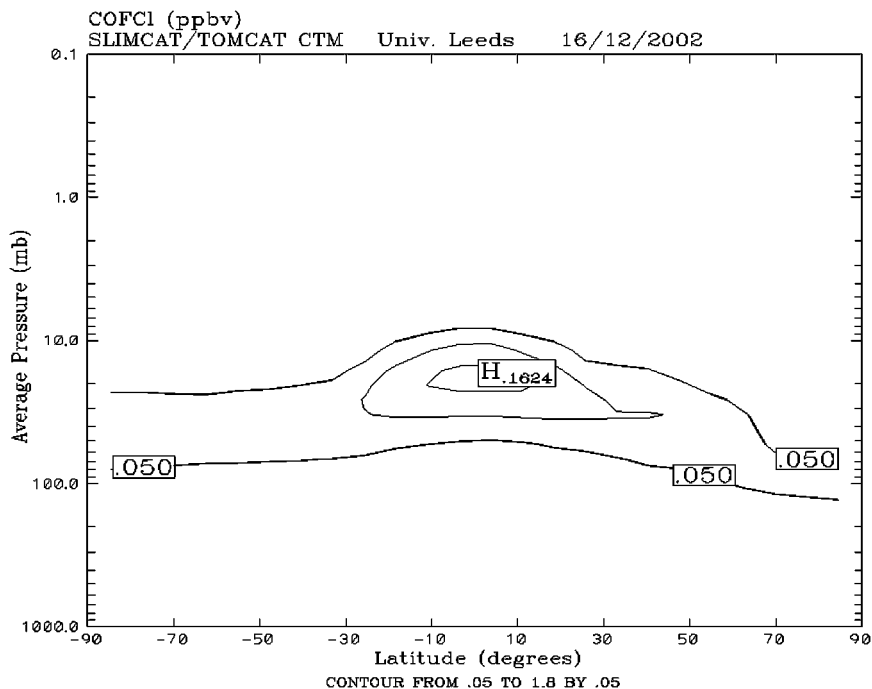
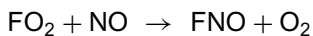
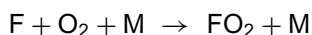
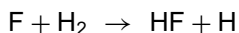
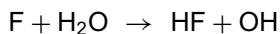
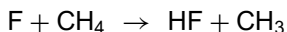


Fig. 7. Latitude vs. pressure distribution of COFCl (ppbv) as calculated by the SLIMCAT 3D chemical-transport model for the December 2002 period (Courtesy M. Chipperfield, University of Leeds). Contour from 0.05 to 1.80 by 0.05 ppbv. $H_{0.1624}$ means local high value of 0.1624 ppbv.

and participate in the following null cycle:

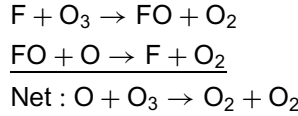


The F atoms eventually react with methane, water vapor, or molecular hydrogen to form hydrogen fluoride (HF):



This set of reactions is similar to that of forming HCl from Cl atoms. Unlike HCl however, HF cannot react with OH, as the reaction is endothermic. In addition,

photolysis cannot occur to any appreciable extent in the stratosphere, making HF an essentially permanent reservoir of stratospheric fluorine. Because of this strong stability, the atmospheric densities of F and FO are very small and prevent the 'classical' odd oxygen-destroying catalytic cycle from being efficient:



Thus, fluorine chemistry does not represent a significant sink for stratospheric ozone. All fluorine released from the source gases ends up in the form of HF, which accumulates in the stratosphere (Fig. 8). It is ultimately removed either by slow diffusion and rainout in the troposphere or by upward transport to the mesosphere where its mixing ratio remains constant up to high altitudes.

The high stability of HF makes it an effective tracer of fluorine input in the stratosphere arising from fluorinated anthropogenic gases. It is also a useful tracer of stratospheric motion and is often used as a reference for chemically more active tracers. Column HF is routinely measured by infrared spectroscopy

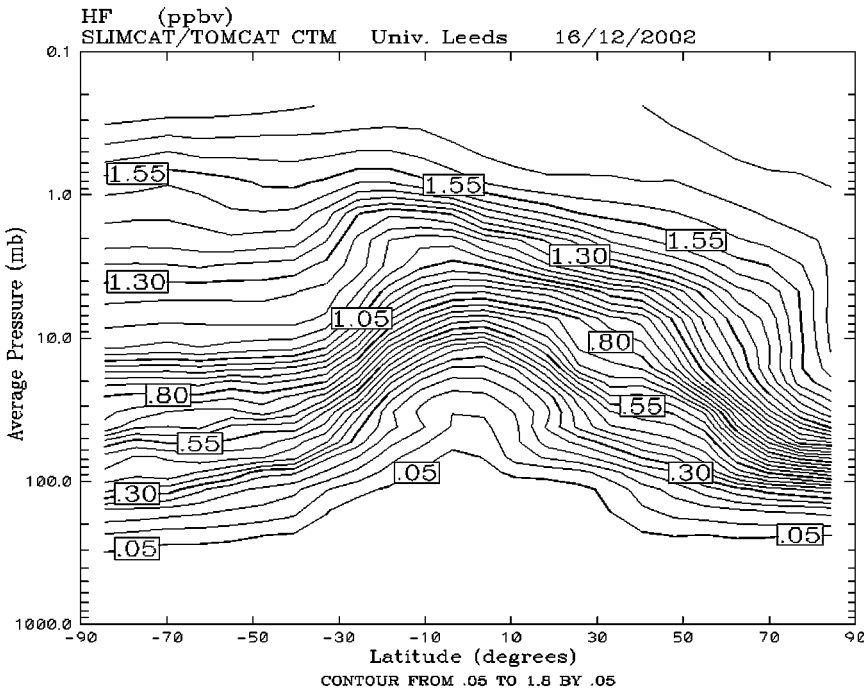


Fig. 8. Latitude vs. pressure distribution of HF (ppbv) as calculated by the SLIMCAT 3D chemical-transport model for the December 2002 period (Courtesy M. Chipperfield, University of Leeds). Contour from 0.05 to 1.80 by 0.05 ppbv.

from the ground [11,13], and numerous observations have been obtained with air-borne, balloon-borne, and space-based instruments. Near global satellite measurements of HF have also been recorded since October 1991 by the HALOE instrument onboard the UARS satellite [14]. At all latitudes, the general morphology of the vertical distribution of the HF abundance shows a continuous increase from the tropopause to the mesosphere (Fig. 9): as altitude increases, organic fluorine compounds decompose due to photolysis and chemistry, forming the intermediate reservoirs COF_2 and CFCIO which dissociate to produce HF. Since HF is not photolyzed or otherwise lost by chemical reaction, its mixing ratio will continue to increase in the stratosphere and mesosphere until all the COF_2 has been photolyzed (Fig. 10). At 55 km, HF is estimated to represent about 90% of the total inorganic fluorine [14]. Based on model calculations, the remaining 10% are believed to be in the form of COF_2 at this altitude [4,9]. In 2004, the total inorganic fluorine burden was estimated to be 1.8 parts per billion volume (ppbv).

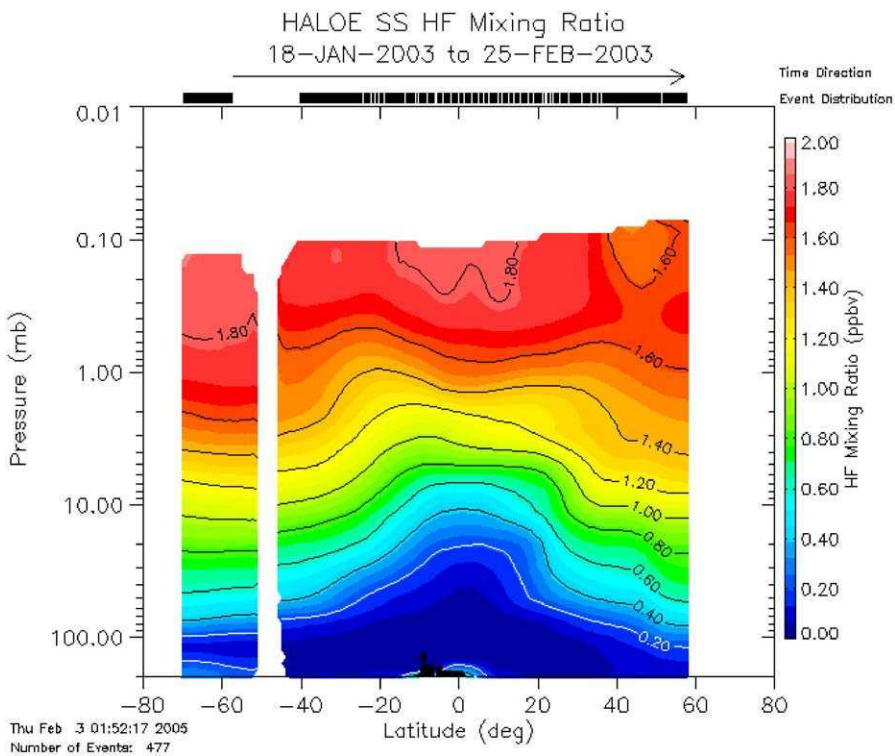


Fig. 9. Latitude vs. pressure cross-section of HF mixing ratio (ppbv) measured by the HALOE instrument on board the UARS satellite between 18 January 2003 and 25 February 2003.

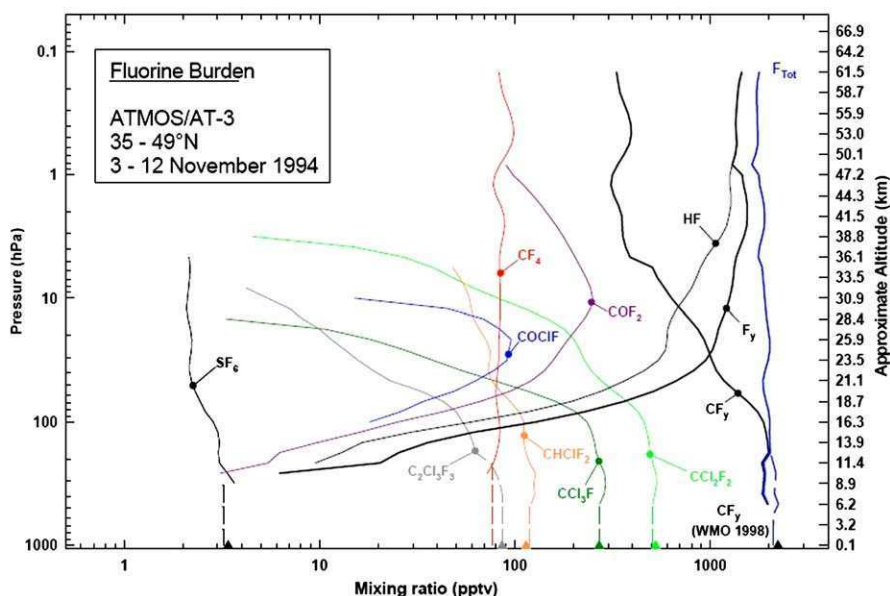
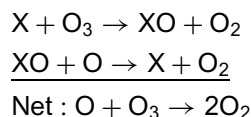


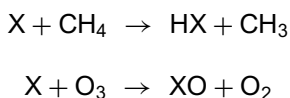
Fig. 10. Fluorine burden estimated from space-borne measurements during the ATMOS mission from Irion *et al.* [6].

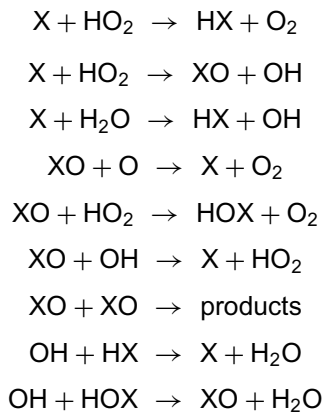
3.2. Chemistry of stratospheric chlorine

Once halogenated compounds are photolyzed or combine with other molecules in the atmosphere, they lead to a rapid release of free halogen atoms which give, after several reactions, inorganic species (see, e.g., Brasseur *et al.* [15]). This latter species belongs to several families (chlorine, fluorine, bromine, iodine) within which they can partition and, for some of them, directly destroy the ozone molecule (active molecules). If not, they are named reservoir molecules. They can indeed destroy O₃ through a catalytic cycle via the reaction:

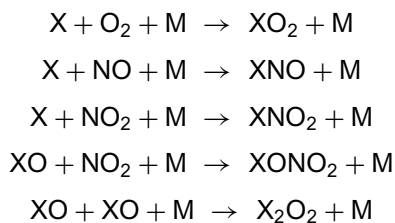


where X can be fluorine (F), bromine (Br), iodine (I), or chlorine (Cl) compounds. The ability of the family to destroy O₃ depends on the thermodynamics and reaction kinetics. Indeed, inorganic halogen species interact with various other molecules and families through bimolecular reactions:

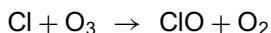




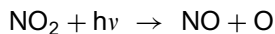
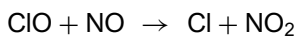
and termolecular reactions:



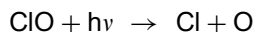
For the reasons given in Section 3.1, fluorine atoms are essentially sequestered in the form of HF in the stratosphere, and thus do not play any significant role in the ozone-destroying catalytic cycles presented here. However, this is not the case for chlorine and bromine atoms. Once a chlorine atom is formed, it rapidly reacts with O_3



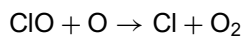
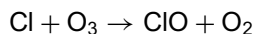
and ClO, once formed, is transformed back into Cl through different pathways



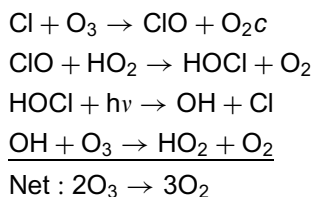
and



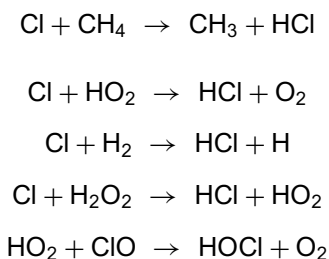
with no change in chemical composition. This is different in the catalytic cycle involving odd oxygen family $\text{O}_x = \text{O} + \text{O}_3$



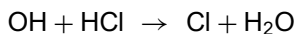
and $\text{HO}_x = (\text{OH} + \text{HO}_2)$ family



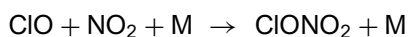
Other reactions can convert active chlorine ($\text{Cl} + \text{ClO}$) into reservoir species (essentially HCl , the most abundant chlorine reservoir, but also HOCl):



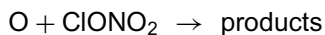
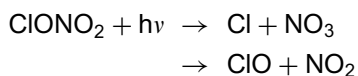
HCl comes back to Cl via the reaction:



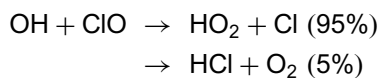
ClO can also react with ClONO_2 via the termolecular reaction:



while ClONO_2 is photolyzed or reacts with the oxygen atom:



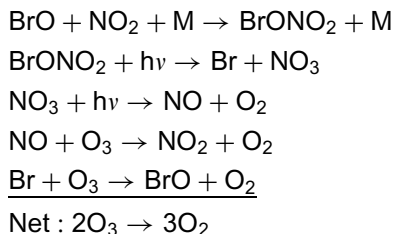
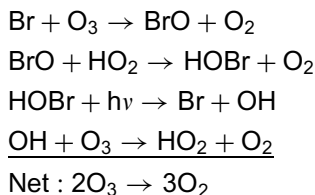
We can also note another pathway converting Cl from active species to reservoir ones:



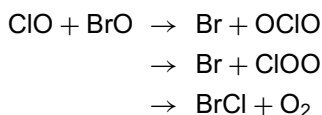
3.3. Links with stratospheric bromine chemistry

As already mentioned in Section 2, bromine, although not as abundant as chlorine, is 45 times more effective per atom in destroying stratospheric ozone. Indeed, bromine family plays a key role in the catalytic ozone destruction cycle

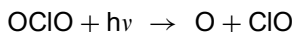
via the two following cycles:



Furthermore, there is a cycle that couples the chemistry of chlorine and bromine through the reaction of ClO with BrO:



Production of OCIO in this reaction results in a null cycle:



but halogen atoms can be regenerated via the reactions:



3.4. Chlorine–bromine reactions in an “Ozone Hole” configuration

At high northern and southern winter latitudes (Fig. 11), the destruction of the ozone layer is governed by reactions that are far different from the ones listed above. Indeed, heterogeneous reactions can occur on the surface of polar stratospheric clouds (PSCs formed of liquid or solid particles composed of HNO_3 and H_2O). This leads to ozone loss, depending upon the occurrence of sunlight combined with gas-phase reactions involving bromine and chlorine chemical reactions [15].

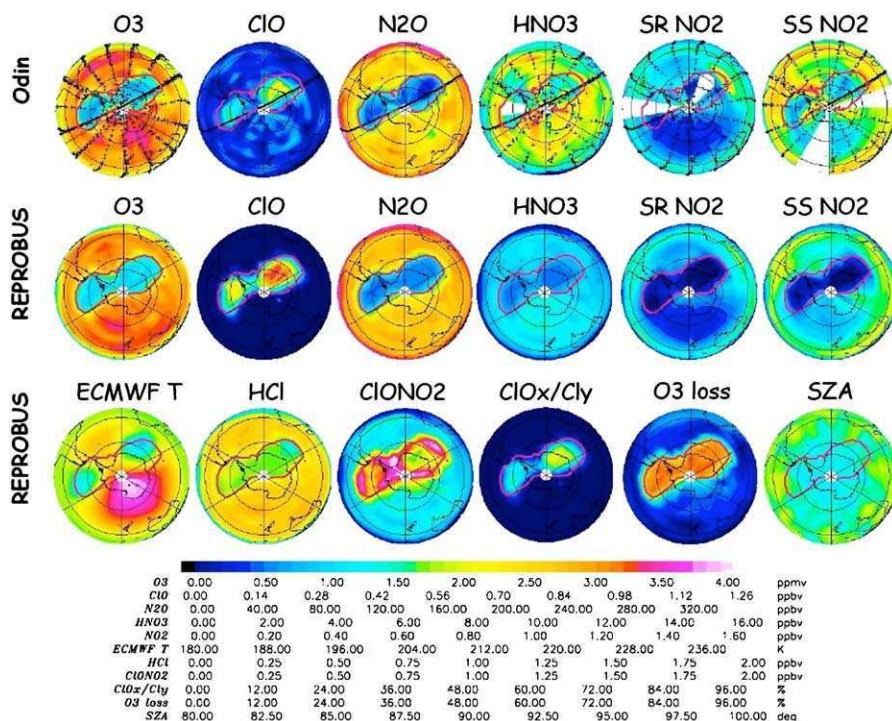
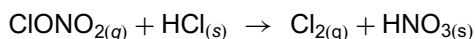
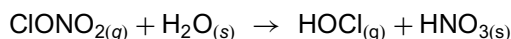
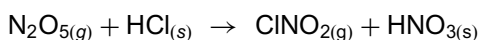
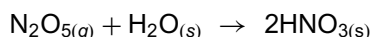


Fig. 11. Polar stereographic projection of the Antarctic polar vortex split in September 2002, as traced by different stratospheric constituents at 20 km as measured by the Odin satellite (top row), and as calculated by a 3D chemical-transport model (middle and bottom rows). Taken from Ricaud *et al.* [16].

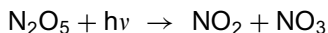
On the surface of PSCs, heterogeneous reactions alter the partitioning of inorganic chlorine, since reservoir species HCl and ClONO₂ convert into Cl₂, HOCl, and ClNO₂:



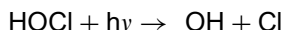
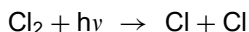
where the subscript (g) means gas phase and (s) means solid phase. Gas-phase N₂O₅ is essentially produced during the night



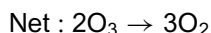
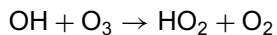
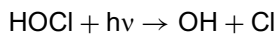
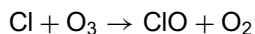
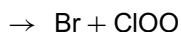
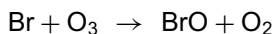
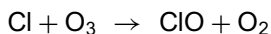
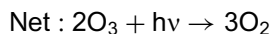
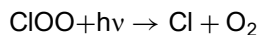
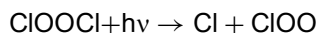
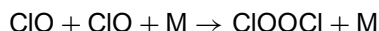
and destroyed during daytime



The gas-phase species produced by heterogeneous reactions photolyze readily at the edge of the polar vortex in winter or later in early spring:



yielding the catalytic ozone-destroying cycles involving both chlorine and bromine families:



Because they do not require the presence of oxygen atoms O, these catalytic cycles can operate at low altitudes where the concentration of ozone is largest.

4. RADIATIVE IMPACTS

Global warming potentials (GWPs) are used to estimate the integrated climate forcing of various greenhouse gases compared with a reference gas, usually chosen to be carbon dioxide (CO₂). They provide a simple way of gauging how

decisions affecting greenhouse gas emissions (e.g., in the Kyoto Protocol) may influence our future climate in a relative sense. Furthermore they allow the effects of these potential actions to be roughly assessed in terms of a “carbon dioxide equivalent” emission. Radiative effects of CFC alternatives are also assessed with the use of GWPs.

Furthermore the accurate calculation of the radiative forcing of the CFCs and related species relies on good quality data on the absorption cross sections at thermal infrared. For some gases, a spread exceeding 25% of the mean cross sections was found and there was little agreement of the sign, or indeed even the existence, of any temperature dependence. The radiative forcing owing to CFCs and their related species also depends on the knowledge of the spectroscopy of overlapping species such as water vapor, carbon dioxide, and ozone. Remaining spectroscopic uncertainties from the HITRAN database [17] are estimated to cause errors of no more than 5% in the radiative forcing. Hence, errors from this source are likely to be smaller than current uncertainties in the absorption cross sections of the halocarbons.

The GWP of a particular compound is defined as the ratio of the time-integrated radiative forcing from the instantaneous emission of 1 kg of some gas relative to that of 1 kg of a reference gas. Mathematically, the GWP is given by

$$\text{GWP}_x(TH) = \frac{\int_0^{TH} a_x[x(t)]dt}{\int_0^{TH} a_r[r(t)]dt}$$

where a_x is the radiative forcing of a unit mass of species x added to the current atmospheric composition, $x(t)$ the atmospheric decay function of the pulse of species x , a_r , and $r(t)$ the corresponding quantities for the reference gas, and TH the time horizon over which the calculation is performed.

The global and annual mean radiative forcing induced by halocarbons is indeed positive at about 0.5 W m^{-2} and of a high degree of scientific understanding (Fig. 12). They participate to the $2.43 (\pm 10\%) \text{ W m}^{-2}$ positive radiative forcing induced by other greenhouse gases (namely CO_2 , CH_4 , and N_2O) within a small uncertainty range.

In addition to the direct GWP of the species listed in Table 2, chlorinated and brominated halocarbons can lead to a significant indirect forcing through their destruction of stratospheric O_3 . Indeed, since O_3 is a greenhouse gas, halocarbons destroying stratospheric O_3 induce a negative indirect forcing that counteracts some or perhaps all (in certain cases) of their direct forcing. Furthermore, decreases in stratospheric O_3 act to increase the ultraviolet field of the troposphere and hence can increase OH and deplete those gases destroyed by reaction with the OH radical (particularly CH_4); this provides an additional negative forcing that is very difficult to quantify.

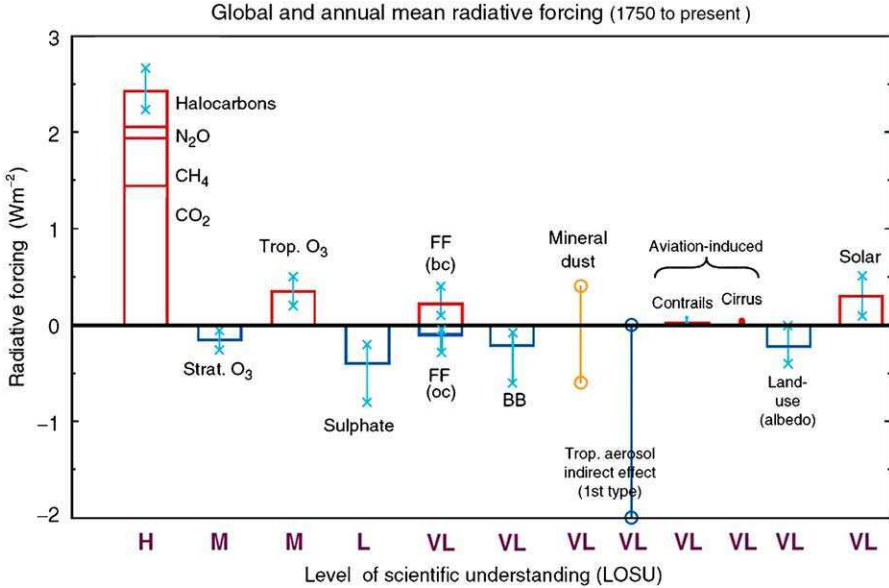


Fig. 12. Global and annual mean radiative forcings ($W m^{-2}$) according to different climate parameters from pre-industrial (1750) to present (2000) and their associated level of scientific understanding (H, high; M, medium; L, low; VL, very low). Taken from IPCC [18].

5. MEASUREMENTS

The monitoring effort on the temporal evolutions of CFCs, HCFCs, HCFs, and PFCs is conducted via two programs: (1) the Atmospheric Lifetime Experiment (ALE), Global Atmospheric Gases Experiment (GAGE), and Advanced Global Atmospheric Gases Experiment, namely ALE/GAGE/AGAGE program and (2) the former NOAA Climate Monitoring and Diagnostics Laboratory (CMDL) which has recently merged into the Earth System Research Laboratory (ESRL) as part of its Global Monitoring Division (GMD).

In the ALE/GAGE/AGAGE global network program [19], continuous high-frequency gas chromatographic measurements of two biogenic/anthropogenic gases (CH_4 and N_2O) and six anthropogenic gases (chlorofluorocarbons $CFCl_3$, CF_2Cl_2 , and $CF_2ClCFCl_2$; methyl chloroform, CH_3CCl_3 ; chloroform, $CHCl_3$; and carbon tetrachloride, CCl_4) are carried out at five globally distributed sites. Additional important species such as hydrogen (H_2), carbon monoxide (CO), methyl chloride (CH_3Cl), methyl bromide (CH_3Br), HFC-134a, HCFC-141b, HCFC-142b, HCFC-22, and Halons-1211 and -1301 have been added at select sites in recent years. The program, which began in 1978, is divided into three parts associated

Table 2. Global warming potential of long-lived fluorinated species in the atmosphere. Taken from WMO [12]

Common name	Chemical formula	Global warming potential		
		20 years	100 years	500 years
Carbon dioxide	CO ₂	1	1	1
<i>Chlorofluorocarbons</i>				
CFC-11	CCl ₃ F	6330	4680	1630
CFC-12	CCl ₂ F ₂	10,340	10,720	5230
CFC-13	CClF ₃	10,160	14,190	16,520
CFC-113	CCl ₂ FCClF ₂	6150	6030	2700
CFC-114	CClF ₂ CClF ₂	7560	9880	8780
CFC-115	CClF ₂ CF ₃	4990	7250	10,040
<i>Hydrochlorofluorocarbons</i>				
HCFC-22	CHClF ₂	4850	1780	552
HCFC-142b	CH ₃ CClF ₂	5170	2270	709
<i>Hydrofluorocarbons</i>				
HFC-23	CHF ₃	9500	12,240	10,350
HFC-125	CHF ₂ CF ₃	5970	3450	1110
HFC-143a	CH ₃ CF ₃	5540	4400	1600
HFC-227ea	CF ₃ CHFCF ₃	5760	3660	1200
HFC-236fa	CF ₃ CH ₂ CF ₃	7620	9650	7700
<i>Bromocarbons</i>				
Halon-1211	CBrClF ₂	4460	1860	578
Halon-1301	CBrF ₃	7970	7030	2780
<i>Fully fluorinated species</i>				
Sulfur hexafluoride	SF ₆	15,290	22,450	32,780
Trifluoromethylsulfurpenta	SF ₅ CF ₃	12,370	17,500	21,500
FC-14	CF ₄	3920	5820	9000
FC-116	C ₂ F ₆	8110	12,010	18,280
FC-218	C ₃ F ₈	5940	8690	12,520
FC-31-10	C ₄ F ₁₀	5950	8710	12,550
FC-318	c-C ₄ F ₈	6870	10090	14,740
FC-41-12	C ₅ F ₁₂	6120	9010	13,330
FC-51-14	C ₆ F ₁₄	6230	9140	13,350
<i>Halogenated alcohols and ethers</i>				
HFE-125	CHF ₂ OCF ₃	12,970	14,670	8530
HFE-134	CHF ₂ OCHF ₂	11,470	6220	1970
H-Galden 1040x				
CHF ₂ OCF ₂ OC ₂ F ₄ OCHF ₂		1840	572	
	5940			
HFE-236ca12	CHF ₂ OCF ₂ OCHF ₂	7560	2780	864
HFE-338pcc13				
CHF ₂ OCF ₂ CF ₂ OCHF ₂		1480	459	
	4770			
<i>Gases whose lifetimes are determined by indirect means</i>				
Nitrogen trifluoride	NF ₃	7780	10,970	13,240
Perfluorocyclopropane	c-C ₃ F ₆	> 11,950	> 17,070	> 21,920
HFE-227ea	CF ₃ CHFOCF ₃	4270	1520	471

with three changes in instrumentation: the ALE, which used Hewlett Packard HP5840 gas chromatographs; the GAGE, which used HP5880 gas chromatographs; and the present Advanced GAGE (AGAGE). AGAGE uses two types of instruments: a gas chromatograph with multiple detectors (GC–MD), and a gas chromatograph with mass spectrometric analysis (GC–MS). The current station

locations are Cape Grim, Tasmania (41°S, 145°E); Cape Matatula, American Samoa (14°S, 171°E); Ragged Point, Barbados (13°N, 59°W); Mace Head, Ireland (53°N, 10°W); and Trinidad Head, California (41°N, 124°W). Stations also previously existed at Cape Meares, Oregon (45°N, 124°W); and Adrigole, Ireland (52°N, 10°W). The current Mace Head station replaced the Adrigole station and the station at Trinidad Head replaced the Cape Meares station.

NOAA measurements of climatically important gases began on an expanded scale in the mid-1970s [20] for carbon dioxide (CO₂), nitrous oxide (N₂O), chlorofluorocarbons (CFCs), and ozone (O₃). Over the years, a number of other gases have been added, including methane (CH₄), carbon monoxide (CO), hydrogen (H₂), hydrochlorofluorocarbons (HCFCs), hydrofluorocarbons (HFCs), methyl halides, and sulfur hexafluoride (SF₆). Numerous types of platforms are used, including ground-based stations, towers, ocean vessels, aircraft, and balloons. Electropolished, stainless-steel flasks are collected weekly in pairs, and analyzed for N₂O, CFC-11, and -12 on an electron-capture gas chromatograph (GC-ECD). Flask samples for HCFCs, HFCs, and other atmospheric halogens are analyzed by gas chromatography with detection by mass spectrometry (GC-MS). Flasks are filled at nine sites, five of which are considered remote locations (Fig. 13): Barrow, Alaska (71.32°N, 156.60°W); Trinidad Head, California (41.05°N, 124.15°W); Mauna Loa, Hawaii (19.53°N, 155.57°W); Samoa (14.23°S, 170.56°W); South Pole (89.99°S, 102.00°W). Measurements of nitrous oxide (N₂O), the chlorofluorocarbons: CFC-12 (CCl₂F₂), CFC-11 (CCl₃F), and CFC-113 (CCl₂F-CClF₂) and the chlorinated solvents: methyl chloroform (CH₃CCl₃) and carbon tetrachloride (CCl₄) are being made once an hour by using gas chromatographs. These instruments also have the capability of measuring sulfur hexafluoride (SF₆), Halon-1211 (CBrClF₂), HCFC-22 (CHClF₂), HCFC-142b (CClF₂-CH₃), carbonyl sulfide (OCS), methyl chloride (CH₃Cl), and methyl bromide (CH₃Br).

In parallel to these two ground-based measurement networks, we must mention some activities within the international Network for the Detection of Stratospheric Change (NDSC), now changed into the Network for the Detection of Atmospheric Composition Change (NDACC). Indeed, combining different sorts of ground-based remote-sensing instruments (essentially within the IR domain using Fourier Transform IR spectrometers), some integrated columns of halogen compounds can be identified over long-term periods. For instance, at the Jungfraujoch (46.5°N) and the Mauna Loa (19.53°N) stations, more than a decade of CFCs measurements are available.

Balloon- and air-borne measurements of halogen compounds are also performed during dedicated campaigns: in situ instruments HALOZ, ASTRID, DESCARTES, DIRAC, BONBON, ACATS, SPIRALE, MANTRA, SAKURA, etc., and the remote sensing spectrometers LPMA, MIPAS-B, FIRS-2, MkIV, etc. Another vector for studying the temporal evolution of halogen compounds comes from



Fig. 13. Two NOAA sites where measurements of CFCs are performed: (above) Barrow, Alaska, USA and (below) Mauna Loa Observatory, Hawaii, USA.

Table 3. Lists of long-lived halogen compounds measured by space-borne instruments

Platform	Instrument	Compounds
UARS	CLAES	CFC-12, CFC-11
UARS	HALOE	HCl, HF
Space station	CRISTA	CFC-11
Space station	ATMOS	HF, HCl, CH ₃ Cl, CF ₄ , CCl ₂ F ₂ , CCl ₃ F, CCl ₄ , COF ₂ , CHF ₂ Cl, SF ₆
ENVISAT	MIPAS	CFC-11, CFC-12
AURA	MLS	HCl
AURA	HIRDLS	CFC-11, CFC-12
SciSat	ACE	HF, HCl, CCl ₃ F ₂ , CCl ₃ F, COF ₂ , CHF ₂ Cl, SF ₆ , CF ₄ , CH ₃ Cl
ADEOS	ILAS	CFC-11, CFC-12
ADEOS II	ILAS-II	CFC-11, CFC-12

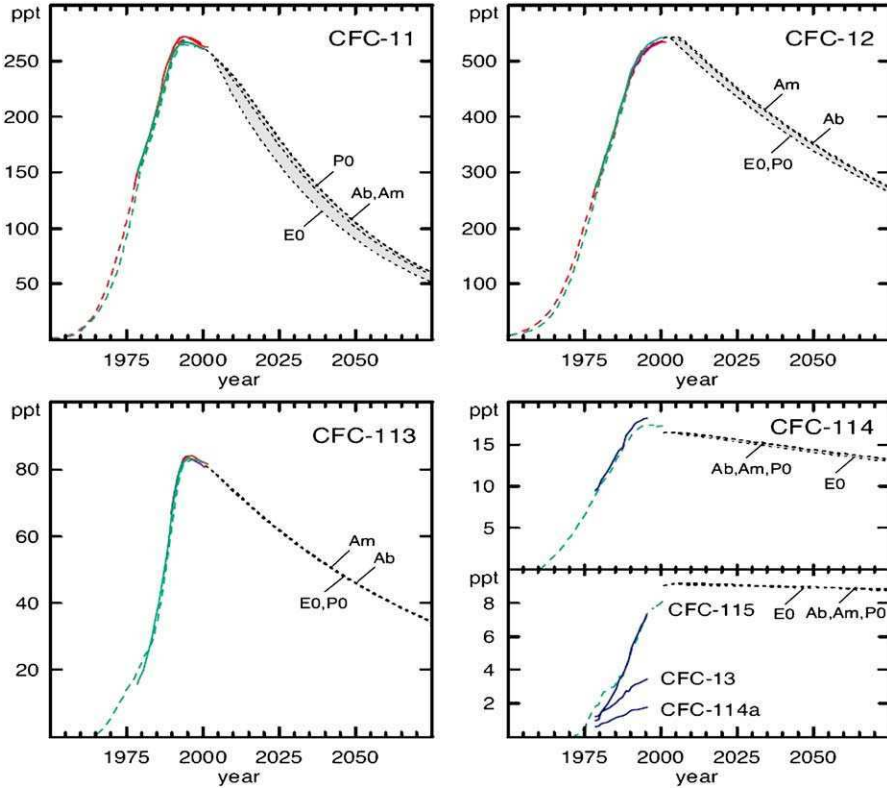


Fig. 14. Past and potential future atmospheric mixing ratios of CFCs using different scenarios. Ab, best guess; E0, zero emissions; Am, maximum allowed production; and P0, zero production. Taken from WMO [12].

space. Table 3 lists different instruments aboard space platforms dedicated to the measurements of halogen compounds, which among them are CLAES [21], HALOE [22], CRISTA [23], MIPAS [24], MLS [25], HIRDLS [26], and ILAS [27].

6. TRENDS AND SCENARIOS

The timetable for the reduction in halogen source gas production and consumption, as outlined by the Copenhagen Amendment, calls for the complete phasing out of the production and consumption of CFCs 11, 12, 113, 114, and 115 by the year 1996; the phasing out of halogen production and consumption by 1994; and the phasing -out of most HCFCs by the year 2040. Projections made following the Copenhagen Amendment indicated that the peak chlorine burden would occur in late 1990s, at a value of about 4 ppbv. The total chlorine burden should decrease,

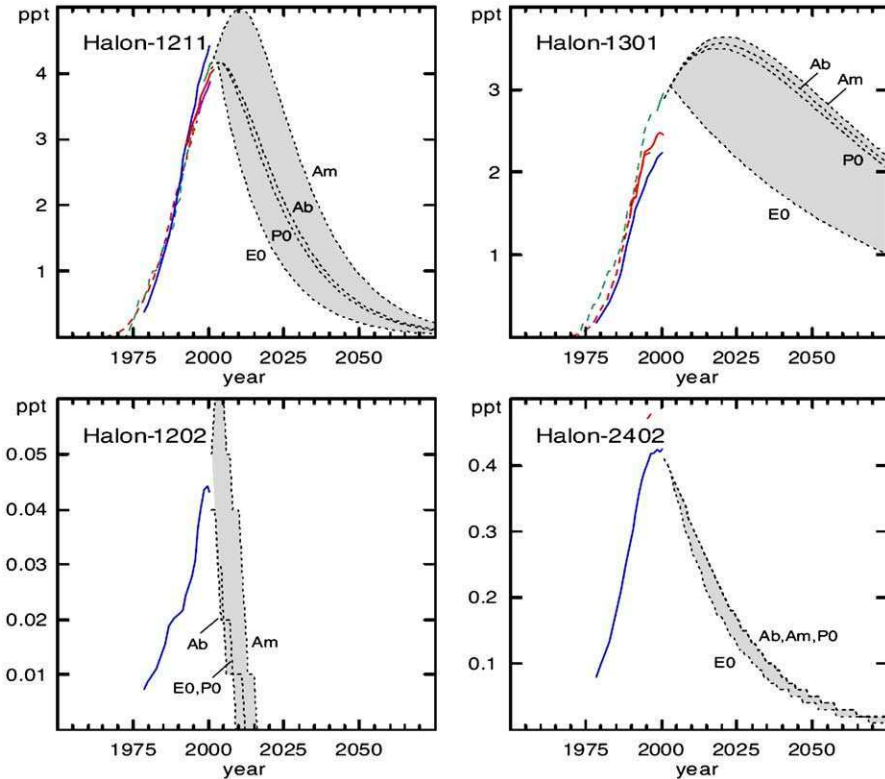


Fig. 15. Same as in Fig. 14 but for halons. Taken from WMO [12].

reaching 3 ppbv in about 2040 and 2 ppbv in about 2060. Recent measurements have indeed shown that the mean global tropospheric chlorine abundance reached a maximum in 1994 and is now decreasing at a rate of about 25 pptv per year. Trends in stratospheric chlorine loading will mirror those observed in the troposphere, after accounting for the 4–6 years time lag associated with transport of air to the stratosphere. It is important to note that the onset of the appearance of the Antarctic ozone hole coincided with chlorine levels of approximately 2 ppbv. Hence, even with current regulations on future emissions of chlorine source gases, ozone depletion in the Antarctic vortex can be anticipated to continue for at least 50 years.

Different scenarios for future ozone depleting substance (ODS) emissions are studied [18]. The Ab scenario represents the best-guess scenario following the Beijing Amendments since the future production of CFCs is supposed to be continued at the current level of capacity for “essential use” for developed countries and is allowed to continue at the current (frozen) level for developing countries. The Am scenario corresponds to the maximum production scenario in which

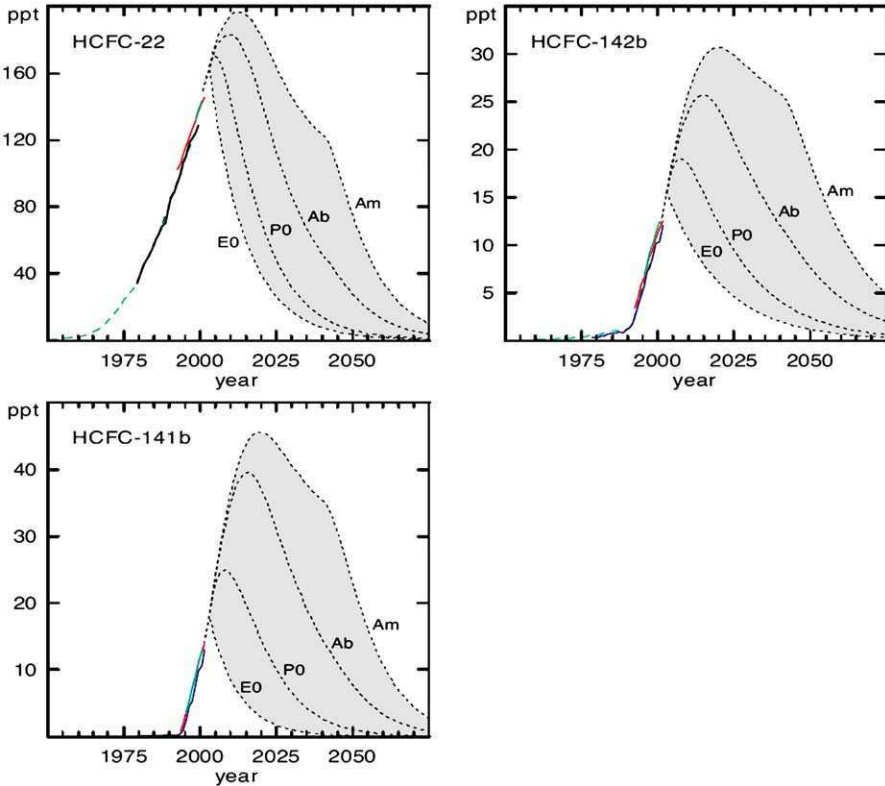


Fig. 16. Same as in Fig. 14 but for HCFCs. Taken from WMO [12].

production of CFCs, halons, and HCFCs is projected forward at the maximum allowed under the protocol. The E0 scenario corresponds to a hypothetical zero-emission scenario. Indeed, anthropogenic emissions of all ODSs (CFCs, CCl_4 , CH_3CCl_3 , halons, HCFCs, and CH_3Br) are set to zero from 2003 onward. Finally, in the P0 scenario, production of all ODSs is set to zero from 2003 onward. Figs. 14–18 and the potential future atmospheric mixing ratios using different scenarios for CFCs, halons, HCFCs, HFCs, fluorocarbons, and sulfur hexafluoride.

The updated, best-estimate scenario for future halocarbon mixing ratios suggests that the atmospheric burden of halogens will return to the 1980, pre-Antarctic-ozon-hole levels around the middle of the century, provided continued adherence is undertaken to the fully amended and adjusted Montreal Protocol. Only small improvements would arise from reduced production allowances in the future. Lack of compliance to the protocol controls would delay or prevent recovery of stratospheric ozone.

About 80% of the equivalent chlorine in today's atmosphere arises from direct anthropogenic release of ODS. Climate change could influence future

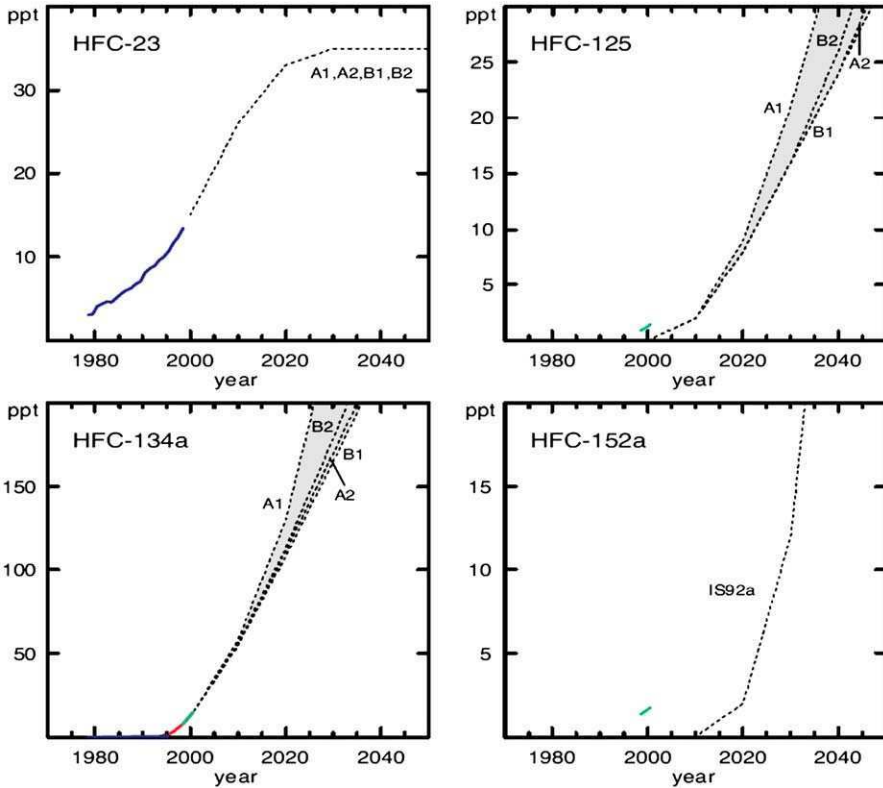


Fig. 17. Long-term trends and possible future levels of HFCs depending upon several scenarios from IPCC (2001). Taken from WMO [12].

atmospheric amounts of these gases by affecting the rates at which gases are removed from the atmosphere. For CFCs, halons, and CCl₄, rates of atmospheric removal are governed by the flux of high-energy light in the stratosphere and the rate at which air is mixed through the stratosphere. If changes in climate were to affect rates of air transport through the stratosphere, trace gas lifetimes would be altered. The lack of predictive understanding of such changes does not allow reliable estimate of whether lifetimes would become longer or shorter in the future in an atmosphere with elevated greenhouse gas abundances. For methylchloroform, HCHCs, methyl halides, and other chemically reduced gases, climate change could influence loss rate through changes in mean global concentrations of hydroxyl radical. This oxidant plays a key role in determining the lifetime of these important ozone-depleting substances. Amounts of this short-lived, but powerful atmospheric oxidant depend directly on humidity, sunlight, temperature, and the abundance of many different trace gases likely to be affected by climate and human behavior in the future.

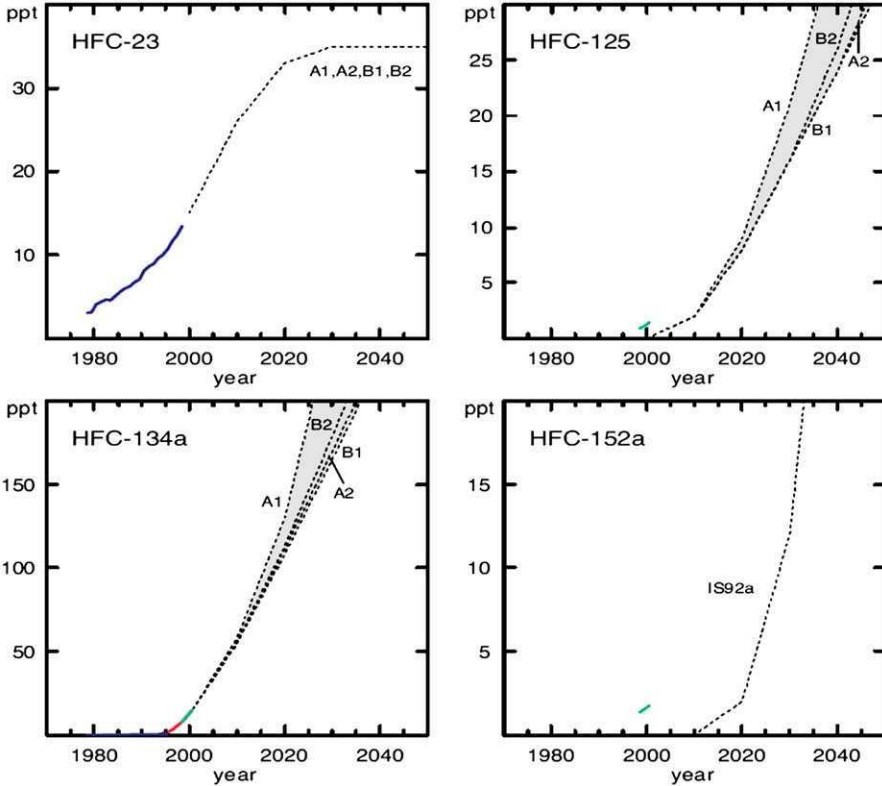


Fig. 18. Same as in Fig. 17, but for fluorocarbons and sulfur hexafluoride. Taken from WMO [12].

REFERENCES

- [1] J.C. Farman, B.G. Gardiner, J.D. Shanklin, Large losses of total ozone in Antarctica reveal seasonal ClO_x/NO_x interaction, *Nature* 315 (1985) 207.
- [2] A. McCulloch, P. Midgley, D. Fisher, Distribution of emissions of chlorofluorocarbons (CFCs) 11, 12, 113, 114, and 115 among reporting and non-reporting countries in 1986, *Atmos. Environ.* 28 (1994) 2567–2582.
- [3] D.L. Baulch, R.A. Cox, R.F. Hampson, J.A. Kerr, J. Troe, R.T. Watson, Evaluated kinetic and photochemical data for atmospheric chemistry, *J. Phys. Chem. Ref. Data* 9 (1980) 295–471.
- [4] J.A. Kaye, A.R. Douglass, C.H. Jackman, R.S. Stolarski, R. Zander, G. Roland, Two-dimensional model calculation of fluorine-containing reservoir species in the stratosphere, *J. Geophys. Res.* 96 (1991) 12865–12991.
- [5] C.P. Rinsland, R. Zander, L.R. Brown, C.B. Farmer, J.H. Park, R.H. Norton, J.M. Russell III, O.F. Raper, Detection of carbonyl fluoride in the stratosphere, *Geophys. Res. Lett.* 13 (1986) 769–772.
- [6] F.W. Irion, M.R. Gunson, G.C. Toon, A. Eldering, A.Y. Chang, E. Mahieu, G.L. Manney, H.A. Michelsen, E.J. Moyer, M.J. Newchurch, G.B. Osterman, M.J. Prather, C.P.

- Rinsland, R.J. Salawitch, B. Sen, Y.L. Yung, R. Zander, Atmospheric Trace Molecule Spectroscopy (ATMOS) Experiment version 3 data retrievals, *Appl. Opt.* 41 (2002) 6968–6979.
- [7] B. Sen, G.C. Toon, J.-F. Blavier, E.L. Fleming, C.H. Jackman, Balloon-borne observations of midlatitude fluorine abundance, *J. Geophys. Res.* 101 (1996) 9045–9054.
- [8] R. Zander, C.P. Rinsland, E. Mahieu, M.R. Gunson, C.B. Farmer, M.C. Abrams, M.K.W. Ko, Increase of carbonyl fluoride (COF_2) in the stratosphere and its contribution to the 1992 budget of organic fluorine in the upper stratosphere, *J. Geophys. Res.* 99 (1994) 16737–16743.
- [9] M.P. Chipperfield, M. Burton, W. Bell, C.P. Walsh, Th. Blumenstock, M.T. Coffey, J.W. Hannigan, W.G. Mankin, B. Galle, J. Mellqvist, E. Mahieu, R. Zander, J. Notholt, B. Sen, G.C. Toon, On the use of HF as a reference for the comparison of stratospheric observations and models, *J. Geophys. Res.* 102 (1997) 12901–12919.
- [10] F. Melen, E. Mahieu, R. Zander, C.P. Rinsland, P. Demoulin, G. Roland, L. Delbouille, C. Servais, Vertical column abundances of COF_2 above the Jungfraujoch station, derived from ground-based infrared observations, *J. Atmos. Chem.* 29 (1998) 119–134.
- [11] E. Mahieu, R. Zander, P. Demoulin, M. De Mazière, F. Melen, C. Servais, G. Roland, L. Delbouille, J. Poels, R. Blomme, Fifteen-year trend characteristics of key stratospheric constituents measured by FTIR above the Jungfraujoch, in *Stratospheric ozone 1999*, Proc. 5th European Symp., Air Pollution Rep. 73, European Commission, Luxembourg, 2000.
- [12] WMO (World Meteorological Organization), Scientific assessment of ozone depletion: 2002, Global Ozone Research and Monitoring Project – Report 47, Geneva, 2003, p. 498.
- [13] C.P. Rinsland, R. Zander, E. Mahieu, L.S. Chiou, A. Goldman, N.B. Jones, Stratospheric HF column abundances above Kitt Peak (31.9°N latitude): trends from 1977 and 2001 and correlations with stratospheric HCl columns, *J. Quant. Spect. Rad. Trans.* 74 (2002) 205–216.
- [14] J. Anderson, J.M. Russell III, S. Solomon, L.E. Deaver, Halogen occultation experiment confirmation of stratospheric chlorine decreases in accordance with the Montreal Protocol, *J. Geophys. Res.* 105 (2000) 4483–4490.
- [15] G. Brasseur, *Atmospheric Chemistry and Global Change*, 2nd edition, Oxford University Press, New York, 1999.
- [16] P. Ricaud, F. Lefèvre, G. Berthet, D. Murtagh, E.J. Llewellyn, G. Mégie, E. Kyrölä, W. Leppelmeier, H. Auvinen, C. Boone, S. Brohede, D.A. Degenstein, J. de La Noë, E. Dupuy, L. El Amraoui, P. Eriksson, W.F.J. Evans, U. Frisk, R.L. Gattinger, F. Girod, C.S. Haley, S. Hassinen, A. Hauchecorne, C. Jiménez, E. Kyrö, N. Lautié, E. Le Flochmoën, N.D. Lloyd, J.C. McConnell, I.C. McDade, L. Nordh, M. Olberg, S.V. Petelina, A. Sandqvist, A. Seppälä, C.E. Sioris, B.H. Solheim, J. Stegman, K. Strong, P. Taalas, J. Urban, C. von Savigny, F. von Scheele, G. Witt, Polar vortex evolution during the 2002 Antarctic major warming as observed by the Odin satellite, *JGR*, 110, D05302, 2005, 10.1029/2004JD005018.
- [17] L.S. Rothman, A. Barbe, D.C. Benner, L.R. Brown, C. Camy-Peyret, M.R. Carleer, K. Chance, C. Clerbaux, V. Dana, V.M. Devi, A. Fayt, J.-M. Flaud, R.R. Gamache, A. Goldman, D. Jacquemart, K.W. Jucks, W.J. Lafferty, J.-Y. Mandin, S.T. Massie, V. Nemtchinov, D.A. Newnham, A. Perrin, C.P. Rinsland, J. Schroeder, K.M. Smith, M.A.H. Smith, K. Tang, R.A. Toth, J.V. Auwera, P. Varanasi, K. Yoshino, The HIT-RAN molecular spectroscopic database: Edition of 2000 including updates Through 2001, *J. Quant. Spectrosc. Radiat. Transfer* 82 (2003) 5–44.
- [18] Intergovernmental Panel on Climate Change (IPCC), *Climate Change 2001: The Scientific Basis*, Contribution of Working Group I to the Third Assessment Report of the IPCC, J. T. Houghton, Y. Ding, D.J. Griggs, M. Noguer, P.J. v.d. Linden, X. Dai, K. Maskell, C.A. Johnson (Eds.), Cambridge University Press, New York, 2001, pp. 881.

- [19] R.G. Prinn, R.F. Weiss, P.J. Fraser, P.G. Simmonds, D.M. Cunnold, F.N. Alyea, S. O'Doherty, P. Salameh, B.R. Miller, J. Huang, R.H.J. Wang, D.E. Hartley, C. Harth, L.P. Steele, G. Sturrock, P.M. Midgely, A. McCulloch, A history of chemically and radiatively important gases in air deduced from ALE/GAGE/AGAGE, *J. Geophys. Res.* 105 (2000) 17751–17792.
- [20] S.A. Montzka, R.C. Myers, J.H. Butler, J.W. Elkins, Early trends in the global tropospheric abundance of hydrochlorofluorocarbon-141b and 142b, *Geophys. Res. Lett.* 21 (1994) 2483–2486.
- [21] A.E. Roche, J.B. Kumer, J.L. Mergenthaler, G.A. Ely, W.G. Uplinger, J.F. Potter, T.C. James, L.W. Sterritt, The cryogenic limb array Etalon spectrometer (CLAES) on UARS: experiment description and performance, *J. Geophys. Res.* 98 (1993) 10763–10775.
- [22] J.M. Russell III., L.L. Gordley, J.H. Park, S.R. Drayson, D.H. Hesketh, R.J. Cicerone, A.F. Tuck, J.E. Frederick, J.E. Harries, P. Crutzen, The halogen occultation experiment, *J. Geophys. Res.* 98 (1993) 10777–10797.
- [23] M. Riese, R. Spang, P. Preusse, M. Ern, M. Jarisch, D. Offermann, K.U. Grossmann, Cryogenic infrared spectrometers and telescopes for the atmosphere (CRISTA) data processing and atmospheric temperature and trace gas retrieval, *J. Geophys. Res.* 104 (1999) 16349–16367.
- [24] H. Fischer, C. Blom, H. Oelhaf, B. Carli, M. Carlotti, L. Delbouille, D. Ehhalt, J.-M. Flaud, I. Isaksen, M. Lopez-Puertas, C.T. McElroy, R. Zander, ENVISAT MIPAS—An Instrument for Atmospheric Chemistry and Climate Research, ESA Special Publication, SP-1229, 2000 pp. 124.
- [25] J.W. Waters, L. Froidevaux, R.S. Harwood, R.F. Jarnot, H.M. Pickett, W.G. Read, P.H. Siegel, R.E. Cofield, M.J. Filipiak, D.A. Flower, J.R. Holden, G.K. Lau, N.J. Livesey, G.L. Manney, H.C. Pumphrey, M.L. Santee, D.L. Wu, D.T. Cuddy, R.R. Lay, M.S. Loo, V.S. Perun, M.J. Schwartz, P.C. Stek, R.P. Thurstans, M.A. Boyles, K.M. Chandra, M.C. Chavez, Gun-Shing Chen, B.V. Chudasama, R. Dodge, R.A. Fuller, M.A. Girard, J.H. Jiang, Y. Jiang, B.W. Knosp, R.C. LaBelle, J.C. Lam, K.A. Lee, D. Miller, J.E. Oswald, N.C. Patel, D.M. Pukala, O. Quintero, D.M. Scaff, W. Van Snyder, M.C. Tope, P.A. Wagner, M.J. Walch, The Earth observing system microwave limb sounder (EOS MLS) on the Aura satellite, *IEEE Trans. Geosci. Remote Sensing* 44 (2006) 1075–1092.
- [26] J.Gille, J.Barnett, J.Gille, G.Visconti (Eds.), *Use of EOS for Studies of Atmospheric Physics*, North-Holland, Netherlands, 1992.
- [27] F. Khosrawi, R. Müller, H. Irie, A. Engel, G.C. Toon, B. Sen, S. Aoki, T. Nakazawa, W.A. Traub, K.W. Jucks, D.G. Johnson, H. Oelhaf, G. Wetzel, T. Sugita, H. Kanzawa, T. Yokota, H. Nakajima, Y. Sasano, Validation of CFC-12 measurements from the Improved Limb Atmospheric Spectrometer (ILAS) with version 6.0 retrieval algorithm, *J. Geophys. Res.* 109 (2004) doi:10.1029/2003JD004325.

CHAPTER 2

Evaluation and Selection of CFC Alternatives

Akira Sekiya,¹ Masaaki Yamabe,² Kazuaki Tokuhashi,³
Yasuo Hibino,⁴ Ryoichi Imasu⁵ and Hidekazu Okamoto⁶

¹*Research Institute for Innovation in Sustainable Chemistry, National Institute of Advanced Industrial Science and Technology (AIST), Central 5-2, 1-1-1 Higashi, Tsukuba, Ibaraki 305-8565, Japan*

²*National Institute of Advanced Industrial Science and Technology (AIST), Tsukuba Headquarters (Central 2), 1-1-1 Umezono, Tsukuba, Ibaraki 305-8568, Japan*

³*Research Institute for Innovation in Sustainable Chemistry, National Institute of Advanced Industrial Science and Technology (AIST), Central 5, 1-1-1 Higashi, Tsukuba, Ibaraki 305-8565, Japan*

⁴*Chemical Research Center, Central Glass Co., Ltd., 2805 Imafuku—Nakadai, Kawagoe, Saitama 350-1151, Japan*

⁵*Center for Climate System Research, The University of Tokyo, General Research Building Room No. 315b, 5-1-5 Kashiwanoha, Kashiwa, Chiba 277-8568, Japan*

⁶*Research & Development Division, Chemicals Company, Asahi Glass Co., Ltd., 10, Goikaigan, Ichihara, Chiba 290-8566, Japan*

Contents

1. CFCs and the global environment	34
1.1. Development of alternative CFCs	34
1.1.1. Market for CFCs	34
1.1.2. Montreal protocol	35
1.1.3. Approaches to alternative CFCs	39
2. Fluorocarbon-related technologies and environmental problems	40
2.1. Refrigerants	40
2.1.1. Demand for refrigerants	40
2.1.2. Fluorine refrigerants and their alternatives	41
2.1.3. Non-fluorine refrigerants	43
2.1.4. Selection of refrigerants	43
2.2. Blowing agents	43
2.2.1. Fluorocarbon blowing agents	43
2.2.2. The development of blowing agents that do not damage the ozone layer	44
2.2.3. Blowing agents by type of application	47
2.2.4. Next-generation blowing agents and methods	48
2.3. Solvents	48
2.3.1. Introduction	48
2.3.2. Physical properties and current application of alternative cleaning solvents	49
2.3.3. Other applications of fluorinated compounds	51

3. Environmental assessment of CFC alternatives	51
3.1. The importance of lifetime of CFC alternatives	51
3.1.1. Reaction rate measurement by the absolute rate method	53
3.1.2. Reaction rate measurement by the relative rate method	58
3.1.3. Atmospheric lifetime of CFC alternatives	59
3.2. Ozone-depletion potential	60
3.3. Global-warming potential	65
4. Evaluation of current alternatives	70
4.1. Environmental impact assessment	71
4.2. Evaluation of the flammability of CFC alternatives	71
4.3. LCCP evaluation	74
4.4. New evaluation of global warming	75
4.4.1. Evaluations using a total warming prediction graph	76
4.4.2. Composite warming potential	79
4.4.3. Atmospheric lifetime of compounds emitted and the greenhouse effect	81
5. Concluding remarks	81
Acronyms and Abbreviations	82
Appendix I: Some chemical symbols used in this chapter	83
References	85

Abstract

This chapter reports on the effect of fluorine compounds in the atmosphere. These compounds have been evaluated for their role in ozone layer depletion and global warming. The state of their application, the use of alternatives and the alternatives themselves were analyzed. There are also explanations of the science behind ozone depletion potential and global-warming potential, of associated evaluation methods, and new methods that can compensate for previous deficiencies. The results suggest that fluorine compounds with short atmospheric lifetimes are suitable as chlorofluorocarbon alternatives.

1. CFCs AND THE GLOBAL ENVIRONMENT

1.1. Development of alternative CFCs

1.1.1. Market for CFCs

The development of fluorine chemical industry in the second half of the twentieth century was triggered by the synthesis of a new non-toxic, non-harmful fluorine-based refrigerant, dichlorodifluoromethane (CCl_2F_2 : CFC-12) by T. Midgley in 1928, and by the serendipitous discovery of polytetrafluoroethene made by R. Plunkett in 1938. DuPont in USA began the industrial production of these compounds, and their use then rapidly expanded in the market worldwide. Following CFC-12, trichlorofluoromethane (CCl_3F : CFC-11) has been extensively used as a foam-blowing agent for plastics such as polyurethane, and trichlorotrifluoroethane ($\text{CF}_2\text{ClCFCl}_2$: CFC-113) has been used as a cleaning solvent mainly in

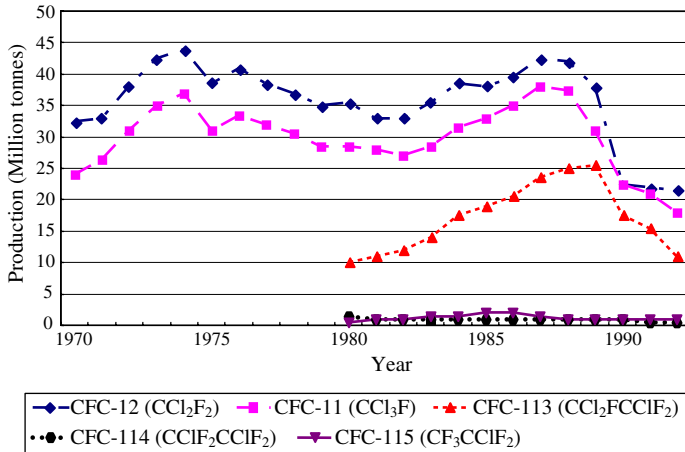


Fig. 1. Worldwide production of chlorofluorocarbons (CFCs).

the electronics industry. These fluorine-based compounds are called chlorofluorocarbons (CFCs) and are characterized by excellent properties and stability together with a relatively low cost (a few dollars per kg). As shown in Fig. 1 [1], from the mid-1970s up to the second half of the 1980s, the global production of CFCs reached about 1 million tonnes.

CFCs are applied mainly to propellants for aerosols, refrigerants for mobile and room air conditioning and refrigerators, blowing agents for plastic foams such as polyurethane and polystyrene, and to solvents for electronic, metal and precision cleaning. As shown in Fig. 2 [1], the demand for CFCs varies according to regions or countries. In the year 1988, almost half of the demand in the United States was for air conditioning refrigerants, mainly for the automobile industry, whereas in Japan, almost half of the consumption was as cleaning agents for electronics and mechanical industries. In Europe, the main uses of CFCs were in aerosols, followed by blowing agents and refrigerants.

1.1.2. Montreal protocol

CFCs were often referred to as a chemical miracle of the twentieth century because of their extraordinary characteristics. However, an unexpected blow struck the fluorine chemical industry when Prof. Sherwood Rowland and Dr Mario Molina of the University of California, reported a hypothesis of the “stratospheric ozone depletion caused by CFCs” at the annual meeting of the American Chemical Society in 1974. According to their publication in *Nature* [2], CFCs have long lifetimes in the atmosphere, and do not decompose in the air; CFC molecules diffuse towards the ozone layer in the stratosphere after a long time, where the effect of strong ultraviolet light causes photo-dissociation of the carbon–chlorine

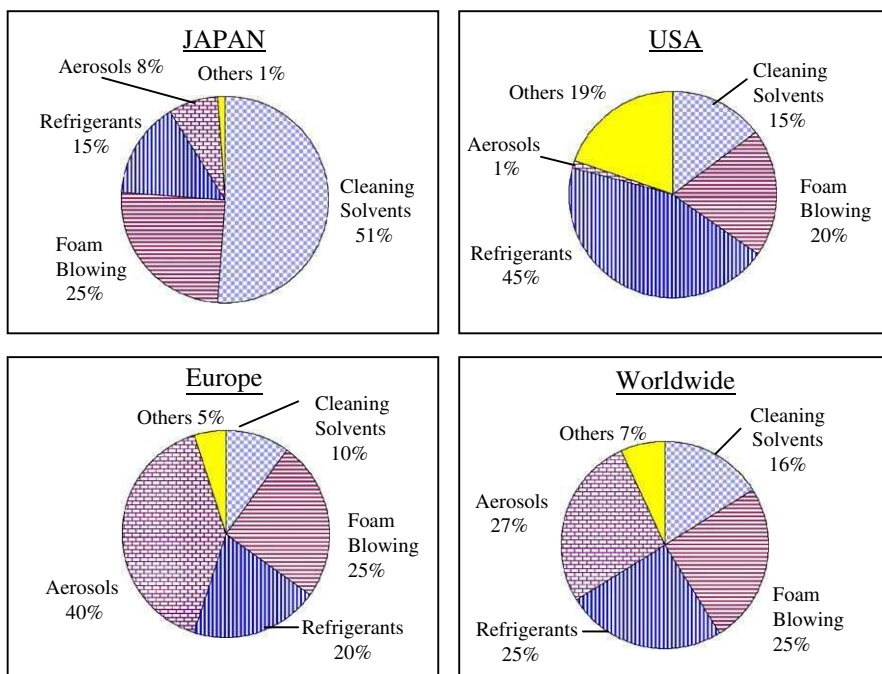


Fig. 2. Regional trends in CFC applications (1988).

bond in the CFC molecule. The excited chlorine atoms then catalytically destroy the ozone molecule, and as a consequence, the ozone layer.

This report prompted projects for monitoring the ozone concentration in the stratosphere, studying the effect on the ecosystem of the increase of the amount of UV-B rays reaching the surface of the Earth as a consequence of ozone depletion and verifying the actual conditions against the claims on ozone depletion caused by the use of CFCs. These monitoring activities have been carried out with the support of industry, NASA and several other research institutions worldwide. At the same time, under guidance from the United Nations Environment Programme (UNEP), governments around the world agreed to endorse the Vienna Convention for the Protection of the Ozone Layer in 1985 after protracted negotiations. In 1987, the Montreal Protocol on Substances that Deplete the Ozone Layer was adopted to reflect the norms in the Vienna Convention. The Montreal Protocol established first that the production and consumption of five types of CFCs (CFC-11, 12, 113, 114 (CClF₂CClF₂), 115 (CF₃CClF₂)) were to be reduced by 50% by the year 2000, and that production and consumption of halons (bromofluoro compounds used as fire extinguishers: Halon-1301 (CBrF₃), 1211 (CBrClF₂) and 2402 (CBrF₂CBrF₂)) with high ozone-depleting potential, was to be frozen at the 1986 level by the year 1992. Several amendments were made to the protocol after reports from the Scientific Assessment Panel (SAP),

Table 1. Schedule for phase-out of ozone-depleting substances (ODSs)

1985: Vienna Convention		
1987–1999: Montreal Protocol with several amendments		
ODSs	Developed countries	Developing countries
Halons	1994	2010
CFCs	1996	2010
HCFCs	2020	2040
Methyl bromide	2005	2015
Carbon tetrachloride	1996	2010
1,1,1-trichloroethane	1996	2015

indicated that the schedules were not comprehensive enough to protect the ozone layer. The schedule for the phasing out of ozone-depleting substances (ODSs) is currently as presented in [Table 1](#).

Following these international agreements, the production of halons was stopped completely in 1994, and production of the so-called controlled substances that cause the depletion of the stratospheric ozone layer was halted in the developed countries at the end of 1995. However, this alone does not guarantee the recovery of the ozone hole. [Table 1](#) shows the established targets which developed countries and developing countries are requested to comply with. In the case of developing countries, there is a grace period of 10 years for compliance, but after the year 2005, the same standards as for the developed countries are to be applied. Technological and economic assistance and support to developing countries are crucial for this to happen. [Fig. 3](#) shows the expected effect on the recovery of the ozone layer by the various adjustments presented by UNEP [3]. From this figure it is evident that recovery of the ozone layer will require a continuous effort by the entire human race for a span of time longer than a hundred years.

Having almost the same relevance as the protection of the ozone layer, global warming is another environmental issue that is related to fluorine compounds. The continuous increase in the emission of carbon dioxide that accompanied the drastic increase in energy consumption from the year 1980 is considered to be the main cause of global warming. In the Earth Summit held in Rio de Janeiro, Brazil in 1992, an agreement known as the United Nations Framework Convention on Climate Change (UNFCCC) was signed. At the third Conference of the Parties to the UNFCCC (COP3) in 1997, specific targets on the decrease of emission of greenhouse gases were introduced as the Kyoto Protocol. [Table 2](#) gives an outline of the Kyoto Protocol which presents six greenhouse gases for specific emission targets with a basket system: besides carbon dioxide, methane

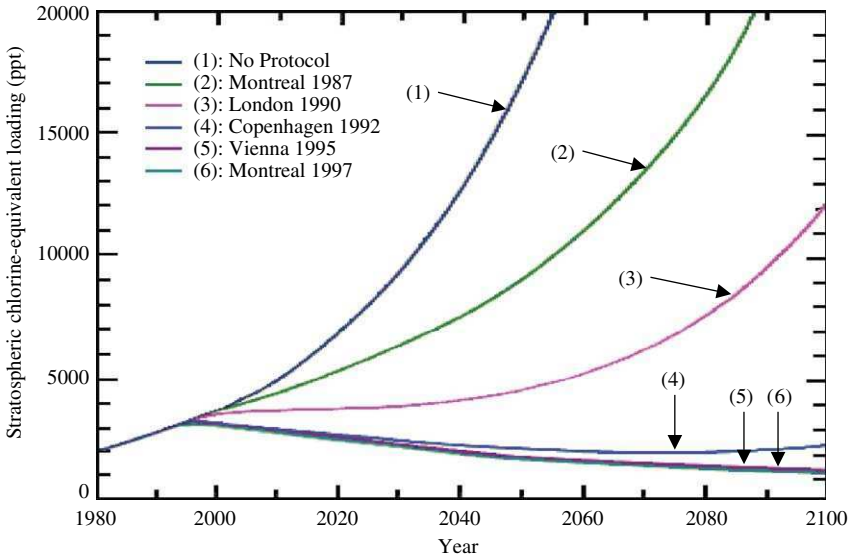


Fig. 3. Effect of the Montreal Protocol.

Table 2. Schedule for reduction of greenhouse gas (GHG) emissions

1992: United Nations Framework Convention on Climate Change (UNFCCC)
 1997: Kyoto Protocol

GHGs	Period	Reduction (total: -5.2%)
CO ₂ , CH ₄ , N ₂ O (base year: 1990)	2008–2012 (1st commitment)	Japan: -6% EU: -8% Canada: -6% Russia, New Zealand: 0
HFC, PFC, SF ₆ (base year: 1995)		Norway: +1% Australia: +8% (USA: -7%)
[Basket System]		

and nitrous oxide, three fluorine compounds, hydrofluorocarbons (HFCs), perfluorocarbons (PFCs) and sulphur hexafluoride (SF₆) are included. The United States of America has not ratified the Kyoto Protocol, but with the endorsement of Russia, it came into force on 16 February 2005. The Japanese government established a “Guideline of Measures to Prevent Global Warming” in March 2002, and Japan signed the Kyoto Protocol in the same year in June. Under the guidance of the Ministry of Economy, Trade and Industry, Japanese industry has

adopted a voluntary action programme that is being evaluated annually by the Industrial Structure Council. As official measures, the government has enacted the “Electric Appliances Recycling Law” and the “CFC Recovery and Destruction Law” for the recovery and destruction of fluorinated greenhouse gases.

The UNEP strongly supports these global environment issues at the international level, and three assessment panels: the SAP, the Technology and Economic Assessment Panel (TEAP) and the Environmental Effects Assessment Panel (EEAP) are playing crucial roles in the implementation of the Montreal Protocol. For the Kyoto Protocol, the Inter-governmental Panel on Climate Change (IPCC) has offered the scientific basis for measures to reduce global warming.¹

From the year 2004 to 2005, scientists as well as technical experts from IPCC and TEAP have cooperated to produce a special report on safeguarding the ozone layer and the global climate system: issues related to HFCs and PFCs [4]. Setting 2015 as the target year, this report analyzes the effect of CFCs and their alternatives on the ozone layer and the climate system, and summarizes possible options for reduction of HFC and PFC emissions, offering solid guidance based on scientific evidence to policy makers [4].

1.1.3. Approaches to alternative CFCs

A wide variety of alternative CFCs has been investigated with the aim of protecting the ozone layer and reducing global warming. Research can be roughly divided into two approaches: development of alternative CFC compounds and development of non-fluorine compounds. Omitting a detailed description of the substitute compounds and of the related technologies here, it can be said that the basic concept or the development of alternative CFCs is the introduction of a hydrogen atom into the CFC molecule to reduce its atmospheric lifetime. Already several alternative CFCs, called hydrochlorofluorocarbon (HCFC), HFC and hydrofluoro-ether (HFE), which have hydrogen atoms introduced into the molecule, have been developed and have found practical use. On the other hand, for those uses where the characteristics of the CFC are not essential, technologies for the development of non-fluorine substitutes (not-in-kind) are being actively pursued. Hydrocarbons for use in aerosols, refrigerants and thermal insulators, natural refrigerants and hydrocarbon and water cleaning systems are examples of this substitution trend. The data regarding substitution of CFCs and halons in industrialized countries indicate that fluorine-based substitutes (HCFC, HFC, HFE) comprise 20% of the transition, and for the remaining 80% non-fluorine products are being used.

Although HFCs were considered to be the most suitable alternative product from the point of view of protection of the ozone layer, they are said to be a strong greenhouse gas and their use has to be controlled. This situation is a clear

¹ See the conclusions of the Montreal Intergovernmental Climate Conference (28 November–9 December 2005) on the United Nations Climate Change Conference website: <http://unfccc.int>.

pointer to the difficulties we encounter while trying to integrate the points of view of the government, the industry and the scientific community. To establish a sustainable society, it is necessary to develop new evaluation standards with a solid scientific base; this issue will be addressed in Section 4.4.

2. FLUOROCARBON-RELATED TECHNOLOGIES AND ENVIRONMENTAL PROBLEMS

2.1. Refrigerants

One of the most important applications of fluorocarbons is as refrigerants in air conditioning equipment for buildings and automobiles, and in refrigerators, coolers (heaters), large turbo cooler equipment, etc.

2.1.1. Demand for refrigerants

A refrigerant works according to the following principles. After the refrigerant is liquefied under pressure, it is adiabatically expanded and the liquid evaporates by taking heat from outside the system. This heat of vaporization translates into “air-conditioning” outside. The air-conditioning temperature is 0°C for domestic air conditioners, about –25°C for domestic refrigerators and about –35°C for warehouses of frozen products for commercial use. The compound selected as a refrigerant must have a boiling point below these temperatures after expansion under pressure.

In the case of heaters, the refrigerant evaporates initially, followed by condensation of the evaporated refrigerant, which means that the refrigerant returns to a liquid state releasing heat in the process, and this condensation heat is used for heating. In order to utilize this latent heat, it is advantageous to set this liquefaction temperature at a value lower than the critical temperature. In the case of air conditioners for domestic use, the critical temperature is set at above 70°C. Therefore, the importance of boiling point and critical temperature in the selection of the refrigerant is evident.

The refrigerant must also be a stable compound. This condition is required to avoid thermal or chemical decomposition inside the equipment. The refrigerant is selected after measuring the amount of compound decomposed in thermal stability tests carried out with metal samples and refrigerant machine oil (lubricant oil). Because the binding energy of carbon and fluorine is large, most fluorine compounds have high thermal stability. Currently, decomposition with production of hydrogen fluoride is tested.

Flammability of the refrigerant will be explained in Section 2.1.2. When the ratio of fluorine to carbon increases, the fluorine compound becomes non-flammable and is safe to use. However, when the fluorine conversion ratio is increased

greatly, its lifetime in the atmosphere becomes longer and the global-warming effect becomes larger. This balance is important.

Regarding the toxicity of the refrigerant, it is said that the amount of chlorine in the molecule raises the toxicity, but in general, toxicity is evaluated from the measurement for each component. The toxicity of a refrigerant [5] expressed as the acceptable level of concentration has been set at higher than 400 ppm by the American Society of Heating, Refrigerating and Air-Conditioning Engineers (ASHRAE), that is, a refrigerant whose exposure limit is higher than 400 ppm can be considered to have low toxicity.

2.1.2. Fluorine refrigerants and their alternatives

Table 3 shows the physical properties of fluorine refrigerants and their alternatives, that is, boiling point, critical temperature (T_c), flammability, exposure limit, ozone-depletion potential (ODP) and global-warming potential (GWP) for 100-year integration time horizon (ITH).

Before the enforcement of regulations for ozone-depletion compounds, CFC-11 (CCl_3F), CFC-12 (CCl_2F_2), HCFC-22 (CHClF_2) and the mixed refrigerant R-502 (HCFC-22/CFC-115 ($\text{CF}_3\text{CF}_2\text{Cl}$) = 48.8/51.2) were used.

CFC-11 and CFC-12 were widely used as ideal refrigerants because of their stability, low toxicity and non-flammability. However, due to their stability, they remain unmodified in the troposphere and are decomposed in the ozone layer of the stratosphere by high-energy ultraviolet rays (wavelength below 280 nm) where they have been connected to the depletion of the ozone layer.

From these facts, research has been devoted to developing an alternative refrigerant which has a short atmospheric lifetime without detrimenting its properties. One approach is the introduction of hydrogen atoms into the molecule to raise the compound's reactivity towards OH radicals as the reactivity with OH radicals is related to the stability of the molecule in the troposphere. Another approach is reduction of the number of chlorine atoms in the molecule, which are responsible for ozone layer depletion, particularly for a refrigerant with long atmospheric lifetime. Following these ideas, the molecular structure of the alternatives has hydrogen atoms which substitute chlorine and/or fluorine atoms in a CFC, and accordingly HFCs and HCFCs have been developed.

The HFCs developed are stable compounds. For example, for mixed HFC refrigerant containing HFC-32 (CH_2F_2), HFC-125 (CHF_2CF_3) and HFC-134a (CH_2FCF_3), the decomposition product, HF, in the refrigerant is less than 1 ppm, under conditions of coexistence with refrigerant machine oil (ester oil) or metal (iron, copper or aluminium) at 175°C for 2 months.

HFCs have a large infrared absorption and a strong greenhouse effect, but the newly developed HFCs can make efficient use of energy by reducing the emission of carbon dioxide which has long atmospheric lifetime. This is one of the deciding factors when compared with natural refrigerants.

Table 3. Properties of refrigerants

Refrigerant no.	Compounds and ratios ^a	Boiling point (°C)	T_c (°C)	Flammability	Exposure limits (ppm)	ODP ^b	GWP ^c (ITH = 100y)
R-11	CFC-11	24.0	198.1	None	1000	1	4600
R-12	CFC-12	-29.8	111.8	None	500	1	10600
R-22	HCFC-22	-40.8	96.5	None	1000	0.055	1700
R-502	CFC-115/HCFC-22 = 51.2/48.8	-45.6	82.2	None	1000	0.33	4500
Alternatives							
R-410A	HFC-32/HFC-125 = 50/50	-51.6	71.4	None	1000	0	2000
R-407C	HFC-32/HFC-125/HFC-134a = 23/25/52	-43.6	85.6	None	1000	0	1700
R-134a	HFC-134a	-26.2	101.1	None	1000	0	1300
R-404A	HFC-125/HFC-143a/HFC-134a = 44/52/4	-46.5	72	None	1000	0	3800
R-507	HFC-125/HFC-143a = 50/50	-46.7	70.9	None	1000	0	3900
	Ammonia	-33.3	132.3	Flammable	25	0	< 1
	Isobutane NH ₃ (CH ₃) ₂ CHCH ₃	-11.9	134.7	Flammable	800	0	< 0

^a For chemical formula of each compound, see “Acronyms and Abbreviations” at the beginning of this chapter.

^b ODP, ozone depletion potential.

^c GWP, global warming potential; ITH, integration time horizon.

The alternative HFC refrigerants are divided into flammable and non-flammable types. Of those used currently as refrigerants, HFC-125 and HFC-134a are non-flammable, and HFC-32, HFC-143a (CF₃CH₃) and HFC-152a (CHF₂CH₃) are flammable. HFC-152a has relatively high flammability, whereas HFC-32 has marginal flammability and is difficult to ignite.

There are also cases in which a refrigerant with marginal flammability is used in combination with non-flammable compounds to produce non-flammable refrigerant which has sufficient properties (see Table 3). One example is the mixed refrigerant of HFC-32, HFC-125 and HFC-134a, which is known as R-407C.

HCFC-123 (CF₃CHCl₂) includes a small amount of chlorine and thus has a depletion effect on the ozone layer. However, as it has a short atmospheric lifetime of 1.5 years, it is considered to be a compound with little effect on the depletion of the ozone layer and on global warming.

R-410A and R-407C are used in air conditioners, R-134a is used in car air conditioners and electric refrigerators, and R-404A and R-507 are used in freezers and showcases.

2.1.3. *Non-fluorine refrigerants*

Non-fluorine compounds are also used as refrigerants. Although the boiling point of carbon dioxide is low at -78°C, it can be used as a heating medium for a hot water supply. Ammonia, which has low flammability, is highly toxic (exposure limit of 25 ppm) and is used only as an industrial refrigerant. Hydrocarbon refrigerants such as propane and isobutane are used for refrigerators.

2.1.4. *Selection of refrigerants*

The contribution to global warming should be estimated by indices such as life cycle climate performance (LCCP), composite warming potential (CWP), total warming prediction graph (TWPG), etc. that is, a combination of the effect from the refrigerant and the energy consumed by the equipment that uses the refrigerant. These indices are explained in Sections 4.3, 4.4.1 and 4.4.2. The combination of the refrigerant and air-conditioning equipment should be selected based on scientific knowledge that optimizes energy-saving characteristic and safety.

2.2. **Blowing agents**

2.2.1. *Fluorocarbon blowing agents*

Foamed plastic insulation is used widely to maintain cold or heat. Because insulation can help reduce energy consumption, it can also help reduce carbon dioxide (CO₂) emissions, which is an integral part of preventing global warming.

Plastic foams include polyurethane foam, polyisocyanurate foam, phenol foam, polystyrene foam and polyethylene foam, and the main fluorocarbon blowing agents are used in producing rigid polyurethane foams and polyisocyanurate foams.

In polyurethane foams, the blowing agent is sealed in closed cells. Besides rigid polyurethane foams which have extremely high insulation capacity, there are flexible polyurethane foams which have a continuous open cell structure and do not have a blowing agent in the resin. Polyisocyanurate foams, which in the broad sense are rigid polyurethane foams, have heterocyclic triisocyanurate groups produced by the cyclotrimerization of the excess isocyanate groups. As a result, they are extremely non-flammable and used as fire-retardant construction material for buildings and other structures that require fire resistance.

Polyurethane foams are synthesized by mixing a compound liquid having polyol, blowing agent, catalyst, surfactant, flame retardant, etc. with liquid diisocyanate.

Unlike chemical blowing agents, which produce gases from chemical reactions, fluorocarbon blowing agents manifest functions as gaseous bodies and as such are classified as physical blowing agents.

CCl_3F (CFC-11), which is a first-generation fluorocarbon blowing agent, has excellent gas thermal conductivity, low odour, good chemical stability, non-flammability, low toxicity, solubility of polyols and mechanical intensity of the foamed body, so it was widely used as a blowing agent of rigid polyurethane foams. With regard to heat insulating properties, rigid polyurethane foams created with CFC-11 (gas thermal conductivity of $8.4 \text{ mW m}^{-1} \text{ K}^{-1}$ at 25°C) have about half of the thermal conductivity after blowing, and twice the insulation effect, as compared with rigid polyurethane foams blown by CO_2 ($16.4 \text{ mW m}^{-1} \text{ K}^{-1}$). In addition, CO_2 has a large diffusion coefficient for urethane resins, so exchanges can easily occur with air. In contrast, rigid polyurethane foams, which use a fluorocarbon blowing agents with small diffusion coefficients, can maintain their insulation capacity over a long period of time [6].

2.2.2. *The development of blowing agents that do not damage the ozone layer*

Among the advantages of rigid polyurethane foams over other types of foamed plastics are the former's low density, high mechanical strength and low thermal conductivity. As shown below, one of their most important factors is the gas thermal conductivity of the blowing agents. Thermal conductivity is generally expressed as a λ value (or a K factor: $\text{mW m}^{-1} \text{ K}^{-1}$). The thermal conductivity, λ_F , of rigid polyurethane foams is shown by the following equation [7]:

$$\lambda_F = \lambda_G + \lambda_S + \lambda_R + \lambda_C \quad (1)$$

where λ_G is the thermal conductivity of the blowing gas, λ_S the thermal conductivity of the solid phase, λ_R the thermal conductivity resulting from radiation

and λ_C the thermal conductivity caused by the convection of the gas (which can be ignored for minute bubbles). The largest contribution from among these values is made by λ_G . Therefore, the blowing agent which is desirable for substances is one that becomes gaseous easily and whose gas thermal conductivity is low.

Fluorocarbon blowing agents that were mainly used at normal temperature are the liquid blowing agent CFC-11 (boiling point 23.8°C) and the low boiling blowing agent CCl_2F_2 (CFC-12: boiling point -29.8°C). CFC blowing agents have extremely high stability in the atmosphere and chlorine atoms in their molecules, so they are considered to be strong ozone-depleting substances (ODSs) in the stratosphere. Their production and use have been prohibited since the Montreal Protocol of 1995.

In 1988, the worldwide sales of CFC-11, a blowing agent for rigid polyurethane foams used as insulation in buildings, refrigerators, etc., peaked at about 166,000 tonnes. As an alternative blowing agent to CFC-11, the HCFC blowing agent CCl_2FCH_3 (HCFC-141b) was developed. However, because its molecules contained chlorine, it still had some ODP issue, albeit slight, so it was considered to be a transitional substance. The worldwide sales of HCFC-141b for rigid polyurethane foams peaked in 2000 to about 125,000 tonnes.

Next, HFC blowing agents were investigated as alternatives to HCFC-141b. Two types, that is, $\text{CF}_3\text{CH}_2\text{CHF}_2$ (HFC-245fa: boiling point 15.3°C) [8] and $\text{CF}_3\text{CH}_2\text{CF}_2\text{CH}_3$ (HFC-365mfc: boiling point 40.2°C) [9] were selected because of their low environmental impact, toxicity and price, and high performance. The use of these materials began in Japan, Europe and the United States in 2003–2004.

As single products, neither HFC-245fa nor HFC-365mfc had sufficient properties to be used without modification as alternatives to HCFC-141b. Therefore, attempts were made to produce various mixtures [10] as shown in Table 4.

Table 5 shows the physical properties and environmental characteristics of CFC-11, HCFC-141b, HFC-245fa, HFC-365mfc and cyclopentane that are used as blowing agents at normal temperature.

However, since there is no ODP and GWP is small, hydrocarbon blowing agents are advantageous for preserving the stratospheric ozone layer and in measures for preventing global warming. Hydrocarbons such as cyclopentane, *n*-

Table 4. Blend ratios of HFC blowing agents

HFCs	Blend ratios (wt./wt.)
HFC-245fa/HFC-365mfc	80/20, 70/30, 50/50
HFC-365mfc/HFC-227ea ^a	94/6
HFC-365mfc/HFC-134a	93/7, etc.

^a HFC-227ea ($\text{CF}_3\text{CHFCF}_3$).

Table 5. Physical and environmental properties of blowing agents

Compounds	CFC-11	HCFC-141b	HFC-245fa	HFC-365mfc	Cyclopentane
Chemical formula	CCl ₃ F	CH ₃ CCl ₂ F	CF ₃ CH ₂ CHF ₂	CF ₃ CH ₂ CF ₂ CH ₃	(CH ₂) ₅
Molecular weight	137.4	116.9	134	148	70.1
Boiling point (°C)	23.8	32	15.3	40.2	49.3
Vapour pressure (MPa, 20°C)	0.0883	0.0647	0.1229	0.059	0.043 (25°C)
Heat of vaporization (kJ mol ⁻¹)	25	25.8	28	26.2	27.3
Liquid density (kg m ⁻³ , 25°C)	1.426	1.228	1.398 (5°C)	1.25	0.75
Gas phase thermal conductivity (mW m ⁻¹ K ⁻¹ , 25°C)	8.4	9.2	12.5	11.6	12.8
Flammable limits (vol.%)	None	7.6–17.7	None	3.8–13.3	1.4–8.0
ODP (CFC-11 = 1)	1	0.11	0	0	0
GWP (ITH = 100y)	4600	700	950	890	11
Atmospheric lifetime (y)	45	9.3	7.2	9.9	Few days

pentane and *i*-pentane are widely used in Europe and Japan in home refrigerators. Unfortunately, hydrocarbon blowing agents are extremely flammable and, near the surface of the ground they can cause photochemical smog as volatile organic compounds (VOCs). Therefore, it is necessary to take sufficient precautions to prevent leakage and maintain safety when using these compounds.

In 1987, use of CFC-12 reached a peak, with worldwide sales of about 60,000 tonnes. As a low boiling blowing agent, CFC-12 was used in froth foaming that was added to the polyol just before mixing with polyurethane foam, and in olefin foaming such as polyethylene and polystyrene. Agents that were developed as alternatives for CFC-12 included CHClF_2 (HCFC-22: boiling point -40.8°C) and CH_3CClF_2 (HCFC-142b: boiling point -9.8°C). The other HFC blowing agents developed for froth foaming were $\text{CF}_3\text{CH}_2\text{F}$ (HFC-134a: boiling point -26.2°C) and CHF_2CH_3 (HFC-152a : boiling point -24.7°C). HFC-134a and HFC-152a maintain stable foam shape at low temperatures, have excellent compressive strength, etc., so their use as blowing agents at normal temperature and as mixed agents with CO_2 (water) is increasing [11]. In the area of olefin foam, hydrocarbon blowing agents such as CO_2 and *i*-butane are coming into practical use.

In 2000, the biggest-selling blowing agent in the world was HCFC-142b, with sales of 41,000 tonnes. However, since then the use of HFC and hydrocarbon blowing agents has been increasing, and sales of HCFC-142b have gradually been decreasing.

2.2.3. Blowing agents by type of application

The main applications of rigid polyurethane foams include home and commercial refrigerators and freezers, sprays, continuous panels, discontinuous panels, blocks, pipes, boards, refrigerated trucks and water heaters [12].

Areas where HFC blowing agents are essential include home refrigerators and freezers (USA), and fields that require on-site blowing. In the Kyoto Protocol that was adopted in 1997, emissions of HFC blowing agents are regulated as global-warming substances. At the same time, they are somewhat more expensive than CFC, HCFC and hydrocarbon blowing agents, so the areas of their use have been shrinking.

In developed countries, HFC-245fa, HFC-134a or hydrocarbons are used as blowing agents for home refrigerators and freezers; in developing countries, HCFC-141b or hydrocarbons are used for this purpose. For European-type home refrigerators that use HFC-245fa or cyclopentane/*i*-pentane (70/30), it has been reported that the HFC-245fa refrigerators consume about 12% less energy than the cyclopentane refrigerators [13]. In the United States, there are strict energy and factory safety regulations, so HFC blowing agents, and not hydrocarbon agents, are used in home refrigerators and freezers.

For on-site blowing, HFC-245fa/HFC-365mfc, HFC-365mfc/ CF_3CHF_2 (HFC-227ea), HFC-245fa, etc., are used in developed countries, while HCFC-141b is used in developing countries. Since there is a risk of fire occurring during

the work at construction sites, it is difficult to use flammable agents for on-site blowing, and consequently there is strong demand for non-flammable agents. In block manufacturing, the centre of the block becomes hot due to exothermic reaction, and there is a risk of discolouration or even fire in extreme cases, so it would be preferable to use non-flammable fluorocarbon blowing agents for this purpose. In addition, it is difficult for small- and medium-sized enterprises to bear equipment costs and maintain work safety when making discontinuous panels [14] and integral skin foams [15], so it is also preferable for them to use non-flammable blowing agents.

2.2.4. Next-generation blowing agents and methods

New technologies that have appeared to replace HFC blowing include vacuum insulation, supercritical or subcritical carbon dioxide blowing [16] and hydrocarbon blowing. However, in fields such as on-site blowing (see above) which use non-flammable fluorocarbon blowing agents, it would be difficult to utilize these new technologies.

Vacuum insulation panels have been developed that use polyurethane, glass wool, etc., as filler materials, and these panels have been used sporadically in pipes and home refrigerators and freezers, but technical and economic issues hinder their utilization in insulating construction materials. Hydrocarbon blowing agents such as cyclopentane are extremely flammable, so they cannot be easily used in applications such as on-site blowing which loathe open flame.

Other additional blowing agents being investigated include dimethoxymethane [17] and *trans*-1,2-dichloroethene [18]. Supercritical or subcritical CO₂-assisted water blown foams are revolutionary new technologies but they impose a high burden on equipment because of their high-pressure blowing conditions. Moreover, because the blowing agent is CO₂, they are poor insulators, and the development of applications is lagging.

It has been proposed that fields requiring such fluorocarbon blowing agents use HFEs because of their relatively low GWP. Some HFEs that have been studied include CF₃CH₂OCHF₂ (HFE-245mf), CHF₂CF₂OCH₃ (HFE-254pc) and CHF₂CF₂OCHF₂ (HFE-236pc) [19], but they have issues regarding production costs, chemical stability, etc., which must be investigated at the practical level.

2.3. Solvents

2.3.1. Introduction

Production of ODSs such as the widely used solvents CFC-113 (CCl₂FCClF₂) and 1,1,1-trichloroethane, was banned in non-Article five countries by the Montreal Protocol in 1996. This measure triggered the development of diverse

technologies for alternatives to ODSs. These technologies include no-clean techniques and aqueous-cleaning as well as solvent-cleaning (including hydrocarbons, alcohols and new fluorinated solvents). This section summarizes recent technological trends in the development of fluorinated solvents.

2.3.2. *Physical properties and current application of alternative cleaning solvents*

2.3.2.1. HCFC cleaning solvent.

HCFCs most widely used as cleaning solvents are HCFC-123 (CF_3CHCl_2), HCFC-141b ($\text{CH}_3\text{CCl}_2\text{F}$), HCFC-225ca ($\text{CF}_3\text{CF}_2\text{CHCl}_2$) and HCFC-225cb ($\text{CClF}_2\text{CF}_2\text{CHClF}$). Table 6 shows a summary of their representative properties.

Although HCFC-141b is most widely used as a cleaning solvent worldwide, in Japan HCFC-225ca and HCFC-225cb are more popular. The properties and the effect on resins of HCFC-225ca and HCFC-225cb are similar to those of CFC-113, enabling them to be used in the CFC-113 cleaning system with little modification (Fig. 4).

2.3.2.2. HFC cleaning solvent.

HFC-365mfc ($\text{CF}_3\text{CH}_2\text{CF}_2\text{CH}_3$), HFC-c-447ef (1,1,2,2,3,3,4-heptafluorocyclopentane), HFC-43-10mee ($\text{CF}_3\text{CHFCHFCF}_2\text{CF}_3$) and HFC-52-13p ($\text{CF}_3(\text{CF}_2)_4\text{CHF}_2$) are the representative HFC solvents. Table 7 shows a summary of their representative properties.

As these HFCs do not contain any chlorine atom, they have very poor solvency. To improve solvency, combinations of these compounds with a surfactant or a second component have been developed. One example of this combination is an HFC and a chlorinated solvent such as *trans*-1,2-dichloroethene to form an azeotropic mixture. This can be used in an open-top-type three-sump vapour degreaser (Fig. 4).

However, in some countries such as Japan which have strict environmental regulations on the use of chlorinated solvents, this kind of mixture is very difficult to use and it is not possible just to substitute the solvent in the traditional vapour degreaser. In such countries, attention is being focused on low surface tension and fast drying properties of fluorinated solvents. As a result, new cleaning systems, in which aqueous cleaning or cleaning with hydrocarbon based solvents is followed by rinsing and drying with fluorinated solvents, have been proposed and put into practical use (Figs. 5 and 6).

2.3.2.3. HFE cleaning solvent.

HFE-449s-c ($\text{C}_4\text{F}_9\text{OCH}_3$), HFE-569sf-c ($\text{C}_4\text{F}_9\text{OCH}_2\text{CH}_3$), HFE-347pc-f ($\text{CHF}_2\text{CF}_2\text{OCH}_2\text{CF}_3$) are the most common HFE solvents. Table 8 summarizes the properties of these representative compounds.

Table 6. Physical properties of HCFCs

Compounds	CFC-113	HCFC-123	HCFC-141b	HCFC-225ca	HCFC-225cb
Chemical formula	$\text{CClF}_2\text{CCl}_2$	CF_3CHCl_2	$\text{CH}_3\text{CCl}_2\text{F}$	$\text{CF}_3\text{CF}_2\text{CHCl}_2$	$\text{CClF}_2\text{CF}_2\text{CHClF}$
Boiling point ($^{\circ}\text{C}$)	47.6	27.6	32.1	51.1	56.1
Freezing point ($^{\circ}\text{C}$)	-35	-107	-103.5	-94	-97
Density (g cm^{-3} , 25°C)	1.57	1.46	1.23	1.55	1.56
Viscosity (mP s , 25°C)	0.65	0.42	0.42	0.58	0.60
Surface tension (mN m^{-1} , 25°C)	17.3	15.5	18.4	15.8	16.7
Flash point ($^{\circ}\text{C}$)	None	None	None	None	None
ODP(CFC-11 = 1)	0.8	0.02	0.11	0.025	0.033
GWP (ITH = 100 y)	6000	120	700	180	620

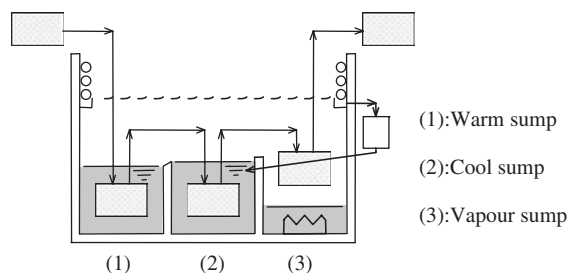


Fig. 4. Typical open-top-type three-sump vapour degreaser.

HFEs have ether oxygen in their molecules. However, the fluorine substitution of hydrogen on the α carbon of the ether decreases the basicity of the ether oxygen. Therefore, most of the HFE solvents have lost the properties as an ether solvent, and have very poor solvency compared with HFC solvents. On the other hand, the GWP values of these commercialized HFEs are smaller than those of commercialized HFCs, and the Kyoto Protocol does not classify them as regulated greenhouse gases.

2.3.3. Other applications of fluorinated compounds

The market volume of non-cleaning applications for HFCs and HFEs is very important. For example, a perfluoropolyether is used as a lubricant to avoid contact between the surface of a hard disc and its reading head, and HFC-43-10mee is used as a carrier solvent for lubricants, as a substitute for perfluorocarbon (PFC), which has a large GWP value.

Besides HFCs and HFEs, attention has also been focused on fluorinated alcohols. An alcohol containing a fluoralkyl group (R_F group) in the α position has an acidic hydroxyl proton based on the strong electron attractive effect of the R_F group, and it has a high affinity for ionic polar compounds. Taking advantage of these characteristics, fluorinated alcohols are widely used as carrier solvent for azo and cyanide dye compounds during the production of recordable optical media such as CD-R or DVD-R. Table 9 summarizes the physical properties of fluorinated alcohols as typical solvents. TFPO ($\text{CHF}_2\text{CF}_2\text{CH}_2\text{OH}$) and OFPO ($\text{CHF}_2(\text{CF}_2)_3\text{CH}_2\text{OH}$) shown in the table have been used as carrier solvents for dyes.

3. ENVIRONMENTAL ASSESSMENT OF CFC ALTERNATIVES

3.1. The importance of lifetime of CFC alternatives

With the objective of minimizing the depletion of the stratospheric ozone layer and reducing global warming, compounds that include the hydrogen atom in the

Table 7. Physical properties of HFCs

HFCs	HFC-365mfc	HFC-c-447ef	HFC-43-10mee	HFC-52-13p
Chemical structure	$\text{CF}_3\text{CH}_2\text{CF}_2\text{CH}_3$	$\begin{array}{c} \text{FHC}-\text{CH}_2 \\ \quad \backslash \\ \text{F}_2\text{C} \quad \text{CF}_2 \end{array}$	$\text{CF}_3\text{CF}_2\text{CHFCHF}_3$	$\text{CF}_3(\text{CF}_2)_4\text{CHF}_2$
Boiling point (°C)	40.2	82.5	55	70.8
Freezing point (°C)	-35	20.5	-80	-85
Density (g cm^{-3} , 25°C)	1.25	1.58	1.58	1.67
Viscosity (mP s, 25°C)	0.433 (20°C)	1.80	0.67	0.81
Surface tension (mN m^{-1} , 25°C)	15 (20°C)	20.3	14.1	13.4
Flash point (°C)	None	None	None	None
ODP (CFC-11 = 1)	0	0	0	0
GWP (ITH = 100 y)	890	250	1500	2000

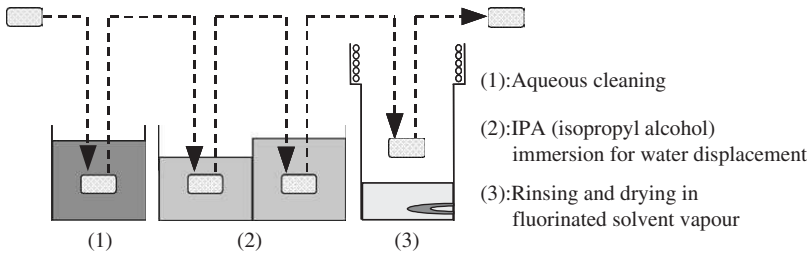


Fig. 5. Aqueous cleaning with rinsing and drying system.

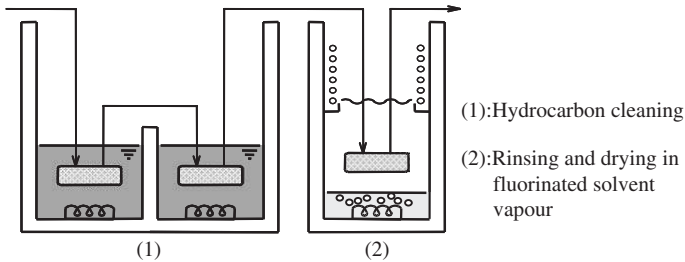


Fig. 6. Hydrocarbon cleaning with rinsing and drying system.

molecule have been developed and are already in use. Examples of these compounds are HCFCs such as HCFC-22 (CHF_2Cl), and HFCs such as HFC-134a ($\text{CF}_3\text{CH}_2\text{F}$). In addition, new compounds of HFEs such as HFE-143a (CH_3OCF_3) have also been developed [20].

As the main decomposition mechanism of compounds that include hydrogen atoms, such as HFCs, is the reaction with the OH radicals in the troposphere, it is possible to determine the atmospheric lifetime of a CFC alternative from its reaction rate with the OH radical. The atmospheric lifetime is a factor for establishing how long the compound remains in the atmosphere, which affects the compound’s greenhouse effect greatly. Therefore, to assess the environmental impact of compounds such as HFCs, it is indispensable to determine their rates of reaction with the OH radical. Measurement methods for the reaction rate with the OH radical can be roughly classified into two kinds: the absolute rate method and the relative rate method. The principles and main measuring techniques for both methods are introduced below.

3.1.1. Reaction rate measurement by the absolute rate method

In the absolute rate method, the reaction is carried out with OH radicals with a large excessive concentration of the target compound such as an HFC, and the

Table 8. Physical properties of HFEs

HFEs	HFE-449s-c (HF-7100 ^a)	HFE-569sf-c (HFE-7200 ^a)	HFE-347pc-f
Chemical formula	C ₄ F ₉ OCH ₃ ^b	C ₄ F ₉ OCH ₂ CH ₃ ^b	CF ₃ CH ₂ OCF ₂ CHF ₂
Boiling point (°C)	61	76	56.2
Freezing point (°C)	-135	-138	-85.9
Density (g cm ⁻³ , 25°C)	1.52	1.43	1.48
Viscosity (mP s, 25°C)	0.58	0.57	0.68
Surface tension (mN m ⁻¹ , 25°C)	13.6	13.6	16.2
Flash point (°C)	None	None	None
ODP (CFC-11 = 1)	0	0	0
FWP (ITH = 100y)	390	55	870

^a Notation in 3M company.

^b *n*-C₄F₉ and *i*-C₄F₉ mixture.

Table 9. Physical properties of fluorinated alcohols

Fluorinated alcohols	PFPO	HFIP	TFPO	OFPO
Chemical formula	CF ₃ CF ₂ CH ₂ OH	(CF ₃) ₂ CHOH	CHF ₂ CF ₂ CH ₂ OH	CHF ₂ (CF ₂) ₃ CH ₂ OH
Boiling point (°C)	80.7	58.6	108	140
Freezing point (°C)	-43	-3.3	-15	< -50
Density (g cm ⁻³)	1.51 (23°C)	1.60 (25°C)	1.48 (20°C)	1.66 (20°C)
Viscosity (mP s)	3.84 (23°C)	1.79 (23°C)	5.48 (23°C)	11.6 (25°C)
Surface tension (mN m ⁻¹)	17.7 (23°C)	16.5 (23°C)	26.6 (25°C)	24.2 (25°C)
Flash point (°C)	None	None	47.5	75.6
ODP (CFC-11 = 1)	0	0	0	0
GWP (ITH = 100 y)	40	190	—	—

reaction rate constant is obtained from the concentration decrease of OH radical during the course of the reaction. The reaction in the system proceeds as follows:



Equation (3) represents the decrease of OH radical due to diffusion, heterogeneous reactions taking place at the wall of the reactor, and with trace amounts of impurities contained in the carrier gas. In the absolute rate method, to ignore the effect of the reaction of OH radical with reaction products, it is necessary to set the initial concentration of OH radical below about 10^{11} molecule cm^{-3} . On the other hand, because the concentration of target compound such as HFC is of the order of 10^{14} – 10^{16} molecule cm^{-3} , pseudo first-order conditions are established, and the changes in HFC concentration during the reaction can be ignored. From equations (2) and (3), the change in OH radical concentration can be expressed as follows:

$$\ln \frac{[\text{OH}]_t}{[\text{OH}]_0} = -(k_1[\text{HFC}]_0 + k_2)t = -k't \quad (4)$$

where, k_1 and k_2 are the reaction rate constants of equations (2) and (3), respectively. $[\text{OH}]_0$ and $[\text{HFC}]_0$ in equation (4) represent the initial concentrations of OH and HFC, and $[\text{OH}]_t$ means the OH concentration at time t of the reaction. The units are as follows: the rate constants k_1 and k_2 are $\text{cm}^3 \text{ molecule}^{-1} \text{ s}^{-1}$, the concentrations of HFC and OH are molecule cm^{-3} , the reaction time, t , in s, and the pseudo first-order rate constant, k' , in s^{-1} . Here, k' can be expressed as follows:

$$k' = k_1[\text{HFC}]_0 + k_2 \quad (5)$$

Using equations (4), the pseudo first-order rate constant, k' , can be obtained using the logarithm of the ratio of OH concentration at a time t against the initial concentration of OH. Then using equation (5), the reaction rate constant, k_1 , can be obtained from the relationship between k' values and $[\text{HFC}]_0$ values for various concentrations. With the absolute rate method, calibration of the OH concentration is not necessary because the absolute value of the reaction rate constant can be obtained from the OH concentration at a time t against the initial concentration of OH, removing the error that would be introduced by calibration of the OH concentration. On the other hand, if reactive impurities such as unsaturated compounds are contained in the target compound of HFC, the reaction of OH with the impurities causes a decrease in the OH concentration. As a result, the measured value is overestimated. Therefore, during measurement with the absolute rate method, it is necessary to use high purity samples to avoid the influence of reactive impurities.

The most frequently used methods for production of OH radicals are flash photolysis, laser photolysis and discharge flow methods. In the flash photolysis method, the pulsed light of a Xe flash lamp causes direct decomposition of H_2O producing OH radicals [21–28]. Laser photolysis methods are illustrated by some examples: a 193-nm ArF excimer laser causes decomposition of N_2O to produce $\text{O}(^1\text{D})$ which is used in the reaction, $\text{O}(^1\text{D}) + \text{H}_2\text{O} \rightarrow 2\text{OH}$ [22,23,29]. A 248-nm KrF excimer laser decomposes H_2O_2 to produce OH radicals [23,25,29], and in another case, a 248-nm KrF excimer laser causes decomposition of HNO_3 to produce OH radicals [25,31], and a third harmonic of Nd:YAG laser (355 nm) causes decomposition of HONO and produces OH [24]. The discharge flow method uses a narrow reaction tube with an internal diameter of several centimetres and a length of approximately 1 m. On the upstream side, microwave discharge on H_2 to produce H atoms used for the reaction $\text{H} + \text{NO}_2 \rightarrow \text{OH} + \text{NO}$ [22,24,25,32–35] produces OH radicals. Pulse radiolysis [35] is also used to produce OH radicals.

To ignore the effect of side reactions, a low concentration of OH radical must be maintained, which means that the methods for detecting the OH radical must be highly sensitive. The laser-induced fluorescence method [22–25,30–32], the resonance fluorescence method [21,28,33], and the laser magnetic resonance method [24,25,34] are often used for this purpose. Compared with these methods, the sensitivity of the absorption method [26–28] is a little lower. For measurement with the absolute rate method, the measurement is carried out under slow flow condition to prevent accumulation of reaction and photofragmentation of the products.

As an example of measurement of reaction rate by the absolute rate method, Fig. 7 shows a schematic of the equipment for flash photolysis-laser-induced fluorescence method used by Tokuhashi *et al.* [22,23]. The gas mixture of the target compound/ $\text{H}_2\text{O}/\text{Ar}$ flows continually into the reactor. OH radicals are pro-

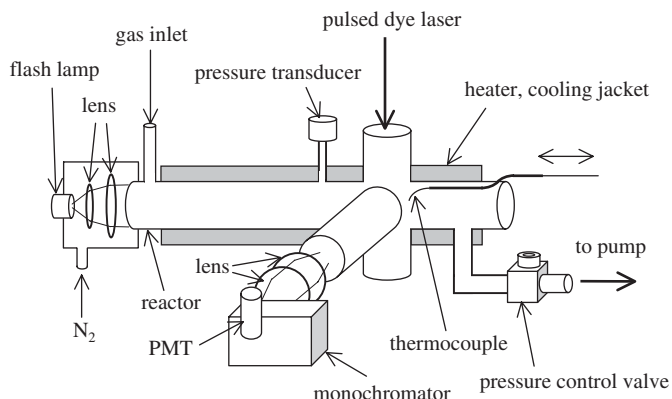


Fig. 7. Absolute rate method reaction equipment [22,23].

duced by direct photolysis of H₂O using the Xe flash lamp ($\lambda \geq 180$ nm). The concentration decrease in OH radical following the reaction with an HFC is measured by laser-induced fluorescence. In this method, the reaction time is defined by the interval between photolysis light and excitation light.

3.1.2. Reaction rate measurement by the relative rate method

For the relative rate method, the reaction with the target compound such as an HFC takes place simultaneously with a reaction with a reference compound which has a known reaction rate. The reactions in the system proceed as follows:



In these reactions, the concentrations of both the HFC and the reference compound decreases. The reaction rate constants k_{HFC} and k_{ref} for equations (6) and (7) can be expressed as follows:

$$\ln \frac{[\text{HFC}]_0}{[\text{HFC}]_t} = \frac{k_{\text{HFC}}}{k_{\text{ref}}} \cdot \ln \frac{[\text{Ref}]_0}{[\text{Ref}]_t} \quad (8)$$

In equation (8), $[\text{HFC}]_0$ and $[\text{Ref}]_0$ correspond to the initial concentrations of HFC and of the reference compound, whereas $[\text{HFC}]_t$ and $[\text{Ref}]_t$ correspond to the concentrations at a given time, t . According to equation (8), the plot of $\ln([\text{Ref}]_0/[\text{Ref}]_t)$ versus $\ln([\text{HFC}]_0/[\text{HFC}]_t)$ gives a straight line, and the slope of the plot allows determination of $k_{\text{HFC}}/k_{\text{ref}}$. The reaction rate constant of HFC with OH radical, k_{HFC} , is obtained using the known reaction rate constant, k_{ref} . In the relative rate method, since $k_{\text{HFC}}/k_{\text{ref}}$ can be obtained from the concentration changes of HFC and of the reference compound, in principle it is not affected by the reactive impurities contained in HFC. On the other hand, as $k_{\text{HFC}}/k_{\text{ref}}$ and k_{ref} contain individual errors, the reaction rate constant calculated for HFC, k_{HFC} , includes the accumulated error from these values, and its precision is lower than that for the absolute rate method. Moreover, because $k_{\text{HFC}}/k_{\text{ref}}$ is obtained from the changes in the concentrations of HFC and of the reference compound, the results might be affected by reactions between chemical compounds in the reactor, heterogeneous reactions at the walls of the reactor and photolysis of HFC or the reference compound.

For the relative rate method, the main sources of the OH radical are (1) the reaction $\text{O}(^1\text{D}) + \text{H}_2\text{O} \rightarrow 2\text{OH}$ [26–40], where $\text{O}(^1\text{D})$ is produced by photolysis of O_3 ; (2) direct photolysis of H_2O [38] by an optical source of short wavelength; and (3) the reactions $\text{CH}_3\text{O} + \text{O}_2 \rightarrow \text{CH}_2\text{O} + \text{HO}_2$ and $\text{HO}_2 + \text{NO} \rightarrow \text{OH} + \text{NO}_2$ [41], where CH_3O and NO originate from photolysis of CH_3ONO . Depending on the reaction involved, the changes in concentrations of HFC and the reference compound are measured using FT-IR [36–41] or gas chromatography [36–38]. The

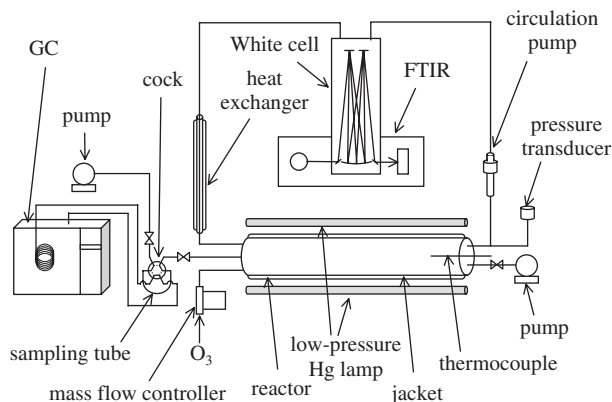


Fig. 8. Relative rate method reaction equipment [36].

sampling for the measurement of concentration using gas chromatography causes change in the pressure of the system, making it necessary to make adjustments. Except for the case of production of OH by direct photolysis of H₂O, the relative rate method is applied under conditions of low OH concentration, below 10⁹ molecule cm⁻³. At this concentration, since the changes of the concentrations of HFC and the reference compound are small, a very long time is required for the measurement, and this causes a negative effect on the precision of the measurement. However, it has recently been reported that it is possible to carry out the measurement at a fixed concentration of the order of 10¹⁰ molecules cm⁻³ of OH using a continuous supply of O₃ in the presence of H₂O.

Fig. 8 shows a schematic of the equipment used by Chen *et al.* [36] for the measurement of reaction rates with the relative rate method. The reactor is filled with the target compound/reference compound/O₃/H₂O/He under a pressure of several hundred Torr. A low-pressure mercury lamp set around the reactor is used for photolysis of O₃ to generate O(¹D) for the O(¹D) + H₂O → 2OH reaction that produces OH radicals. The target compound and the reference compound react with the OH radicals simultaneously and the concentrations of both the compounds are measured by gas chromatography or FT-IR.

3.1.3. Atmospheric lifetime of CFC alternatives

The atmospheric lifetime of compounds such as HFCs can be estimated from the reaction with OH radicals according to the following equation:

$$\tau_{\text{HFC}} = \frac{k_{\text{MC},272\text{K}}}{k_{\text{HFC},272\text{K}}} \cdot \tau_{\text{MC}} \quad (9)$$

where MC refers to methyl chloroform (CH₃CCl₃), τ_{HFC} and τ_{MC} correspond to the atmospheric lifetimes of HFC and MC (τ_{MC} = 6.0 years) [42], respectively,

Table 10. Reaction rate constants [43] and atmospheric lifetimes for main CFC alternatives

Compounds	Chemical formula	$k_{272\text{ K}}$ ($\text{cm}^3 \text{ molecule}^{-1} \text{ s}^{-1}$)	Lifetime (y)
HFC-32	CH_2F_2	6.9×10^{-15}	5.3
HFC-125	CF_3CHF_2	1.2×10^{-15}	31.1
HFC-134a	CH_2FCF_3	2.6×10^{-15}	13.8
HFC-143a	CH_3CF_3	6.8×10^{-16}	53.1
HFC-152a	CH_3CHF_2	2.5×10^{-14}	1.5
HFC-227ea	$\text{CF}_3\text{CHFCF}_3$	1.0×10^{-15}	36.2
HFC-245fa	$\text{CHF}_2\text{CH}_2\text{CF}_3$	4.6×10^{-15}	7.9
HCFC-22	CHClF_2	2.9×10^{-15}	12.3
HCFC-123	CF_3CHCl_2	2.8×10^{-14}	1.3
HCFC-141b	$\text{CH}_3\text{CCl}_2\text{F}$	3.5×10^{-15}	10.4
HCFC-225ca	$\text{CF}_3\text{CF}_2\text{CHCl}_2$	1.9×10^{-14}	2.0
HCFC-225cb	$\text{CClF}_2\text{CF}_2\text{CHClF}$	6.0×10^{-15}	6.0
HFE-143a	CH_3OCF_3	7.3×10^{-15}	5.0
HFE-245cb2	$\text{CF}_3\text{CF}_2\text{OCH}_3$	7.1×10^{-15}	5.1
HFE-254cb2	$\text{CHF}_2\text{CF}_2\text{OCH}_3$	1.4×10^{-14}	2.5
HFE-347mcc3	$\text{CF}_3\text{CF}_2\text{CF}_2\text{OCH}_3$	7.0×10^{-15}	5.1

and $k_{\text{HFC},272\text{ K}}$ and $k_{\text{MC},272\text{ K}}$ correspond to the reaction rate constants of HFC or MC with the OH radical at 272 K ($k_{\text{MC},272\text{ K}} = 6.0 \times 10^{-15} \text{ cm}^3 \text{ molecule}^{-1} \text{ s}^{-1}$) [43]. Table 10 presents the atmospheric lifetimes and rate constants for reactions with the OH radical for the main chemical compounds at 272 K. The atmospheric lifetimes for HFCs, HCFCs and HFEs are shorter than 50 years, and most of the compounds have an atmospheric lifetime of 10 years or less, which indicates that these compounds are removed from the atmosphere in a relatively short span of time.

3.2. Ozone-depletion potential

The depletion of the stratospheric ozone layer is caused by the catalytic reaction of chlorine released from compounds such as CFCs. The ODP is the index used to give a numerical value to the influence of various substances on this kind of reaction in the ozone layer. As is shown below, it is very simple to determine the ODP for a compound x.

$$\text{ODP}_x = \frac{\text{Total amount of depleted ozone due to x}}{\text{Total amount of depleted ozone due to CFC-11}} \quad (10)$$

However, because the mechanism of depletion of the ozone layer is complicated, the actual calculation is not so easy. It is impossible to express in a simple formula the complicated photochemical reaction processes, the heterogeneous reaction processes taking place on the surface of polar stratospheric clouds (PSCs), or the dynamical transport processes related to the polar vortex. Therefore, generally, calculation of the ODP is carried out using a two- or three-dimensional chemical transport model (CTM), which includes the photochemical reaction processes, dynamic processes and radiative processes.

Using a CTM, the evaluation of a compound, x , is carried out by measuring changes in the amount of ozone in the stratosphere. This amount of ozone destroyed is assumed to be the difference between the amount before the release of the compound from the ground and the amount after its release. The same calculation is carried out for the reference substance, CFC-11, and the effect on depletion of the ozone layer of compound x is compared to that of CFC-11. This ratio becomes the ODP index for compound x . Fig. 9 shows a schematic of this calculation. This index is relative to CFC-11; the ODP of a substance with a depletion effect on the ozone layer equivalent to that of CFC-11 will be 1. There are cases when the calculation regarding changes in the ozone layer is carried out after the instantaneous release from the ground of a given substance. But as the amount of ozone and the photochemical reactions in the stratosphere are seasonally dependent, and the substances from the ground are continuously discharged at a constant flux, this loss of ozone can generally be

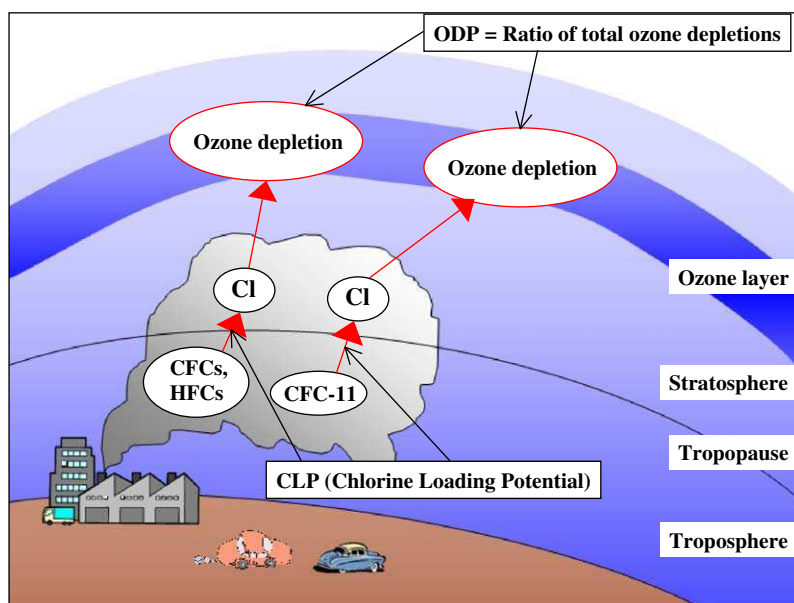


Fig. 9. Schematic of ozone-depletion potential (ODP) calculation.

used for calculation of ODP when the ozone-depletion process becomes stable. As the results from the model calculation are in a steady state, this ODP is called steady-state ODP.

However, as was explained earlier, this CTM-based method can be applied only to the groups which have CTM, and the results may vary according to the model used, so it was necessary to introduce a simpler index based on easier calculations. One of these indexes is the chlorine loading potential (CLP). The calculation of this index assumes that the depletion of the stratospheric ozone is proportional to the amount of chlorine released into the stratosphere, and uses the amount of substances which include chlorine flowing from the troposphere into the stratosphere as indices. The following equation is used:

$$\text{CLP} = \frac{\text{Cl(tropo) for compound } x}{\text{Cl(tropo) for CFC-11}} = \frac{\tau_x}{\tau_{\text{CFC-11}}} \cdot \frac{M_{\text{CFC-11}}}{M_x} \cdot \frac{n_x}{3} \quad (11)$$

where Cl is the total amount of chlorine transported from the troposphere to the stratosphere (molecule), τ_x the tropospheric lifetime of compound x (year), $\tau_{\text{CFC-11}}$ the tropospheric lifetime of CFC-11 (year), M_x the molecular weight of compound x , $M_{\text{CFC-11}}$ the molecular weight of CFC-11, n_x the number of chlorine atoms per molecule in compound x and 3 the number of chlorine atoms per molecule in CFC-11.

It is assumed that, for a given compound released from the Earth's surface, the amount that flows into the stratosphere is proportional to the lifetime of this compound in the troposphere. In other words, it is assumed that compounds with a short lifetime decompose in the troposphere before reaching the stratosphere. Fig. 9 also shows a schematic of the CLP. In this definition, the number of chlorine atoms arriving at the stratosphere is standardized by dividing the mass of the compound by its molecular weight and multiplying by the number of chlorine atoms per molecule. In contrast to the steady-state ODP, which deals with the CTM as a black box, calculation of CLP is straightforward once the value of the troposphere lifetime is determined. However, as this troposphere lifetime value is calculated using a CTM, some model dependency remains. For the relative comparison of compounds that do not decompose in the troposphere such as CFCs, comparison of the number of chlorine atoms in the molecule is the easiest index to use. Similar to chlorine, bromine also causes depletion of the ozone layer in the stratosphere and the bromine loading potential (BLP) is calculated using a similar equation.

In the case of CLP, the evaluation of the compounds loaded into the stratosphere assumes complete decomposition of these compounds, and that all the chlorine atoms are discharged into the stratosphere and contribute to the depletion of the ozone layer. Actually not all the amount of chlorine included in the compounds loaded into the stratosphere is released; one portion is removed midway or changes into other compounds before having any effect on the

depletion of the ozone layer. Taking this fact into account, an index that also takes into account the decomposition ratio of the substance has been proposed. First, if μ_{enter} is the amount of a compound loaded into the stratosphere from the troposphere, and $\mu_{\theta,z}$ is the concentration at latitude θ and altitude z , the amount of substance decomposed by reaching this place is the difference $(\mu_{\text{enter}} - \mu_{\theta,z})$. The fractional amount of chlorine $\text{FC}_{\text{release}}$ is defined as the ratio of the decomposed substance to the total amount of substance loaded.

$$\text{FC}_{\text{release}} = \frac{\mu_{\text{enter}} - \mu_{\theta,z}}{\mu_{\text{enter}}} \quad (12)$$

Usually, the compounds enter the stratosphere from the troposphere at low latitudes, near the equator, and spread towards high latitude regions, decomposing and, gradually releasing chlorine atoms. Therefore, $\text{FC}_{\text{release}}$ is expressed as a function of latitude and altitude. Using this $\text{FC}_{\text{release}}$, as well as the CLP already described, we will now define the relative stratospheric chlorine release, $\text{Cl}_{\text{release}}$:

$$\text{Cl}_{\text{release}} = \frac{\text{FC}_{\text{release}}(x)}{\text{FC}_{\text{release}}\text{CFC-11}} \cdot \text{CLP} \quad (13)$$

CLP represents the ratio of a given compound x released from the ground that is loaded into the stratosphere. $\text{FC}_{\text{release}}$ shows the extent of decomposition of the compounds entering the stratosphere and the proportion of chlorine released. As $\text{Cl}_{\text{release}}$ represents the number of chlorine atoms causing depletion of the stratospheric ozone layer, the value of $\text{Cl}_{\text{release}}$ can be regarded as ODP in the region where the catalytic reaction of the chlorine is dominant to the dynamical transport.

To calculate the relative stratospheric chlorine release $\text{Cl}_{\text{release}}$, it is necessary to calculate $\text{FC}_{\text{release}}$. However, this value has to be determined after complicated photochemical reactions have taken place in the stratosphere, which cannot be represented in a simple equation. Solomon [44] proposed a method in which ODP/CLP ratios corresponding to $\text{FC}_{\text{release}}$ are calculated based on observed data and these values are used for calculation of ODP. The ODP calculated from this method is called the semi-empirical ODP. Table 11 shows values of the model-derived ODP and the semi-empirical ODP.

The instantaneous ozone loss (IOL) is defined as the ozone loss after a time t following the instantaneous release of a substance that flows into the stratosphere. It can be understood from this definition that this quantity is directly related to $\text{FC}_{\text{release}}$. In general, it is assumed that the amount of substance with the lifetime, τ , decreases exponentially in the stratosphere, and the amount of ozone depletion is proportional to the amount of this substance decomposed.

The time integration value of this IOL, that is the amount of ozone destroyed after this substance flows into the stratosphere, is called the time-dependent ODP, and is a function of time, t , elapsed since the substance was loaded into the

Table 11. Examples of model-derived ODP and semi-empirical ODP

Compounds	Chemical formula	Model-derived ODP	Semi-empirical ODP
CFC-11	CCl ₃ F	1.0	1.0
CFC-12	CCl ₂ F ₂	0.82	0.9
CFC-113	CCl ₂ FCClF ₂	0.90	0.9
CFC-114	CClF ₂ CClF ₂	0.85	
CFC-115	CF ₃ CClF ₂	0.40	
Carbon tetrachloride	CCl ₄	1.20	
Methyl chloroform	CH ₃ CCl ₃	0.12	0.12
HCFC-22	CHClF ₂	0.04	0.05
HCFC-123	CF ₃ CHCl ₂	0.014	0.02
HCFC-124	CF ₃ CHClF	0.03	
HCFC-141b	CH ₃ CCl ₂ F	0.10	0.1
HCFC-142b	CH ₃ CClF ₂	0.05	0.066
HCFC-225ca	CF ₃ CF ₂ CHCl ₂	0.02	0.025
HCFC-225cb	CClF ₂ CF ₂ CHClF	0.02	0.03
HFC-134a	CH ₂ FCF ₃	< 1.5 × 10 ⁻⁵	< 5 × 10 ⁻⁴
HFC-23	CHF ₃	< 4 × 10 ⁻⁴	
HFC-125	CHF ₂ CF ₃	< 3 × 10 ⁻⁵	
Methylbromide	CH ₃ Br	0.64	0.57
Halon-1301	CF ₃ Br	12	13
Halon-1211	CF ₂ ClBr	5.1	5
Trifluoroiodomethane	CF ₃ I		< 0.008
Methylchloride	CH ₃ Cl	0.02	

stratosphere.

$$\text{ODP}_x(t) = \frac{F_x}{F_{\text{CFC11}}} \cdot \frac{M_{\text{CFC11}}}{M_x} \cdot \frac{n_x}{3} \cdot \alpha \cdot \frac{\int_{t_s}^t \exp[-(t-t_s)/\tau_x] dt}{\int_{t_s}^t \exp[-(t-t_s)/\tau_{\text{CFC11}}] dt} \quad (14)$$

Here, F_x is the fraction of compound x that is injected into the stratosphere, M_x the molecular weight of compound x , t_s the time required for a molecule to be transported from the surface to the region of the stratosphere in question (year) and α the enhanced efficiency of Br or I atoms for ozone loss compared to Cl ($\alpha = 40$ for Br and $\alpha = 2000$ for I).

When the time-dependent ODP is integrated to an infinite time, it becomes the steady-state ODP (Fig. 10(a) and (b)).

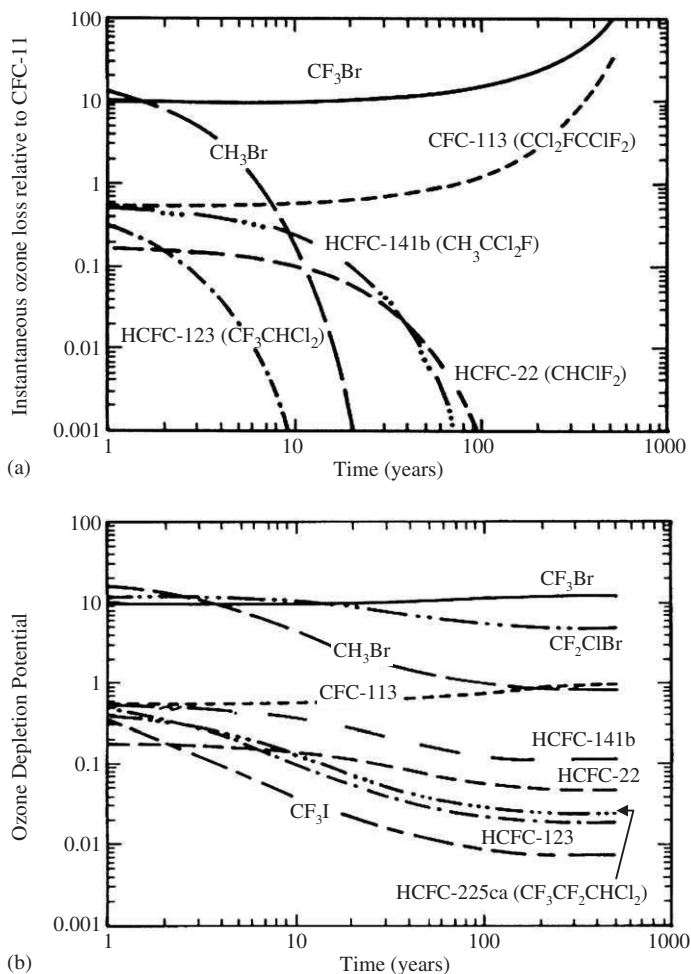


Fig. 10. (a) Examples of instantaneous ozone loss (IOL). (b) Examples of time-dependent ODP.

3.3. Global-warming potential

Similar to the concept of ODP as an index for the degradation of the ozone layer, another index was proposed: the GWP, that is a measure of the contribution to global warming of a compound released into the atmosphere. In contrast to ODP where the main compounds under evaluation are those containing chlorine or bromine, in the case of GWP, the compounds under calculation are those that

absorb infrared radiation and cause a greenhouse effect. GWP is defined by

$$GWP_x(ITH) = \frac{\int_0^{ITH} R_x(t) C_x(t) dt}{\int_0^{ITH} R_{CO_2}(t) C_{CO_2}(t) dt} \tag{15}$$

where $R(t)$ is the instantaneous radiative forcing at time t from a pulse release of the compound, $C(t)$ the concentration of the compound at time t (ppbv) and ITH the integration time horizon (year).

The subscripts correspond to compound x and to CO_2 .

As can be observed from the above equation, GWP is a relative value that uses CO_2 as the reference substance. When the absolute climatic impacts of the substance are under discussion, the absolute GWP (AGWP), which is the numerator of the formula, is used. In some cases, CFC11 is used as the standard and such a GWP is called halocarbon global-warming potential (HGWP).

Instantaneous radiative forcing for a substance is defined as the difference in radiation flux in the tropopause. The difference is measured between the time when the substance is present in the atmosphere and the time when it is not present, and is usually expressed in units of $Wm^{-2}ppmv^{-1}$. Fig. 11 shows the schematic of GWP calculation. This quantity is related to the strength of infrared absorption of the substance: the higher the concentration, the higher the forcing. However, if the absorption band of the substance overlaps other components of the atmosphere, especially the absorption band of water vapour, even if the substance has a strong absorption, its forcing is not large because of the sat-

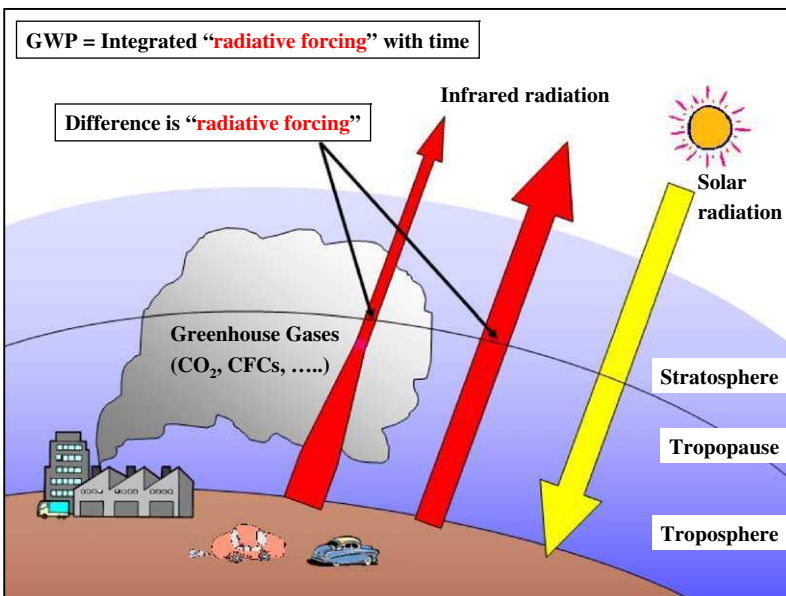


Fig. 11. Schematic of global-warming potential (GWP) calculation.

uration of water vapour absorption. Thus water vapour blocks the effect of a new substance on the radiation field.

There are two methods for calculating instantaneous radiative forcing. One is to use a determined atmospheric model, and the other is to use a two- or three-dimensional model, which calculates the radiative transfer by latitude and area and determines a global average. In any of the models, the vertical distribution of the concentration of target substance must be known in order to calculate the instantaneous radiative forcing. The mixing ratio is assumed to be homogeneous because the substance is thoroughly mixed in the troposphere. On the other hand, the concentration distribution in the stratosphere is calculated based on the decomposition rate, which is frequently obtained from the photochemical reaction model.

Once the vertical distribution of the concentration of the target substance and other atmosphere components, as well as of temperature, is established, the instantaneous radiative forcing of the substance can be calculated. However, in the troposphere, when the radiative forcing is added, it takes more than a few years before the next equilibrium condition is reached, whereas in the stratosphere this radiative equilibrium is reached in a few months. Therefore, to calculate the instantaneous radiative forcing, the vertical distribution of the temperature, not at the initial conditions but after radiative equilibrium is reached, is used in the stratosphere. This instantaneous radiative forcing is called adjusted radiative forcing.

From the method described above, radiative forcing for CO_2 : $R_{\text{CO}_2}(t)$ can be calculated, but because a high concentration of CO_2 already exists in the atmosphere, it is necessary to calculate radiative forcing for minute changes of CO_2 , and therefore, the accuracy in measurement is comparatively low. The dependence on the model becomes strong and the results differ between different researchers. IPCC (1995) [45] and World Meteorological Organization (WMO) (1998) [46] recommend the use of a conversion equation to unify the values of $R_{\text{CO}_2}(t)$.

Another important term in equation (15) is the time change of concentration after discharge of the substance $C(t)$. The concentration in the atmosphere is characterized by lifetime in atmosphere, τ , which is determined by the decomposition reactions and removal processes of the substance. Using this atmospheric lifetime, the time change of the concentration of the substance in the atmosphere can be expressed as $C(t) = C(t=0) \exp(-t/\tau)$. In general, the decomposition and removal processes of the CFC alternatives take place by reaction with OH radicals, photodissociation caused by ultraviolet radiation, ocean uptake, etc. For example, if the atmospheric lifetimes determined by these reactions are called τ_{OH} , τ_{UV} and τ_{w} , the actual atmospheric lifetime, τ , can be calculated from $1/\tau = 1/\tau_{\text{OH}} + 1/\tau_{\text{UV}} + 1/\tau_{\text{w}}$, when these reactions occur simultaneously.

Because of the time dependence of the CO₂ concentration, the denominator of equation (15) cannot be expressed as a simple exponential function. This is because the process of removal of CO₂ from the atmosphere is very complicated. CO₂ is absorbed differently according to the vegetation, the oceanic surface and the ocean depth, and its atmospheric lifetime extends from a few years to a thousand and a few hundred years. To estimate the lifetime of CO₂, it is necessary to use a very complicated carbon cycle model, but this has been developed in only a few institutions, and the results of the calculations differ greatly. Similar to radiative forcing, IPCC (1995) [45] and WMO (1998) [46] have recommended a simple arithmetic expression to apply to time changes in CO₂ concentration.

Thus $R(t)$ and $C(t)$ in equation (15) can be calculated as described above.

Here, it is possible to calculate $R(t)$ without integral calculus if it is a time-independent uniform process. This hypothesis is almost exact unless the substance concentration undergoes extreme change in the system. Integral calculus of the numerator becomes integration $C(t)$ with respect to t ,

$$\begin{aligned} \int_0^{\text{ITH}} C_x(t) dt &= C_x(0) \int_0^{\text{ITH}} \exp(-t/\tau_x) dt \\ &= C_x(0)\tau_x [1 - \exp(-\text{ITH}/\tau_x)] \end{aligned} \quad (16)$$

and can be expressed as

$$\text{GWP}_x(\text{ITH}) = \frac{R_x C_x(t=0) \tau_x [1 - \exp(-\text{ITH}/\tau_x)]}{C_{\text{CO}_2}(t=0) \text{AGWP}_{\text{CO}_2}(\text{ITH})} \quad (17)$$

The denominator of $\text{AGWP}_{\text{CO}_2}$, as mentioned above, can be calculated following the equation recommended by IPCC and WMO.

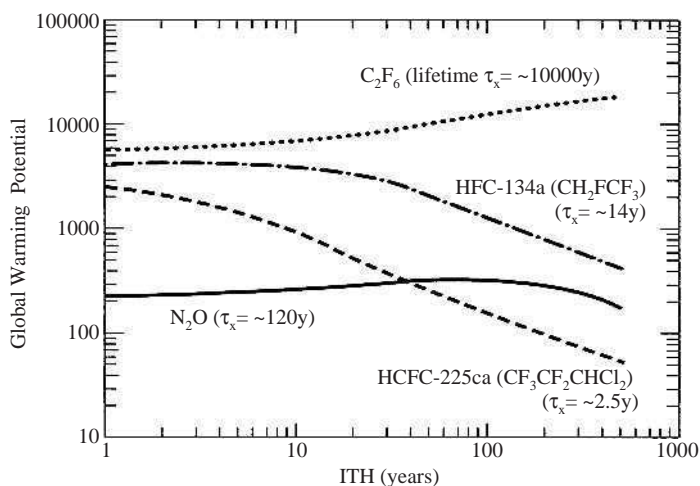
However, for calculation of R_x , each researcher uses a different model, and when calculation of $\text{AGWP}_{\text{CO}_2}$ is carried out following the IPCC recommended equation, the model dependence of radiative forcing is not cancelled and problems remain. Therefore, in order to slightly this influence, equation (17) is calculated for CFC-11, and the obtained value is standardized by equation (17) to obtain

$$\text{GWP}_x(\text{ITH}) = \frac{\mu_{\text{CFC-11}} R_x}{\mu_x R_{\text{CFC-11}}} \cdot \text{GWP}_{\text{CFC-11}}(\text{ITH}) \cdot \frac{\tau_x [1 - \exp(-\text{ITH}/\tau_x)]}{\tau_{\text{CFC-11}} [(1 - \exp(-\text{ITH}/\tau_{\text{CFC-11}}))]} \quad (18)$$

With this equation, if the GWP values for CFC-11, $\text{GWP}_{\text{CFC-11}}(\text{ITH})$, are calculated by other methods, the resulting GWP is independent of the radiative transfer calculation model for the target substance. Recently, this equation has been currently used to calculate GWP. Examples of the GWP value calculated in this way are presented in Table 12 together with atmospheric lifetimes. Values for $\text{ITH} = 20, 100$ and 500 years are commonly used. Fig. 12 shows a plot of GWP

Table 12. Lifetimes and GWPs (selected from IPCC (2001))

Compounds	Chemical formula	Lifetime (y)	GWP		
			Integration time horizon (y)		
			20	100	500
Carbon dioxide	CO ₂	—	1	1	1
Methane	CH ₄	12.0	62	23	7
Methyl chloroform	CH ₃ CCl ₃	4.8	450	140	42
Carbon tetrachloride	CCl ₄	35	2700	1800	580
Sulphur hexafluoride	SF ₆	3200	15100	22200	32400
Perfluoromethane	CF ₄	50000	3900	5700	8900
CFC-11	CCl ₃ F	45	6300	4600	1600
CFC-12	CCl ₂ F ₂	100	10200	10600	5200
CFC-113	CCl ₂ FCClF ₂	85	6100	6000	2700
CFC-114	CClF ₂ CClF ₂	300	7500	9800	8700
HCFC-22	CHClF ₂	11.9	4800	1700	540
HCFC-141b	CH ₃ CCl ₂ F	9.3	2100	700	220
HCFC-225cb	CClF ₂ CF ₂ CHClF	6.2	2000	620	190
HFC-134a	CH ₂ FCF ₃	13.8	3300	1300	400
HFC-143	CHF ₂ CH ₂ F	3.4	1100	330	100
HFC-236ea	CHF ₂ CHFCF ₃	10.0	3600	1200	390
HFE-245cb2	CF ₃ CF ₂ OCH ₃	4.3	1900	580	180
HFE-347mcc3	CF ₂ CF ₂ CF ₂ OCH ₃	4.5	1600	480	150
HFE-356pcf3	CHF ₂ CF ₂ CH ₂ OCHF ₂	3.2	1500	430	130

**Fig. 12.** GWPs as a function of integration time horizon (ITH) [45].

(ITH) as a continuous function. It is found that a peak of GWP for each substance is located in the vicinity of the end of atmospheric lifetime of the substance.

Some problems remain after calculating GWP using the method described above. The first is that CO₂ is used as the standard substance. A proportion of the original CO₂ discharged into the atmosphere still remains even after a period of a thousand years. Because of this, if equation (15) is integrated over an infinite time, the denominator becomes infinite, and the GWP value becomes zero. Despite this limitation, CO₂ is still used as a standard to determine GWP, because CO₂ is the principal greenhouse gas. In the calculation of GWP, a thorough mixture of the target substance is assumed in order to carry out the radiative transfer calculation. However, for substances with a short atmospheric lifetime, this assumption is sometimes not correct. It has been suggested that instead of assessing global climate impact using values such as GWP, we should concentrate on the accurate assessment of regional climate impact. On the other hand, concerning substances with an extremely long atmospheric lifetime, GWP does not reach a peak even after ITH = 500 years, and there is concern about the effect on climate over such a long span of time. But, despite this concern, ITH = 500 has become a common value for assessment because of difficulty in calculation for longer ITH. For example, in the case of CF₄, the radiative forcing is not very different from other substances, and despite the long lifetime of 50,000 years, a value is kept at the 8900 level even for a GWP (ITH = 500). There is currently a lot of discussion on how to evaluate the climatic influence of a substance with such a long atmospheric lifetime.

Until now, radiative forcing has been evaluated just for the target substances. The GWP calculated based on these results is called direct GWP. However, the products of the decomposition of the target substance remain in the atmosphere and they may also have a greenhouse effect. The GWP based on this effect should be called indirect GWP, to include the effect on atmosphere of the original substance. However, it is generally difficult to identify the products of decomposition, and to predict their infrared absorption strength and atmospheric lifetime. For the substances shown in Table 12, indirect GWP is not included in GWP. In the case of methane, the decomposition process in the stratosphere is quite simple, and in addition the decomposition products are CO₂ and water, so it is possible to add this radiation effect, which is calculated as several 10% of the value of direct GWP. It is necessary to sufficiently investigate the indirect effects of other substances.

4. EVALUATION OF CURRENT ALTERNATIVES

Evaluation of alternatives and associated topics discussed so far have included atmospheric lifetime, ODP and GWP. With that, just how are the evaluations

made in the real world? Furthermore, are these evaluations sufficient in themselves? The following points may be necessary to make a proper evaluation.

4.1. Environmental impact assessment

While ozone layer depletion and photochemical smog produced by VOCs are serious problems, most attention has been focused on global warming. Atmospheric lifetime and GWP have been already discussed as a means of evaluating global warming. There are mechanical methods also for evaluating global warming, such as life cycle assessment (LCA), LCCP and total equivalent warming impact (TEWI). In addition, there are other factors that must be evaluated, including toxicity, flammability, legal, social and ethical considerations, resources, properties for use and economic impact. Here we will focus on flammability and LCCP.

4.2. Evaluation of the flammability of CFC alternatives

CFC alternatives such as HFCs and HFEs contain hydrogen atoms in their molecules to adjust their atmospheric lifetimes. As some of the compounds contained therein are flammable, it is very important from a safety perspective to evaluate their flammability. When fluorinated compounds catch fire, it is believed that the fluorine atoms produced during combustion react with chemically active hydrogens and other atoms/radicals to reduce the flammability. Generally speaking, as the proportion of fluorine atoms in the compound decreases, flammability increases.

For example, in compounds of the ethane series, PFC-116 (C_2F_6), HFC-125 (CF_3CHF_2) and HFC-134a (CF_3CH_2F) are not flammable, whereas HFC-143a (CH_3CF_3) and HFC-152a (CH_3CHF_2) are flammable. HFC-23 (CHF_3) and HFC-227ea ($CF_3CHF_2CF_3$) are non-flammable by themselves and are used as alternatives for the fire extinguisher chemical Halon-1301 (CF_3Br).

Thus, we can see that fluorinated compounds have various levels of flammability, from the strongly flame-suppressing compounds used in fire extinguishers to highly flammable compounds such as HFC-152a. In addition, there are numerous matters that are still unknown about the flammability of fluorinated compounds, such as why structural isomers HFC-245eb (CF_3CHFCH_2F) and HFC-245fa ($CF_3CH_2CHF_2$) have the same ratio of fluorine atoms in their molecules, as the former is flammable while the latter is not.

When evaluating the flammability of compounds, it is necessary to consider two factors. The first factor is the probability of ignition, and the second factor is the intensity when ignition actually occurred. The first factor is related to the flammability limit, and the second factor is related to the burning velocity and the heat of combustion. ISO (International Organization for Standardization) and

ASHRAE (American Society of Heating, Refrigerating and Air-Conditioning Engineers) have been investigating the flammability classification of refrigerants based on these indices.

The flammability limit is measured from the processes of ignition by high-voltage electric discharge, etc. of a flammable compound/air mixture. Flammable or non-flammable is judged by the subsequent flame propagation. While the measured value of the flammability limit is affected by the vessel size, shape, etc., a relatively constant value can be obtained when the inner diameter and the height are above a certain threshold. For example, with a 12-L spherical vessel, the ASHRAE method [47] can produce results similar to those of large vessels [48]. The burning velocity can be measured using various methods such as the spherical vessel method [49], the Schlieren method [49], the tube method [50] and the burner method [51,52].

The combustibility of flammable compounds can be classified based on values of flammability limit, combustion velocity, etc. In addition, numerical methods have been proposed which are based on the values of flammability limit, burning velocity, etc. An index called RF number [53] is shown in equation (19) as a function of lower limit (L), upper limit (U), heat of combustion (Q) and molecular weight (M). The units are as follows: RF number (kJ g^{-1}), L and U (vol.%), Q (kJ mol^{-1}) and M (g mol^{-1}). In equation (20), RF2 (revision of RF number, the unit is $\text{kJ mol}^{-1} \text{m s}^{-1}$) is a function of the lower limit, upper limit, the heat of combustion per one mole of stoichiometric mixture (Q_{ST}) in kJ mol^{-1} and the burning velocity (S_U) in m s^{-1} , and in equation (21), the R-index [55] is shown as a function of the lower limit and the stoichiometric concentration (C_{ST}) in unit of vol.%.

$$\text{RF} = \frac{\sqrt{UL} - L}{L} \cdot \frac{Q}{M} \quad (19)$$

$$\text{RF2} = \frac{\sqrt{UL} - L}{L} \cdot Q_{\text{ST}} \cdot S_U \quad (20)$$

$$\text{R} = \frac{C_{\text{ST}}}{L} \quad (21)$$

Table 13 shows values related to the combustibility of flammable compounds such as ammonia and methane as well as the major flammable HFCs. The numerical indices of RF numbers, etc., are small for compounds with low combustibility such as HFC-32 (CH_2F_2) and ammonia, and large for ordinary flammable gases such as methane and propane. Among the HFCs, the highly flammable HFC-152a, has a value that is intermediate, or is close to methane. These indices have the advantage of enabling numerical comparisons to be made of the combustibility of each compound.

Table 13. Flammability indices of major flammable compounds

Compounds	HFC-32	HFC-143	HFC-143a	HFC-152a	Ammonia	Methane	Propane
Chemical formula	CH ₂ F ₂	CHF ₂ CH ₂ F	CH ₃ CF ₃	CH ₃ CHF ₂	NH ₃	CH ₄	C ₃ H ₈
Stoichiometric concentration (vol.%)	17.32	9.48	9.48	7.73	21.8	9.48	4.02
Heat of combustion (kJ mol ⁻¹)	489	939	864	1073	317	799	2041
Flammability limits (vol.%)	13.3–29.3 [56]	6.2–22.6 [56]	7.4–17.0 [57]	4.35–17.5 [57]	15–28 [58]	4.9–15.8 [60]	2.1–9.5 [61]
Burning velocity (cm s ⁻¹)	6.7 [49]	13.1 [49]	7.1 [49]	23.6 [49]	8.0 [59]	36.5 [49]	38.7 [49]
RF number [53] (kJ mol ⁻¹ s ⁻¹)	4.6	10	5.3	17	6.8	40	52
RF2 [54] (kJ mol ⁻¹ ms ⁻¹)	2.8	11	3.0	20	2.0	22	36
R-index [55]	1.31	1.53	1.28	1.79	1.45	1.94	1.90

4.3. LCCP evaluation

The evaluation of the greenhouse effect is divided into evaluation of the compounds themselves, and evaluation of the systems used [62]. While the scope of LCCP evaluations differs from that of LCA, TEWI, it is essentially a method for making wide-ranging evaluation of greenhouse effects, and is most commonly used.

This method enables evaluations of greenhouse effects to be compared by varying CFC alternatives themselves and/or their use conditions, and also includes the use efficiency of equipment that derives from the characteristics of CFC alternatives. Therefore, it is the most important method for selecting a CFC alternative. This is because, even if GWP value is small, if the usage efficiency is not very good, there is a lot of emission of CO₂ originating from the energy use of equipment and thus cannot be said to be a good selection.

LCCP can make a comprehensive evaluation in both the above situations. In nearly all the cases, evaluations have been made with the 100-year value of GWP (evaluations made with a variable time axis are discussed in the following section). As shown in the following example of automobile air conditioners, the evaluation covers both direct effects induced by the emission of compounds, and indirect effects which are indirectly induced by the use of energy, etc.

Fig. 13 shows a comparison between R-134a (CF₃CH₂F) and R-744 (CO₂) as an example of automobile air conditioners. R-744 reduces the greenhouse effect in cold regions, while R-134a reduces it in warm regions.

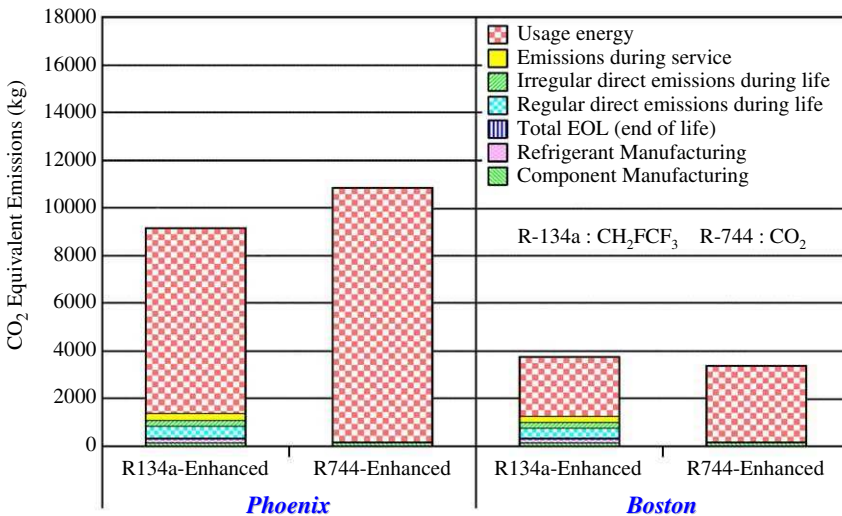


Fig. 13. Breakdown of total CO₂ equivalent emissions for R-134a and R-744 in different cities. Reported by Papasavva and Hill [63] [Using these data, time depending analysis is shown in the next section].

4.4. New evaluation of global warming

New approaches are being taken to the evaluation of global warming. This section will examine the following two approaches:

- (1) Improving the evaluation of global warming along a time axis.
- (2) Reflecting not only direct warming, but also indirect warming in the evaluation.

The first approach is an attempt to compensate for the shortcomings of the GWP. The GWP is calculated by determining the ITH, that is, the length of time of integration. The integrated warming effect of a certain compound is obtained by designating "1" as the standard value of integrated warming effect of CO₂ during this ITH [64]. If the ITH is determined to be X years, the warming value of the compound for X years is expressed as a relative value to that of CO₂. Thus, evaluations can be made by changing the time period of the ITH. However, currently the only GWP value used is the one which is calculated from a 100-year value of ITH. This overlooks the fact that GWP is a function of time.

This problem begins by making CO₂ the standard; even for different values of ITH, CO₂ is always a standard value of "1". CO₂ is removed from the atmosphere through different processes from other normal compounds. CO₂ is absorbed by plants and by oceans, quite unlike hydrocarbons and HFCs which are removed from the atmosphere by reaction with OH radicals. In addition, it is known from the carbon cycle model [46] that two-thirds of CO₂ can be quickly removed after its release into the atmosphere (within a few decades), the remaining amounts need thousands of years to be removed.

The warming effects for GWP (n) and GWP (m) of CO₂ after n and m years, respectively, are always set to "1," regardless of any actual differences after n and m years. Therefore, a comparison between different ITH values is essentially impossible because it involves different unit values, so it is usually evaluated based on the values for 100 years. The use of GWP makes the evaluation of warming biased. It is reported in IPCC as well that quantitative evaluation based on a single ITH value is erroneous [65]. Evaluations for different time frames are essential for comparing substances which have different atmospheric lifetimes.

With respect to the second approach, research is progressing to make better evaluations. New evaluations based on the following concepts are reported in scientific journals. It involves the concept of Net GWP [64] in which warming is suppressed as the ozone layer becomes depleted, and compounds with a short atmospheric lifetime reduce the concentration of OH radicals which reacts with methane in the atmosphere; thus methane increases the warming effect [66]. In addition, it also involves that decomposition of components released into the atmosphere induces the warming effect [66,67], and compounds released into the atmosphere can cause the production of tropospheric ozone which induces warming [66,67].

4.4.1. Evaluations using a total warming prediction graph

In the Kyoto Protocol, evaluation is based on a comparison between CO₂ and other greenhouse gases, which is called as a “basket-type” formula. Therefore, integration values are used in quantitative evaluations, and the standard unit is that for CO₂. As mentioned in Section 4.4 temporary evaluation is difficult to obtain. Because of the cumulative evaluation, even if substances released into the atmosphere disappear, the past cumulative value is displayed, resulting in an illusion that some warming effect remains. To solve these problems and to show what kind of warming effect is caused over time by substances released today, the depiction of each compound for each application appears to be the easiest method to be undertaken.

This scheme does not show cumulative values, but simple depictions of greenhouse effects at various times. Based on this concept, an attempt was made to convert gases released into the atmosphere, energy used, etc., into radiative force (RF) and plot the results on a graph called the TWPG [68,69]. Because this method is concerned with a sustainable global environment, the atmosphere is assumed to be the same for the present and the future, and the reduction curve from the carbon cycle model [48] is used for CO₂, while the reduction curve from the chemical kinetic equation is used for normal compounds [64]. The TWPG analysis is done in Fig. 14 to Fig. 17; and Fig. 19 for various types of applications.

4.4.1.1. Evaluation of mobile air conditioning (MAC).

Boston, MA, USA was selected as the cool zone city for the MAC evaluation. In an initial phase, the enhanced R-134a model (R-134a coolant) showed significant warming, but from approximately the 50th year onwards the enhanced R-744 model (CO₂ coolant) showed a greater warming effect (Fig. 14).

The warming effect in the latter half was 127% for R744-enhanced (enhanced R-744 model), with R134a-enhanced (enhanced R-134a model) at 100%, indicating that R134a-enhanced helped to stabilize CO₂ concentrations. Furthermore, in the GWP 100-year evaluation, R-134a was considered to make a larger contribution to warming, but in the TWPG analysis, it was clearly seen that in the long term the total greenhouse effect from R-134a was less than that of R-744, indicating that R-134a was the optimum choice for a coolant. Such quantitative evaluations of the greenhouse effect should be referred to the CWP evaluations, as will be discussed later. The excellent properties of R-134a act to reduce emissions of CO₂.

Fig. 15 shows another evaluation for Phoenix, AZ, USA which is an example of a warm zone city. For nearly all time frames, the TWPG analysis showed that R-134a was superior. In this case, calculations which were similar to the previous calculations indicated that R-134a helped to reduce CO₂ concentrations by 38%.

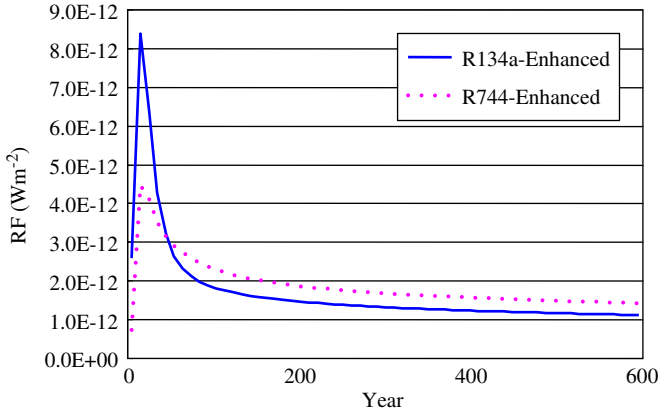


Fig. 14. Total warming prediction graph (TWPG) analysis of MAC (mobile air conditioning) in Boston (example of a cool zone city). Reported by Sekiya [68,69]. The analysis was performed using the data from Papasavva and Hill [63] p. 21.

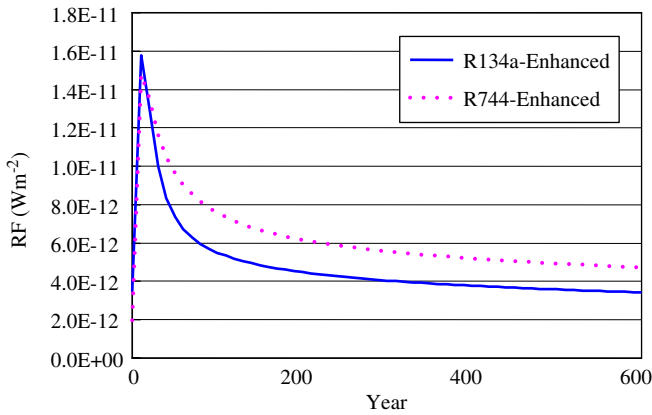


Fig. 15. TWPG analysis of mobile air conditioning (MAC) in Phoenix, Arizona, USA (example of a warm zone city). Reported by Sekiya [68,69]. The analysis was performed using the data from Papasavva and Hill [63] p. 21.

4.4.1.2. Evaluation of refrigerators.

Fig. 16 shows an evaluation of refrigerators used in Europe. In this case, the blowing agent HFC-245fa ($CF_3CH_2CHF_2$) showed a significant contribution to the greenhouse effect in the initial stage up to about 50 years, but after that, the pentane blend contributed more. Thus, it is apparent that in this case as well, HFC-245fa can be a next-generation contributor to greenhouse effect reduction. Furthermore, we can expect HFC-245fa to emit a smaller total volume of greenhouse gas than pentane.

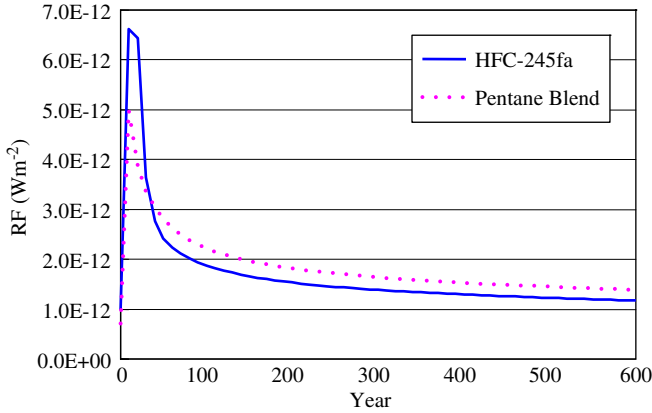


Fig. 16. The effect of blowing agents in refrigerators in Europe (Calculated using the data from R.W. Johnson [70] p. 7). TWPG Analysis of 358-L refrigerators (Refrigerant R-600: C3H8). Emissions comparison, current disposal practices, 60% Landfilled [69].

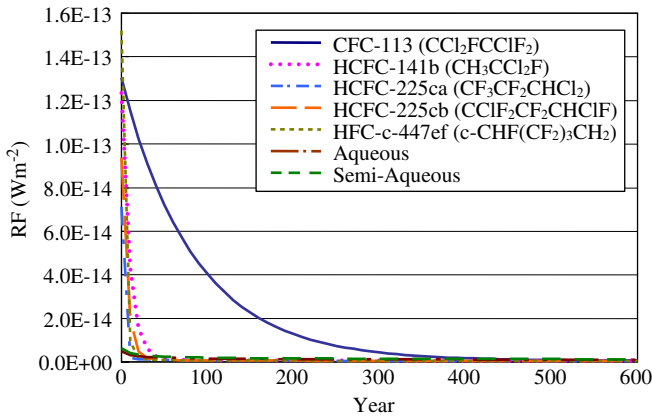


Fig. 17. TWPG analysis of solvents (per m² board). Batch PWA (printed wire assembly) cleaning processes [69]. Calculated from the data in alternative fluorocarbons environmental acceptability study (AFEAS) [71].

4.4.1.3. Evaluation of solvents.

Fig. 17 shows an evaluation of detergents. Fluorine-based detergents contributed to the greenhouse effect in the initial stage, but in this case as well, HFCs, which are short-lived in the atmosphere, clearly reversed their contribution compared with aqueous and semi-aqueous detergents.

From these results, it appears again that HFCs with a short lifetime in the atmosphere are generally a much better alternative for CFCs than non-fluorine-based alternatives. These results show that a more scientific and wider evaluation should be applied without relying solely on 100-year values of GWP evaluations. Thus, TWPG evaluations should proceed to help develop the optimal alternatives.

4.4.2. Composite warming potential

While TWPG can give us a qualitative understanding, there have also been investigations to determine whether or not it can be used quantitatively by changing the cumulative time frames. This consideration has led to the development of CWP [67,72,73]. While the standard value “1” in GWP changes with the integrated time horizon (ITH), if the standard value is made constant, comparisons can be made even if the time changes. The following is an examination of the GWP formula and the integrated warming effect (IWE), which is part of CWP.

The IWE for a compound x is calculated by the following equation. The 100-year absolute GWP value of carbon dioxide, $AGWP_{CO_2}(100y)$, is $1 \text{ Wm}^{-2} \text{ kg}^{-1} \text{ y}$.

$$IWE_x(ITH) = \frac{AGWP_x(ITH)}{AGWP_{CO_2}(100y)} \quad (22)$$

It is comparable to the following calculation of GWP:

$$GWP_x(ITH) = \frac{AGWP_x(ITH)}{AGWP_{CO_2}(ITH)} \quad (23)$$

As shown below, CWP is a summation of the values for warming effect of decomposed compounds (WEDC), warming effect of created ozone (WECO) and IWE. Table 14 lists some examples. WEDC expresses the warming effect of decomposed compounds in which hydrocarbons react with OH radicals in the atmosphere to create CO_2 . WECO uses the Carter equation [74] to calculate the upper limit maximum incremental reactivities (ULMIR) of the amount of created tropospheric ozone which is converted with a simple method into greenhouse effect.

$$CWP_x(ITH) = IWE_x(ITH) + WEDC_x(ITH) + WECO_x(ITH) \quad (24)$$

Fig. 18 shows an example of a comparison of automobile (mobile) air conditioners (Fig. 14) made using CWP analyses for 100-, 500- and 1000-year time frames. The greenhouse effect for 100-year CO_2 is evaluated as “1”. Therefore, CWP enables mutual analyses to be made, even for different evaluation periods. Because there are emissions of long-lived CO_2 , the total emission volume of greenhouse gas increases with the evaluation period. R134a-enhanced, which has a high position in terms of 100-year greenhouse effect, is surpassed at the

Table 14. Examples of composite warming potential (CWP) values

Compounds	CWP (total, ITH)				GWP		
	ITH (y)	100	500	1000	∞	100	500
CO ₂		1.0	3.2	5.4	60.0	1	1
CFC-11		4600	5160	5161	5172	4600	1600
HFC-134a		1301	1304	1306	1347	1300	400
HC, <i>n</i> -C ₃ H ₈		5.1	11.7	18.0	182.1	—	—
HFC-245fa		950.9	953.1	955.3	1005.9	950	300
HFC-365mfc		891.1	893.8	896.4	956.0	890	280
HC, <i>cyclo</i> -C ₅ H ₁₀		7.81	14.78	21.59	193.11	—	—
HCFC-225ca/cb (blend)		422.7	424.1	425.5	459.8	422	129
HFC, <i>cyclo</i> -C ₅ F ₇ H ₃		251.1	253.6	256.1	317.5	250	80
HC, <i>n</i> -C ₅ H ₁₂		6.73	13.51	20.13	186.86	—	—
CF ₄		5700	28,386	56,490	2,470,000	5700	8900
NF ₃		10,800	41,968	63,322	85,443	10,800	13,100
COF ₂		0.7	2.1	3.6	40.0	—	—
HFC, <i>cyclo</i> -C ₅ F ₈		91.0	93.4	95.6	151.8	90	30

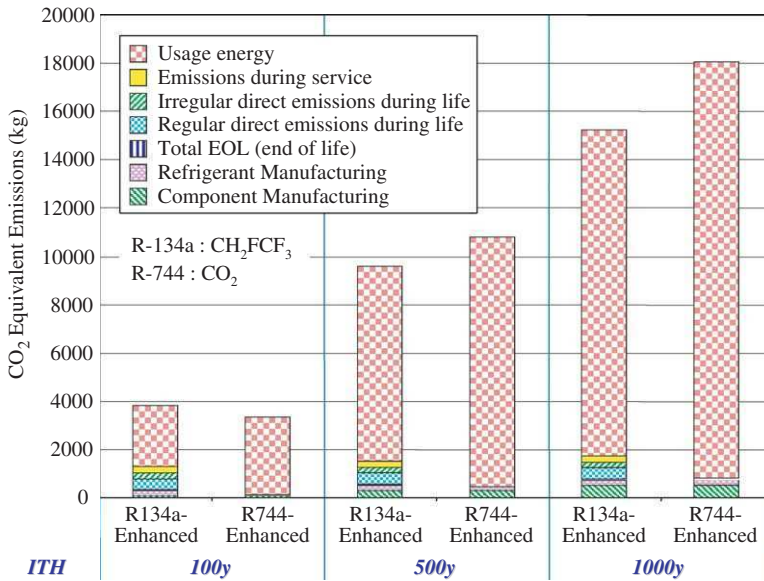


Fig. 18. Composite warming potential (CWP) analysis of MAC for R-134a and R-744 in Boston. Reported by Sekiya [73]. The analysis was performed using the data from Papasavva and Hill [63] p. 21.

500-year level and above by R744-enhanced in the CWP analysis. However, a quantitative analysis indicates that R-134a is superior.

This trend was also found for both blowing agents and detergents, revealing that HFCs, which have a relatively short lifetime in the atmosphere, are excellent alternatives.

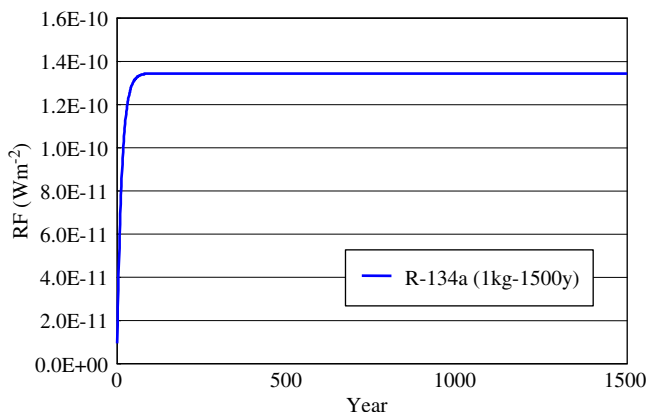


Fig. 19. TWPG analysis of the sustainability of R-134a (CH_2FCF_3). Year-by-year greenhouse/global-warming effect of the release of 1 kg of R-134a every year into the atmosphere for 1500 years [69,75].

4.4.3. Atmospheric lifetime of compounds emitted and the greenhouse effect

Fig. 19 shows the greenhouse effect at X years up to 1500 years for R-134a which has an atmospheric lifetime of 13.8 years and which had been released into the atmosphere at the rate of 1 kg per year. The concentration of short-lived compounds quickly stabilizes and does not increase [75]. Analyzing CO_2 in the same way shows a very different result, that is, a continuous increase. Stabilization occurs when the amount released and the amount decomposed in the atmosphere are in balance. The time needed to reach stability depends on the lifetime of the substance. When the lifetime is very short, it can cause photochemical smog. Thus, it appears clearly that HFCs, whose lifetime is neither too long nor too short, can make excellent alternatives for CFCs.

5. CONCLUDING REMARKS

Fluorine compounds are used widely not only in energy-related applications such as fuel cells and lithium electric batteries, but also in the well-established fields of bioactive substances for chemical products for medicine and agriculture; in ion-exchange membranes; liquid crystals for TV displays; as etching gases for industrial semiconductors; and cleaning gases for (chemical vapour deposition) CVD chambers, fluorine resins, paints, etc. The reason for this widespread use of fluorine is that it has the largest electronegativity of all atoms, and that it can form chemical compounds with special characteristics. These make fluorine very attractive for applications as a refrigerant, blowing agent or washing agent.

Because of their excellent properties, CFCs, HCFCs and HFCs have been highly regarded in society. On the other hand, as these compounds have caused the depletion of the ozone layer and global warming, international efforts are being devoted to take improved measures to solve these problems. In this chapter, statuses of various CFC alternatives have been explained. In Section 1 CFCs and their present conditions were explained from an international point of view, showing the changes in industrial production as well as the international measures that have been taken. In Section 2 the principles and characteristics of the use of CFCs as refrigerants, blowing agents and washing agents were presented, and the present status of CFC alternatives described. In Section 3 three important terms were explained as follows: the life span in the atmosphere, which is an important indicator of the behaviour of chemical compounds released into the atmosphere, methods of evaluating the ODP which triggered the establishment of international measures restricting the CFC production, and the assessment of problems involved in alternative compounds using the GWP. In Section 4 evaluations of CFCs were introduced according to their use as refrigerants, blowing agents and washing agents. In order to compare suitable CFC alternative technologies, methods of assessing global warming in terms of CFCs applications were explained using CWP and TWPG together with the traditional factors, the total equivalent of warming impact (TEWI) and LCCP.

From the present situation of CFC alternatives, it may be concluded that the most important measures are related to chemical compounds with a long life span in the atmosphere to reach the objective of Article 2 in the United Nations Framework Convention on Climate Change (UNFCCC), "to achieve stabilization of greenhouse gas concentrations in the atmosphere at a level that would prevent dangerous anthropogenic interference with the climate system." From this point of view, it is necessary to control the amount of carbon dioxide discharged into the atmosphere. It is found that the effective use of the excellent properties of fluorine compounds such as HFCs with a relatively short life span in the atmosphere would contribute to the preservation of the environment. It is important to preserve the global environment by advancing technical measures based not on a one-sided assessment such as the GWP for a hundred years but on a comprehensive scientific assessment covering short-, middle- and long terms.

ACRONYMS AND ABBREVIATIONS

AFEAS	Alternative fluorocarbons environmental acceptability study
AGWP	Absolute global warming potential
ASHRAE	American Society of Heating, Refrigerating and Air-Conditioning Engineers

BLP	Bromine loading potential
CLP	Chlorine loading potential
COP	Conference of the Parties (to the UNFCCC)
CTM	Chemical transport model
CVD	Chemical vapour deposition
CWP	Composite warming effect
EEAP	Environmental Effects Assessment Panel
EOL	End of life
FC	Fractional amount of chlorine
GHG	Greenhouse gas
GWP	Global warming potential
HGWP	Halocarbon global warming potential
IOL	Instantaneous ozone loss
IPCC	Intergovernmental Panel on Climate Change
ISO	International Organisation for Standardisation
ITH	Integration time horizon
IWE	Integrated warming effect
LCA	Life cycle assessment
LCCP	Life cycle climate performance
MAC	Mobile air conditioning
ODP	Ozone-depleting potential
ODS	Ozone-depleting substance
PSC	Polar stratospheric clouds
PWA	Printed wire assembly
RF	Radiative forcing
SAP	Scientific Assessment Panel
TEAP	Technology and Economic Assessment Panel
TEWI	Total equivalent warming impact
TWPG	Total warming prediction graph
ULMIR	Upper limit maximum incremental reactivities
UNEP	United Nations Environment Programme
UNFCCC	United Nations Framework Convention on Climate Change
VOC	Volatile organic compounds
WECO	Warming effect of created ozone
WEDC	Warming effect of decomposed compounds
WMO	World Meteorological Organization

APPENDIX I: SOME CHEMICAL SYMBOLS USED IN THIS CHAPTER

CFC	Chlorofluorocarbon
CFC-11	CCl ₃ F (trichlorofluoromethane)

CFC-12	CCl_2F_2 (dichlorodifluoromethane)
CFC-113	$\text{CCl}_2\text{FCClF}_2$ (trichlorotrifluoroethane)
CFC-114	$\text{CClF}_2\text{CClF}_2$ (dichlorotetrafluoroethane)
CFC-115	CF_3CClF_2 (chloropentafluoroethane)
Halon-1211	CBrClF_2
Halon-1301	CBrF_3
Halon-2402	$\text{CBrF}_2\text{CBrF}_2$
HCFC	Hydrochlorofluorocarbon
HCFC-22	CHClF_2
HCFC-123	CF_3CHCl_2
HCFC-124	CF_3CHClF
HCFC-141b	$\text{CH}_3\text{CCl}_2\text{F}$
HCFC-142b	CH_3CClF_2
HCFC-225ca	$\text{CF}_3\text{CF}_2\text{CHCl}_2$
HCFC-225cb	$\text{CClF}_2\text{CF}_2\text{CHClF}$
HFC	Hydrofluorocarbon
HFC-23	CHF_3
HFC-32	CH_2F_2
HFC-125	CHF_2CF_3
HFC-134a	CH_2FCF_3
HFC-143	$\text{CHF}_2\text{CH}_2\text{F}$
HFC-143a	CF_3CH_3
HFC-152a	CH_3CHF_2
HFC-227ea	$\text{CF}_3\text{CHF}_2\text{CF}_3$
HFC-236ea	$\text{CHF}_2\text{CHF}_2\text{CF}_3$
HFC-245eb	$\text{CF}_3\text{CHFCH}_2\text{F}$
HFC-245fa	$\text{CHF}_2\text{CH}_2\text{CF}_3$
HFC-365mfc	$\text{CF}_3\text{CH}_2\text{CF}_2\text{CH}_3$
HFC-43-10mee	$\text{CF}_3\text{CHFCH}_2\text{CF}_2\text{CF}_3$
HFC-52-13p	$\text{CF}_3(\text{CF}_2)_4\text{CHF}_2$
HFC-c-447ef	<i>cyclo</i> - $\text{CHF}(\text{CF}_2)_3\text{CH}_2$ (1,1,2,2,3,3,4-heptafluorocyclopentane)
HFE	Hydrofluoroether
HFE-143a	CH_3OCF_3
HFE-236pc	$\text{CHF}_2\text{CF}_2\text{OCHF}_2$
HFE-245cb2	$\text{CF}_3\text{CF}_2\text{OCH}_3$
HFE-245mf	$\text{CF}_3\text{CH}_2\text{OCHF}_2$
HFE-254cb2	$\text{CHF}_2\text{CF}_2\text{OCH}_3$
HFE-254pc	$\text{CHF}_2\text{CF}_2\text{OCH}_3$
HFE-347mcc3	$\text{CF}_3\text{CF}_2\text{CF}_2\text{OCH}_3$
HFE-347pc-f	$\text{CHF}_2\text{CF}_2\text{OCH}_2\text{CF}_3$
HFE-356pcf3	$\text{CHF}_2\text{CF}_2\text{CH}_2\text{OCHF}_2$
HFE-449s-c	$\text{CF}_3(\text{CF}_2)_3\text{OCH}_3$
HFE-569sf-c	$\text{CF}_3(\text{CF}_2)_3\text{OCH}_2\text{CH}_3$
HFIP	$(\text{CF}_3)_2\text{CHOH}$ (hexafluoroisopropanol)
MC	CH_3CCl_3 (methyl chloroform)

OFPO	(CF ₂) ₄ CH ₂ OH (octafluoropentanol)
PFC	perfluorocarbon
PFC-116	C ₂ F ₆ (perfluoroethane)
PFPO	CF ₃ CF ₂ CH ₂ OH (pentafluoropropanol)
TFPO	CHF ₂ CF ₂ CH ₂ OH (tetrafluoropropanol)

REFERENCES

- [1] M. Yamabe, H. Matsuo, Development of Fluorine Materials H. Matsuo (Ed.), CMC Publishing Co., Ltd., Tokyo, Japan, 1994, pp. 8–9.
- [2] S. Rowland, M. Molina, *Nature* 249 (1974) 810.
- [3] Synthesis of Assessment Panel Report, UNEP, 1988, 155pp.
- [4] IPCC/TEAP Special Report on Safeguarding the ozone layer and the global climate system: issues related to hydrofluorocarbons (HFCs) and perfluorocarbons (PFCs), URL: <http://www.ipcc.ch>.
- [5] ASHRAE34 Standard (Measurement ATM E681-94, Evaluation ASTM E681–85).
- [6] G. Biesmans, R. De Vos, I.D. Rosbotham, Proceedings of the Polyurethanes World Congress, 1993, 498pp.; M. Modesti, A. Lorenzetti, C. Dall'Acqua, *Polym. Eng. Sci.* 45 (2005) 260.
- [7] O.R. McIntire, R.N. Kennedy, *Chem. Eng. Prog.* 44 (1948) 727.
- [8] C.-D. Sommerfeld, W.M. Lamberts, D. Bielefeldt, A. Marhold, M. Negele, Ger. Pat. 298419, 1990; D.J. Williams, R.C. Parker, M.C. Bogdan, *Utech* 96. Conference Proceedings, 1996, 14pp.; J. Wu, D. Mouton, A. Albouy, Proceedings of the Polyurethanes Expo'98, 1998, 79pp.
- [9] P. Barthelemy, A. Leroy, Proceedings of the Polyurethanes Expo'96, 1996, 404pp. L. Zipfel, K. Borner, W. Kruecke, P. Barthelemy, P. Dournel, *J. Cellular Plastics* 35 (1999) 328.
- [10] L. Zipfel, W. Kruecke, DE 19822944 A1, 1999.
- [11] R.E. Wiedermann, G.G. Heilig, E.M. Hoppe, Proceedings of the Polyurethanes World Congress, 1991, 160pp.; J.A. Creazzo, H.S. Hammel, K.J. Cicalo, Proceedings of the Polyurethanes World Congress, 1993, 456pp.
- [12] P. Ashford, M.W.Q. Guzman, Proceedings of the Polyurethanes EXPO 2003, 2003, 435pp.
- [13] R.W. Johnson, *Int. J. Refrigeration* 27 (2004) 794.
- [14] M.A. Dobransky, Proceedings of the Polyurethanes EXPO 2003, 2003, 37pp.
- [15] M. Jeffs, *Urethane Technology*, December 2004/January 2005, 32pp.
- [16] Y. Ohnuma, J. Mori, Proceedings of the Polyurethanes EXPO 2003, 2003, 61pp.
- [17] M. Modesti, A. Lorenzetti, G. Basile, Proceedings of the Polyurethanes EXPO 2001, 2001, 611pp.; M. Modesti, A. Lorenzetti, G. Gavasso, Bevilaqua, Proceedings of the Polyurethanes EXPO 2003, 2003, 660pp.
- [18] J. Wu, C. Bertelo, *J. Cellular Plastics* 41 (2005) 15.
- [19] L. Fishback, C.J. Reichel, Proceedings of the Polyurethanes '92, 1992, 23pp. N. Takada, R. Tamai, H. Yamamoto, A. Sekiya, N. Tsukida, H. Takeyasu, *J. Cellular Plastics* 35 (1999) 389. R. Tamai, S. Urata, H. Takeyasu, H. Sato, A. Sekiya, Proceedings of the Polyurethanes Expo 2001, 2001, 619pp.
- [20] A. Sekiya, S. Misaki, *Chemtech* 26 (1996) 44–48.
- [21] Z. Zhang, S. Padmaja, R.D. Saini, R.E. Huie, M.J. Kurylo, *J. Phys. Chem.* 98 (1994) 4312–4315.
- [22] K. Tokuhashi, H. Nagai, A. Takahashi, M. Kaise, S. Kondo, A. Sekiya, M. Takahashi, Y. Gotoh, A. Suga, *J. Phys. Chem. A* 103 (1999) 2664–2672.

- [23] K. Tokuhashi, A. Takahashi, M. Kaise, S. Kondo, A. Sekiya, E. Fujimoto, *Chem. Phys. Lett.* 325 (2000) 189–195.
- [24] R.K. Talukdar, A. Mellouki, T. Gierczak, J.B. Burkholder, S.A. McKeen, A.R. Avishankara, *J. Phys. Chem.* 95 (1991) 5815–5821.
- [25] T. Gierczak, R.K. Talukdar, G.L. Vaghjani, E.R. Lpvejoy, A.R. Ravishankara, *J. Geophys. Res.* 96 (1991) 5001–5011.
- [26] V. Handwerk, R. Zellner, *Ber. Bunsenges. Phys. Chem.* 82 (1978) 1161–1166.
- [27] G. Paraskevopoulos, D.L. Singleton, R.S. Irwin, *J. Phys. Chem.* 85 (1981) 561–564.
- [28] R. Atkinson, D.A. Hansen, J.N. Pitts Jr., *J. Chem. Phys.* 63 (1975) 1703–1706.
- [29] T.D. Fung, P.H. Taylor, R.J. Berry, *J. Phys. Chem. A* 103 (1999) 2700–2704.
- [30] A. Mellouki, S. Teton, G. Le Bras, *Geophys. Res. Lett.* 22 (1995) 389–392.
- [31] N.L. Garland, H.H. Nelson, *Chem. Phys. Lett.* 248 (1996) 296–300.
- [32] D.D. Nelson Jr., M.S. Zahniser, C.E. Kolb, H. Magid, *J. Phys. Chem.* 99 (1995) 16301–16306.
- [33] J.S. Chang, F. Kaufman, *J. Phys. Chem.* 66 (1977) 4989–4994.
- [34] C.J. Howard, K.M. Evenson, *J. Chem. Phys.* 64 (1976) 197–202.
- [35] O.J. Nielsen, *Chem. Phys. Lett.* 187 (1991) 286–290.
- [36] L. Chen, S. Kutsuna, K. Tokuhashi, A. Sekiya, *Int. J. Chem. Kinet.* 35 (2003) 317–325.
- [37] L. Chen, S. Kutsuna, K. Tokuhashi, A. Sekiya, K. Takeuchi, T. Ibusuki, *Int. J. Chem. Kinet.* 35 (2003) 239–245.
- [38] W.B. DeMore, E.W. Wilson Jr., *J. Phys. Chem. A* 103 (1999) 573–576.
- [39] T.J. Wallington, W.F. Schneider, J. Sehested, M. Bilde, J. Platz, O.J. Nielsen, L.K. Christensen, M.J. Molina, L.T. Molina, P.W. Wooldridge, *J. Phys. Chem. A* 101 (1997) 8264–8274.
- [40] J. Barry, H. Sidebottom, J. Treacy, J. Franklin, *Int. J. Chem. Kinet.* 27 (1995) 27–36.
- [41] M. Mashino, M. Kawasaki, T.J. Wallington, M.D. Hurley, *J. Phys. Chem. A* 104 (2000) 2925–2930.
- [42] R.G. Prinn, J. Huang, R.F. Weiss, D.M. Cunnold, P.J. Fraser, P.G. Simmonds, A. McCulloch, C. Harth, P. Salameh, S. O'Doherty, R.H.J. Wang, L. Porter, B.R. Miller, *Science* 292 (2001) 1882–1888.
- [43] S.P. Sander, R.R. Friedl, D.M. Golden, M.J. Kurylo, R.E. Huie, V.L. Orkin, G.K. Moortgat, A.R. Ravishankara, C.E. Kolb, M.J. Molina, B.J. Finlayson-Pitts, *Chemical Kinetics and Photochemical Data for Use in Atmospheric Studies, Evaluation No. 14, JPL Publication 02-25, California Institute of Technology, Pasadena, CA, 2003.*
- [44] S. Solomon, M. Mills, L.E. Heidt, W.H. Pollock, A.F. Tuck, *On the evaluation of ozone depletion potentials, J. Geophys. Res.* 97 (1992) 825–842.
- [45] IPCC, *Climate Change 1995, Scientific Basis, Cambridge University Press.*
- [46] *Scientific Assessment of Ozone Depletion: 1998, WMO, 10.21, 1998.*
- [47] American Society of Heating, Refrigerating and Air-conditioning Engineers, *Number designation and safety classification of refrigerants – Third public review. BSR/ASHRAE Addendum “p” to ANSI/ASHRAE 34-1992, Atlanta GA, 2000.*
- [48] A. Takahashi, Y. Urano, K. Tokuhashi, S. Kondo, *J. Hazard. Mater.* A105 (2003) 27–37.
- [49] K. Takizawa, A. Takahashi, K. Tokuhashi, S. Kondo, A. Sekiya, *Combust Flame* 141 (2005) 298–307.
- [50] D. Clodic, T. Jabbour, *Burning velocity as an additional criterion for flammability classification of refrigerants, Seminar 10, ASHRAE Annual Meeting, Kansas City, June 29, 2003.*
- [51] G.T. Linteris, L. Truett, *Combust Flame* 105 (1996) 15–27.
- [52] W.L. Grosshandler, M.K. Donnelly, C. Womeldrof, *Trans. ASME Series C J. Heat Transfer* 122 (2000) 92–98.
- [53] S. Kondo, A. Takahashi, K. Tokuhashi, A. Sekiya, *J. Hazard. Mater.* A93 (2004) 259–267.

- [54] S. Kondo, K. Takizawa, A. Takahashi, K. Tokuhashi, A. Sekiya, ASHRAE Trans 110 (2) (2004) 534–539.
- [55] O. Kataoka, Trans. of JSRAE 18 (2001) 289–298 (in Japanese).
- [56] Y. Urano, S. Horiguchi, K. Tokuhashi, M. Iwasaka, S. Kondo J. High Press. Gas Safety Inst. Japan 27 (1990) 416–422; (in Japanese).
- [57] S. Kondo, K. Takizawa, A. Takahashi, K. Tokuhashi, J. Hazard. Mater. A109 (2004) 13–21.
- [58] T. Hikita, K. Akita, Outline of Combustion – Physics and Chemistry of Flames, 4th Edn, Corona Publishing Co., Ltd., (in Japanese).
- [59] P.D. Ronny, Combust. Sci. Technol. 59 (1987) 123–141.
- [60] S. Kondo, A. Takahashi, K. Tokuhashi, J. Hazard. Mater. A100 (2003) 27–36.
- [61] S. Kondo, Y. Urano, K. Takizawa, A. Takahashi, K. Tokuhashi, A. Sekiya, Fire Safety Journal 41 (2006) 46–56.
- [62] H. Onishi, 15th Annual Earth Tech. Forum and Mobile Air Conditioning Summit, Washinton, DC, USA, 2004.
- [63] S. Papasavva and W. Hill, MAC Summit, New Delhi, India, 2005.
- [64] IPCC, Climate Change 2001, Scientific Basis, Cambridge University Press, England
- [65] IPCC Technical Paper, February 1997, 13pp.
- [66] W.J. Collins, R.G. Derwent, C.E. Johnson, D.S. Stevenson, Climate Change 52 (2002) 453–479.
- [67] A. Sekiya, 15th Annual Earth Technical Forum and Mobile Air Conditioning Summit, Washington, DC, USA.
- [68] A. Sekiya, 12th Annual International Semiconductor Environment Safety & Health Conference, Portland, June 2005.
- [69] A. Sekiya, 17th International Symposium on Fluorine Chemistry, Shanghai, July 2005.
- [70] R.W. Johnson, 14th Annual Earth Tech. Forum and Mobile Air Conditioning Summit,, Washington, DC, USA, 7pp.
- [71] AFEAS, Ref. 46342, Arthur D. Little, Cambridge, MA, USA, October.
- [72] A. Sekiya, Polyurethane Expo 2004, Las Vegas, USA, October.
- [73] A. Sekiya, 17th Winter Fluorine Conference, Florida, USA, January.
- [74] W.P.L. Carter, Documentation of the SAPRC-99 Chemical Mechanism for VOC Reactivity Assessment. Final Report to California Air Resources Board Contract, No. 92-329 and 95-308, May 2000.
- [75] A. Sekiya, Expected Mater. Future 1 (6) (2001) 30–35.

This page intentionally left blank

CHAPTER 3

Trifluoromethyl Sulphur Pentafluoride, SF_5CF_3 : Atmospheric Chemistry and Its Environmental Importance via the Greenhouse Effect

Richard P. Tuckett

School of Chemistry, University of Birmingham, Edgbaston, Birmingham, B15 2TT, UK

Contents

1. Introduction	90
2. Structure, spectroscopy and thermochemistry of SF_5CF_3	92
3. The greenhouse effect and SF_5CF_3 : how serious is the problem?	93
4. Kinetics and removal processes of SF_5CF_3 from the earth's atmosphere	97
5. The VUV photoionisation and photofragmentation spectroscopy of SF_5CF_3	98
5.1. Definition of the first dissociative ionisation energy: application to CF_4 and SF_6	98
5.2. Experimental details	102
5.3. Determination of the first dissociative ionisation energy of SF_5CF_3 and the S–C bond strength	103
5.4. Threshold photoelectron spectrum of SF_5CF_3	106
5.5. Ion yields and fixed-energy TPEPICO spectra of SF_5CF_3	108
6. Removal processes of SF_5CF_3 from the earth's atmosphere in the mesosphere	110
6.1. Reactions of SF_5CF_3 with cations and anions	110
6.2. Reactions of SF_5CF_3 with low-energy electrons	114
6.3. Reactions of SF_5CF_3 with vacuum-UV photons, especially Lyman- α (121.6 nm) radiation	117
7. Lifetime of SF_5CF_3 in the earth's atmosphere and conclusions	122
Table of Acronyms	125
Acknowledgments	125
References	125

Abstract

One molecule of SF_5CF_3 , an adduct of the SF_5 and CF_3 free radicals, causes more global warming than one molecule of any other greenhouse gas yet detected in the atmosphere, that is, it has the highest *per molecule* radiative forcing of any greenhouse pollutant, and the value of its global warming potential is only exceeded by that of SF_6 . Using tunable vacuum-UV radiation from a synchrotron and coincidence spectroscopy, the strength of the central S–C bond in SF_5CF_3 is determined to be $3.86 \pm 0.45 \text{ eV}$ or $372 \pm 43 \text{ kJ mol}^{-1}$, and this molecule is highly unlikely to be removed from the Earth's atmosphere by

UV photolysis in the stratosphere. Complementary laboratory-based experiments have shown that the main sink route of this greenhouse gas is low-energy electron attachment in the mesosphere, with Lyman- α photodissociation at 121.6 nm being only a minor channel. On comparison with data for SF₆, the lifetime of SF₅CF₃ in the Earth's atmosphere is estimated to be ca. 1000 years. The principal reason for the current low level of concern about the impact of SF₅CF₃ on our environment is that the concentration levels are still very low, at the sub parts per trillion level. The high growth rate of ca. 6% per annum, however, should cause concern for policymakers.

1. INTRODUCTION

Trifluoromethyl sulphur pentafluoride, SF₅CF₃, has recently been termed as the super greenhouse gas. This claim to fame arises because, *per molecule*, it makes more contribution to global warming via the greenhouse effect than any other molecule yet detected in the atmosphere. Within this headline phrase, however, caution must be exercised as the amounts of SF₅CF₃ in the Earth's atmosphere are still very low at the sub parts per trillion level by volume (pptv): ca. 0.15 pptv; 1 pptv is equivalent to a number density of 2.46×10^7 molecules cm⁻³ for a pressure of 1 bar and a temperature of 298 K. By contrast, carbon dioxide has a current concentration of ca. 370 parts per million by volume in the Earth's atmosphere, which is over nine orders of magnitude greater than that of SF₅CF₃. Despite a much lower environmental impact *per molecule*, CO₂ makes a much greater impact on global warming, simply because its concentration is much higher. Nevertheless, the Kyoto Protocol of 1997, now ratified as an International Treaty in 2005 (see the conclusions of the *Montreal Intergovernmental Climate Conference* (28 November–9 December 2005) on the *United Nations Climate Change Conference* website – <http://unfccc.int>), to limit emissions of greenhouse gases has meant that scientists and industry are now legally bound to determine the most environmentally benign and cost-effective materials in large-scale industrial applications. It is therefore essential to understand the reactive and photochemical properties of molecules used in industry, which are emitted into the atmosphere and even gases that at first sight might seem benign and harmless. It is within this near-worldwide political consensus for control of global warming that one can understand the huge upsurge in interest in SF₅CF₃ since its potential for global warming was first raised by Sturges *et al.* [1] 5 years ago.

SF₅CF₃ is a gas at room temperature, with a boiling point of 253 K and an enthalpy of vapourisation of 20.2 kJ mol⁻¹ over the temperature range 223–253 K [2], and such thermochemical data have been available for some time. The paper by Sturges *et al.* [1], however, was the first to describe detection of SF₅CF₃ in the Earth's atmosphere. Its source was believed to be anthropogenic in nature, and most likely a breakdown product of SF₆ in high-voltage equipment. Since the

trends in concentration levels of SF₆ and SF₅CF₃ have tracked each other very closely over the last 30–40 years, Sturges *et al.* [1] suggested that SF₅CF₃ has mainly been produced in the electronics industry via the recombination of SF₅ and CF₃ free radicals. This claim has since been disputed [3]. Infrared (IR) absorption measurements showed that SF₅CF₃ has the highest radiative forcing per molecule of any gas found in the atmosphere to date ($0.57 \text{ W m}^{-2} \text{ ppb}^{-1}$, a figure since updated to $0.60 \pm 0.03 \text{ W m}^{-2} \text{ ppb}^{-1}$ [4,5]). Antarctic firm measurements suggested that it has grown from a concentration of near zero in the late 1960s to ca. 0.12 pptv in 1999 with a current growth rate of ca. 6% per annum, and stratospheric profiles suggested that the lifetime of this species in the atmosphere is between several hundred and a few thousand years. It was estimated that the global warming potential (GWP) of SF₅CF₃ is 18,000 relative to CO₂, with only SF₆ having a higher value. Sturges *et al.* [1] concluded that, while still a relatively minor problem, nevertheless, it was important to control the source(s) of SF₅CF₃ into the atmosphere in order to guard against an undesirable accumulation of this potent greenhouse gas. These comments remain as true now as they were then. Furthermore, in historical terms, the story of the chlorofluorocarbons, and their ‘conversion’ from industrially produced benign molecules to serious ozone-depleting molecules in the stratosphere over a period of less than 20 years, is still fresh in the memory of many atmospheric scientists. Small problems have a tendency to become big problems in atmospheric science. Thus, although the best estimate 2 years ago was that SF₅CF₃ only contributes 0.003% to the total greenhouse effect [6], it is not surprising that there has been huge interest in studying the reactive and photochemical properties of SF₅CF₃.

The purpose of this chapter is to review the microscopic properties of SF₅CF₃, most of the measurements and calculations made since Sturges *et al.* [1] published their paper. Emphasis will be on those measurements that pertain to the atmospheric properties of SF₅CF₃ and the processes that remove it from the Earth’s atmosphere. Only limited descriptions of the macroscopic properties of SF₅CF₃ will be given. Since the readership of this chapter will be wide, the terms *microscopic* and *macroscopic* may mean different things to different readers. As a chemical physicist, I define a microscopic property to be that of one molecule of the system under study (e.g. a spectroscopic, kinetic, photochemical or thermodynamic property). A macroscopic property relates to the system as a whole (e.g. industrial production sources of SF₅CF₃, the geographical properties that determine the transport of SF₅CF₃ through the atmosphere via convection and diffusion). The chapter will conclude with a review of the properties of SF₅CF₃ that determine its lifetime in the Earth’s atmosphere. The *lifetime* of a pollutant is another term that can mean different things to different scientists, and I will bring together all the many interpretations of this term in the context of the physical, chemical and geographical properties of SF₅CF₃ in our atmosphere.

2. STRUCTURE, SPECTROSCOPY AND THERMOCHEMISTRY OF SF₅CF₃

It is of some surprise to note that SF₅CF₃ is not a new molecule, and its microwave spectrum was recorded by Kisliuk and Silvey [7] as long ago as 1952. The S–C bond distance was determined to be 0.186 nm, and in 1985 all the geometrical parameters for SF₅CF₃ were reported by Marsden *et al.* [8] from an electron diffraction study. Fig. 1 shows an unpublished structure of the highest occupied molecular orbital (HOMO) of SF₅CF₃ by Knowles [9] using the MOL-PRO *ab initio* suite of programmes. The particular points to note are the substantial dipole moment of the molecule of 0.95 D; the significant σ -bonding electron density along the S–C bond; the S–C bond length of 0.187 nm in almost exact agreement with the microwave study; and the FSF and FCF bond angles of approximately 90° or 109.3°, respectively. SF₅CF₃ can therefore either be regarded as a perturbed SF₆ molecule in which one fluorine atom has been replaced by a CF₃ group of tetrahedral symmetry, or as a perturbed CF₄ molecule in which one fluorine has been replaced by an SF₅ group with octahedral symmetry. This will form a recurring theme of this chapter. The only major difference from SF₆ and CF₄ is that the HOMO of these two molecules is F 2p π non-bonding in character, whereas the HOMO of SF₅CF₃ is S–C σ -bonding in character. The

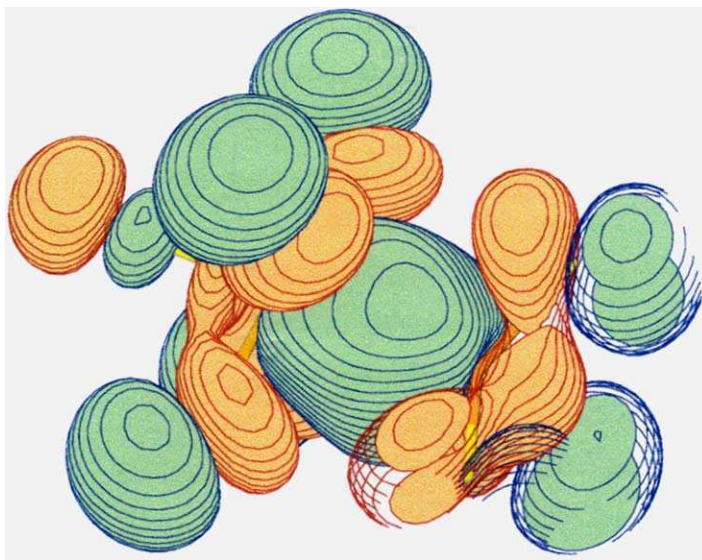


Fig. 1. Electron density map of the highest occupied molecular orbital of SF₅–CF₃. The FSF and FCF bond angles are all either 90° or 109.3°. The S–C bond length is 0.187 nm, the three C–F lengths are all 0.130 nm, the three S–F_{equatorial} lengths are 0.158 nm and the two S–F_{axial} lengths are 0.157 nm. The dipole moment is calculated to be 0.95 D.

gas-phase IR and liquid-phase Raman spectra at low resolution over the extended range of 100–4000 cm⁻¹ were reported over 40 years ago [10,11]. These measurements have been made at a much higher resolution in the last 3 years, and all the important IR-active vibrations in the atmospheric window region of ca. 700–1500 cm⁻¹ have been determined [12–14]. Of particular note is the determination of the integrated absorption coefficient over this range as a function of temperature between 200 and 300 K by two groups [13,14], with both studies demonstrating that the coefficient showed little variation with temperature. There were no other spectroscopic details (e.g. UV/visible electronic, vacuum-UV photoionisation) on this molecule before the Sturges *et al.* [1] paper was published. Since 2000, there have been a large number of new studies: some of direct importance to the atmospheric properties of SF₅CF₃ and some of more general and pure scientific interest. They include VUV and XUV absorption [4,15–19], valence photoelectron [4,15,20–22], electron energy loss spectroscopy [4,23], electron scattering [24–26], protonation [27] and photofragmentation studies [20–22,28].

As with the spectroscopic situation, there was scant information on the thermochemistry of SF₅CF₃ prior to 2000. The JANAF tables of 1998 [29] quote an enthalpy of formation of -1700 ± 63 kJ mol⁻¹ at 0 K and -1717 ± 63 kJ mol⁻¹ at 298 K, although these data are indirect and it is not clear how these numbers are derived. The strength of the SF₅–CF₃ σ -bond will also be determined by the enthalpies of formation of the SF₅ and CF₃ radicals, where improved values since the tables were published are now available. As the strength of this bond is related to possible photochemistry of SF₅CF₃ that may occur in the stratosphere, a *direct* determination of $\Delta_f H^\circ$ (SF₅CF₃) is therefore essential to explain any possible atmospheric reactions. Such an experiment is described in Section 5.3. As with experimental spectroscopic studies, there have been many theoretical studies on SF₅CF₃ since 2000 [30–34]. Their main aim has been to determine properties that relate to the atmospheric chemistry of SF₅CF₃, such as integrated IR intensities, vibrational frequencies and thermochemical and structural parameters.

3. THE GREENHOUSE EFFECT AND SF₅CF₃: HOW SERIOUS IS THE PROBLEM?

The greenhouse effect is usually associated with small polyatomic molecules such as CO₂, H₂O, CH₄, N₂O and O₃. The ‘natural’ greenhouse gases, notably CO₂ and H₂O, have been responsible for maintaining the temperature of the Earth at ca. 290 K, suitable for habitation for hundreds of years. The ‘enhancing’ greenhouse gases, mainly CH₄, N₂O and O₃, have concentrations in the atmosphere which have increased in the last 50–100 years and have IR absorptions in

the atmospheric window region where CO_2 and H_2O do not absorb, and are believed to be the main culprits for global warming. It is now clear, however, that there are larger polyatomic gases of low concentrations in the atmosphere, which can contribute significantly to global warming, as they possess exceptionally strong IR absorption bands in regions where other greenhouse gases do not absorb. Two notable examples are SF_6 , which has a GWP of 22,200 relative to CO_2 over a time horizon of 100 years [35] and SF_5CF_3 , which is the subject of this review. In qualitative terms, the physical and chemical properties that are necessary for a molecule to have a large GWP are as follows: (a) it must absorb IR radiation in the black-body range of the Earth's emission, ca. $5\text{--}25\ \mu\text{m}$ ($2000\text{--}400\ \text{cm}^{-1}$) with a peak at $15\ \mu\text{m}$ ($667\ \text{cm}^{-1}$), in regions where CO_2 and H_2O do not absorb; in practice this means that many C–F and C–Cl stretching vibrations around $900\text{--}1100\ \text{cm}^{-1}$ contribute strongly, (b) the integrated absorption intensities of the IR-active vibrations must be strong due to large dipole moment derivatives, (c) the molecule must have a long lifetime (defined in Section 7) in the Earth's atmosphere; it must not be photodissociated by solar UV radiation in either the troposphere ($\lambda > 290\ \text{nm}$) or the stratosphere ($200 < \lambda < 290\ \text{nm}$), and it must not react with either the OH or $\text{O}^*(^1\text{D})$ free radicals. Furthermore, a greenhouse gas whose concentration is increasing rapidly due to man's activity, while not affecting an integrated absorption coefficient or the GWP value directly, is a special cause for concern for policymakers in Government.

SF_5CF_3 appears to obey all these criteria, and Table 1 shows data for five greenhouse gases which demonstrate how serious or otherwise the presence of SF_5CF_3 in the Earth's atmosphere as a pollutant should be regarded. The five compounds are CO_2 and CH_4 which contribute ca. 70% to the overall greenhouse effect, N_2O , a chlorofluorocarbon (CF_2Cl_2) and SF_5CF_3 . Most of the data are taken from the Intergovernmental Panel of Climate Change report of 2001 [35], an associated paper whose data were fed into the IPCC2001 report [36], and one of many websites from an environmental pressure group highlighting statistics on global warming [37]. While some of the data may now be slightly out of date, the long-term trends should be unchanged. The term that is used to characterise the IR absorption properties of a greenhouse gas is the *radiative forcing*, while the overall effect of this pollutant on the Earth's climate is described by the GWP. The former measures the strength of the absorption bands over the IR black-body region of the Earth, ca. $400\text{--}2000\ \text{cm}^{-1}$. Essentially, it is a (per molecule) microscopic property, is given the symbol a_0 , and is usually expressed in units of $\text{W m}^{-2}\ \text{ppbv}^{-1}$. If this value is multiplied by the change in concentration of pollutant over a defined time window, usually the 250 years from before the Industrial Revolution to the current day, the macroscopic radiative forcing in units of W m^{-2} is obtained. One may then compare the radiative forcing of different pollutant molecules over this time window.

Table 1. Examples of greenhouse gases and their contribution to global warming [35–37].

Greenhouse gas	CO ₂	CH ₄	N ₂ O	CF ₂ Cl ₂	SF ₅ CF ₃
Concentration in 1998 (ppmv)	365	1.75	0.31	0.0005	1.2×10^{-7}
Δ Concentration (1750–1998) (ppmv)	87	1.045	0.044	0.0005	1.2×10^{-7}
Δ Concentration (ca. 2000) (% pa)	0.45	0.60	0.25	ca. 5.0	ca. 6.3
Radiative forcing a _o (W m ⁻² ppbv ⁻¹)	1.68×10^{-5}	4.59×10^{-4}	3.41×10^{-3}	0.32	0.60
Total radiative forcing ^a (W m ⁻²)	1.46	0.48	0.15	0.16	7.2×10^{-5}
Lifetime ^b (years)	50–200 ^c	12	120	102	ca. 1000
Global warming potential ^d	1	23	296	10600	> 17500
Contribution to greenhouse effect (%)	52	17	5	ca. 15 ^e	0.003 ^f

^a Owing to change in concentration of greenhouse gas from the pre-Industrial era to the present time.

^b Assumes a single-exponential decay for removal of greenhouse gas from the atmosphere.

^c CO₂ does not show a single-exponential decay [37,38].

^d Calculated for a time period of 100 years.

^e Cumulative effect of all chlorofluorocarbons.

^f Reference [6].

The GWP measures the radiative forcing, A_x , of a pulse emission of a greenhouse gas, x , over a defined time period, t , usually 100 years, relative to the time-integrated radiative forcing of a pulse emission of an equal mass of CO₂ [35]:

$$\text{GWP}_x(t) = \frac{\int_0^t A_x(t).dt}{\int_0^t A_{\text{CO}_2}(t).dt} \quad (1)$$

The GWP is therefore a dimensionless number that informs how important one molecule of pollutant x is to the greenhouse effect via global warming, compared to one molecule of CO₂. The GWP of CO₂ is defined to be unity. For most

greenhouse gases, the radiative forcing following an emission at $t = 0$ takes a simple exponential form:

$$A_x(t) = A_{o,x} \exp\left(\frac{-t}{\tau_x}\right) \quad (2)$$

where τ_x is the lifetime for removal of species x from the atmosphere. For CO_2 , the lifetime ranges from 50 to 200 years [37,38]. A single exponential decay is therefore not appropriate, and we can write,

$$A_{\text{CO}_2}(t) = A_{o,\text{CO}_2} \left[b_0 + \sum_i b_i \exp\left(\frac{-t}{\tau_i}\right) \right] \quad (3)$$

where the response function, the bracket in the right-hand-side of equation (3), is derived from more complete carbon cycles. Values for b_i ($i = 0-4$) and τ_i ($i = 1-4$) have been given by Shine *et al.* [38]. It is important to note that the radiative forcing, A_o , in equations (1)–(3) has units of $\text{W m}^{-2} \text{ kg}^{-1}$. For this reason, it is given a different symbol to the microscopic radiative forcing, a_o , which has units of $\text{W m}^{-2} \text{ ppbv}^{-1}$. Conversion between the two units is simple [38]. The time integral of the large bracket on the right-hand-side of equation (3), defined K_{CO_2} , has units of time, and takes values of 13.44 and 45.73 years for a time period of 20 and 100 years, respectively, the values of t for which GWP values are quoted most often. Within the approximation that the greenhouse gas x follows a single-exponential time decay in the atmosphere, it is then possible to parameterise equation (1) to give an exact analytical expression for the GWP of x over a time period t :

$$\frac{\text{GWP}_x(t)}{\text{GWP}_{\text{CO}_2}(t)} = \frac{\text{MW}_{\text{CO}_2}}{\text{MW}_x} \cdot \frac{a_{o,x}}{a_{o,\text{CO}_2}} \cdot \frac{\tau_x}{K_{\text{CO}_2}} \cdot \left[1 - \exp\left(\frac{-t}{\tau_x}\right) \right] \quad (4)$$

In this simple form, the GWP only incorporates values for the microscopic radiative forcing of greenhouse gases x and CO_2 , $a_{o,x}$ and a_{o,CO_2} , in units of $\text{W m}^{-2} \text{ ppbv}^{-1}$; the molecular weights of x and CO_2 ; the lifetime of x in the atmosphere, τ_x ; the time period over which the effect of the pollutant is determined; and the constant K_{CO_2} which can easily be determined for any value of t . This equation is not given in this specific form in [38], but is easy to derive from equations given therein. Note that a similar equation given in Section 6 of Ref. [5] by Mason *et al.* has numerous typographical errors, and should be disregarded. The *recent* increase in concentration per unit time interval of a pollutant (e.g. the rise in concentration per annum over the last 5–10 years), one of the factors of greatest concern to policymakers, does not contribute directly to the GWP value. This and other factors [38] have caused some criticism over the use of GWPs in policy formulation. That said, the important point to note from Table 1 is that CO_2 and CH_4 contribute most to the greenhouse effect simply due to their high atmospheric concentration; note that the radiative forcing per molecule and GWP of

both gases are relatively low. By contrast, SF₅CF₃ has the highest radiative forcing per molecule of any greenhouse gas and its GWP value is therefore very high, but its contribution to the overall greenhouse effect is relatively small because the concentration of SF₅CF₃ in the atmosphere is still very low.

4. KINETICS AND REMOVAL PROCESSES OF SF₅CF₃ FROM THE EARTH'S ATMOSPHERE

Even if the presence of SF₅CF₃ in our atmosphere contributes only a very small amount to global warming, nevertheless, it is important to understand the physical and chemical properties of this new greenhouse gas better. It is especially important to determine what are the chemical and photolytic reactions that remove it from the atmosphere, as they will contribute to its lifetime and GWP value. The total rate of removal of SF₅CF₃ per unit volume per unit time is given by

$$\text{Rate} = [\text{SF}_5\text{CF}_3] \left(k_1[\text{OH}] + k_2[\text{O}^*(^1\text{D})] + \sum_{\text{ions}} k_{\text{ion}}[\text{ion}] + k_e[\text{e}^-] + \sum_{\lambda} \sigma_{\lambda} J_{\lambda} \Phi_{\lambda} \right) \quad (5)$$

where each of the five terms in the large bracket of equation (5) is a pseudo-first-order rate constant. The first four terms represent reactions of SF₅CF₃ with OH, O^{*}(¹D), cations and electrons, respectively; k_1 , k_2 , k_{ion} and k_e are the corresponding second-order bimolecular rate coefficients. The first term will dominate in the troposphere ($0 < \text{altitude } (h) < 10 \text{ km}$), the second term in the stratosphere ($10 < h < 50 \text{ km}$) and the third and fourth terms in the mesosphere ($h > 50 \text{ km}$). In the fifth term of the bracket, σ_{λ} and J_{λ} are the absorption cross-section for SF₅CF₃ and the solar flux at wavelength λ , respectively, and Φ_{λ} the quantum yield for dissociation following photoabsorption at wavelength λ . In the troposphere, the summation for λ is over the range ca. 290–700 nm, in the stratosphere ca. 200–290 nm and in the mesosphere the solar flux at the Lyman- α wavelength of 121.6 nm dominates all other vacuum-UV wavelengths. We note that equation (5) assumes that the ion–molecule and electron attachment reactions lead to the removal of every SF₅CF₃ molecule by formation of dissociation products. Furthermore, secondary reactions of such products must not recycle SF₅CF₃. This assumption is true for ion–molecule reactions, but is not necessarily so for electron attachment (Section 6.2).

Having no hydrogen atoms, SF₅CF₃ is very unlikely to be removed by reaction with OH in the troposphere, and the rate coefficient for this reaction is almost certainly too small to be measured by conventional laboratory techniques (e.g. discharge flow or pulsed photolysis with laser-induced fluorescence detection of OH). Likewise, the reaction of O^{*}(¹D) with SF₅CF₃ has not been measured. There are therefore no *chemical* processes that remove SF₅CF₃ from the troposphere

and stratosphere. Furthermore, the electron energy loss spectrum of SF_5CF_3 , in effect a pseudo-absorption spectrum, showed that no bound excited electronic states exist for $h\nu < \text{ca. } 8 \text{ eV}$ (i.e. $\lambda > 150 \text{ nm}$) [23]. Therefore, σ_λ is effectively zero in both the relevant wavelength ranges of the troposphere and stratosphere. These laboratory measurements confirm field measurements from stratospheric profiling that the lifetime of SF_5CF_3 in the Earth's atmosphere is very long as reported by Sturges *et al.* [1]. In Section 5.2, an experiment is described to determine the strength of the $\text{SF}_5\text{--CF}_3$ bond, leading to an improved value for the enthalpy of formation of SF_5CF_3 [20,21]. This experiment was performed in the middle of 2000, the authors having obtained an early preprint of the Sturges *et al.* paper. The principal concern of meteorologists then was to determine this bond strength. The result, that the S–C bond has strong σ -character with a dissociation energy of ca. 4 eV or 400 kJ mol^{-1} , confirmed that UV photolysis in the stratosphere was very unlikely to contribute to the rate of removal of SF_5CF_3 from the atmosphere. In retrospect, and given experiments that have been performed since, this is an obvious result. Attention in recent years has therefore turned to laboratory-based measurements relevant to the mesosphere, where ionic processes involving cations, anions and electrons dominate, and where the only significant photolytic wavelength is 121.6 nm. These experiments are described in Section 6. In Section 7, I draw together all these data, and describe how the lifetime of SF_5CF_3 , ca. 1000 years, is defined and determined.

5. THE VUV PHOTOIONISATION AND PHOTOFRAGMENTATION SPECTROSCOPY OF SF_5CF_3

5.1. Definition of the first dissociative ionisation energy: application to CF_4 and SF_6

Photodissociation generally occurs through excitation of a molecule to a repulsive electronic state which lies above a dissociation threshold. Close to threshold, the cross section for photodissociation can be negligibly small, and this makes the experimental determination of a dissociation energy notoriously difficult. Thus, CF_4 has a dissociation energy (to $\text{CF}_3 + \text{F}$) of 5.61 eV, but VUV photons with energies in excess of 12 eV are required to photodissociate CF_4 . Likewise, the bond dissociation energy of SF_6 (to $\text{SF}_5 + \text{F}$) is 3.82 eV, but photodissociation is not observed until the photon energy exceeds ca. 10 eV. SF_5CF_3 seems to show similar properties. The electron energy loss spectrum [23] suggests that there are no excited electronic states of SF_5CF_3 lying less than ca. 8 eV above the ground state. In the stratosphere, the highest energy solar photons have an energy of ca. 6 eV ($\lambda = \text{ca. } 200 \text{ nm}$). It is therefore very unlikely that SF_5CF_3 will be photodissociated in the stratosphere, irrespective of the strength of the S–C bond, simply

because dissociative electronic states at energies accessible with stratospheric UV photons are not present. The use of *neutral* excited states of SF₅CF₃ to determine its dissociation energy to SF₅ + CF₃ is therefore not viable.

CF₄, SF₆ and SF₅CF₃, however, also share the common property that the parent cation is not observed in a conventional 70 eV electron-impact mass spectrum [39]. Thus the ground electronic state of these cations is repulsive in the Franck–Condon region, dissociating on a time scale much faster than the transit time of an ion through a magnetic or quadrupole mass spectrometer. With CF₄ and SF₆, CF₃–F and SF₅–F bond cleavage to form CF₃⁺ or SF₅⁺ + F + e[−] must occur. With SF₅CF₃, we assume that cleavage of the central S–C bond occurs, forming either SF₅⁺ + CF₃ + e[−] or CF₃⁺ + SF₅ + e[−]. As the threshold energy of the latter dissociation channel lies ca. 0.8 eV lower than that of the former, we assume dissociation within the mass spectrometer to CF₃⁺ + SF₅ + e[−] dominates. (We note that dissociation to SF₄⁺ + CF₄ + e[−] requires even less energy [20,22], driven by the large and negative enthalpy of formation of CF₄, but the significant re-arrangement of chemical bonds needed in the transition state makes this reaction kinetically unfavourable.) Taking SF₅CF₃ as an example, we can define the first *dissociative ionisation energy* (DIE) of these molecules to be the 0 K energy of CF₃⁺ + SF₅ + e[−] relative to the ground vibronic level of the neutral molecule (Fig. 2). This energy has alternatively been called the adiabatic ionisation energy (AIE) of the neutral molecule, but it is this author’s belief that this latter terminology is inappropriate in cases such as CF₄, SF₆ and SF₅CF₃ where the Franck–Condon overlap at threshold is zero. The determination of the DIE of a

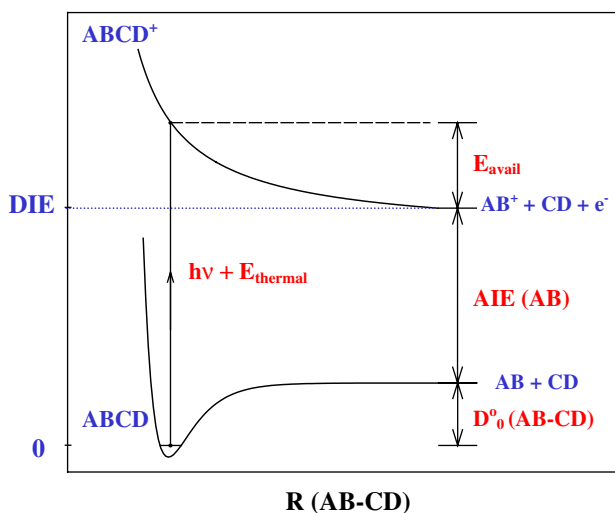


Fig. 2. Definition of the dissociative ionisation energy (DIE) of a generalised polyatomic molecule AB–CD. In the particular application to SF₅CF₃, AB represents CF₃ and CD represents SF₅.

molecule whose ground state of the parent ion is totally repulsive in the Franck–Condon region is a difficult problem because its value is likely to be significantly less than the energy corresponding to the onset of ionisation of the neutral precursor; in the opinion of this author, *onset of ionisation* is a more appropriate phrase to use than AIE for such molecules, as the latter term has ambiguous meanings. Thus the photoelectron spectrum of the parent molecule can only give an upper bound to its first DIE.

This problem is well known for CF_4 and SF_6 , and for many years the DIE of these molecules has been the subject of controversy. However, Fig. 2 can also apply to dissociation of a polyatomic molecule to two molecular free radicals. From the figure, it is clear that,

$$\text{DIE}(\text{ABCD}) = D_o(\text{AB-CD}) + \text{AIE}(\text{AB}) \quad (6)$$

where ABCD refers to a general polyatomic molecule which dissociates along the central B–C bond, $D_o(\text{AB-CD})$ is the dissociation energy of the AB–CD bond and AIE (AB) the adiabatic ionisation energy of the AB free radical; in this situation, the use of AIE is appropriate so long as the ground state of AB^+ is bound in the Franck–Condon region. For SF_5CF_3 , AB will clearly be the CF_3 , and CD the SF_5 radical. For SF_5CF_3 , the estimation of its first DIE requires a knowledge of both the $\text{SF}_5\text{-CF}_3$ bond energy and the AIE of the CF_3 radical. The latter value is now well determined as 9.04 ± 0.04 eV [40], after many years of uncertainty. When Sturges *et al.* [1] published their paper, however, the former value was only known within a broad range of ca. 2–4 eV.

One method to determine the DIE of such molecules directly is to turn the problem around, and use the fact that, in the Franck–Condon region, the ground state of the parent cation lies above the DIE as a benefit rather than a hindrance. The fragments will be formed with translational kinetic energy, and we can perform a photoelectron–photoion coincidence (PEPICO) experiment to measure the mean translational kinetic energy, $\langle \text{KE} \rangle_{\text{T}}$, released into the $\text{AB}^+ + \text{CD}$ fragments; CD is atomic F for dissociation of CF_4 or SF_6 . Using tunable vacuum-UV radiation, it is most convenient to use *threshold* photoelectron detection, and the acronym for this mode of spectroscopy then becomes threshold photoelectron–photoion coincidence (TPEPICO). From an analysis of the width and shape of the fragment ion (AB^+) time-of-flight (TOF) distribution in the TPEPICO spectrum measured at a photon energy $h\nu$, it is possible to determine $\langle \text{KE} \rangle_{\text{T}}$. This KE release will correspond to some fraction of the available energy, where

$$E_{\text{avail}} = h\nu + (\text{thermal energy of ABCD}) - \text{DIE}(\text{ABCD}) \quad (7)$$

The thermal energy of the parent neutral molecule comprises contributions from rotational energy ($3k_{\text{B}}T/2$ per molecule) and vibrational energy ($h\nu_i/\exp(h\nu_i/k_{\text{B}}T) - 1$, summed up for all vibrational modes ν_i). The size of this fraction, $\langle \text{KE} \rangle_{\text{T}}/E_{\text{avail}}$, is governed by the dynamics of the decay mechanism [41]. The

mechanism cannot unambiguously be determined from a measurement at one single photon energy. By measuring $\langle KE \rangle_T$ continuously as a function of $(h\nu + \text{thermal energy of ABCD})$, however, and assuming that the fractional KE release is independent of energy, an extrapolation to a KE release of zero gives an intercept on the x-axis corresponding to the DIE of ABCD (Fig. 3). As the AB⁺–CD bond breaks, if dissociation involves an impulsive release of energy so great that it results in intramolecular collisions between the recoiling fragments (the ‘pure’ impulsive model), then $\langle KE \rangle_T$ and E_{avail} are related only by the kinematics of the dissociation [42]:

$$\langle KE \rangle_T = \frac{\mu_{B,C}}{\mu_{AB,CD}} E_{\text{avail}} \quad (8)$$

where $\mu_{B,C}$ is the reduced mass of the two atoms in the dissociating bond, and $\mu_{AB,CD}$ the reduced mass of the two products of the dissociation. Thus the slope of the graph in Fig. 3 is given simply by the ratio of two reduced masses. As a test of the experiment, we used this method to determine the first DIE for CF₄ and SF₆, where there is some degree of certainty in the correct values now. From the former experiment, we determined the first DIE of CF₄ to be 14.45 ± 0.20 eV. Hence we were able to determine the 0K enthalpy of formation of CF₃⁺ to be 390 ± 20 kJ mol⁻¹ and, via $\Delta_f H_0^0$ (CF₃) [40], the AIE of the CF₃ free radical. Our value, 8.84 ± 0.20 eV, was in good agreement with the now-accepted best experimental determination of 9.04 ± 0.04 eV [40]. The SF₆ experiment determined its first DIE to be 13.6 ± 0.1 eV, leading to a value for $\Delta_f H_0^0$ (SF₅⁺) of 29 ± 10 kJ mol⁻¹. Using the recommended value for $\Delta_f H_0^0$ (SF₅) from the ion beam study of Fisher *et al.* [43], we obtained a value for the AIE for the SF₅ free radical of 9.8 ± 0.2 eV. Within error limits, this value is also in good agreement

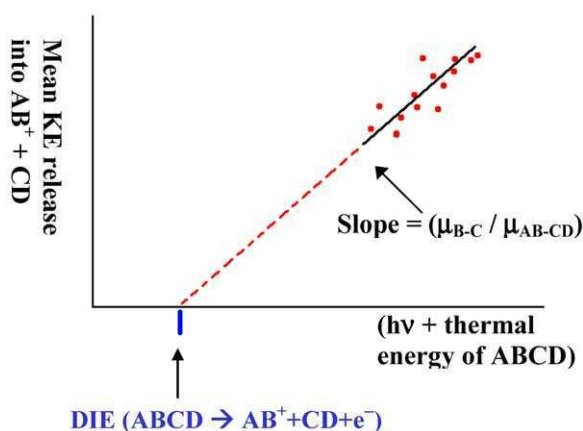


Fig. 3. Extrapolation method to determine the first dissociative ionisation energy of AB–CD.

with the guided ion beam result of 9.60 ± 0.05 eV [43]. Following these test experiments, full details of which are given elsewhere [20,21], we measured the first DIE of SF_5CF_3 (Section 5.3). Using the now well-established ionisation energy (IE) of CF_3 , we were able to determine, admittedly in an indirect manner, the dissociation energy of the $\text{SF}_5\text{--CF}_3$ bond.

5.2. Experimental details

The apparatus used for the TPEPICO study [44] is shown in Fig. 4, the source of radiation being beamline 3.1 (1 m Seya-Namioka monochromator) of the UK Daresbury Synchrotron Radiation Source operating at a resolution of 0.3 nm. The monochromatised radiation is coupled into the interaction region via a capillary, and its flux is monitored from the fluorescence of a sodium salicylate-coated window. Threshold photoelectrons and fragment cations from the interaction

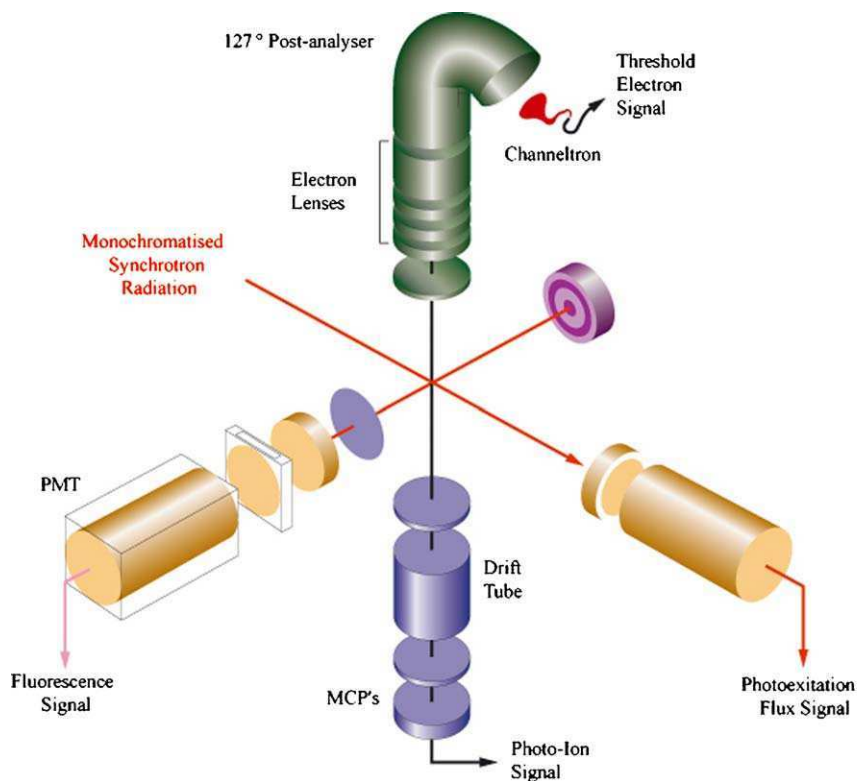


Fig. 4. Schematic of the threshold photoelectron–photoion coincidence apparatus. The apparatus can also study coincidences between threshold photoelectrons or mass-resolved cations with fluorescence photons, but these modes of operation are not used in this work.

region are extracted in opposite directions by an electric field of 20 V cm⁻¹. The threshold electron analyser consists of a cylindrical electrostatic lens followed by a 127° post analyser, which rejects energetic electrons. The lens has a shallow depth of field and poor chromatic aberrations, so that only electrons with low initial energies produced in the centre of the interaction region focus efficiently at the entrance of the post analyser. Simulations suggest a high degree of space focusing, so a finite interaction volume is relatively unimportant. The resolution of the electron analyser, ca. 10 meV, is superior to that of the monochromator in these experiments; therefore, the overall resolution of the experiment is limited by that of the photon source. Ions pass through a two-stage acceleration region followed by a linear TOF drift tube. This arrangement satisfies the space focusing condition, yielding sufficient TOF resolution so that kinetic energy releases from dissociative ionisation events can be measured. Signals from the channeltron and microchannel plate detectors are discriminated and conveyed to a time-to-digital converter (TDC) card via pulse-shaping electronics. The electron signal provides the start pulse, the ion signal provides the stop pulse, and delayed coincidences can be recorded. Concurrently, the total ion yield and threshold photoelectron spectrum (TPES) can also be measured.

With this apparatus, three different spectra can be recorded. First, the TPES spectrum is obtained by recording the threshold electron signal as a function of photon energy. Second, a TPEPICO spectrum is obtained by recording the coincidence spectrum continuously as a function of photon energy. The data record as a 3D map of coincidence counts vs. ion time of flight vs. photon energy. Sections from this map can yield either the TOF mass spectrum at a defined photon energy or the yield of a particular ion. Third, with a fixed photon energy, high-resolution TOF spectra can be recorded and values for $\langle KE \rangle_T$ obtained [45,46]. Briefly, for each TPEPICO–TOF spectrum a small basis set of peaks, each with a discrete energy release ε_t is computed, and assigned a probability. The discrete energies are given by $\varepsilon_t(n) = (2n-1)^2\Delta E$, where $n = 1, 2, 3, 4 \dots$. ΔE depends on the statistical quality of the data; the higher the signal-to-noise ratio, the lower ΔE and the higher n can be set to obtain the best fit. Each computed peak in the kinetic energy release distribution spans the range $4(n-1)^2\Delta E$ to $4n^2\Delta E$, centred at $\varepsilon_t(n) + \Delta E$. The reduced probability of each discrete energy, $P(\varepsilon_t)$, is varied by linear regression to minimise the least-squared errors between the simulated and experimental TOF peak. From the basis set of ε_t and $P(\varepsilon_t)$, $\langle KE \rangle_T$ is easily determined.

5.3. Determination of the first dissociative ionisation energy of SF₅CF₃ and the S–C bond strength

The three modes of experiment described above were performed for SF₅CF₃ [20]. In addition, to determine the first DIE, important aspects of the second and

third mode were combined. Thus the TOF spectrum for CF_3^+ was recorded over a narrow time window with a resolution of 16 ns, close to the optimum of the TDC card of 8 ns, and 64 wavelength channels were scanned over the energy range 12.9–15.7 eV, encompassing the Franck–Condon zone of the ground state of SF_5CF_3^+ . The results are shown in Fig. 5. Only those datapoints that define the Franck–Condon region, ca. 13.2–14.8 eV, were used to determine the slope and intercept of the graph. The onset of ionisation for SF_5CF_3 , 12.9 ± 0.2 eV, lies significantly lower in energy than that in either CF_4 or SF_6 , reflecting the different character of the HOMO. The mean KE releases over these channels range from 0.05 eV to 0.4 eV. As one example, Fig. 6 shows the TPEPICO–TOF spectrum of $\text{CF}_3^+/\text{SF}_5\text{CF}_3$ recorded at 14.09 eV and the best simulated fit, from which a mean KE release of 0.24 ± 0.05 eV was determined. Within experimental error, the 35 lowest energy data points which encompass the Franck–Condon region of the ground state of SF_5CF_3^+ fit to a straight line with a slope of 0.19, in excellent agreement with the prediction of the pure-impulsive model of 0.20. Extrapolation to a KE release of zero on the y -axis yields the first DIE of SF_5CF_3 to

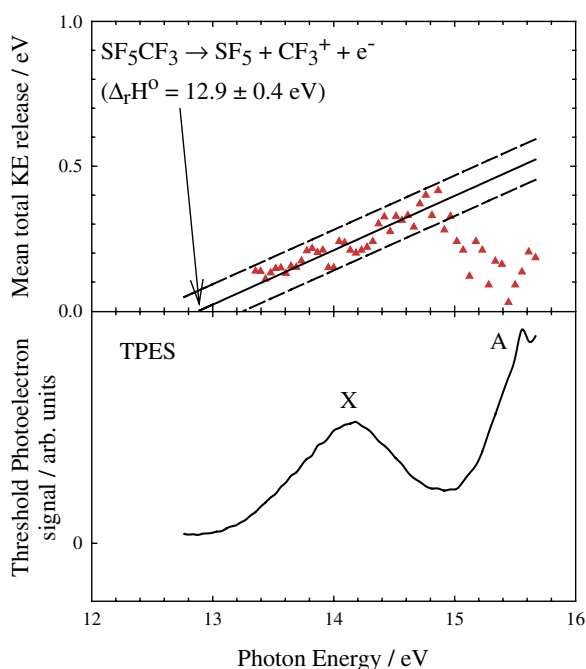


Fig. 5. Results of the extrapolation experiment for $\text{CF}_3^+ + \text{SF}_5$ from SF_5CF_3 . Only datapoints that define the Franck–Condon region of the ground state of SF_5CF_3^+ are used to define the slope and intercept of the graph [20]. The slope is 0.19 and the first dissociative ionisation energy of SF_5CF_3 is determined to be 12.9 ± 0.4 eV. (Reproduced with permission from *J. Phys. Chem. A*, 105 (2001) 8403–8412.)

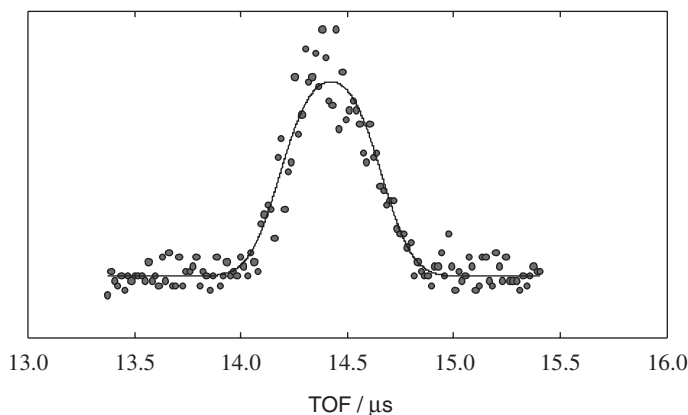


Fig. 6. TPEPICO–TOF spectrum (closed circles) for CF₃⁺/SF₅CF₃ recorded at a photon energy of 14.09 eV. Shown as a solid line is the data fit to a mean translational KE release, $\langle KE \rangle_T$, of 0.24 ± 0.05 eV. (Reproduced with permission from *J. Phys. Chem. A*, 105 (2001) 8403–8412.)

CF₃⁺ + SF₅ + e[−] to be 12.9 ± 0.4 eV. The relatively large error in the DIE reflects the small slope of the $\langle KE \rangle_T$ vs. photon energy graph, and hence the shallow nature of the extrapolation. We should note that the DIE, unlike that of CF₄ and SF₆, is coincidentally isoenergetic with the ionisation onset of the first photoelectron band of SF₅CF₃; for both CF₄ and SF₆, the first DIE lies over 1 eV lower than the onset of ionisation, leading to a longer extrapolation to zero $\langle KE \rangle_T$.

Two important thermochemical data can now be determined. First, using values for the 0 K enthalpies of formation of CF₃⁺ (409 ± 3 kJ mol^{−1}) [40] and SF₅ (-915 ± 18 kJ mol^{−1}) [43], we determine $\Delta_f H_0^0$ (SF₅CF₃) to be -1750 ± 47 kJ mol^{−1}, significantly lower than that quoted in the 1998 JANAF tables [29]. Second, using the now-accepted value for AIE (CF₃) of 9.04 ± 0.04 eV [40], we determine the dissociation energy of the SF₅–CF₃ bond at 0 K to be 3.86 ± 0.45 eV or 372 ± 43 kJ mol^{−1}. (We note that these values are updates of those published in ref. [20], following improvements in the published thermochemical values for CF₃ and CF₃⁺.) Using the value for AIE (SF₅) with the highest claim for accuracy from Fisher *et al.* [43], 9.60 ± 0.05 eV, the *second* DIE of SF₅CF₃ (defined here to be SF₅⁺ + CF₃ + e[−]) is calculated to be 13.46 ± 0.45 eV. This energy is ca. 0.6 eV higher than the first DIE to CF₃⁺ + SF₅ + e[−], and presumably explains why only CF₃⁺ is observed for dissociation of the low-energy regions of the ground-state potential of SF₅CF₃⁺.

At this stage it is only proper to highlight the assumptions and limitations of this extrapolation technique. The errors quoted for the first DIE of CF₄, SF₆ and SF₅CF₃ arise from random statistical errors in the data for $\langle KE \rangle_T$. Two factors have been ignored which might produce systematic errors. First, the theory assumes that dissociation is 100% impulsive with no statistical component. The

simple relation between $\langle KE \rangle_T$ and E_{avail} (equation (8)) arises from classical mechanics, with linearity in the extrapolation graph (Fig. 3) applying even for very low values of $\langle KE \rangle_T$. This is most likely to be true when the onset of ionisation to $ABCD^+$ is significantly greater than the DIE of $ABCD$. This is the situation for CF_4 and SF_6 , but not perhaps for SF_5CF_3 . Second, anisotropic effects are ignored in the analysis, despite the vacuum-UV radiation source being close to fully plane-polarised perpendicular to the TOF axis. More details of these potential problems are given elsewhere [20].

Theoretical values for $\Delta_f H_0^0$ (SF_5CF_3) are significantly less negative than the experimental value, yielding weaker SF_5-CF_3 bond strengths. Ball [30] and Miller *et al.* [32], both using Gaussian-2 (G2) and Gaussian-3 (G3) Moller–Plesset perturbation methods, found $\Delta_f H_0^0$ to be -1615 and -1623 kJ mol^{-1} , respectively, the former being the average of G2 and G3 calculations. Using experimental values for the 0 K enthalpy of formation of CF_3 and SF_5 [40,43], they yield S–C bond strengths of 237 and 245 kJ mol^{-1} , respectively. It is worth noting that, while there has been convergence in recent years between experiment and theory yielding an accepted value for $\Delta_f H_0^0$ (CF_3), this has not been the case for the SF_5 radical where theory [47] and experiment [43] differ by over 70 kJ mol^{-1} . Using Irikura's value for $\Delta_f H_0^0$ (SF_5) [47], for example, Ball [30] predicts a S–C bond strength of 311 kJ mol^{-1} , much closer to our experimental value of 372 ± 43 kJ mol^{-1} . Xu *et al.* [33], using varying density functional methods but without zero point vibrational energy corrections, obtained dissociation energies for $SF_5CF_3 \rightarrow SF_5 + CF_3$ ranging between 1.9 and 3.1 eV (ca. 180–300 kJ mol^{-1}). While there are no atmospheric implications for SF_5CF_3 from these differing values for its enthalpy of formation, it is surprising and slightly concerning that experiment and theory differ by as much as 100 kJ mol^{-1} , ca. 1 eV, for a microscopic property as fundamental as the 0 K enthalpy of formation. State-of-the-art *ab initio* calculations on the SF_5-CF_3 bond strength are currently being performed with full configuration interaction and a much larger basis set than has been used to date [48]. The calculations are not yet complete, but early indications are that the S–C bond strength may be much closer to the experimental value [20] than the earlier calculations.

5.4. Threshold photoelectron spectrum of SF_5CF_3

In the final two parts of Section 5, I describe additional and important information on an isolated SF_5CF_3 molecule that resulted from this TPEPICO study. The valence TPES of SF_5CF_3 was measured from 12.7 to 26.4 eV with a resolution of 0.3 nm (Fig. 7). No vibrational structure was observed. The onset of ionisation, defined as the energy at which signal is first observed above the background noise, is 12.92 ± 0.18 eV. The vertical IE of this first band occurs at 14.13 eV. The

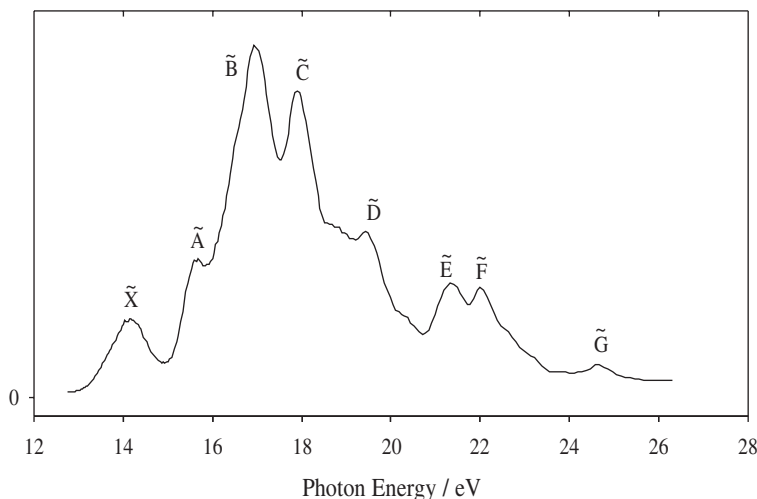


Fig. 7. Threshold photoelectron spectrum of SF₅CF₃ recorded at a resolution of 0.3 nm. Assignment of the bands to the ground state (\tilde{X}) and excited electronic states ($\tilde{A}, \tilde{B}, \tilde{C}$, etc.) of SF₅CF₃⁺ is shown. (Reproduced with permission from J. Phys. Chem. A, 105 (2001) 8403–8412.)

low value of this vertical IE, ca. 2 eV lower than that in both CF₄ and SF₆ where the HOMO has F 2p π non-bonding character, has already been noted. The large difference between the onset of ionisation and the vertical IE suggests a significant change in geometry between neutral ion and cation, probably in the S–C bond length, compatible with a repulsive ground state of the parent cation along this coordinate. *Ab initio* calculations on the structure of SF₅CF₃ by Knowles [9] at the Hartree–Fock level were described briefly in Section 2. The predicted structure, detailed in the caption of Fig. 1, is in good agreement with that from gas-phase electron diffraction [8]. No other structures of molecules with stoichiometry C₁S₁F₈ are stable. The HOMO of SF₅CF₃ has a large S–C σ -bonding character, whereas the next three orbitals lie ca. 2.7 eV lower in energy and are F 2p π non-bonding in character. No minimum-energy geometry of the ground state of SF₅CF₃⁺ can be obtained at either the Hartree–Fock or the MP2(full)/6–31 g(d) level, giving further evidence that this state is indeed unbound. Results from these simple calculations have recently been confirmed using the GAMESS-UK suite of programs with a variety of basis sets [15]. Higher energy peaks in the TPES are observed at 15.68, 16.94, 17.86, 19.44, 21.34, 22.01 and 24.67 eV. Attempts have now been made to assign these peaks in the TPES and to know how they correlate with peaks in the (T)PES of both CF₄ and SF₆ [15]. The evidence from the vacuum-UV absorption and valence photoelectron spectrum of SF₅CF₃ is that this molecule behaves more like a perturbed SF₆ than a perturbed CF₄ molecule [15].

5.5. Ion yields and fixed-energy TPEPICO spectra of SF₅CF₃

The TOF spectrum of the fragment ions from SF₅CF₃, integrated over the whole range of VUV photoexcitation energies 12.7–26.4 eV, is shown in Fig. 8. The parent ion is not observed. CF₃⁺ and SF₃⁺ are the dominant ions, then SF₅⁺, with CF₂⁺ and SF₄⁺ being very weak. Table 2 shows threshold energies for their production. We first consider the *major* ions, defined as those formed by a single bond cleavage; reactions in which there is no barrier in the exit channel and hence, in the conventional sense, no transition state. The ion yield of CF₃⁺ follows that of the TPES of SF₅CF₃ from the onset of ionisation to ca. 20 eV, and states of the parent ion with vertical energies below 20 eV dissociate predominantly to this ion. By contrast, the SF₅⁺ signal is so weak that it is not possible to say whether its ion yield shows any correlation with electronic states of SF₅CF₃⁺. Even well above the SF₅⁺ threshold of 13.9 eV, its ion yield relative to that of CF₃⁺ remains very weak. These thresholds and relative intensities are in good agreement with a tunable electron energy beam study over the same range of energies [22]. This behaviour is somewhat surprising for a large polyatomic cation with ten atoms and a correspondingly large density of vibronic states. These dissociation properties of SF₅CF₃⁺ suggest that it behaves more like a pseudo-diatomic molecule

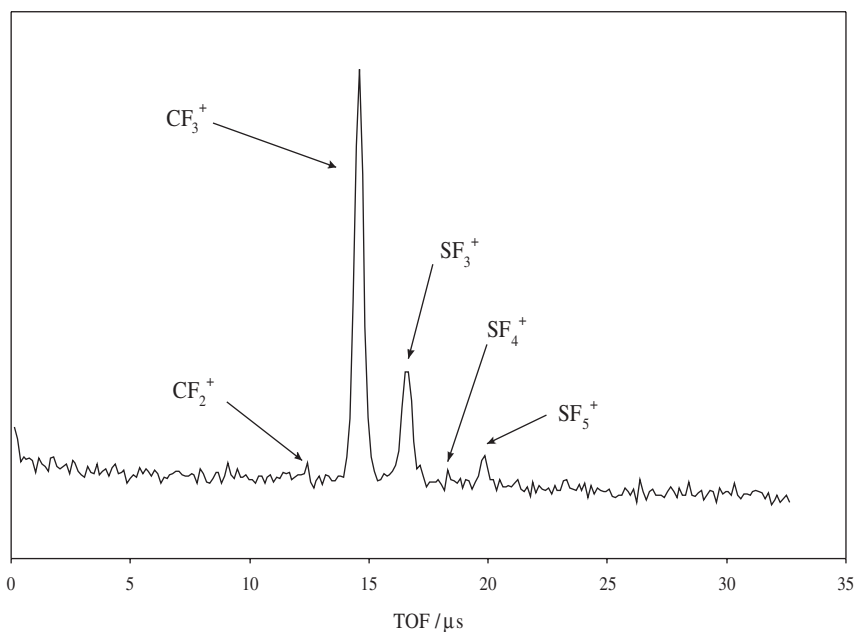


Fig. 8. Time-of-flight spectrum of fragment ions from SF₅CF₃ integrated over the photoexcitation energies of 12.7–26.4 eV. (Reproduced with permission from J. Phys. Chem. A, 105 (2001) 8403–8412.)

Table 2. Appearance energies of fragment ions from SF₅CF₃ over the photo-excitation energy range 12.7–26.4 eV.

Fragment ion	AE_{298} (eV)	Neutral partner	$\Delta_r H_0^\circ$ (eV)
Major ions ^a			
CF ₃ ⁺	12.92 ± 0.18	SF ₅	12.90
SF ₅ ⁺	13.9 ± 1.2	CF ₃	13.67
Minor ions ^b			
SF ₄ ⁺	13.5 ± 1.3	CF ₄	12.42
SF ₃ ⁺	14.94 ± 0.13	CF ₄ + F	12.36
CF ₂ ⁺	16.0 ± 2.0	SF ₆	15.22

^a A *major* ion is defined as one formed by a single bond cleavage; formation of CF₃⁺ and SF₅⁺ involves cleavage of the S–C bond.

^b A *minor* ion is defined as one in which intramolecular rearrangement must occur. Note that the formation of SF₄⁺, SF₃⁺ and CF₂⁺ is only possible at their observed appearance energies given in Column 2 if migration of F[−] across the S–C bond occurs in the transition state to form CF₄ and SF₆, respectively, as accompanying neutrals.

with a much lower density of states, dissociating only on one repulsive potential energy surface with no curve crossings. By contrast, the *minor* ions are defined as those which can only form following intramolecular rearrangement within a transition state of the unimolecular reaction following photoexcitation. The threshold energy for the strongest minor ion, SF₃⁺, is 14.94 ± 0.13 eV. Energetically, it can only form at this energy if the accompanying neutral fragments are CF₄ + F. Likewise, the two very weak minor ions, SF₄⁺ and CF₂⁺, can only form at their thresholds (Table 2) if migration of F[−] across the S–C bond occurs in the transition state to form CF₄ and SF₆, respectively. Such migrations in unimolecular reactions are usually only associated with H(D) atoms, but F-atom migration across a C–X bond has been observed in fragmentation of other long-lived greenhouse gases, for example the perfluorocarbon cations, C_xF_y⁺ [49].

Table 3 shows values for the mean translational KE release into CF₃⁺ + SF₅ when SF₅CF₃ is excited into the ground and first four excited states of the parent ion. The procedure is described in Section 5.2. Columns 5–7 show the experimental fractional release into translational energy ($f_{\text{expt}} = \langle \text{KE} \rangle_{\text{T}} / E_{\text{avail}}$) and the predictions of statistical [50] and pure-impulsive [42] models. It was noted in Section 5.3 that for dissociation of the ground state of SF₅CF₃⁺, the value for f_{expt} at 14.25 eV, 0.21, is very close to that predicted by the pure-impulsive model. This is as expected, because the Franck–Condon maximum of the ground state of SF₅CF₃⁺ lies ca. 1.3 eV higher than the dissociation threshold to CF₃⁺ + SF₅ + e[−]. Dissociation from this repulsive potential energy surface is therefore expected to occur rapidly on a sub-picosecond timescale, with a relatively large amount of the available energy being released into translation of the

Table 3. Total mean translational kinetic energy release, $\langle KE \rangle_T$, for the two-body fragmentation of the valence states of $SF_5CF_3^+$.

Fragment	E (eV)	E_{avail} (eV) ^a	$\langle KE \rangle_T$ (eV)	f_{expt}	$f_{statistical}$ ^b	$f_{pure\ impulsive}$ ^c
CF_3^{+d}	14.25	1.52	0.32 (5)	0.21	0.04	0.20
	15.69	2.96	0.29 (2)	0.10	0.04	0.20
	16.98	4.25	0.38 (1)	0.09	0.04	0.20
	17.97	5.24	0.40 (1)	0.08	0.04	0.20
	19.07	6.34	0.37 (1)	0.06	0.04	0.20

^a E_{avail} is defined in equation (7). The average thermal energy of SF_5CF_3 is 0.17 eV.

^b From Klots [50].

^c From Holdy, Klotz and Wilson [42].

^d Assumes the neutral fragment is SF_5 .

two fragments. As the photon energy increases to 19 eV, however, f_{expt} decreases by a factor of ca. 3–4. It appears that as higher energy electronic states of $SF_5CF_3^+$ are populated, there is a reduced coupling of the initially excited vibrational modes into the reaction coordinate, behaviour that is normally associated with a multi-atom polyatomic species. This phenomenon, that the value of $\langle KE \rangle_T$ does not increase as rapidly with photon energy as a pure-impulsive model would predict, has also been observed in dissociation reactions in other polyatomic molecules, CF_3^+ from CF_4 and SF_5^+ from SF_6 [51].

6. REMOVAL PROCESSES OF SF_5CF_3 FROM THE EARTH'S ATMOSPHERE IN THE MESOSPHERE

The larger-than-expected value of the S–C bond strength [20] and the absence of excited electronic states of SF_5CF_3 lying below ca. 8 eV [23] led scientists to study processes in the mesosphere that could remove this greenhouse gas from the atmosphere; reactions with cations, electrons and vacuum-UV photodissociation (the last three terms in the bracket of equation (5)).

6.1. Reactions of SF_5CF_3 with cations and anions

Two papers have described the reactions of cations with SF_5CF_3 [52,53] and one with anions [54]. All these studies have been made in a selected ion flow tube (SIFT), and a schematic of this apparatus is shown in Fig. 9. Such an experiment can determine the rate coefficient and product ions and their branching ratios for the reactions of small anions or cations with neutral molecules, generically $A^\pm + BC \rightarrow D^\pm + EF$, where the ions can be atomic or molecular. Only fast

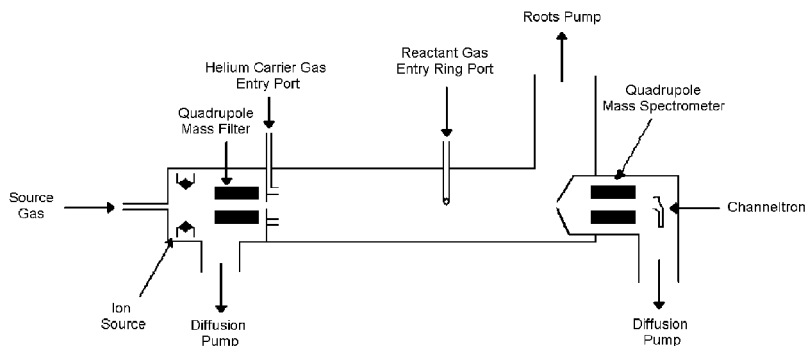


Fig. 9. Schematic of the selected ion flow tube used to determine rate coefficients and product ion yields of ion–molecule reactions. (Reproduced with permission of Dr C.R. Howle, PhD thesis, University of Birmingham, 2004.)

reactions with rate coefficient greater than ca. $10^{-13} \text{ cm}^3 \text{ molecule}^{-1} \text{ s}^{-1}$ can be studied. In brief, a reagent ion of interest is produced in a high-pressure electron impact ion source containing an appropriate source gas. The cation or anion is injected through a quadrupole mass filter into a flow tube holding ca. 0.5 Torr of high purity helium as a buffer gas. The neutral reactant of choice is then admitted through an inlet at one of various points down the flow tube. The resultant ionic products are detected using a quadrupole mass spectrometer. The loss of reagent ion signal, alongside the increase in the various product ion signal(s), is recorded as a function of neutral reactant concentration. The amount of neutral is altered between zero and a concentration that depletes the reactant ion signal by ca. 90%. As the experiment operates under pseudo-first-order conditions with $[A^\pm] \ll [BC]$, and with knowledge of the reaction length and ion flow velocity, a plot of the logarithm of the reagent ion signal vs. neutral molecule concentration allows the rate coefficient to be determined. Percentage branching ratios for each product ion are derived from graphs of the relative product ion counts vs. neutral molecule concentration, with extrapolation to zero neutral gas flow to allow for the effect of any secondary reactions. Most of the Birmingham, UK studies are made at 298 K, whereas the Air Force Research Laboratories, US apparatus can operate over the temperature range ca. 250–500 K.

Unrelated to the atmospheric importance of such reactions for SF₅CF₃, an additional motivation for such studies is to understand the importance of long-range charge transfer in cation–molecule reactions. Charge transfer can occur either at long range or at short range. In the long-range mechanism, assuming BC has a permanent dipole moment, A⁺ and BC approach under the influence of their charge–dipole interaction, until at some critical distance (R_c) the A⁺-BC and A-BC⁺ potential energy curves cross. At this point an electron jump can take place. We have shown [55] that R_c depends on the difference in energy between the recombination energy (RE) of A⁺ and the IE of BC; the smaller this difference, the

larger the R_c . (The RE is defined as the energy that is released when a cation forms its neutral compound.) Furthermore, two important factors for a rapid electron transfer and an efficient long-range charge transfer process are a non-zero energy resonance connecting BC to an electronic state of BC^+ at the RE of A^+ , and the transferring electron coming from a molecular orbital of BC that is not shielded from the approaching cation. So long as there is some overlap of vibrational wavefunction between BC and BC^+ at the RE of A^+ , the magnitude of the photoionisation Franck–Condon factor for BC is not as important as originally thought in determining the efficiency of such a reaction. We note that if this long-range charge transfer mechanism operates, then the branching ratios for fragmentation of $(BC^+)^{(*)}$, where (*) denotes the possibility of BC^+ being in an excited electronic state, are expected to be independent of how this state is produced. Hence, we would expect similar product branching ratios from the ion–molecule study and the TPEPICO photoionisation study, assuming that the photon energy in the latter experiment matches the RE of A^+ in the former.

When long-range charge transfer is unfavourable, A^+ and BC move closer together. As their separation decreases, distortion of the potential energy surface of interaction occurs. Eventually, a curve crossing can occur through which efficient charge transfer takes place. This is called short-range charge transfer. As an intermediate complex has formed, a chemical reaction, defined as the breaking and making of new bonds, may, in addition, compete with short-range charge transfer. This means that it is unlikely that the product branching ratios from the ion–molecule and the TPEPICO experiments will mimic each other. Thus, a comparison of the fragmentation patterns from the SIFT and TPEPICO experiments, together with an analysis of the TPES of BC at the energy of the RE of A^+ , may indicate which mechanism, be it long-range or short-range, is dominant for the reaction of each cation. Agreement within ca. $\pm 15\%$ is taken as evidence for possible long-range charge transfer [56]. We have made this comparison for the reactions of SF_5CF_3 with those cations whose concentrations are the highest in the mesosphere, and might therefore be expected to contribute to the removal of SF_5CF_3 from the Earth's atmosphere.

The results of the SIFT study for reactions of SF_5CF_3 with the important atmospheric cations N_2^+ , N^+ , CO^+ , CO_2^+ , O^+ , N_2O^+ , H_2O^+ and O_2^+ are shown in Table 4. The RE values of these cations range from 15.58 (for N_2^+) to 12.07 eV (for O_2^+). The first five ions have RE values greater than the onset of ionisation of SF_5CF_3 , so in principle long-range charge transfer may occur. The last three cations have RE values below the onset of ionisation, so can only react via a short-range process and the formation of a reaction intermediate. Seven of the eight ions react with a rate coefficient close to or equal to the Langevin capture value [57]. O_2^+ reacts significantly slower. The reactions of the six cations with RE in the range 12.89 to 15.58 eV (i.e. those equal to or greater than the onset of ionisation of SF_5CF_3) appear to occur by dissociative charge transfer, with CF_3^+

Table 4. Rate coefficients, cation product ions and their branching ratios for the reactions of cations with possible atmospheric importance with SF₅CF₃. The recombination energies of the reagent cations are listed in eV in brackets under the cations. The capture rate coefficients, calculated using Langevin theory [57], are presented in square brackets under the experimental values. Zero K enthalpies of reaction for these channels are given in Column 5. For formation of SF₃⁺ and SF₄⁺, two values for $\Delta_r H_0^\circ$ are given. The first value is calculated using the data set of Fisher *et al.* [43]; whereas, the second corresponds to that of Irikura [47]. The two values given for $\Delta_r H_0^\circ$ for formation of SF₅⁺ by dissociative charge transfer result from taking the IE (SF₅) to be either 9.60 eV [43] or 9.71 eV [47].

Reagent ion	Rate coefficient ($\times 10^{-9} \text{ cm}^3 \text{ s}^{-1}$)	Product ion (%)	Proposed neutral products	$\Delta_r H_0^\circ$ (kJ mol ⁻¹)
N ₂ ⁺ (15.58)	1.6 [1.4]	CF ₃ ⁺ (65)	SF ₅ + N ₂	-258
		SF ₃ ⁺ (28)	CF ₄ + F + N ₂	-248, -289
		SF ₄ ⁺ (trace)	CF ₄ + N ₂	-283, -345
		SF ₄ ⁺ CF ₃ (2)	F + N ₂	?
		SF ₅ ⁺ (5)	CF ₃ + N ₂	-185, -175
N ⁺ (14.53)	2.2 [1.9]	CF ₃ ⁺ (80)	SF ₅ + N	-157
		SF ₃ ⁺ (17)	CF ₄ + F + N	-147, -187
		SF ₄ ⁺ (trace)	CF ₄ + N	-181, -243
		SF ₅ ⁺ (3)	CF ₃ + N	-84, -73
		CF ₃ ⁺ (75)	SF ₅ + CO	-107
CO ⁺ (14.01)	1.6 [1.4]	SF ₃ ⁺ (22)	CF ₄ + F + CO	-96, -137
		SF ₄ ⁺ (trace)	CF ₄ + CO	-131, -193
		SF ₅ ⁺ (3)	CF ₃ + CO	-34 (± 43), -23 (± 46)
		CF ₃ ⁺ (76)	SF ₅ + CO ₂	-84
		SF ₃ ⁺ (14)	CF ₄ + F + CO ₂	-73, -114
CO ₂ ⁺ (13.77)	1.2 [1.1]	SF ₄ ⁺ (8)	CF ₄ + CO ₂	-108, -170
		SF ₅ ⁺ (2)	CF ₃ + CO ₂	-11 (± 43), 0 (± 46)
		CF ₃ ⁺ (83)	SF ₅ + O	-69
		SF ₃ ⁺ (16)	CF ₄ + F + O	-59, -100
		SF ₄ ⁺ (trace)	CF ₄ + O	-93, -156
O ⁺ (13.62)	1.9 [1.8]	SF ₅ ⁺ (1)	CF ₃ + O	4 (± 43), 14 (± 46)
		CF ₃ ⁺ (75)	SF ₅ + N ₂ O	1 (± 39)
		SF ₃ ⁺ (19)	CF ₄ + F + N ₂ O	12 (± 45), -29 (± 47)
		SF ₄ ⁺ (5)	CF ₄ + N ₂ O	-23 (± 45), -85
		SF ₅ ⁺ (1)	CF ₃ + N ₂ O	74, 84
H ₂ O ⁺ (12.61)	1.6 [1.7]	CF ₃ ⁺ (8)	SF ₅ + H ₂ O	28 (± 39)
		SF ₃ ⁺ (92)	CF ₄ + F + H ₂ O	39 (± 45), -2 (± 47)
		SF ₄ ⁺ (trace)	CF ₄ + H ₂ O	4 (± 45), -58
		CF ₃ ⁺ (63)	SF ₅ + O ₂	80, 62, 43 (± 39) ^a
		SF ₃ ⁺ (31)	CF ₄ + F + O ₂	91, 50 (± 47)
O ₂ ⁺ (12.07)	0.01 [1.3]	SF ₄ ⁺ (2)	CF ₄ + O ₂	56, -6 (± 46)
		SF ₅ ⁺ (4)	CF ₃ + O ₂	153, 164

^a The three values given are for the $\nu = 0, 1$ and 2 vibrational levels of O₂⁺, respectively.

and SF_3^+ being the dominant product ions. It seems likely that CF_3^+ forms by direct breaking of the S–C bond, whereas SF_3^+ may form from dissociation of $(\text{SF}_4^+)^*$ following intramolecular rearrangement within a reaction intermediate. The evidence for formation of such an intermediate lies in the SF_3^+ branching ratios. Significant values, ca. 10–20%, are observed for reactions of N^+ , CO^+ , CO_2^+ , O^+ and N_2O^+ despite the fact that these ions have RE values less than 14.94 eV, the appearance energy at 298 K (AE_{298}) of this cation in the photon-induced study (Section 5.5) [20]. Only the yield of SF_3^+ from the N_2^+ reaction, 28%, gets close to approaching that from the photon-induced reaction at $h\nu = 15.58$ eV, 25%. Note also that the SF_3^+ ion is dominant for the H_2O^+ reaction, 92%, although this ion has an RE value 0.3 eV below the onset of ionisation of SF_5CF_3 . Thus the evidence is that, with the possible exception of N_2^+ , all reactions yielding SF_3^+ proceed via the formation of an intermediate at short range, followed by intramolecular re-arrangement and migration of F^- across the S–C bond to form CF_4 as an accompanying, thermochemically stable neutral partner. Table 4 also highlights the difficulties in using the experimental values of Fisher *et al.* [43] for the enthalpies of formation of $\text{SF}_x^{(+)}$, in that some ‘fast’ reactions are calculated to be significantly endothermic. Thus, Column 5 of Table 4 also shows values for $\Delta_r H_0^\circ$ calculated using the theoretical values of Irikura [47] for $\Delta_f H_0^\circ$ ($\text{SF}_x^{(+)}$), where his more negative values make such reactions exothermic.

In theory, the rate coefficients and products of such reactions should be used to model the fate of SF_5CF_3 in the mesosphere and hence its atmospheric lifetime. However, despite the fact that these reactions are fast, ca. 10^{-9} cm^3 molecule $^{-1}$ s $^{-1}$, they are still over an order of magnitude slower than low-energy electron attachment (Section 6.2). Furthermore, the concentrations of such positive ions in the mesosphere are also at least an order of magnitude lower than that of free electrons [58]. Therefore, the reactions of both cations and anions with SF_5CF_3 , while yielding a huge amount of information at the microscopic level, makes very little contribution to the atmospheric chemistry of this molecule as the reactions are too slow and the ion concentrations too low; the third term in the bracket in the right-hand-side of equation (5) is negligibly small. Although this section has concentrated on the reactions of *cations* with SF_5CF_3 , mainly because of the comparison with the TPEPICO data and hence an understanding of reaction mechanisms, the arguments in this paragraph also hold true for the reactions of *anions* with SF_5CF_3 .

6.2. Reactions of SF_5CF_3 with low-energy electrons

As the mesosphere is electrically neutral, the total concentration of positive ions must be balanced by the concentration of anions and free electrons, and Adams

and Smith [58] estimated a mean electron number density of 10^5 cm^{-3} for altitudes in the range $100 < h < 200 \text{ km}$, falling rapidly to 10^3 cm^{-3} for $h \approx 80 \text{ km}$. The mesosphere is thermalised with a temperature in the range 170–250 K, the lowest temperature occurring at the mesopause, $h \approx 85 \text{ km}$. The average thermal energy of the electrons, $3k_{\text{B}}T/2$, is therefore low, ca. 0.02–0.03 eV, and laboratory studies of low-energy electron attachment to SF₅CF₃ can give an important guide to reactions that may occur in the mesosphere.

Several groups have made such measurements. The group of Mayhew in Birmingham, UK [59] uses a Swarm apparatus to determine absolute electron attachment cross sections, rate coefficients and products of the low-energy attachment. The Air Force Research Laboratory group of Viggiano [32] uses a flowing afterglow Langmuir probe (FALP) apparatus whose temperature can be controlled between ca. 300 and 550 K. They can also measure the rate coefficient for low-energy electron attachment and the products of such reactions. Both give near-identical results for SF₅CF₃. Mayhew and Kennedy [59] measured the thermal attachment rate coefficient to be $7.7 \pm 0.6 \times 10^{-8} \text{ cm}^3 \text{ molecule}^{-1} \text{ s}^{-1}$, with the only anionic product being SF₅⁻. Miller *et al.* [32] measured the rate coefficient at 296 K to be slightly higher, $8.6 \pm 2.2 \times 10^{-8} \text{ cm}^3 \text{ molecule}^{-1} \text{ s}^{-1}$, the rate constant increasing very slightly with increasing temperature giving an Arrhenius activation barrier of 25 meV or 2.4 kJ mol⁻¹. Again, the only observed charged product is SF₅⁻. The groups of Illenberger (Berlin, Germany) [25] and Märk (Innsbruck, Austria) [26] operate under collision-free beam conditions and use a tunable electron beam with energies in the range ca. 0–15 eV. Absolute cross sections and rate coefficients cannot be determined, but the presence of low-energy resonances leading to the production of certain anions can be measured. For SF₅CF₃, both beam studies show a large dissociative electron attachment cross section at 0 eV to form SF₅⁻ + CF₃, in excellent agreement with the Swarm and FALP studies. The 0 eV CF₃⁻ peak is over four orders of magnitude weaker [25]. Of less importance to the atmospheric chemistry of SF₅CF₃, absolute cross sections for electron scattering at much higher electron energies, 100–10,000 eV, have been measured [24].

A schematic of the Birmingham Swarm apparatus, described in detail elsewhere [60], is shown in Fig. 10. The source of electrons is a radioactive ⁶³Ni β-emitting sample which is located in front of a drift tube. An electric potential can be applied along this drift tube, creating a uniform electric field, *E*, which draws electrons towards a Faraday plate detector. An electron energy distribution is established, determined by a dynamic balance between the kinetic energy gained from the electric field and energy loss through multiple collisions with the high-pressure buffer gas (either Ar or N₂, number density *N*). Anions formed by electron attachment can be distinguished from electrons by a simple timing arrangement in which the electrons are admitted into the drift tube as a short (ca. 1 ms) pulse via an electron gate. By monitoring the attenuation of electron pulses as

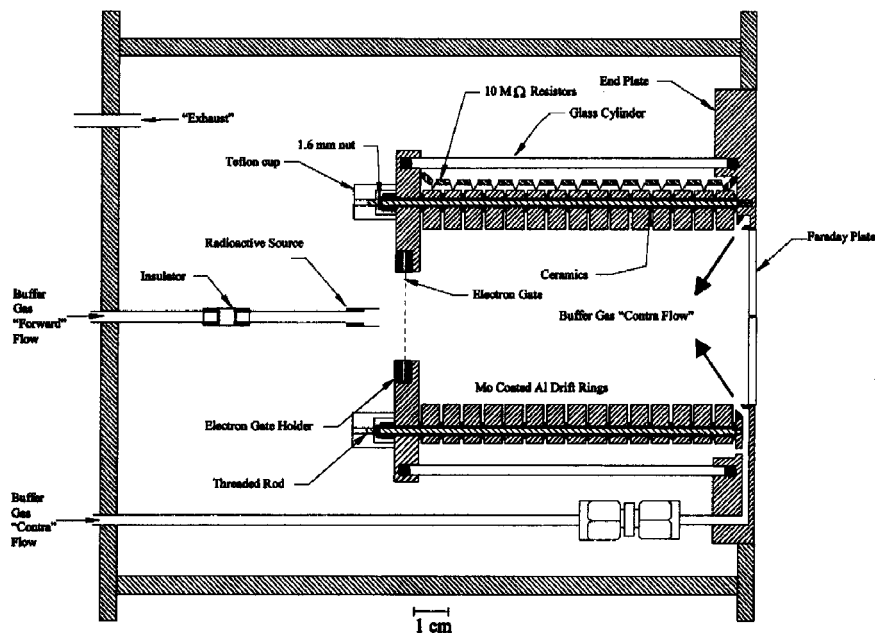


Fig. 10. Schematic of the electron swarm drift tube used in Birmingham for the SF_5CF_3 measurements. A small pinhole at the right-hand end of the drift tube leads, via differential pumping, to a quadrupole mass spectrometer for detection of the anionic products. (Reproduced with permission from *Int. J. Mass Spectrom.*, 205 (2001) 253–270.)

a function of the reactant gas concentration, the density-reduced electron attachment coefficient, α , is determined as a function of E/N . Multiplication of α by the mean electron drift speed gives the electron attachment rate constant, k_a , again as a function of E/N . A small hole in the Faraday plate allows anions formed within the drift tube to enter a differentially pumped region and a quadrupole mass spectrometer. The product anions formed from electron attachment can thus be determined, which is the major advantage of this instrument compared to more conventional electron swarm apparatus [61].

Using Ar or N_2 buffer gas, electrons in the Swarm apparatus have a non-thermal energy distribution. However, many detectors commercially used for the detection of electronegative molecules rely on *thermal* electron attachment in high-pressure buffer gas. Furthermore, if the concentration of an electron-attaching gas is to be accurately determined, thermal attachment rate coefficients are needed. Until recently, we could only obtain such rate coefficients, such as for SF_5CF_3 [59], by extrapolation of our data to zero electric field strengths (Fig. 11). We have now developed a new drift tube ideally suited for thermal electron attachment in a high pressure (ca. 1 bar) of CO_2 buffer gas, and confirmed its correct mode of operation with SF_6 , where α is now determined to be independent of E/N [62].

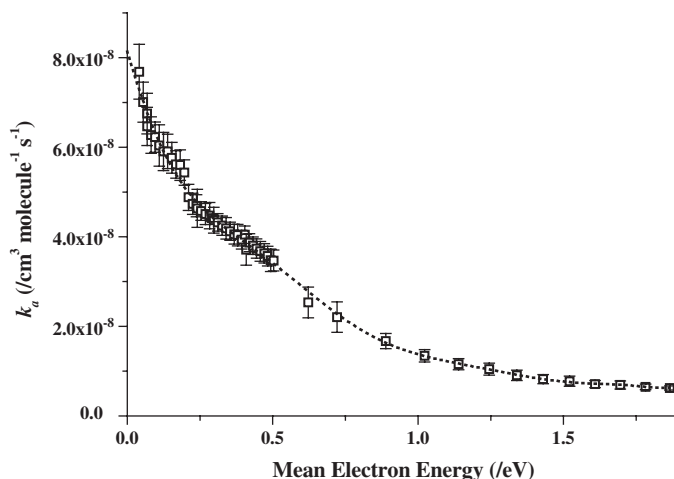


Fig. 11. Graph of electron attachment rate coefficient, k_a , as a function of mean electron energy for SF₅CF₃ in atmospheric pressure of N₂ ($\langle \varepsilon \rangle$ less than 0.5 eV) and Ar ($\langle \varepsilon \rangle$ greater than 0.5 eV) buffer gas. (Reproduced with permission from Int. J. Mass Spectrom., 206 (2001) i–iv.)

The electron attachment rate coefficient for SF₅CF₃, $7.7 \pm 0.6 \times 10^{-8} \text{ cm}^3 \text{ molecule}^{-1} \text{ s}^{-1}$, is fast, but significantly slower than that for SF₆, $2.38 \pm 0.15 \times 10^{-7} \text{ cm}^3 \text{ molecule}^{-1} \text{ s}^{-1}$ [62], which is close to the theoretical maximum for pure s-wave capture [63]. From an atmospheric point of view, however, perhaps the most important result is that the product of such low-energy electron attachment to SF₅CF₃ is not the parent anion, but a fragment anion SF₅⁻. Assuming SF₅CF₃ is not recycled by subsequent reactions of SF₅⁻, low-energy electron attachment is therefore one route to remove SF₅CF₃ from the Earth's atmosphere, and the pseudo-first-order rate constant for this process, the fourth term in the bracket on the right-hand-side of equation (5), will be significant. Energetically, this removal process is also possible. Table 5 shows that, within the error for $\Delta_f H_0^0$ (SF₅CF₃) quoted in Section 5.3, the reaction SF₅CF₃ + e⁻ (0 eV) → SF₅⁻ + CF₃ is exothermic, using both the 0 K enthalpy of formation for SF₅CF₃ from experiment [20] and the less negative value from theory [32]. Using either value for $\Delta_f H_0^0$ (SF₅CF₃), formation of CF₃⁻ + SF₅ is significantly endothermic, explaining the almost total absence of this anion in the 0 eV peak in the electron beam studies [25,26].

6.3. Reactions of SF₅CF₃ with vacuum-UV photons, especially Lyman- α (121.6 nm) radiation

The VUV absorption spectrum of SF₅CF₃, including a determination of the absorption cross section at the Lyman- α wavelength of 121.6 nm, has been

Table 5. Possible products from e^- attachment and Lyman- α excitation of SF_5CF_3 .

Reaction	$\Delta_r H_0^0$ (kJ mol $^{-1}$) (eV)		
	Scheme A ^a	Scheme B ^b	
$SF_5CF_3 + e^-$ (0 eV) (−1623 or −1750)	$\rightarrow SF_5^-$ (−1282) ^c + CF_3 (−463) ^c	−122 (−1.26)	+ 5 (+ 0.05)
	$\rightarrow CF_3^-$ (−639) + SF_5 (−915)	+ 69 (+ 0.72)	+ 196 (+ 2.03)
$SF_5CF_3 + h\nu$ (10.2 eV) (−1623 or −1750)	$\rightarrow SF_5$ (−915) + CF_3 (−463)	−739 (−7.66)	−612 (−6.34)
	$\rightarrow CF_3^+$ (+ 409) + SF_5^- (−1282)	−234 (−2.43)	−107 (−1.11)
	$\rightarrow SF_5^+$ (+ 29) + CF_3^- (−639)	+ 29 (+ 0.30)	+ 156 (+ 1.62)

^a Scheme A assumes $\Delta_r H_0^0$ (SF_5CF_3) = −1623 kJ mol $^{-1}$ (theory [32]).

^b Scheme B assumes $\Delta_r H_0^0$ (SF_5CF_3) = −1750 kJ mol $^{-1}$ (experiment: updated value from [20]).

^c Values in brackets are $\Delta_r H_0^0$ in kJ mol $^{-1}$.

measured by five groups using either direct absorption and the Beer–Lambert law [4,16,17] or a double-ion chamber [15,18]. Measurements have been made using VUV laser radiation [17], fixed-energy lamp sources [18] and tunable VUV radiation from a synchrotron [4,15–17]. The synchrotron experiments have been performed with wavelengths both above [4,17] and below [15,16] the lithium fluoride window cutoff of ca. 105 nm (or 11.8 eV). The apparatus used by the Birmingham group, described in detail by Hoxha *et al.* [64] and used at both the Bessy-I, Berlin and SuperAco, Paris synchrotron sources, is shown in Fig. 12.

In brief, radiation from the synchrotron passes through the exit slit of a VUV monochromator (a 1.5 m normal incidence at Bessy-I), a two-stage differential pumping section and a 1 mm thick stainless-steel microchannel plate into an absorption cell of length, L , 300 mm. A pressure differential of 1000:1 across the microchannel plate is possible. This plate can transmit wavelengths well below 100 nm, so this experiment can measure absorption spectra below the LiF cut off, and yet the path length of the absorption ‘cell’ is defined. The gas pressure in the absorption cell, in the range 10–50 μ bar, is maintained constant via a slow controlled flow of gas. The VUV radiation at the end of the cell is detected through a sodium-salicylate-coated window and a visible photomultiplier tube. Since the pressure of gas and optical path length are known, measurement of the ratio of transmitted intensity observed for background (no gas) and sample spectra (with gas) can yield, via the Beer–Lambert law $\ln(I_0/I) = \sigma cL$, absolute absorption cross sections, σ , in units of $\text{cm}^2 \text{molecule}^{-1}$; c is the number density of the gas in units of molecules cm^{-3} and L has units of cm. In the calculation of I_0/I at every value of the VUV energy, allowance is made for the natural decay of the VUV flux over the time of an experiment. No allowance is made for the small pressure gradient

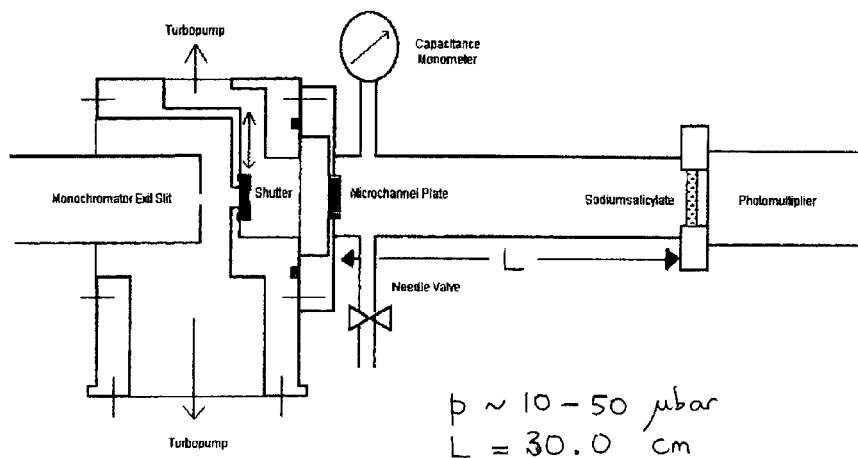


Fig. 12. Apparatus used to record the vacuum-UV absorption spectrum of SF₅CF₃. (Reproduced with permission from Chem. Phys., 260 (2000) 237–247.)

within the absorption cell due to gas leakage through the microchannel plate, and the small effects of second-order radiation from the VUV monochromator are ignored. We estimate that cross sections are accurate to ca. 15–20%, and the ignorance of second-order effects may make this error greater at wavelengths close to twice the blaze wavelength of the grating in the VUV monochromator. Absorption spectra in the range ca. 50–200 nm at a resolution of better than 0.1 nm can routinely be measured. The range of cross sections that can be determined span ca. 10^{-16} to 10^{-20} cm². The absorption spectrum of SF₅CF₃ measured with this apparatus is shown in Fig. 13 [16], and the cross section at 121.6 nm is determined to be $1.3 \pm 0.2 \times 10^{-17}$ cm² (or 13 ± 2 Mb); note that, following a re-analysis of the data, this value is 2 Mb lower than that reported in Ref. [16]. This value is significantly greater than that for SF₆ where $\sigma_{121.6}$ is 1.76×10^{-18} cm², and orders of magnitude greater than for CF₄ which shows negligible absorption at this wavelength ($\sigma_{121.6} < 8 \times 10^{-22}$ cm²) [65]. As commented in Section 5.4, the evidence from the assignment of the absorption spectrum by Holland *et al.* [15] is that SF₅CF₃ behaves more like SF₆ than CF₄ in its VUV photoabsorption properties. The value of $\sigma_{121.6}$ from Chim *et al.* [16] is slightly higher than that determined by others. Holland *et al.* [15], Takahashi *et al.* [17] and Limao-Vieira [4] obtained 6.4, 7.8 and 6.5 Mb, respectively, and the result of Chim *et al.* may be anomalously high because higher order effects are

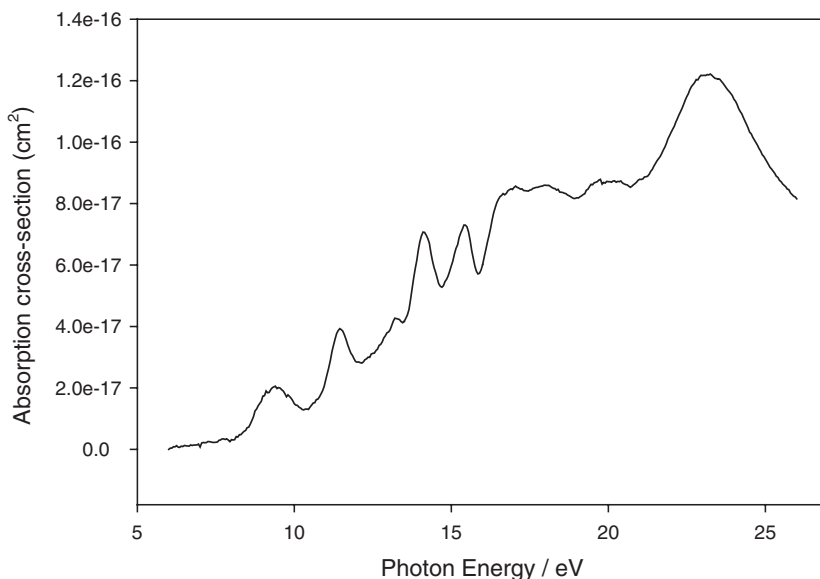


Fig. 13. Absorption spectrum of SF₅CF₃ recorded with a photon resolution of 0.08 nm. The absorption cross section at 121.6 nm is $1.3 \pm 0.2 \times 10^{-17}$ cm² or 13 ± 2 Mb. (Reproduced with permission from Chem. Phys. Lett., 367 (2003) 697–703.)

ignored. That said, using the known value of $J_{121.6}$ [66], the absolute value of this cross section makes negligible difference to the lifetime of SF₅CF₃ in the mesosphere, because VUV photodissociation only contributes ca. 1% to the removal of SF₅CF₃ by processes that occur in the mesosphere (Section 7).

As with the states of SF₅CF₃⁻ excited by low-energy electrons, VUV photo-absorption will only contribute to the removal of SF₅CF₃ from the atmosphere if the valence or Rydberg electronic states, photoexcited at 121.6 nm, are dissociative. The bottom half of Table 5 shows that while dissociation to neutral SF₅ and CF₃ is clearly energetically possible as the SF₅-CF₃ bond strength is only 3.86 eV (Section 5.3), dissociation to the ion pair CF₃⁺ + SF₅⁻ (but not to SF₅⁺ + CF₃⁻) can also occur with 10.2 eV photon excitation. In determining the energetics of these reactions, we use values for the electron affinity of the CF₃ and SF₅ radicals of 1.82 and 3.8 eV, respectively [67,68]. Although the quantum yields for dissociation into ion pairs are generally unknown, their formation following VUV photoexcitation of polyatomic molecules should be prevalent, but this process for SF₅CF₃ has not yet been observed.

Table 6 summarises the electron attachment rate coefficient and Lyman- α absorption cross section for SF₅CF₃, SF₆ and CF₄; reactions of these molecules with small cations and anions are not included as these processes make negligible contribution to their removal from the mesosphere. It is clear that SF₅CF₃ behaves much more like a modified SF₆ than a modified CF₄ molecule. The electron attachment rate coefficient for SF₅CF₃ is ca. three times slower than that for SF₆, $\sigma_{121.6}$ is ca. seven times larger, but k_e and $\sigma_{121.6}$ for CF₄ are orders of magnitude smaller. The only aspect of the photochemistry of SF₅CF₃ where it behaves like a modified CF₄ molecule is its vacuum-UV fluorescence properties. Following VUV photoexcitation in the range 8–25 eV, weak UV/visible emission is observed from CF₃, CF₂ and possibly the parent ion in the energy ranges ca. 10–12, 15–17 and $h\nu > 20$ eV [70]. In this aspect, SF₅CF₃ appears to behave like the group of molecules CF₃X (X = H,F,Cl,Br) [71]. This work does not relate to

Table 6. Thermal electron attachment rate constants, absorption cross sections at 121.6 nm and atmospheric lifetimes for CF₄, SF₆ and SF₅CF₃.

Perfluoro compound	k_e (298 K) (cm ³ s ⁻¹)	$\sigma_{121.6}$ (cm ²)	Lifetime (years)
CF ₄	$< 10^{-16}$ ^a	$< 8 \times 10^{-22}$ ^b	> 50000
SF ₆	2.38×10^{-7} ^c	1.76×10^{-18} ^b	> 800
SF ₅ CF ₃	7.7×10^{-8} ^d	1.3×10^{-17} ^e	ca. 1000

^a Schumacher *et al.* [69].

^b Ravishankara *et al.* [65].

^c Mayhew *et al.* [62].

^d Kennedy and Mayhew [59].

^e Re-analysis of the data of Chim *et al.* [16], resulting in a reduction of $\sigma_{121.6}$ by 2 Mb.

the atmospheric chemistry of SF₅CF₃, but will be described in detail in a future publication [70].

7. LIFETIME OF SF₅CF₃ IN THE EARTH'S ATMOSPHERE AND CONCLUSIONS

The lifetime of a pollutant or greenhouse gas is a term that can mean different things to different people, and sometimes confusion can arise [72]. To a laboratory-based physical chemist, the lifetime usually means the inverse of the pseudo-first-order rate constant of the dominant chemical or photolytic process that removes the pollutant from the atmosphere. Using CH₄ as an example, it is predominantly removed in the troposphere via oxidation by the OH free radical, OH + CH₄ → H₂O + CH₃. The rate coefficient for this reaction at 298 K is 6.39 × 10⁻¹⁵ cm³ molecule⁻¹ s⁻¹ [73], so the lifetime is approximately equal to (k₂₉₈[OH])⁻¹. Using an average value for the tropospheric OH concentration of 10⁶ molecules cm⁻³, the atmospheric lifetime of CH₄ is calculated to be ca. 5 years. This is within a factor of 2.4 of the accepted value of 12 years (Table 1). The difference arises because CH₄ is not emitted uniformly from the Earth's surface, a finite time is needed to transport CH₄ via convection and diffusion into the troposphere, and oxidation occurs at different altitudes in the troposphere where the concentration of OH will vary from its average value of 10⁶ molecules cm⁻³. In simple terms, this is an example of a two-step kinetic process, A → B → C with first-order rate constants k₁ and k₂. The first step, A → B, defines the transport of the pollutant into the atmosphere, while the second step, B → C, defines the chemical or photolytic process (e.g. reaction with an OH radical in the troposphere, electron attachment in the mesosphere) that removes the pollutant from the atmosphere. In general, the overall rate of the process (whose inverse is called the *lifetime*) will be a function of both k₁ and k₂, but its value will be dominated by the *slower* of the two steps. Thus, in writing the lifetime of CH₄ simply as (k₂₉₈[OH])⁻¹, we are assuming that the first step, transport into the region of the atmosphere where chemical reactions occur, is infinitely fast.

SF₅CF₃, perfluorocarbons such as CF₄, and SF₆ behave in the opposite sense. The slow, rate-determining process is now the first step, transport of the greenhouse gas from the surface of the Earth into the mesosphere, and the chemical or photolytic processes that remove SF₅CF₃ etc. in the mesosphere will have very little influence on the lifetime. We can define a chemical lifetime, τ_{chemical}, as (k_e[e⁻] + σ_{121.6}J_{121.6})⁻¹, assuming the quantum yield for dissociation at 121.6 nm is unity, but the value will be a function of position, particularly altitude, in the atmosphere. In the troposphere, τ_{chemical} will be infinite because both the concentration of electrons and J_{121.6} are effectively zero at low altitude, but in the mesosphere τ_{chemical} will be much less. In other words, multiplication of k_e for

SF₅CF₃ etc. by a typical electron density in the mesosphere, ca. 10⁴ cm⁻³ [58], yields a chemical lifetime which is far too small and bears no relation to the true atmospheric lifetime, simply because most of the SF₅CF₃ etc. does not reside in the mesosphere.

The global atmospheric lifetime is obtained from globally averaged loss frequencies. In forming the average, the pseudo-first-order destruction rate coefficient for each region of the atmosphere is weighted according to the number of molecules of compound in that region,

$$\langle k \rangle_{\text{global}} = \frac{\sum_i k_i V_i n_i}{\sum_i V_i n_i} \quad (9)$$

where i is a region, k_i the pseudo-first-order rate coefficient for region i , V_i the volume of region i , and n_i the number density of the greenhouse gas under study in region i . The averaging process thus needs input from a 2D or 3D model of the atmosphere in order to supply the values of n_i . This is essentially a meteorological problem, and may explain why such scientists and physical chemists sometimes have different interpretations of what the lifetime of a greenhouse gas actually means. The only sensible definition is the inverse of $\langle k \rangle_{\text{global}}$. Many such studies have been made for SF₆ [65,74,75], and differences in the kinetic model (k_i) and the atmospheric distributions (n_i) from different climate or transport models account for the variety of atmospheric lifetimes that have been reported. For molecules such as SF₆ (and SF₅CF₃) which are only destroyed in the mesosphere above 60 km, the importance of both these factors has been explored by Hall and Waugh [76]. Their results show that because the fraction of the total number of SF₆ molecules in the mesosphere is very small, the global atmospheric lifetime is much longer than the mesospheric, chemical lifetime. Thus, they quote that if the mesospheric loss frequency is 9 × 10⁻⁸ s⁻¹, corresponding to a local lifetime of 129 days, then the global lifetime ranges between 1424 and 1975 years, according to which climate or transport model is used. In conclusion, therefore, the lifetime of SF₆, SF₅CF₃ and CF₄ is dominated by the meteorology that transports these pollutants into the mesosphere, but the fate of each molecule when it reacts with low-energy electrons and Lyman- α radiation may make a small contribution to $\langle k \rangle_{\text{global}}$.

To the author's knowledge, no full meteorological analysis of SF₅CF₃ in the atmosphere has been performed. Both SF₆ and SF₅CF₃ attach electrons with a fast rate coefficient (> 10⁻⁸ cm³ molecule⁻¹ s⁻¹) and show significant absorption with Lyman- α radiation. Furthermore, the height profiles of SF₆ and SF₅CF₃ are similar in the atmosphere [1]. It should therefore be appropriate to make quantitative comparisons between these two molecules, expecting them to have similar lifetimes in the atmosphere. By contrast, the almost infinite value for the lifetime of CF₄, greater than 50,000 years [65,77], arises because this molecule

shows no absorption at 121.6 nm [65] and attaches electrons at a negligibly slow rate [69]. k_e for SF_5CF_3 at 298 K is 3.1 times smaller than for SF_6 , whereas the absorption cross section is 7.4 times larger (Table 6). Therefore, the pseudo-first-order rate constant for removal of SF_5CF_3 by electrons divided by that due to photons at the same altitude of the mesosphere, $k_e[\text{e}^-]/\sigma_{121.6}J_{121.6}$, is 22.9 times smaller than this ratio for SF_6 . (This calculation assumes that electron attachment to both SF_6 and SF_5CF_3 leads only to the formation of a fragment anion, SF_5^- , which is not recycled.) Assuming an incorrect value for k_e of $1 \times 10^{-9} \text{ cm}^3 \text{ molecule}^{-1} \text{ s}^{-1}$, Ravishankara *et al.* [65] initially determined that this ratio of pseudo-first-order rate constants for SF_6 was 3.2, and obtained an atmospheric lifetime of 3200 years. Using the much larger and correct value for k_e (SF_6) of $2.3 \times 10^{-7} \text{ cm}^3 \text{ molecule}^{-1} \text{ s}^{-1}$, Morris *et al.* [74] showed that this ratio of pseudo-first-order rate constants was 1998, and determined a lower limit to the atmospheric lifetime of 800 years. The lower limit arises because they assumed that every electron attachment event led to the permanent removal of SF_6 from the atmosphere. Reddmann *et al.* [75] considered a number of scenarios for the destruction of SF_6^- . They found that if less than 100% was destroyed, the lifetime, not surprisingly, increased. They calculated values spanned 400 to 10000 years, depending on the loss mechanism and the value for the electron density in the upper stratosphere and mesosphere.

Assuming that the analysis of Morris *et al.* [74] for SF_6 is correct, the predominant 'chemical' removal process for SF_5CF_3 remains electron attachment and not VUV photolysis, as the ratio of the pseudo-first-order rate constants for SF_5CF_3 is 1998/22.9 or 87.2, which is still much greater than unity. Without a full meteorological study, however, as explained above, it is very difficult to convert these first-order rate constants into a global lifetime for SF_5CF_3 . What can be said is that, *per molecule*, the quantum yield for electron attachment to SF_5CF_3 in the mesosphere is 87.2/88.2 or 0.989, and for Lyman- α photodissociation 1/88.2 or 0.011. The atmospheric lifetime is dominated by the meteorology that transports SF_5CF_3 to the upper altitudes of the atmosphere and is likely to be ca. 1000 years, with an uncertainty in this number possibly as large as ± 300 years.

In conclusion, it is quite clear that, while the current concentrations of SF_5CF_3 in the atmosphere are still very low, mankind is stuck with this problem for a very long time. Since the original paper by Sturges *et al.* [1] was published 5 years ago, a huge amount of fundamental research has meant that the atmospheric properties and reactions of SF_5CF_3 are now well understood, and further research effort will only contribute at the edges to understand the environmental impact of this greenhouse gas. It is suggested that reliable monitors, probably using the IR absorption properties of this molecule, are installed to determine the concentration of SF_5CF_3 both at the Earth's surface and in the atmosphere. It is also suggested that policymakers should be concerned at the high annual growth rate of SF_5CF_3 , and measures should be put in place world wide to control its emissions.

TABLE OF ACRONYMS

GWP	global warming potential
DIE	dissociative ionisation energy
PEPICO	photoelectron–photoion coincidence
TPEPICO	threshold photoelectron–photoion coincidence
TOF	time-of-flight
TDC	time-to-digital converter
TPES	threshold photoelectron spectrum
SIFT	selected ion flow tube

ACKNOWLEDGMENTS

I thank members of my research group who participated in our laboratory-based experiments on SF₅CF₃, and EPSRC, UK and the EU for funding. I particularly thank Professor K.P. Shine, Reading University UK, for discussions on radiative forcing and global warming potentials, and Dr C.R. Howle, Bristol University UK, for a critical reading of the manuscript.

REFERENCES

- [1] W.T. Sturges, T.J. Wallington, M.D. Hurley, K.P. Shine, K. Sihra, A. Engel, D.E. Oram, S.A. Penkett, R. Mulvaney, C.A.M. Brenninkmeijer, A potent greenhouse gas identified in the atmosphere: SF₅CF₃, *Science* 289 (2000) 611–613.
- [2] J.S. Chickos, W.E. Acree, Enthalpies of vaporisation of organic and organometallic compounds, 1880–2002, *J. Phys. Chem. Ref. Data* 32 (2003) 519–878.
- [3] L. Huang, L. Zhu, X. Pan, J. Zhang, B. Ouyang, H. Hou, One potential source of the potent greenhouse gas SF₅CF₃: the reaction of SF₆ with fluorocarbons under discharge, *Atmos. Environ.* 39 (2005) 1641–1653.
- [4] P. Limao-Vieira, S. Eden, P.A. Kendall, N.J. Mason, A. Giuliani, J. Heinesch, M.J. Hubin-Franskin, J. Delwiche, S.V. Hoffmann, An experimental study of SF₅CF₃ by electron energy loss spectroscopy, VUV photo-absorption and photoelectron spectroscopy, *Int. J. Mass Spectrom.* 233 (2004) 335–341.
- [5] N.J. Mason, A. Dawes, R. Mukerji, E.A. Drage, E. Vasekova, S.M. Webb, P. Limao-Vieira, Atmospheric chemistry with synchrotron radiation, *J. Phys. B* 38 (2005) S893–S911.
- [6] A. McCulloch, Fluorocarbons in the global environment: a review of the important interactions with atmospheric chemistry and physics, *J. Fluorine Chem.* 123 (2003) 21–29.
- [7] P. Kisliuk, G. A. Silvey, The microwave spectrum of SF₅CF₃, *J. Chem. Phys.* 20, (1952) 517–517.
- [8] C.J. Marsden, D. Christen, H. Oberhammer, The trans influence of CF₃: gas-phase structure of SF₅CF₃, *J. Mol. Struct.* 131 (1985) 299–307.
- [9] P.J. Knowles, private communication, 2005.
- [10] D.F. Eggers, H.E. Wright, D.W. Robinson, The infrared spectrum of SF₅CF₃, *J. Chem. Phys.* 35 (1961) 1045–1050.

- [11] J.E. Griffiths, The infrared and Raman spectra of SF₅Cl and SF₅CF₃, *Spectrochim. Acta A* 23 (1967) 2145–2157.
- [12] O.J. Nielsen, F.M. Nicolaisen, C. Bacher, M.D. Hurley, J.T.J. Wallington, K.P. Shine, Infrared spectrum and global warming potential of SF₅CF₃, *Atmos. Environ.* 36 (2002) 1237–1240.
- [13] P.A. Kendall, N.J. Mason, G.A. Buchanan, G. Marston, P. Tegeder, A. Dawes, S. Eden, P. Lima-Vieira, D.A. Newnham, Temperature dependent high-resolution infrared photoabsorption cross sections of SF₅CF₃, *Chem. Phys.* 287 (2003) 137–142.
- [14] C.P. Rinsland, S.W. Sharpe, R.L. Sams, Temperature-dependent absorption cross-sections in the thermal infrared bands of SF₅CF₃, *J. Quant. Spec. Rad. Transfer* 82 (2003) 483–490.
- [15] D.M.P. Holland, D.A. Shaw, I.C. Walker, I.J. McEwen, E. Apra, M.F. Guest, Study of the valence shell photoelectron and photoabsorption spectra of SF₅CF₃, *J. Phys. B* 38 (2005) 2047–2067.
- [16] R.Y.L. Chim, R.A. Kennedy, R.P. Tuckett, The vacuum-UV absorption spectrum of SF₅CF₃; implications for its lifetime in the earth's atmosphere, *Chem. Phys. Lett.* 367 (2003) 697–703.
- [17] K. Takahashi, T. Nakayama, Y. Matsumi, S. Solomon, T. Gejo, E. Shigemasa, T.J. Wallington, Atmospheric lifetime of SF₅CF₃, *Geophys. Res. Lett.* 29 (2002) 1712–1715.
- [18] P.A. Hatherly, A.J. Flaxman, On the absolute absorption cross-section of SF₅CF₃, *Chem. Phys. Lett.* 380 (2003) 512–515.
- [19] T. Ibuki, Y. Shimada, S. Nagaoka, A. Fujii, M. Hino, T. Kakiuchi, K. Okada, K. Tabayashi, T. Matsudo, Y. Yamana, I.H. Suzuki, Y. Tamenori, Total photoabsorption cross-sections of SF₅CF₃ in the C, F and S K-shell regions, *Chem. Phys. Lett.* 392 (2004) 303–308.
- [20] R.Y.L. Chim, R.A. Kennedy, R.P. Tuckett, W. Zhou, G.K. Jarvis, D.J. Collins, P.A. Hatherly, Fragmentation of energy-selected SF₅CF₃⁺ probed by threshold photoelectron photoion coincidence spectroscopy: bond dissociation energy of SF₅–CF₃ and its atmospheric implications, *J. Phys. Chem. A* 105 (2001) 8403–8412.
- [21] R.Y.L. Chim, R.A. Kennedy, R.P. Tuckett, W. Zhou, G.K. Jarvis, C.A. Mayhew, D.J. Collins, P.A. Hatherly, Determination of the first dissociative ionisation energy of polyatomic molecules by TPEPICO Spectroscopy: application to CF₄, SF₆, SeF₆, TeF₆ and SF₅CF₃, *Surf. Rev. Lett.* 9 (2002) 129–135.
- [22] B. Gstir, G. Hanel, J. Fedor, M. Probst, P. Scheier, N.J. Mason, T.D. Märk, Electron impact ionisation studies of SF₅CF₃, *J. Phys. B* 35 (2002) 2567–2574.
- [23] P.A. Kendall, N.J. Mason, Excitation and relative differential oscillator strengths for trifluoromethyl sulphur pentafluoride, SF₅CF₃, in the UV-VUV region by electron energy loss spectroscopy, *J. Elec. Spec. Rel. Phen.* 120 (2001) 27–31.
- [24] P. Lima-Vieira, F. Blanco, J.C. Oller, A. Munoz, J.M. Perez, M. Vinodkumar, G. Garcia, N.J. Mason, Electron scattering cross sections for SF₆ and SF₅CF₃ at intermediate and high energies (100–10,000 eV), *Phys. Rev. A* 71 (2005) 0327201–0327206.
- [25] R. Balog, M. Stano, P. Lima-Vieira, C. König, I. Bald, N.J. Mason, E. Illenberger, Low energy electron interaction with free and bound SF₅CF₃: negative ion formation from single molecules, clusters and nanofilms, *J. Chem. Phys.* 119 (2003) 10396–10403.
- [26] W. Sailer, H. Drexel, A. Pelc, V. Grill, N.J. Mason, E. Illenberger, J.D. Skalny, T. Mikoviny, P. Scheier, T.D. Märk, Low energy electron attachment to SF₅CF₃, *Chem. Phys. Lett.* 351 (2002) 71–78.
- [27] F. Pepi, A. Ricci, M. Di Stefano, M. Rosi, Gas phase protonation of trifluoromethyl sulphur pentafluoride, *Phys. Chem. Chem. Phys.* 7 (2005) 1181–1186.

- [28] T. Ibuki, Y. Shimada, R. Hashimoto, S. Nagaoka, M. Hino, K. Okada, I.H. Suzuki, Y. Morishita, Y. Tamenori, Photofragmentation of C, F and S *K*-shell excited SF₅CF₃ studied by PEPICO and PIPICO spectroscopy, *Chem. Phys.* 314 (2005) 119–126.
- [29] M.W. Chase, NIST-JANAF thermochemical tables, 4th edition, *J. Phys. Chem. Ref. Data*, 1998, monograph no. 9.
- [30] D.W. Ball, Formation and vibrational spectrum of trifluoromethyl sulphur pentafluoride, SF₅CF₃, a new greenhouse gas: Gaussian-2 and Gaussian-3 calculations, *J. Mol. Struct. (Theochem.)* 578 (2002) 29–34.
- [31] Z. Li, J. Yang, J.G. Hou, Q. Zhu, Hybrid density functional study of SF₅CF₃, *Chem. Phys. Lett.* 359 (2002) 321–325.
- [32] T.M. Miller, S.T. Arnold, A.A. Viggiano, W.B. Knighton, Electron attachment to SF₅CF₃ (296–563 K), and calculations of the neutral and anion thermochemistry, *J. Chem. Phys.* 116 (2002) 6021–6027.
- [33] W. Xu, C. Xiao, Q. Li, Y. Xie, H.F. Schaefer, Structures, thermochemistry, vibrational frequencies and integrated infrared intensities of SF₅CF₃ and SF₅CF₃⁻, with implications for global temperature patterns, *Mol. Phys.* 102 (2004) 1415–1439.
- [34] M. Turki, W. Eisfeld, Theoretical investigation of the absorption and ionisation spectrum of the super greenhouse gas SF₅CF₃, *Phys. Chem. Chem. Phys.* 7 (2005) 1700–1708.
- [35] Intergovernmental Panel on Climate Change, 3rd report, 2001, Chapter 6.
- [36] K. Sihra, M.D. Hurley, K.P. Shine, T.J. Wallington, Updated radiative forcing estimates of 65 halocarbons and nonmethane hydrocarbons, *J. Geophys. Res.* 106 (2001) 20493–20505.
- [37] <http://earthfuture.com/stormyweather/greenhouse/>
- [38] K.P. Shine, J.S. Fuglested, K. Hailemariam, N. Stuber, Alternatives to the global warming potential for comparing climate impacts of emissions of greenhouse gases, *Climatic Change* 68 (2005) 281–302.
- [39] <http://webbook.nist.gov/>
- [40] G.A. Garcia, P.M. Guyon, I. Powis, The ionisation energy of CF₃ deduced from photoionisation of jet-cooled CF₃Br, *J. Phys. Chem. A* 105 (2001) 8296–8301.
- [41] D.P. Secombe, R.Y.L. Chim, G.K. Jarvis, R.P. Tuckett, The use of threshold photoelectron – photoion coincidence spectroscopy to probe the spectroscopic and dynamic properties of valence states of CCl₃F⁺, CCl₃H⁺ and CCl₃Br⁺, *Phys. Chem. Chem. Phys.* 2 (2000) 769–780.
- [42] K.E. Holdy, L.C. Klotz, K.R. Wilson, Molecular dynamics of photodissociation: quasi-diatom model for ICN, *J. Chem. Phys.* 52 (1970) 4588–4598.
- [43] E.R. Fisher, B.L. Kickel, P.B. Armentrout, Collision-induced dissociation and charge-transfer reactions of SF_x⁺ (*x* = 1–5); thermochemistry of sulphur fluoride ions and neutrals, *J. Chem. Phys.* 97 (1992) 4859–4870.
- [44] P.A. Hatherly, M. Stankiewicz, K. Codling, J.C. Creasey, H.M. Jones, R.P. Tuckett, A threshold electron analyser for use in coincidence experiments, *Meas. Sci. Tech.* 3 (1992) 891–896.
- [45] I. Powis, P.I. Mansell, C.J. Danby, Photoelectron photoion coincidence spectrometer for the study of translational energy release distributions, *Int. J. Mass Spectrom. Ion Phys.* 32 (1979) 15–26.
- [46] G.K. Jarvis, D.P. Secombe, R.P. Tuckett, The effects of isotopomers in the state-selected photofragmentation of BCl₃⁺, PCl₃⁺ and PBr₃⁺, *Chem. Phys. Lett.* 315 (1999) 287–292.
- [47] K.K. Irikura, Structure and thermochemistry of sulphur fluorides SF_{*n*} and their ions SF_{*n*}⁺ (*n* = 1–5), *J. Chem. Phys.* 102 (1995) 5357–5367.
- [48] M. Hanrath, S.D. Peyerimhoff, R.P. Tuckett, unpublished data.
- [49] G.K. Jarvis, K.J. Boyle, C.A. Mayhew, R.P. Tuckett, Threshold photoelectron photoion coincidence spectroscopy of saturated perfluorocarbons C₂F₆, C₃F₈ and *n*-C₄F₁₀, *J. Phys. Chem. A* 102 (1998) 3219–3229.

- [50] C.E. Klots, Thermochemical and kinetic information from metastable decomposition of ions, *J. Chem. Phys.* 58 (1973) 5364–5367.
- [51] J.C. Creasey, H.M. Jones, D.M. Smith, R.P. Tuckett, P.A. Hatherly, K. Codling, I. Powis, Fragmentation of valence electronic states of CF_4^+ and SF_6^+ studied by threshold photoelectron photoion coincidence spectroscopy, *Chem. Phys.* 174 (1993) 441–452.
- [52] C. Atterbury, R.A. Kennedy, C.A. Mayhew, R.P. Tuckett, A study of the reactions of trifluoromethyl sulphur pentafluoride, SF_5CF_3 , with several positive ions of atmospheric interest, *Phys. Chem. Chem. Phys.* 3 (2001) 1949–1953.
- [53] C. Atterbury, A.D.J. Critchley, R.A. Kennedy, C.A. Mayhew, R.P. Tuckett, A study of the gas-phase reactions of several cations with two derivatives of SF_6 : SF_5CF_3 and SF_5Cl , *Phys. Chem. Chem. Phys.* 4 (2002) 2206–2223.
- [54] S.T. Arnold, T.M. Miller, A.A. Viggiano, C.A. Mayhew, A temperature-dependent selected ion flow tube study of anions reacting with SF_5CF_3 , *Int. J. Mass Spectrom.* 223 (2003) 403–409.
- [55] G.K. Jarvis, R.A. Kennedy, C.A. Mayhew, R.P. Tuckett, Charge transfer from neutral perfluorocarbons to various cations: long-range versus short-range reaction mechanisms, *Int. J. Mass Spectrom.* 202 (2000) 323–343.
- [56] M.A. Parkes, R.Y.L. Chim, C.A. Mayhew, V.A. Mikhailov, R.P. Tuckett, Threshold photoelectron photoion coincidence spectroscopy and selected ion flow tube reactions of CHF_3 : comparison of product branching ratios, *Mol. Phys.* 104 (2006) 263–272.
- [57] G. Gioumousis, D.P. Stevenson, Reactions of gaseous molecular ions with gaseous molecules. V: theory, *J. Chem. Phys.* 29 (1958) 294–299.
- [58] N.G. Adams, D. Smith, Ionic reactions in atmospheric, interstellar and laboratory plasmas, *Contemp. Phys.* 29 (1988) 559–578.
- [59] R.A. Kennedy, C.A. Mayhew, A study of the low energy electron attachment to trifluoromethyl sulphur pentafluoride, SF_5CF_3 : atmospheric implications, *Int. J. Mass Spectrom.* 206 (2001) i–iv.
- [60] G.K. Jarvis, R.A. Kennedy, C.A. Mayhew, Investigations of low energy electron attachment to SF_6 , SeF_6 and TeF_6 using an electron swarm mass spectrometric technique, *Int. J. Mass Spectrom.* 205 (2001) 253–270.
- [61] A.A. Christodoulides, L.G. Christophorou, R.Y. Pai, C.M. Tung, Electron attachment to perfluorocarbon compounds. I: $c\text{-C}_4\text{F}_6$, $2\text{-C}_4\text{F}_6$, $1,3\text{-C}_4\text{F}_6$, $c\text{-C}_4\text{F}_8$ and $2\text{-C}_4\text{F}_8$, *J. Chem. Phys.* 70 (1979) 1156–1168.
- [62] C.A. Mayhew, A.D.J. Critchley, D.C. Howse, V.A. Mikhailov, M.A. Parkes, Measurements of thermal electron attachment rate coefficients to molecules using an electron swarm technique, *Eur. Phys. J. D* 35 (2005) 307–312.
- [63] E.P. Grimsrud, S. Chowdbury, P. Kebarle, The electron affinity of SF_6 and perfluoromethyl cyclohexane; the unusual kinetics of electron transfer reactions $\text{A}^- + \text{B} \rightarrow \text{A} + \text{B}^-$, *J. Chem. Phys.* 83 (1985) 1059–1068.
- [64] A. Hoxha, R. Loch, B. Leyh, D. Dehareng, K. Hottmann, H.W. Jochims, H. Baumgärtel, Photoabsorption and constant ionic state spectroscopy of vinyl bromide, *Chem. Phys.* 260 (2000) 237–247.
- [65] A.R. Ravishankara, S. Solomon, A.A. Turnipseed, R.F. Warren, Atmospheric lifetimes of long-lived halogenated species, *Science* 259 (1993) 194–199.
- [66] T.N. Woods, W.K. Tobiska, G.J. Rottman, J.R. Worden, Improved solar Lyman- α irradiance modelling from 1947–1999 based on UARS observations, *J. Geophys. Res.* D 105 (2000) 27195–27215.
- [67] H.J. Deyerl, L.S. Alconel, R.E. Continetti, Photodetachment imaging studies of the electron affinity of CF_3 , *J. Phys. Chem. A* 105 (2001) 552–557.
- [68] H.P. Fenzlaff, R. Gerhard, E. Illenberger, Associative and dissociative electron attachment to SF_6 and SF_5Cl , *J. Chem. Phys.* 88 (1988) 149–155.

- [69] R. Schumacher, H.R. Sprunken, A.A. Christodoulides, R.N. Schindler, Studies of electron cyclotron resonance technique; electron scavenging properties of CCl₃F, CCl₂F₂, CClF₃ and CF₄, *J. Phys. Chem.* 82 (1978) 2248–2252.
- [70] J. Alvarez Ruiz, S. Ali, R.P. Tuckett, Vacuum-UV fluorescence excitation spectroscopy of SF₅CF₃ in the range 8–25 eV, *Phys. Chem. Chem. Phys.* (2006) in preparation.
- [71] H. Biehl, K.J. Boyle, R.P. Tuckett, H. Baumgärtel, H.W. Jochims, Vacuum-UV fluorescence excitation spectroscopy of CF₃X (X = F, H, Cl, Br) in the range 10–30 eV, *Chem. Phys.* 214 (1997) 367–382.
- [72] A.R. Ravishankara, E.R. Lovejoy, Atmospheric lifetime, and its application and determination: CFC-substitutes as a case study, *J. Chem. Soc. Faraday Trans.* 90 (1994) 2159–2169.
- [73] T. Gierczak, R.K. Talukdar, S.C. Herndon, G.L. Vaghjiani, A.R. Ravishankara, Rate coefficients for the reaction of the OH radical with methane and substituted methanes, *J. Phys. Chem. A* 101 (1997) 3125–3134.
- [74] R.A. Morris, T.M. Miller, A.A. Viggiano, J.F. Paulson, S. Solomon, G. Reid, Effects of electron and ion reactions on atmospheric lifetimes of fully fluorinated compounds, *J. Geophys. Res. D* 100 (1995) 1287–1294.
- [75] T. Reddman, R. Ruhnke, W. Kouker, Three-dimensional model simulations of SF₆ with mesospheric chemistry, *J. Geophys. Res. D* 106 (2001) 14525–14537.
- [76] T.M. Hall, D.W. Waugh, Influence of nonlocal chemistry on tracer distributions: inferring the mean age of air from SF₆, *J. Geophys. Res. D* 103 (1998) 13327–13336.
- [77] R.J. Cicerone, Atmospheric carbon tetrafluoride: a nearly inert gas, *Science* 206 (1979) 59–61.

This page intentionally left blank

CHAPTER 4

Production of Second- or Third-Generation Fluorine-based Refrigerants from (Photo)-Dechlorination of Fluorocarbon Wastes

Hideo Nishiumi,* Koichi Sato and Ryo Kato

Department of Materials Chemistry, Hosei University 3-7-2 Kajino-cho, Koganei-city, Tokyo 184-8584, Japan

Contents

1. Introduction	133
2. Decomposition of fluorocarbons	134
2.1. A review of the decomposition technologies	134
2.1.1. Incineration decomposition method	134
2.1.2. Thermal decomposition method	134
2.1.3. Plasma decomposition method	135
2.1.4. Catalytic reactions	136
2.1.5. Reductive dehalogenation in sodium naphthalenide-THF solution	136
2.1.6. Supercritical water hydrolysis	137
2.1.7. Superoxide-induced decomposition by pyridine and dipyridinium ion-type compounds	137
2.1.8. γ -ray radiation	137
2.1.9. Photochemical decomposition	137
2.2. Decomposition of CFCs and HCFCs in alcoholic alkali solution	138
2.2.1. Decomposition of CCl_2F_2 (CFC-12)	138
2.2.2. Decomposition of 1,1,2-trichlorotrifluoroethane $\text{C}_2\text{Cl}_3\text{F}_3$ (CFC-113)	139
2.2.3. Influence of solvents and light sources	139
2.2.4. Dechlorination of PCBs in transformer oil by alkaline methanol	139
3. Production of useful compounds from fluorocarbon wastes	141
3.1. Decomposition products of fluorocarbons	141
3.2. Difluorodimethyl ether CH_3OCHF_2 obtained from CCl_2F_2 or CHClF_2	143
3.2.1. CH_3OCHF_2 production from CHClF_2 (HCFC-22)	143
3.2.2. Vapor pressure measurement of CH_3OCHF_2	144
4. Reaction rate and reaction mechanism	146
4.1. Solubility of fluorocarbons in alcohols	146
4.2. Decomposition rate of CHClF_2 (HCFC-22)	148

*Corresponding author. Tel. and Fax: 81-42-387-6142;
E-mail: nishi@k.hosei.ac.jp

4.3. Photodecomposition rate of CCl_2F_2 (CFC-12)	150
4.4. Photodecomposition rate of C_2ClF_5 (CFC-115) and reaction mechanism	151
5. Effect of mass transfer rate on reaction rate	156
5.1. Effect of NaCl precipitation on the decomposition of CHClF_2	156
5.2. Competitive mass transfer rate and reaction rate	159
6. Conclusion	162
References	162

Abstract

Chlorofluorocarbons (CFCs) and hydrochlorofluorocarbons (HCFCs) are called first-generation fluorocarbons because they contain chlorine atoms. Because they deplete the ozone layer, the production of CFCs has been banned and HCFCs will soon share the same fate. From this trend one can predict that hundreds of thousands of tons of CFCs or HCFCs presently being used will become harmful wastes in the near future. On the other hand, if these chlorinated wastes could be converted into either nonhazardous or useful compounds, CFCs or HCFCs could be regarded as chemical feedstocks. In this work, our first objective was to develop a decomposition method for CFCs or HCFCs at moderate conditions. Combustion of CFCs is an obvious choice, but has the disadvantage of producing toxic compounds such as dioxins. In our work, we found that photodecomposition of chlorinated compounds in dissolved alcohol–NaOH solutions under ultraviolet (UV) irradiation is possible under mild conditions of room temperature and atmospheric pressure. Chlorine atoms are easily removed yielding NaCl. Among the 12 chlorinated compounds tested, low-pressure mercury lamps were more effective than high-pressure ones. Chlorodifluoromethane (HCFC-22) and dichlorotrifluoroethane (HCFC-123a) is decomposed by only bubbling into methanol–NaOH solution and did not require UV irradiation. The second objective of our work was to determine the reaction products and their possible application to environmental fields. Three kinds of solutions, methanol plus NaOH, 2-propanol plus NaOH, and 2-propanol, were tested using 10 types of CFCs and HCFCs. Results showed that the main products were either hydrofluorocarbons (HFCs) or fluoroethers. HFCs are known as second-generation fluorocarbons because – although they have low effects on the ozone layer – they still have a large greenhouse gas potential. Fluoroethers are known as third-generation refrigerants, because they have neither the ozone layer depleting potential nor the greenhouse gas potential. Our work showed the possibility that wastes such as CFCs and HCFCs could be converted into resources. From our results, a possible system for producing 1,1-difluoromethyl ether, CH_3OCHF_2 , is via HCFC-22, because the reaction occurs in the absence of UV irradiation at room temperature and atmospheric pressure, and is widely used in air conditioners. As vapor pressure of the ether is similar to that of chlorodifluoroethane (HCFC-142b), the ether has a good possibility of use as an alternative refrigerant for HCFC-142b. The third objective of our work was to know the effect of process factors such as agitation in addition to reaction mechanism for designing a photochemical reactor. The process is composed of two steps: a mass transfer process of fluorocarbons dissolving in solutions from vapor bubbles and the reaction rate in a solution. To estimate the mass transfer, we measured the solubility of fluorocarbons in alcohol–NaOH solutions. Using these values, a stationary state model, in which mass transfer rates and reaction rates are balanced, was set up. Using the stationary state model with the kinetic data, we obtained a model for the reaction rate and were able to propose a reaction mechanism.

1. INTRODUCTION

Chlorofluorocarbons (CFCs) and hydrochlorofluorocarbons (HCFCs) are termed first-generation fluorocarbon refrigerants because they have chlorine atoms. Because they deplete the ozone layer, the production of CFCs has been banned and HCFCs will soon share the same fate. From this trend, one can predict that hundreds of thousands of tons of CFCs or HCFCs presently being used will need to be treated or disposed in safety. On the other hand, if these chlorinated wastes could be converted into either nonhazardous or useful compounds, CFCs or HCFCs would be regarded as chemical feedstocks. In this chapter, we propose a process to re-form CFCs or HCFCs into useful compounds, i.e., the second- or third-generation refrigerants.

Our first objective was to develop a decomposition method for CFCs or HCFCs. Combustion of CFCs is an obvious choice, but has the disadvantage of possibly producing toxic compounds such as dioxins. In our work, we found that photodecomposition of chlorinated compounds in dissolved alcohol–NaOH solutions under UV irradiation is possible under mild conditions of room temperature and atmospheric pressure. Chlorine atoms are easily removed yielding NaCl.

The second objective was to determine the reaction products of our work and their possible application in environmental fields. Results showed that the main products were either hydrofluorocarbons (HFCs) or fluoroethers. HFCs are known as second-generation fluorocarbon refrigerants because – although they have no effects on the ozone layer – they still have the greenhouse gas potential. Compounds containing oxygen such as fluoroethers are known as third-generation refrigerants because they have neither the ozone layer depleting potential nor the greenhouse effect. The possibility was therefore revealed that wastes such as CFCs and HCFCs could be converted into resources.

Especially, 1,1-difluoromethyl ether, CH_3OCHF_2 , is a practically interesting fluoroether converted from CHClF_2 (HCFC-22), which is widely used in air conditioners. As the vapor pressure of the ether is similar to that of $\text{C}_2\text{H}_3\text{ClF}_2$ (HCFC-142b), the ether has a good possibility of use as an alternative refrigerant for $\text{C}_2\text{H}_3\text{ClF}_2$.

The third objective was to reveal the process factors that determine the reaction rate, which is very important for designing photochemical reactors. The process is composed of the following two steps: (1) a mass transfer process of fluorocarbons dissolving in solutions from vapor bubbles and (2) the reaction rate in a solution. To estimate the mass transfer rate, solubility data of fluorocarbons in alcohol–NaOH solutions are reviewed. Using the stationary state model with the kinetic data, a model was obtained for the reaction rate from which a reaction mechanism could be proposed.

2. DECOMPOSITION OF FLUOROCARBONS

2.1. A review of the decomposition technologies

2.1.1. Incineration decomposition method

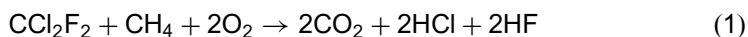
Using a cylindrical burner, Kondo and Miyazaki [2] found that CCl_2F_2 (CFC-12), $\text{C}_2\text{Cl}_2\text{F}_4$ (CFC-114), and C_2ClF_5 (CFC-115) in methane and air were completely decomposed in premixed and/or semipremixed combustion method conditions, although in diffusion flames a great amount of soot formation was observed.

Oyumi and Nagayama [38] investigated thermal decomposition and the burning properties of fluorocarbon/boron/admixed ammonium perchlorate (AP) propellant granule. The fluorocarbon binder was oxidized by the decomposition products of AP, and its decomposition products rate was 423 K lower in the slow thermolysis. The characteristic exhaust velocity significantly decreased at below the characteristic chamber of 11 cm.

Burgess *et al.* [39] developed a comprehensive chemical mechanism consisting of elementary reactions to describe the destruction of fluorinated hydrocarbons and their influence on flame chemistry.

2.1.2. Thermal decomposition method

Kondo and Miyazaki [2,16,17] conducted thermal decomposition of 1,1,2-trichlorotrifluoroethane $\text{C}_2\text{Cl}_3\text{F}_3$ (CFC-113) in hexane or methane under the condition of excess oxygen. They revealed that the major halogenated compound in the emission gas was CCl_2F_2 (CFC-12), which was decomposed completely above 1000 K as follows (equation (1)):



In this case, treatment of the outlet gas at high temperatures is a severe problem. However, if this reaction is carried out at 1400°C with calcium carbonate in a cement plant, the HCl and CaF_2 produced are converted to harmless CaCl_2 and CaF_2 . When CCl_2F_2 is added to an 8-m long rotary kiln, 100% of the feed was decomposed [17].

Lin and Yates [37] carried out thermal reactions of fluorocarbon and hydrofluorocarbon species on $\text{Si}(100)-(2 \times 1)-\text{CF}_3\text{I}$, $\text{CF}_3\text{CH}_2\text{I}$, and C_2F_4 .

Angellino and Invernizzi [44] tested five zero ODP (ozone depletion potential) hydrofluorocarbon refrigerants (HFC-23, HFC-143a, HFC-227ea, HFC-236fa, HFC-245fa) to define their maximum usable temperature and their thermal degradation threshold. Pyrolysis detected excellent thermal stability up to 570–700 K depending on the compounds. Clear degradation signs were observed at temperatures 25–50 K or higher.

2.1.3. Plasma decomposition method

Mizuno *et al.* [3,18–20] reported the conversion of CCl_3F (CFC-11) using radio frequency (RF) argon plasma at atmospheric pressure. In the region of 7–14 kW, decomposition yield increased from 63% to 98%. Analysis of fine particles of soot deposited on the reactor wall revealed that CCl_3F was converted to fluoromethanes, especially CCl_2F_2 or fluoroethanes.

Addition of water increased the decomposition of CCl_3F and decreases soot formation. The major products were CO_2 and CO ; an efficiency of 99.9% was attained with a 15-kW plasma. Decomposition of CCl_2F_2 with water can be expressed as follows (equation (2)), and the outlet gas is neutralized by alkaline aqueous solution.



A demonstration plant of Ichikawa Environmental Engineering Co., which has 50 kg h^{-1} capacity, is working in the suburbs of Tokyo. However, treatment is expensive, about \$4 per kg.

Kanazawa *et al.* [4] carried out similar plasma decomposition of CCl_2F_2 with thermal argon plasma generated by d.c. arc discharge. The results were similar to that of CCl_3F (CFC-11).

Breitbarth *et al.* [40] studied, by Fourier transform infrared (FTIR) spectroscopy, the kinetics of the plasma-chemical conversion of a number of saturated, as well as of unsaturated, fluorocarbon compounds in an oxygen-based RF discharge. Unsaturated fluorocarbons are rapidly converted into CF_4 and C_2F_6 , which, in the presence of silica walls, are finally converted quantitatively into SiF_4 . The results of this investigation are used to design a plasma-chemical reactor for the conversion of fluorocarbon exhaust gases into SiF_4 in the vacuum line of a technological low-pressure plasma reactor.

Sato *et al.* [41] investigated the thermal decomposition products of fluorine-graphite intercalation compounds ($\text{C} \times \text{F}$) with a first stage structure. Residual carbon obtained by the decomposition of $\text{C}_{2.5}\text{F}$ at 770 K possesses graphite structure with a low crystallinity. Reactive fluorocarbon gases are evolved by the decomposition, and successively react to give a deposit of carbon and fluorocarbons on the reactor wall as well as gaseous perfluoroalkanes.

Jasinski *et al.* [43] presented a novel plasma method and its application for the destruction of fluorocarbon C_2F_6 (CFC-116) in atmospheric-pressure flowing nitrogen using a moderate-power (several hundred watts) microwave torch discharge (MTD). The results showed that the decomposition efficiency of C_2F_6 was up to 100% with the removal rate of several hundred g h^{-1} and energy efficiency of several hundred g kWh^{-1} . This energy efficiency of C_2F_6 decomposition was much higher than that of the conventional methods.

Hayashi *et al.* [45] investigated a nonthermal plasma produced by the streamer corona discharge at atmospheric pressure for the treatment of fluorocarbons. The

effective treatment of fluorocarbons was performed by controlling the discharge parameters of the plasma. The decomposition rate of fluorocarbon was investigated by varying discharge modes, dilution gases, and discharge characteristics, that is, applied voltage V of the main discharge gap and its steepness dV/dt . Maximum decomposition rate of 92% was achieved by the streamer corona discharge.

Hayashi and Satoh [46] investigated a nonthermal plasma produced by the streamer corona discharge at atmospheric pressure. The effectiveness of fluorocarbon treatment was investigated by using a mixture of Ar or N gas with CF_4 . A maximum decomposition rate of 86% and a maximum energy efficiency of 0.6 g kWh^{-1} were achieved using the mixture of CF_4 (1%) and Ar (99%).

2.1.4. Catalytic reactions

Mizuno *et al.* [5] catalytically hydrolyzed chlorofluorocarbons. In the presence of water, $\text{CCl}_n\text{F}_{4-n}$ ($n < 4$) gave CO_2 , HCl , and HF . Although HY and NaY zeolites showed high initial activities, they were deactivated within a few tens of hours. Using 30 different catalysts, Imamura [6] decomposed CCl_2F_2 . He concluded that selection of catalysts for the treatment of fluorocarbons seemed difficult because fluorine is more corrosive than chlorine. Ichikawa and Ohnishi [7], catalytically transformed $\text{C}_2\text{Cl}_3\text{F}_3$ (CFC-112) on reacting with hydrogen via $\text{C}_2\text{H}_3\text{ClF}_2$ and C_2HF_3 into $\text{C}_2\text{H}_2\text{F}_4$ (HFC-134a), which has no ozone depleting effect.

Ogata *et al.* [36] decomposed fluorocarbons (1%) in Ar using a surface discharge-type plasma reactor. When TiO_2 pellets were packed as a catalyst, the removal rate increased; however, significant UV emission and temperature increase were not observed in the plasma reactor. The removal rate was also enhanced when water vapor, oxygen, or hydrogen was added to the reactant.

Howe *et al.* [42] undertook Al and Ni K-edge XANES and EXAFS experiments to characterize the chemical states of aluminum and nickel in NiZSM-5 catalysts used for the pyrolysis and hydrodehalogenation with methane of Halon 1301 (CF_3Br). Pyrolysis of Halon 1301 over NiZSM-5 involved both extra-framework aluminum fluoride or hydroxyfluoride species and aggregated nickel species, probably fluorides. The reaction products were CF_4 and C_2F_6 . In the presence of CH_4 framework, dealumination and aggregation of nickel was inhibited.

2.1.5. Reductive dehalogenation in sodium naphthalenide-THF solution

Oku [8] accomplished reductive transformation of organic halogen atoms into halide ions. He decomposed $\text{C}_2\text{Cl}_3\text{F}_3$ (CFC-113) in sodium naphthalenide-THF solution at temperature ranging from 0 to 150°C , and almost over 80% Cl^- and F^- was dehalogenated. Both gaseous CHClF_2 (HCFC-22) and CCl_2F_2 (CFC-112) were dehalogenated almost completely by an analogous method. To avoid the

addition of additives as well as high temperature, UV light irradiation was used to accelerate the reaction.

2.1.6. *Supercritical water hydrolysis*

Fluorocarbons are easily hydrolyzed in supercritical water above 647 K and 22 MPa. Hakuta [9] decomposed CFC-11 completely to produce HCl and HF in 45 min.

2.1.7. *Superoxide-induced decomposition by pyridine and dipyridinium ion-type compounds*

Decomposition of CFCs can happen at room temperature by superoxide continuously generated by the use of pyridine and dipyridinium ion-type compounds. Matsunaga [10] decomposed CFC-113, CFC-112, and other chlorinated compounds over 85% degradation at 32°C.

2.1.8. *γ -ray radiation*

Toriyama *et al.* [14] irradiated C₂Cl₃F₃/hexane with γ -ray radiation. The main products were mono-chlorinated alkane and mono-hydrogenated fluorocarbons. HCl is also found as a by-product.

2.1.9. *Photochemical decomposition*

Tanaka and Hisanaga [11] photolyzed air containing CCl₃F, CCl₂F₂ and C₂Cl₃F₃, CHClF₂, and C₂H₄F₂ (HCFC-152) with vacuum ultraviolet (UV) irradiation (185 nm). The final products were Cl₂, F₂, CO₂, and COCl₂. Koyama *et al.* of Toshiba Corporation [13] developed a decomposition process of CFCs by UV irradiation in alcohol–NaOH. While stirring magnetically, CCl₃F was irradiated with a high-pressure mercury lamp at 303 K. The ratio of the product NaCl to that of NaF was over 3.0. They obtained similar results for C₂Cl₃F₃ and a few chlorohydrocarbons.

Nishiumi and Sato [12] independently discovered the same reaction as Koyama [13]. Dissolving chlorofluorocarbons containing chlorine atoms, RCl, in a sodium alcoholate R'ONa alcohol solution under UV irradiation at room temperature and atmospheric pressure, chlorofluorocarbons easily decomposed to produce a precipitate of sodium chloride and ether, R'OR, as follows (equation (3)):



The following sections will be mainly concerned with the above reaction done by Nishiumi *et al.*

2.2. Decomposition of CFCs and HCFCs in alcoholic alkali solution

2.2.1. Decomposition of CCl_2F_2 (CFC-12)

Fig. 1 shows a schematic diagram of the experimental apparatus for CCl_2F_2 photochemical decomposition [15]. Bubbling CCl_2F_2 through methanol or 2-propanol solvent (200 ml) containing 28% CH_3ONa or NaOH , CCl_2F_2 was irradiated with a 100-W high-pressure mercury lamp ($\lambda_{\text{max}} = 365 \text{ nm}$). Astonishingly, after bubbling through the solvent at room temperature and atmospheric pressure, for a few minutes, as shown in Fig. 2 [48] a white precipitate of NaCl was observed.

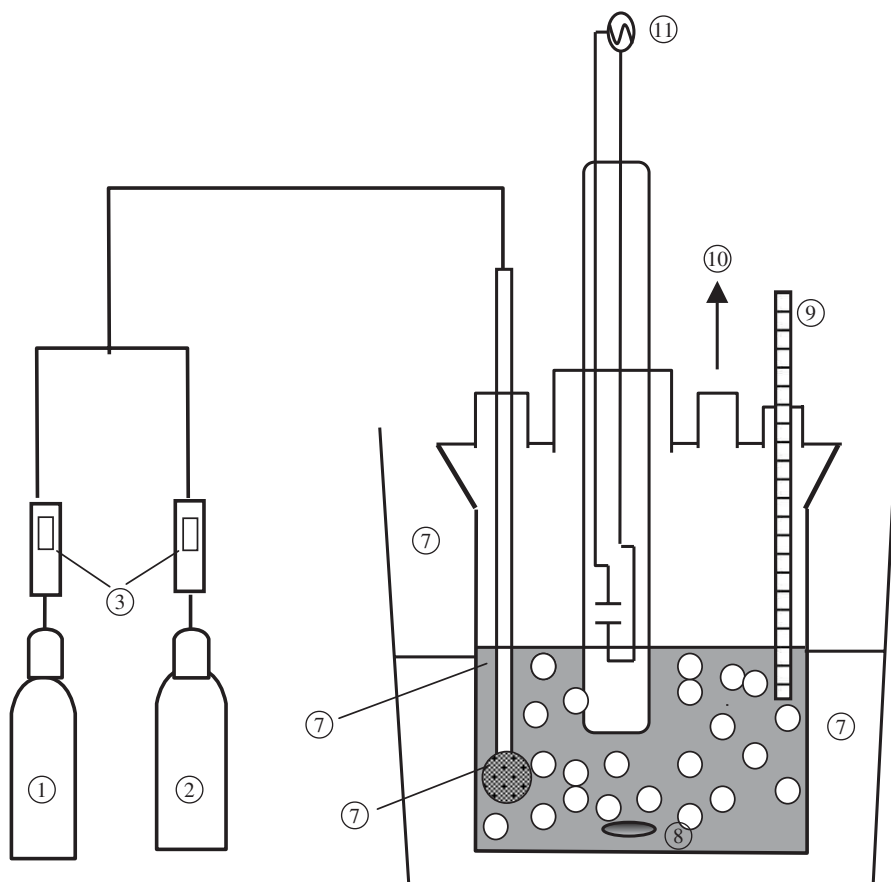


Fig. 1. Schematic diagram of experimental apparatus for CFC-12 photochemical decomposition (Reproduced with permission from H. Nishiumi, 6th World Congress of Chemical Engineering, Melbourne, Australia, 2001); 1, CFC-12; 2, N_2 ; 3, flowmeter; 4, reactor; 5, methanol + NaOH or CH_3ONa ; 6, glass ball filter; 7, water (278 K); 8, stirring magnet; 9, thermometer; 10, sampling; 11: low-pressure mercury lamp.

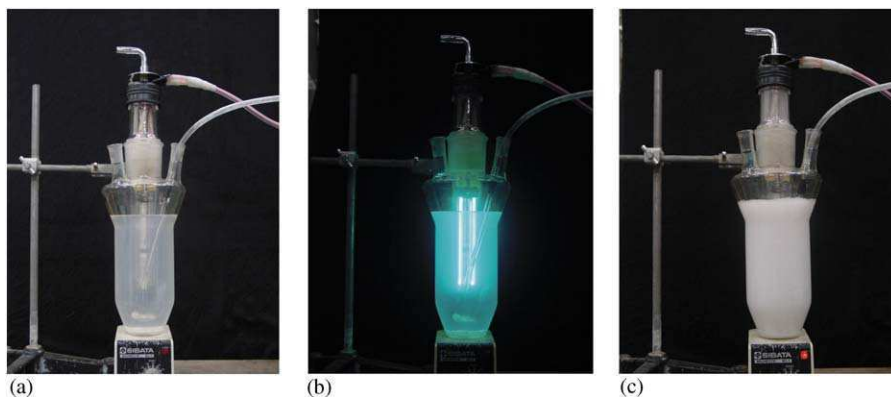


Fig. 2. CFC-12 decomposition under UV irradiation.

The quantity of NaCl was determined by the Mohr method. UV spectral changes in the solution and the produced compounds were characterized using gas chromatogram in the outlet gas [15,34].

2.2.2. Decomposition of 1,1,2-trichlorotrifluoroethane $C_2Cl_3F_3$ (CFC-113)

Reaction occurs in a homogeneous liquid phase because $C_2Cl_3F_3$ is a liquid. Fig. 3 shows that the reaction attained equilibrium in 10 min [34]. Gas chromatography mass spectrometry (GC-MS) detected ethers from intermediates.

2.2.3. Influence of solvents and light sources

All chlorofluorocarbons indicated in Table 1 were decomposed by low-pressure mercury lamp irradiation in NaOH plus 2-propanol solution [21,22]. It was surprising that $CHClF_2$ (HCFC-22) and $CHClFCClF_2$ (HCFC-123a) could be easily decomposed at room temperature in alcoholic alkali solution in the absence of UV irradiation. Chlorofluorocarbons, which were decomposed in methanol or 2-propanol solution with a sodium source, did not react in $C_2H_5ONa-C_2H_5OH$ solution. C_2ClF_5 (CFC-115) could be decomposed only in NaOH plus 2-propanol solution under the irradiation of a low-pressure UV lamp. Decomposition rate in CH_3ONa -alcohol was much faster than in NaOH-alcohol solvent. Since fast sampling in CH_3ONa -alcohol solvent appeared to be difficult, experiments were carried out in NaOH-methanol solvent.

2.2.4. Dechlorination of PCBs in transformer oil by alkaline methanol

Ikeda *et al.* [47] developed a solvothermal decomposition process for polychlorinated biphenyls (PCBs) decomposition in transformer oil using methanol and

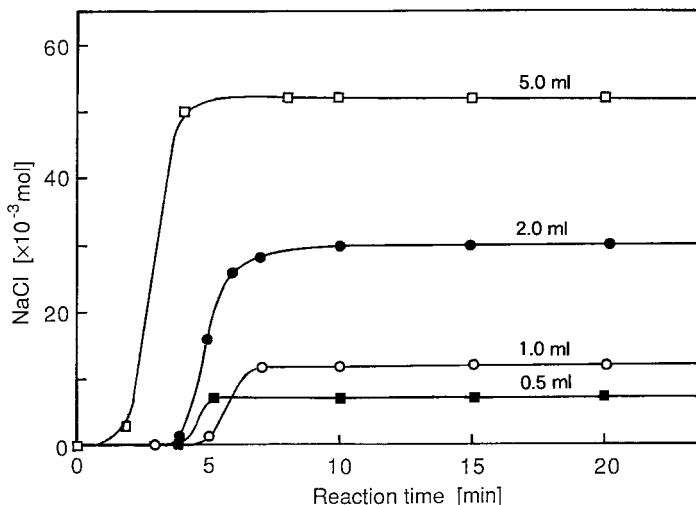


Fig. 3. Effect of CFC-113 on production of sodium chloride. (Reproduced with permission from Japan Committee of Technologies for Destruction of Substances that Deplete the Stratospheric Ozone Layer, Industrial Conference for Ozone Layer Protection (JICOP), 1991.) [1].

Table 1. Comparison of dechlorination in sodium source–alcohol solution [21]

Chlorinated compounds	Thermal at room temperature ^a	UV irradiation	
		High-pressure mercury lamp	Low-pressure mercury lamp
CFC-11	N	Y	Y
CFC-12	N	Y	Y
CFC-113	N	Y	Y
CFC-114	N	Y	Y
CFC-115	N	N	Y ^{b,c}
HCFC-22	Y	Y	Y
HCFC-123	N	Y	Y
HCFC-123a	Y	Y	Y
HCFC-141b	N	Y ^c	Y ^c

Y, dechlorinated; N, not reacted.

For NaOH plus 2-propanol solution, results are stated above.

^a Without UV irradiation.

^b Is 'N' for 28% CH₃ONa–methanol solution.

^c Is 'N' for NaOH–methanol solution.

sodium hydroxide (alkaline methanol solvent). They found that PCB concentration could be decreased below 0.5 g per kg-oil (regulated value of PCBs in waste oil) by using thermal alkaline methanol solvent. The new method is particularly effective at temperatures near the critical point of alkaline methanol. Initial PCB concentration from low (200 ppm) to high (10,000 ppm) range can be treated effectively. The spent solvent after reaction was easily separated from oil, and this solvent could be reused as a fresh solvent. Furthermore, after dechlorination, transformer oil could be reused without decomposition and polymerization. Therefore, the process proposed in this chapter offers a suitable closed system for treatment of dispersed PCBs in transformer oil with high dechlorination efficiency.

3. PRODUCTION OF USEFUL COMPOUNDS FROM FLUOROCARBON WASTES

3.1. Decomposition products of fluorocarbons

Products in solution were analyzed by GC-MS. Comparison of products under irradiation at either 254 or 185 nm are shown in Tables 2 and 3, respectively [23].

Table 2. Decomposition products of chlorofluorocarbons using low-pressure mercury lamp (254 nm) [23]

CFCs	Solvent		
	Methanol + NaOH	2-Propanol + NaOH	2-Propanol
CFC-11	CFC-21	HCFC-31	—
CFC-12	CHF ₂ OCH ₃	CHF ₂ OCH(CH ₃) ₂	HCFC-22
CFC-112	CCIF = CCIF	CHF = CCIF	CCIF = CCIF
	CHF = CCIF	CHCIFCHCIF	CHCIFCCl ₂ F
CFC-113	CHCIFCF ₂ OCH ₃	CHCIFCF ₂ OCH(CH ₃) ₂	HCFC-123a
		(CH ₃) ₂ CHOCHFCHF ₂	
		HFC-143	
CFC-114	No reaction	HFC-124a	HFC-124a
CFC-115	No reaction	HFC-125	No reaction
HCFC-22	CHF ₂ OCH ₃	CHF ₂ OCH(CH ₃) ₂	No reaction
HCFC-123	HCFC-133a	HFC-143	HCFC-133a
HCFC-123a	CHCIFCF ₂ OCH ₃	CHCIFCF ₂ OCH(CH ₃) ₂	No reaction
		(CH ₃) ₂ CHOCHFCHF ₂	
		HFC-143	
HCFC-141b	HCFC-151a	HCFC-151a	No reaction

Produced Cl⁻ ions were detected by the Mohr method.

Table 3. Decomposition products of fluorocarbons with low-pressure mercury lamp (185 nm) [23]

CFCs	Solvent	
	2-Propanol + NaOH	2-Propanol
CFC-12	HCFC-22 HFC-32 CHF ₂ OCH(CH ₃) ₂	HCFC-22 HFC-32
CFC-113	CHClFCF ₂ OCH(CH ₃) ₂ CHF ₂ CHFOCH(CH ₃) ₂	HCFC-123a HCFC-133
CFC-115	HFC-125	No reaction
HCFC-22	HFC-32 CHF ₂ OCH(CH ₃) ₂	HFC-32
HCFC-123	HCFC-133a	HCFC-133a
HCFC-123a	CHClFCF ₂ OCH(CH ₃) ₂ HCFC-133	HCFC-133
HCFC-141b	HCFC-151a	HCFC-151a
CCl ₄	CHCl ₃ CH ₂ Cl ₂	CHCl ₃ CH ₂ Cl ₂
CCl ₂ = CCl ₂	CHCl = CCl ₂	CHCl = CCl ₂
CHCl = CCl ₂	Reacted	Reacted

Produced Cl⁻ ions were detected by the Mohr method.

The produced compounds are found to belong to second-generation HFCs refrigerants, third-generation refrigerant fluoroethers, and fluoroalkenes, with a different number of compounds depending on the starting product. These results show that CFC or HCFC wastes can be re-formed to second- or third-generation refrigerants. Even in 2-propanol solvent without NaOH, dechlorination occurs as shown in Table 2. However, if NaOH is added, the dechlorination rate is much faster because of the easy removal of chloride.

As shown in Table 4, an excimer lamp decomposes CFCs and HCFCs in methanol solvent [23]. However, reaction rate is slower than low-pressure mercury lamps. When an excimer lamp irradiates 2-propanol, the solvent is also decomposed because of the high power of the beam. So, excimer lamps do not seem to be good for decomposition of fluorocarbons.

Takita *et al.* [24] reported an interesting reaction in which UV irradiation of CCl₂F₂ (CFC-12) or C₂Cl₂F₄ (CFC-114) in the presence of oxygen produces tetrafluoroethylene monomer as follows (equation (4)):

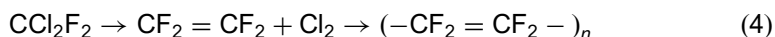


Table 4. Decomposition products of fluorocarbons in methanol with excimer lamp (172 nm) [23]

CFCs	Products
CFC-113	HCFC-123a
CFC-115	No reaction
HCFC-22	Reacted
HCFC-123	HCFC-133a
HCFC-123a	CH ₃ OCCIFCCIF ₂
HCFC-141b	Reacted

Produced Cl⁻ ions were analyzed by the Mohr method.

3.2. Difluorodimethyl ether CH₃OCHF₂ obtained from CCl₂F₂ or CHClF₂

3.2.1. CH₃OCHF₂ production from CHClF₂ (HCFC-22)

Sato, Nishiumi, and Kasatani [25] used two kinds of apparatus (circulating and flow types) for the production of difluorodimethyl ether CH₃OCHF₂ from CHClF₂. By circulating the injected CHClF₂ into methanol-containing saturated sodium methoxide at room temperature and atmospheric pressure, they found sodium chloride and 1,1-difluoromethyldimethyl ether CH₃OCHF₂ produced according to the following reaction (equation (5)):



Products were analyzed with GCMS. The by-product was identified as trimethyl orthoformate CH(OCH₃)₃. It was formed by the following reaction from the fluoroether (equation (6)):



To prevent the increase in the by-product formation, a flow method was used. Finally, 94.5% CH₃OCHF₂ was obtained by distillation with small amounts of CHClF₂ and CH(OCH₃)₃. Fig. 4 shows the gas chromatogram of fluoroether (Porapak-T 3m; injection temperature at 120°C).

To make the process practicable, Matsuyama *et al.* set up a circulating bubble tower of 40 mm I.D. with a sparger as shown in Fig. 5 [48]. At room temperature and atmospheric pressure, the effects of solution volume on the one pass yield of CH₃OCHF₂ are shown in Fig. 6 [48]. Circulation of vapor phase for 20 min brought about complete decomposition of CHClF₂.

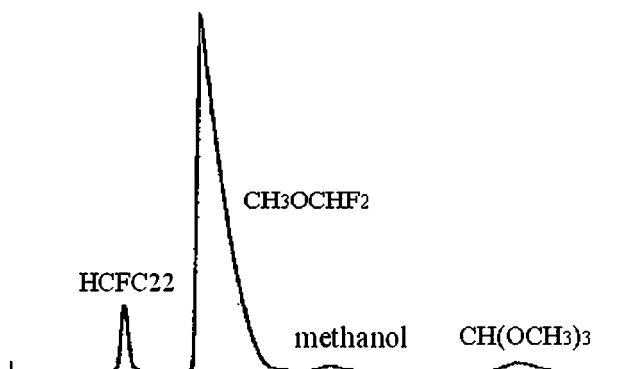


Fig. 4. Gas chromatogram of distilled solution from HCFC-22 decomposition. (Reproduced with permission from *Fluid Phase Equilibria*, 144 (1998) 211–216.)

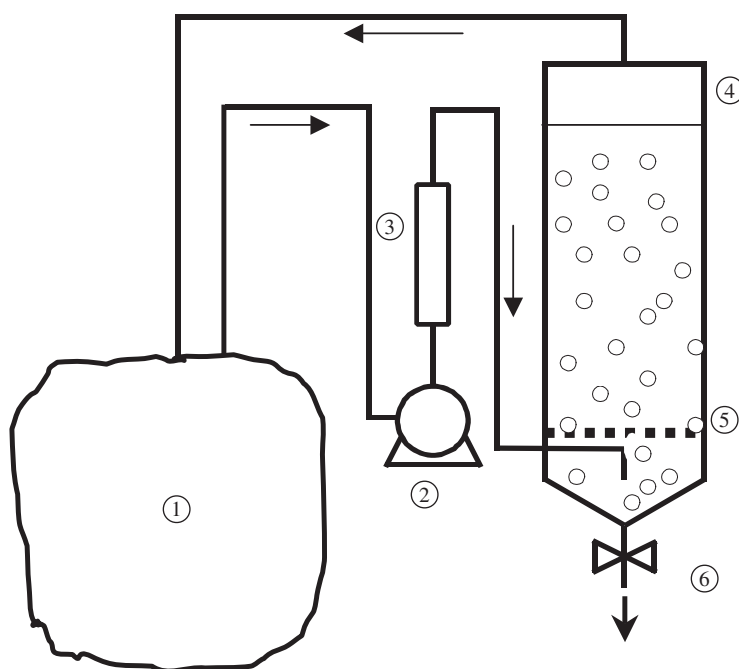


Fig. 5. Circulating bubble tower; 1, tedlar bag; 2, pump; 3, flowmeter; 4, bubble tower; 5, sintered plate; 6, NaCl product [48].

3.2.2. Vapor pressure measurement of CH_3OCHF_2

Using the above sample, Satoh, Nishiumi, and Kasatani [25] measured the vapor pressures between 266 and 393 K with no decomposition due to thermal decomposition detected. As shown in Fig. 7, the vapor pressure of the fluoroether is

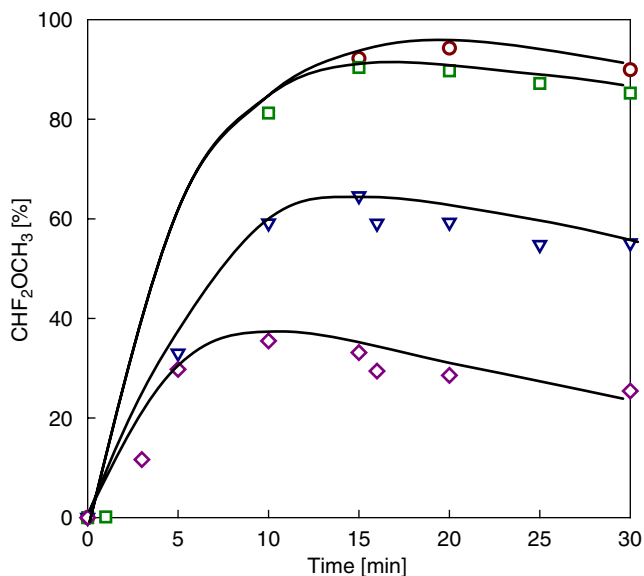


Fig. 6. Effect of volume of NaOH + methanol on CHF_2OCH_3 production; HCFC-22 flow rate 2.0 L min^{-1} , 1 atm; ○, 2.5; □, 2.0; ▽, 1.0; ◇, 0.5 L [48].

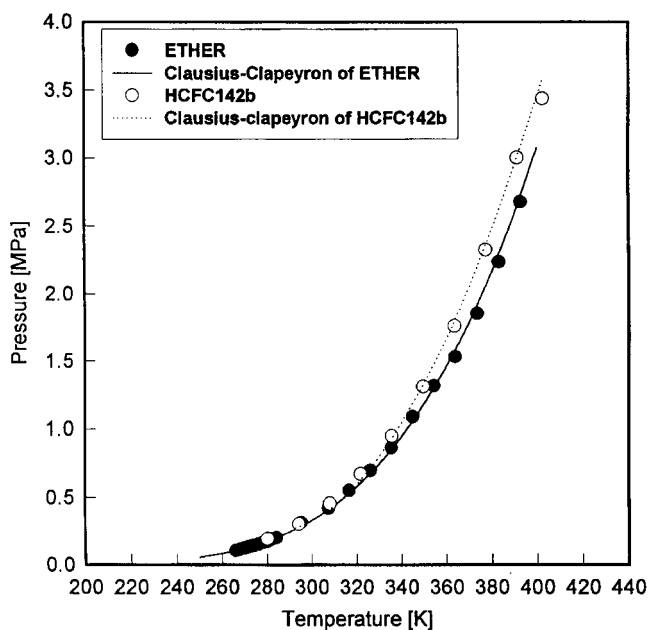


Fig. 7. Comparison of vapor pressure between HCFC-142b and CH_3OCHF_2 . (Reproduced with permission from Fluid Phase Equilibria, 144 (1998) 211–216.)

slightly lower than that of $C_2H_3ClF_2$ (HCFC-142b). With respect to the vapor pressure, the second-generation fluorocarbon $C_2H_3ClF_2$ can be replaced by the third-generation compound CH_3OCHF_2 .

Normal boiling points and critical properties of fluoroethers were estimated by a group-contribution technique according to Joback's equation [26]. Table 5 lists the estimated normal boiling point and critical properties of CH_3OCHF_2 together with those of other fluoroethers using Joback's equation. The measured normal boiling temperature of CH_3OCHF_2 was 264.92 K (8.23°C), whose deviation with correlation was 0.3%.

The fluoroether CH_3OCHF_2 may be a hopeful alternative fluorocarbon for $C_2H_3ClF_2$ in the sense that it neither depletes the ozone layer nor promotes the greenhouse effect. We may use fluorocarbon wastes as a new resource through recycling techniques presented in this work [25].

4. REACTION RATE AND REACTION MECHANISM

4.1. Solubility of fluorocarbons in alcohols

After fluorocarbon vapor dissolves in alcohol, the dissolved fluorocarbons react with the solution components. If a reaction rate is much smaller than a mass transfer rate, the reaction rate is the rate-determining step, and concentration of fluorocarbons in the solution is in equilibrium with the partial pressure of fluorocarbon vapor. So, solubility is a very important information. Takenouchi, Kato, and Nishiumi [27] measured the Henry's law constants of CCl_2F_2 , $CHClF_2$, CH_2F_2 , C_2ClF_5 , C_2HF_5 (HFC-125), and $C_2H_3ClF_2$ (HCFC-115) in methanol, ethanol, and 2-propanol. The experimental apparatus is similar to that shown in Fig. 1 except that there is no lamp. The samples were injected into a gas chromatograph with the thermal conductivity detector (TCD) to determine a vapor- or liquid-phase composition. They correlated experimental data as the Valentiner equation (equation (7)),

$$\ln H = a + \frac{b}{T} + c \ln T \quad (7)$$

where H is the Henry's law constant and T the temperature. The Valentiner constants a , b , and c are listed in Table 6. Deviations from the experiments are thought to be $\pm 3.0\%$. Comparison of the experimental data and the correlation are in excellent agreement as shown in Fig. 8. Measuring solubilities in five types of fluorocarbons in ethanol and methanol with headspace gas chromatography, Kato and Nishiumi [28] obtained similar results as those of Takenouchi *et al.* [27].

Table 5. Estimated normal boiling points and critical properties of some fluoroethers and the observed values for HCFC-142b [25]

Fluoroethers	Formula	Normal boiling temperature [K]	Critical temperature [K]	Critical pressure [MPa]
Difluoromethylmethyl ether	CH_3OCHF_2	265.68 (264.92) ^a	411.15	4.392
Difluoromethyltrifluoroethyl ether	CF_3OCHF_2	260.26	390.22	3.786
Difluoromethyl-2,2,2-trifluoroethyl ether	$\text{CF}_3\text{CH}_2\text{OCHF}_2$	283.29	420.98	3.376
Difluoromethylpentafluoropropyl ether	$\text{CF}_3\text{CF}_2\text{CH}_2\text{OCHF}_2$	278.45	404.56	3.114
HCFC-142b ^b	CF_3CCIF_2	264.0	410.4	4.05

^a Observed values [25].^b ASHRAE [35].

Table 6. Valentiner constants a , b and c of fluorocarbon–alcohol systems ranging 283–313 K [27]

Fluorocarbon	In methanol			In ethanol			In 2-propanol		
	a^*	b^*	c^*	a^*	b^*	c^*	a^*	b^*	c^*
CFC-115	196.3	-9595	-27.46	212.9	-10,591	-29.89	236.4	-11,574	-33.49
HFC-125	-211.0	-7822	33.49	115.3	-6763	-15.22	78.0	-4755	-9.85
HFC-134a	-25.0	-961	5.92	61.4	-4239	-7.32	232.0	-11,566	-32,933
HFC-152a	-482.5	18,819	74.57	-14.3	-926	4.01	179.6	-9501	-24.96
CFC-12	97.1	-5870	-12.50	142.9	-8045	-19.34	378.8	-18,288	-54.76
HCFC-22	86.5	-5660	-10.95	-102.0	2972	17.07	51.2	-3613	-5.89
HFC-32	-65.5	1663	11.60	111.1	-6132	-14.80	8.5	-1292	0.40

* Constant of equation (7).

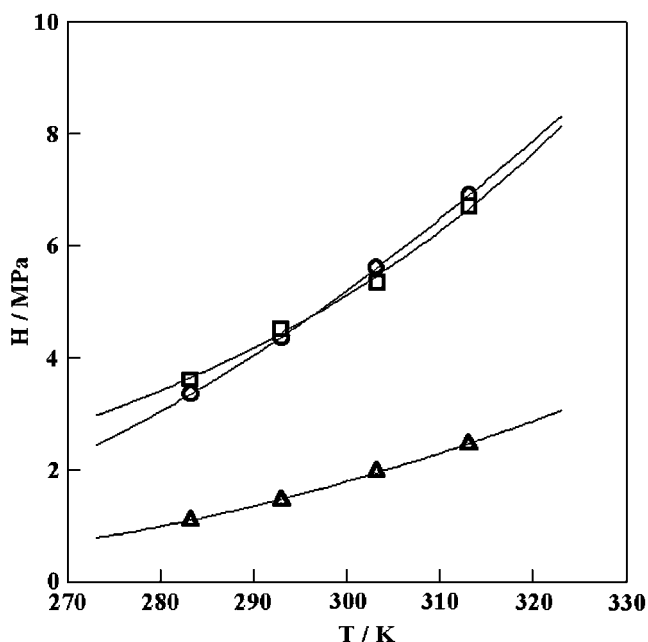


Fig. 8. Henry's law constants of CCl_2F_2 (CFC-12), CHClF_2 (HCFC-22), and CH_2F_2 (HFC-32) in methanol. \circ , CFC-12; Δ , HCFC-22; Δ , HFC-32; solid line, Valentiner equation (7). (Reproduced with permission from *J. Chem. Eng. Data* 46 (2001) 746–749.)

4.2. Decomposition rate of CHClF_2 (HCFC-22)

Nishiumi [21] carried out the decomposition of CHClF_2 by bubbling it in methanol–sodium methoxide at room temperature and atmospheric pressure. From the effect of flow rate on NaCl production, it could be concluded that over

0.8 L min^{-1} reaction rate is a rate-determining step. So, the experiments were carried out at 0.8 L min^{-1} of the inlet gas flow rate. Fig. 10 shows that decomposition rate of CHClF_2 below 101 kPa partial pressure increases with the concentration of CH_3ONa . For high NaCl concentrations, however, there are deviations from regularity because sampling gathers not only liquid but also well-mixed NaCl particles. The reaction rate was found to be proportional to both the concentration of CH_3ONa , $[\text{CH}_3\text{ONa}]$, and the partial pressure of CHClF_2 , $p_{\text{HCFC-22}}$.

Material balance of NaCl concentration $[\text{NaCl}]$ is written as follows if we neglect the production of the by-product, orthotrimethyl formate (equation (8)):

$$\frac{d[\text{HCFC-22}]}{dt} = \frac{d[\text{NaCl}]}{dt} = \frac{k}{H} p_{\text{HCFC-22}} [\text{CH}_3\text{ONa}] \quad (8)$$

where t , k , $p_{\text{HCFC-22}}$ are the reaction time, reaction coefficient, and partial pressure of HCFC-22, respectively. The value of Henry's law constant of CHClF_2 in methanol at 313.15 K, H , was estimated to be $97.9 \text{ kPa L mol}^{-1}$ from the measurement by Takenouchi *et al.* [27]. Fitting the above equation to the experimental data, an optimal value of reaction rate constant k was 0.0260 min^{-1} . Back-calculated results are shown as solid lines in Fig. 9. Results at initial reaction are in excellent agreement; however, experimental data at high NaCl concentrations

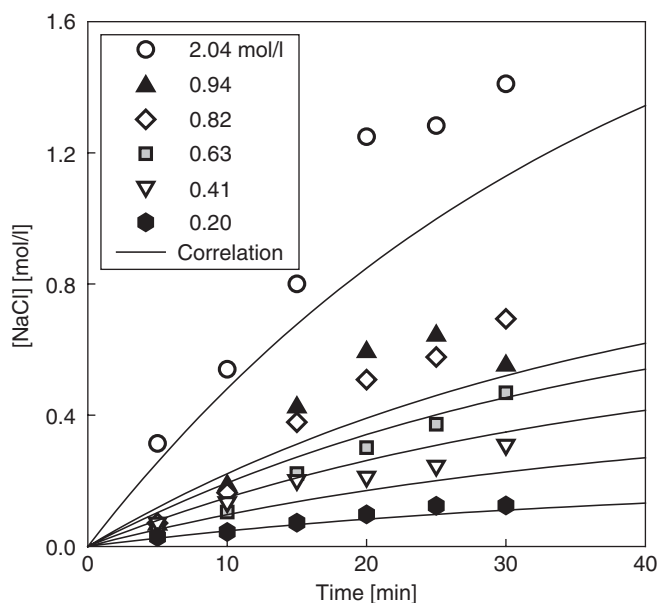
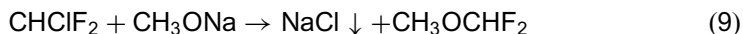


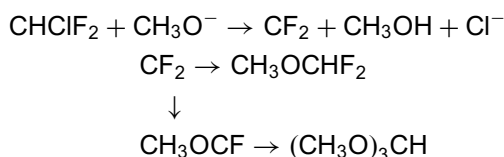
Fig. 9. Effect of CH_3ONa concentrations on NaCl production when partial pressure of HCFC-22 is 101 kPa. (Reproduced with permission from H. Nishiumi, 6th World Congress of Chemical Engineering, Melbourne, Australia, 2001.)

were scattered because of an experimental problem of sampling precipitates, as stated above. Applying equation (3) to the reaction in this work,



The chemical reaction scheme (equation (9)) coincides with the reaction mechanism because the partial pressure $p_{\text{HCFC-22}}$ is proportional to the concentration of HCFC-22 in equation (8).

Early in 1957, Hine and Porter [31] reported that CHClF_2 decomposed to produce CH_3OCHF_2 and $\text{CH}(\text{OCH}_3)_3$; however, they had no idea of its practical use. They studied how the reaction was so fast in comparison to the $\text{S}_{\text{N}}2$ reaction and proposed a reaction model in which an active CF_2 intermediate simultaneously resulted both in 1,1-difluoromethyldimethyl ether CH_3OCHF_2 as given in equation (5) and trimethyl orthoformate $\text{CH}(\text{OCH}_3)_3$ as given in equation (6). They proposed the following reaction scheme:

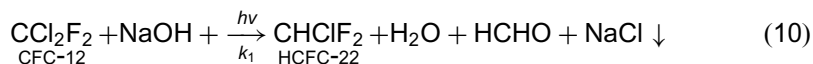


To bring another proof, they carried out the reaction with thiophenoxide ion $\text{C}_6\text{H}_5\text{S}^-$ instead of methoxide ion CH_3O^- , and found it to be a very slow process. Since in other $\text{S}_{\text{N}}2$ reactions $\text{C}_6\text{H}_5\text{S}^-$ was found to be twenty to ten thousand times as reactive as CH_3O^- , the fast reaction with methoxide ion was not $\text{S}_{\text{N}}2$ in character. When methanol– NaOH solution is used instead of CH_3ONa , similar reaction rate equation was obtained [29,30].

4.3. Photodecomposition rate of CCl_2F_2 (CFC-12)

Nishiumi [21] measured the photodecomposition rate of CCl_2F_2 using the apparatus shown in Fig. 1. Under the condition that the reaction is the rate-determining step, he carried out a vapor–liquid consecutive reaction of the photodecomposition of CCl_2F_2 to produce CH_3OCHF_2 *via* CHClF_2 .

First, photodecomposition of CCl_2F_2 produced CHClF_2 :



Second, decomposition of CHClF_2 produced CH_3OCHF_2 :



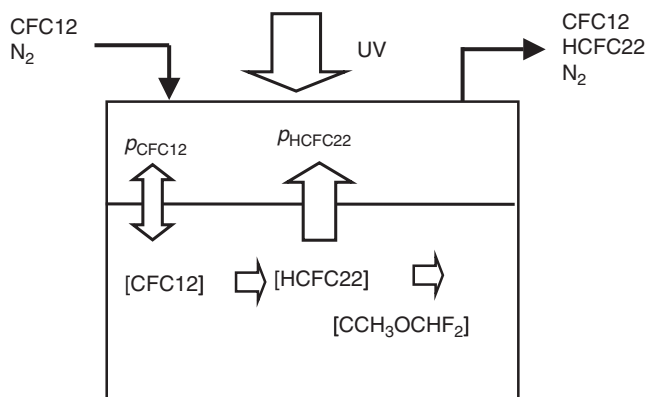


Fig. 10. Reaction model for photodecomposition of CFC-12. (Reproduced with permission from H. Nishiumi, 6th World Congress of Chemical Engineering, Melbourne, Australia, 2001.)

The reaction rate of equation (11) is faster than that of equation (10). Fitting a reaction model to experimental values, the rate constants were determined, and are found to be in excellent agreement with the calculated ones.

The reaction model is shown in Fig. 10. As the inlet gases, CCl_2F_2 and nitrogen bubble into methanol containing NaOH ; after the vapor–liquid equilibrium is attained for CCl_2F_2 , the reaction starts under UV irradiation. The resulting CHClF_2 either transforms into ether or vaporizes. The ether CH_3OCHF_2 does not vaporize and remains in the solution. Nitrogen, unreacted CCl_2F_2 , and CHClF_2 are evacuated from the reactor. Assuming a perfect mixing in both phases, steady state and the rate-determining step of reaction, material balances for components were set up. The rate constants were determined by fitting the reaction model to experimental values. Based on these values, back-calculated results are shown as solid lines in Fig. 11. Experimental values are in excellent agreement with the calculated ones. Profiles of the ether concentration seem to indicate saturation. This may be due to the production of by-product, orthotrimethyl formate, according to scheme (6).

4.4. Photodecomposition rate of C_2ClF_5 (CFC-115) and reaction mechanism

Aruga, Nishiumi, and Sato [32] measured the photodecomposition rate of C_2ClF_5 using the equipment represented in Fig. 1. Once the saturation of C_2ClF_5 was attained, UV irradiation initiated the reaction. From the effect of the flow rate on NaCl production, it could be concluded that over 2.0 L min^{-1} the reaction rate is a rate-determining step. So, the experiments were carried out with an inlet gas flow rate of over 2.0 L min^{-1} .

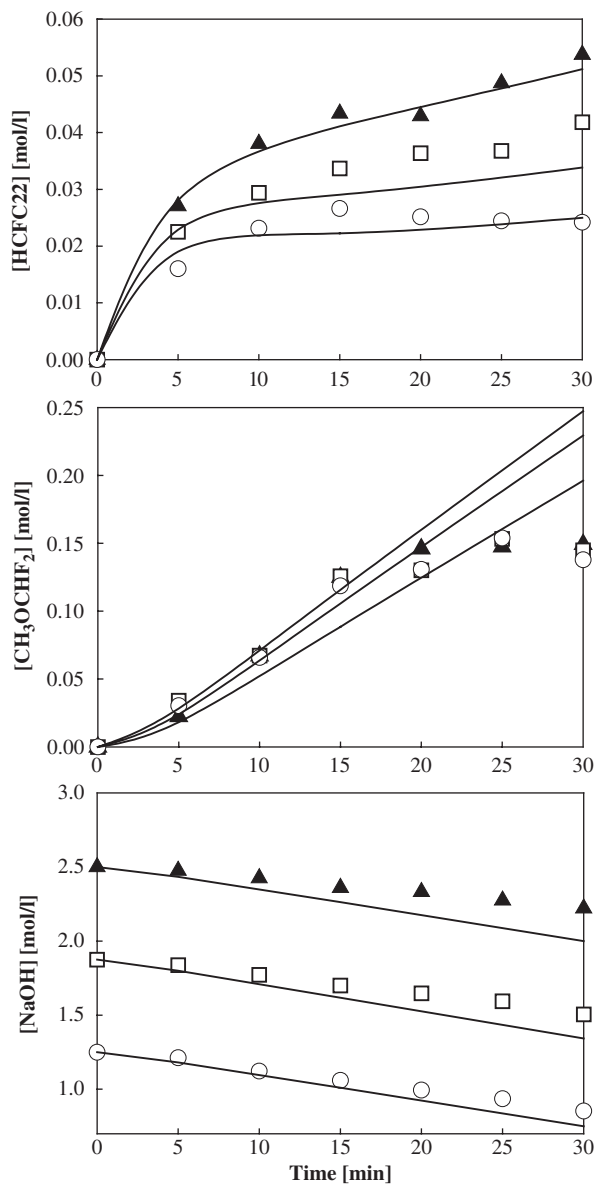
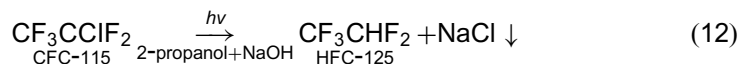


Fig. 11. Concentration profiles of HCFC-22, CH_3OCHF_2 , and NaOH in liquids when partial pressure of HCFC-12 is 16.6 kPa, for different concentrations of NaOH: \blacktriangle , 2.50 mol L^{-1} ; \square , 1 mol L^{-1} ; \circ , 1.26 mol L^{-1} . Solid lines are back-calculated values based on reaction model presented in this work. (Reproduced with permission from H. Nishiumi, 6th World Congress of Chemical Engineering, Melbourne, Australia, 2001.)

The photodecomposition of C_2ClF_5 to produce C_2HF_5 (HFC-125) occurs according to equation (12):



Product C_2HF_5 was identified in the solution by GC-MS. The reaction occurred only in a 2-propanol–NaOH solution, whereas no reaction occurred in methanol–NaOH or 2-propanol only. The effective wavelength of mercury lamp was 253.7 nm. During the manufacture of C_2HF_5 , which was an alternative refrigerant, a very small quantity of C_2HF_5 was also produced. This was very difficult to separate by distillation because the boiling points of both are close. So, this reaction is interesting from the point of view of not only the reaction scheme but also its possible practical use.

The effects of partial pressure of C_2HF_5 on NaCl production are shown in Fig. 12. When the partial pressure is over 20 kPa, the reaction rate increases slowly. It was observed that the color of the solution changes to yellowish; however, no by-product could be detected by GC-MS. In Fig. 13, the initial reaction rate data were plotted against the partial pressures of C_2HF_5 . It reveals that the photodecomposition rate of C_2HF_5 increases with increasing partial pressure or

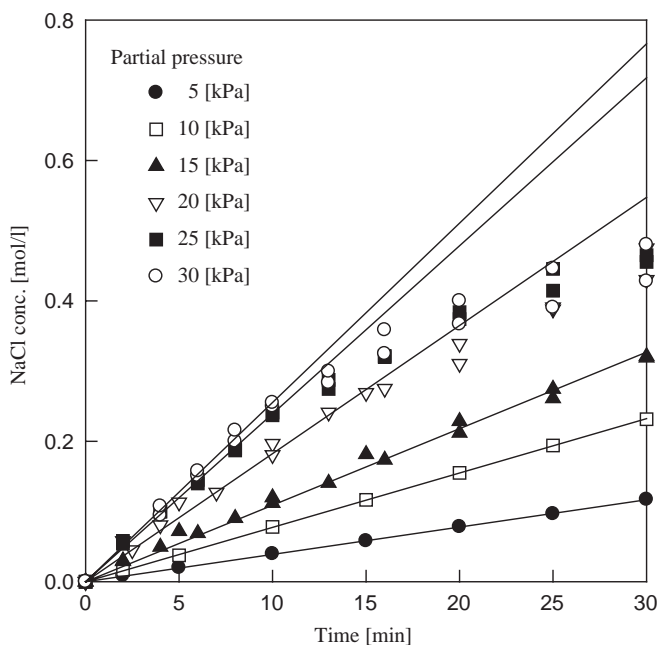


Fig. 12. Effect of partial pressure of CFC-115 on NaCl production. (Reproduced with permission from Kagaku Kogaku Ronbunshu 25 (1999) 837–841.)

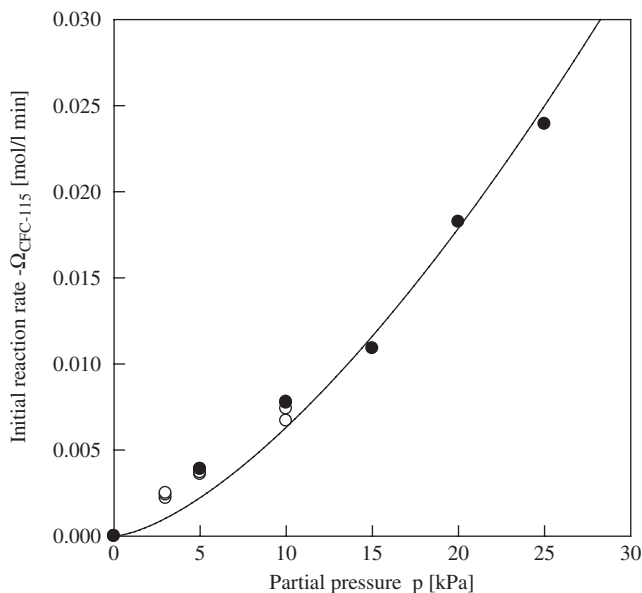


Fig. 13. Relationship between partial pressure of CFC-115 and initial reaction rate; ●, this work; ○, Suda, M. (unpublished); solid line, correlation. (Reproduced with permission from Kagaku Kogaku Ronbunshu 25 (1999) 837–841.)

concentration of C_2HF_5 in the solution. The concentration of NaOH had no effects on reaction rate ranging from 0.10 to 0.24 mol/L.

To control light intensity at 253.7 nm, a $CuSO_4$ filter solution at 30°C was circulated using a similar apparatus as that shown in Fig. 1. The effects of light intensity on NaCl production at a flow rate of $2.0 L min^{-1}$ and partial pressure of 10 kPa are shown in Fig. 14. Relative light intensity is expressed based on the light intensity for $8.0 g L^{-1}$ $CuSO_4$. The data show that the reaction rate increases with light intensity; however, the induction period increases as the light intensity decreases. Linear slopes of the initial period are plotted on a log scale against relative intensities as shown in Fig. 15. They reveal that the initial reaction rate is proportional to the square root of the light intensity. According to the experimental results, the initial reaction rate $\Omega_{CFC-115}$ is expressed as follows (equation (13)):

$$-\Omega_{CFC-115} = \frac{d[CFC-115]}{dt} \propto I_0^{1/2} [CFC-115]^a \quad (13)$$

The concentration of NaOH has no effect on the reaction rate. Comparison of the radiation energy data at 253.7 nm from the lamp maker “Riko Kagaku Sangyo Co.” with the rate of NaCl produced reveals that the minimum overall quantum yield is over 50. It means that the reaction is a chain reaction. Based on the above

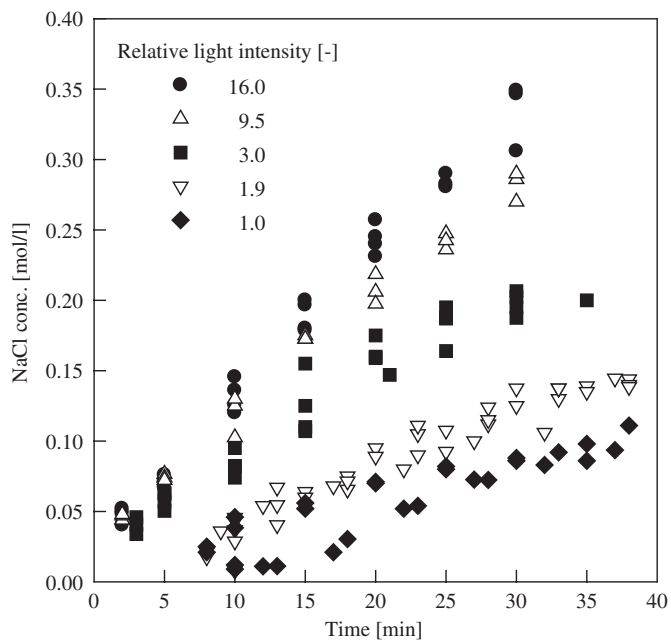


Fig. 14. Effect of light intensity on NaCl production. (Reproduced with permission from Kagaku Kogaku Ronbunshu 25 (1999) 837–841.)

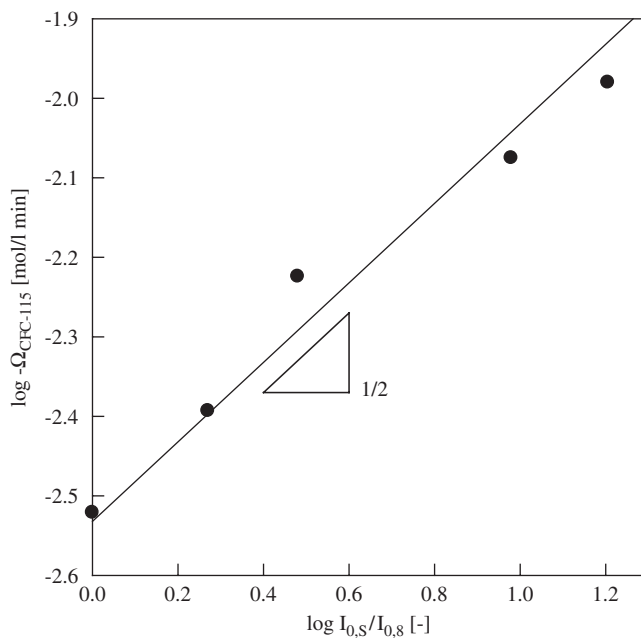
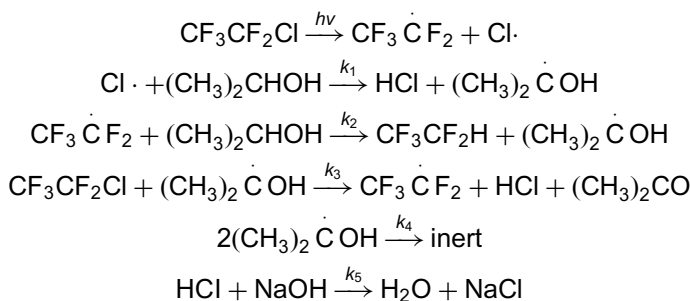


Fig. 15. Relationship between light intensity $I_{0,S}/I_{0,8}$ and initial decomposition rate of CFC-115 [32].

information, the following reaction mechanism was proposed [32]:



where k_i ($i = 1-5$) is a reaction coefficient for each elementary reaction. Material balances from the above mechanism were set up. Assuming that light absorption is very small, application of the material balance to an immersed batch-type photochemical reactor leads to the following expression (equation (14)):

$$-\frac{d[\text{CFC-115}]}{dt} = k_3 \left(\frac{4\pi LR_1(R_2 - R_1)\varepsilon\phi}{Vk_4} \right)^{1/2} I_0^{1/2} [\text{CFC-115}]^{3/2} \quad (14)$$

where L , R_1 , R_2 , V , I_0 , ε , and ϕ are the length of a light source, radii of a reaction cell, liquid volume, light intensity at 253.7 nm, light absorption coefficient of C_2HF_5 in the solution, and primary quantum yield, respectively. The solid line in Fig. 13 is based on the correlation from equation (14) and is in good agreement with the experimental data.

5. EFFECT OF MASS TRANSFER RATE ON REACTION RATE

5.1. Effect of NaCl precipitation on the decomposition of CHClF_2

Nishiumi and Kato [30] described that the NaCl precipitating during the CHClF_2 decomposition may have disturbed the mixing of the solution. Decomposition of CHClF_2 does not need UV irradiation. The experimental apparatus is similar to the one shown in Fig. 1 without the use of a UV lamp. Reactions were carried out in a 1L sealed glass batch reactor. Gas mixtures were bubbled into the 700 cm^3 NaOH–methanol solution through a glass ball filter. The solution was also agitated strongly by a magnetic stirrer. Using a 2 cm^3 solution containing uniformly dispersed precipitation, the concentration of NaCl in solution after dissolving small-sized precipitation was determined using the Mohr method to estimate the quantity of decomposed CHClF_2 and produced ether.

The reaction scheme is shown in equation (10). Experiments were carried out over 5.5 L min^{-1} which is the rate-limiting step of the reaction. Initial reaction rate was found to be proportional to the partial pressure of CHClF_2 , $p_{\text{HFCF-22}}$ and to the NaOH initial concentration C_{NaOH}^0 [30].

As shown in Fig. 17 (broken lines), the deviations from the initial reaction rate increased as the reaction proceeded. In every run, a well-dispersed white NaCl precipitate was observed because of the poor solubility of NaCl in methanol. Considering that NaCl precipitate prevented the mixing of a solution, a model was formulated on the premise that NaCl precipitation would cause a reduction in the mass transfer coefficients of CHClF_2 gas into the solvent.

Measurement of the mass transfer rate of CHClF_2 from the gas phase to the liquid phase was carried out using the same apparatus as shown in Fig. 1, bubbling a gas mixture of nitrogen and CHClF_2 in methanol at 303 K without NaOH, and measuring the CHClF_2 concentration in the liquid directly using gas chromatography.

Assuming perfect mixing of a solution, a material balance can be written as follows:

$$\frac{dC_{\text{HCFC-22}}}{dt} = K_L a (C_{\text{HCFC-22}}^* - C_{\text{HCFC-22}}) \quad (15)$$

Initial conditions: $t = 0$, $C_{\text{HCFC-22}} = C_{\text{HCFC-22}}^*$

where $C_{\text{HCFC-22}}^*$ is the solubility of CHClF_2 in methanol [27].

Then, the volumetric coefficient $K_L a$ is obtained by

$$K_L a = \frac{1}{t} \ln \left(\frac{C_{\text{HCFC-22}}^*}{C_{\text{HCFC-22}}^* - C_{\text{HCFC-22}}} \right) \quad (16)$$

From the experimental data of the concentration of dissolved CHClF_2 vs. time, the values of $K_L a$ were determined from equation (16). Fig. 16 shows the example of $K_L a$ determination at 1.5 L min^{-1} flow rate, 303 K and 101.3 kPa of CHClF_2 pure gas together with the back-calculated results. For this case, the average value of $K_L a$ was 0.179 min^{-1} with 16% average deviation. The back-calculation values agreed well with the experimental data at low concentrations of CHClF_2 .

The volumetric coefficient $K_L a$ was found to be proportional to the flow rate Q . The values of $K_L a$ decreases experimentally as the concentration of NaCl increases. Finally, the following function form of $K_L a$ was used (equation (17)):

$$K_L a = 0.170 Q \exp(-3.0 C_{\text{NaCl}}) \quad (17)$$

where $K_L a$ is expressed in min^{-1} , flow rate Q in L min^{-1} , and concentration of NaCl C_{NaCl} in mol L^{-1} .

The material balance for CHClF_2 in a solution can be expressed as follows:

$$\frac{dC_{\text{HCFC-22}}}{dt} = K_L a (C_{\text{HCFC-22}}^* - C_{\text{HCFC-22}}) - k C_{\text{HCFC-22}} C_{\text{NaOH}} \quad (18)$$

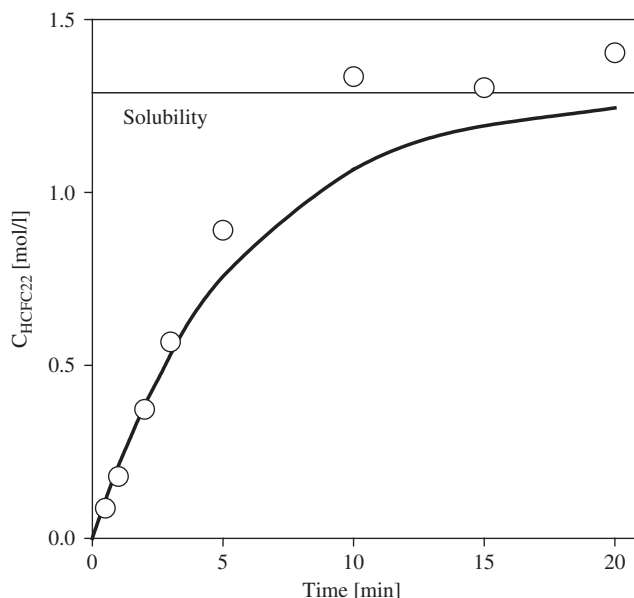


Fig. 16. Mass transfer measurements without NaCl when solution temperature, HCFC-22 partial pressure, and total flow rate were 303 K, 101.3 kPa, and 1.5 L min^{-1} , respectively; \circ , experimental data; solid line, equation (25) for $K_L a = 170 \text{ min}^{-1}$; —, solubility of HCFC-22. (Reproduced with permission from *J. Chem. Technol. Biotechnol.* 78 (2003) 298–302.)

For NaCl,

$$\frac{dC_{\text{NaCl}}}{dt} = k C_{\text{HCFC-22}} C_{\text{NaOH}} \quad (19)$$

Initial conditions: at $t = 0$, $C_{\text{HCFC-22}} = C_{\text{HCFC-22}}^*$, $C_{\text{NaCl}} = 0$

Moreover,

$$C_{\text{NaOH}} = C_{\text{NaOH}}^* - C_{\text{NaCl}} \quad (20)$$

where C_{NaOH}^* is the initial concentration of NaOH.

Simultaneous equations (17)–(20) were numerically solved using the Runge–Kutta method. Fig. 17 shows the effect of mass transfer reduction by NaCl precipitation (solid lines) with respect to the lines calculated without mixing disturbance by the NaCl produced (broken lines). In the initial period, reduction has little effect on the reaction. The effect of $K_L a$ on the reaction becomes noticeable as the reaction proceeds. The model provides qualitative agreement, but a quantitative description still needs further investigation.

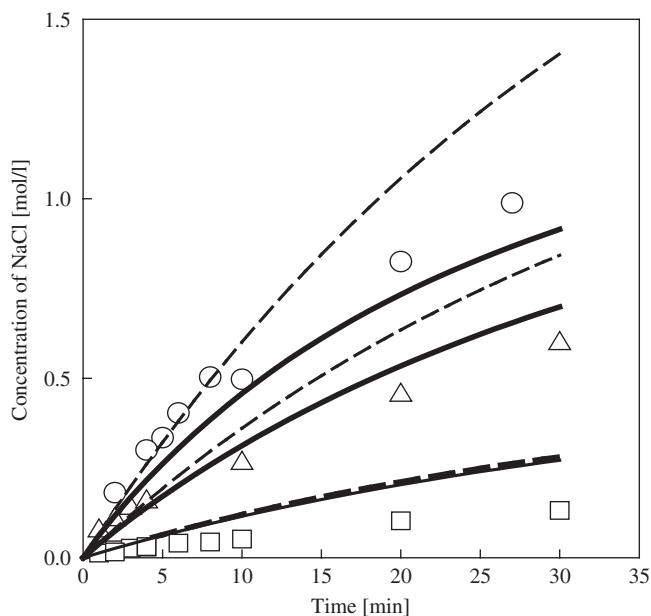


Fig. 17. Comparison between model and experimental data at 303 K and 5.5 L/min for an HCFC-22 partial pressure of 25 kPa in methanol–NaOH solutions. The agitation by NaCl precipitation was taken into account in the calculation. Concentration of NaOH: \circ , 2.5; \triangle , 1.5; \square , 0.5 mol L⁻¹; — —, calculated based on initial reaction rate; —, calculation considering mixing effects at 303 K, and the value of reaction rate coefficient k could be determined to be 0.0871 L min⁻¹ mol⁻¹. (Reproduced with permission from J. Chem. Technol. Biotechnol. 78 (2003) 298–302.)

5.2. Competitive mass transfer rate and reaction rate

Let us consider the decomposition reaction of CHClF_2 according to the scheme equation (10). If the reaction is very slow, vapor–liquid equilibrium for CHClF_2 is attained, which means that mass transfer controls the process. On the other hand, if the reaction is very fast, we cannot find CHClF_2 in the solution, which means that the reaction controls the process. Kato and Nishiumi [33] found that the concentrations reached a stationary state and the values were smaller than the solubility. It means that both the mass transfer and the reaction rates affect each other. They measured the concentration of NaCl with the Mohr method and CHClF_2 in the solution directly by gas chromatography.

Fig. 18 shows that the measured concentrations of CHClF_2 decrease in solubility and reach a steady state as a reaction proceeds at 15 kPa. At lower partial pressure, no decrease in the concentration could be observed with respect to the saturated solubility, because of small reaction rate.

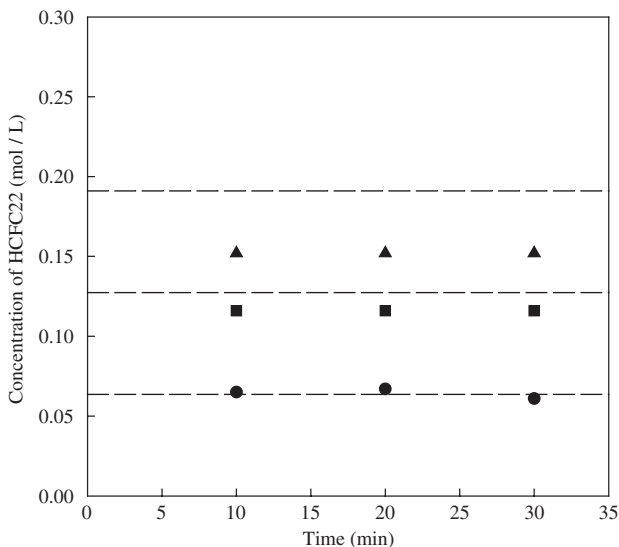


Fig. 18. Relation between partial pressure of HCFC-22 and concentration of HCFC-22 in 0.5 mol L^{-1} NaOH–methanol solution at 303 K; partial pressure of HCFC-22: ●, 5; ■, 10; ▲, 15 kPa; —, saturated solubility. (Reproduced with permission from *Can. J. Chem. Eng.* 81 (2003) 543–548.)

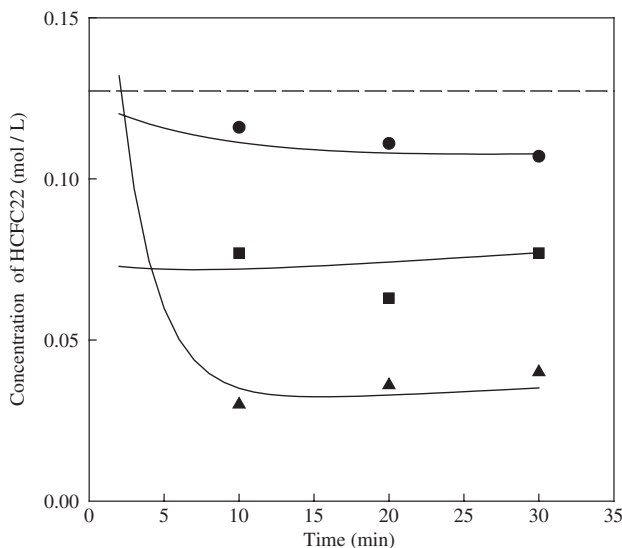


Fig. 19. Comparison between calculated HCFC-22 concentration and experimental data at 303 K and 10 kPa HCFC-22 partial pressure in methanol–NaOH solution; initial concentration of NaOH: ●, 0.5; ■, 1.0; ▲, 2.0 mol L^{-1} ; —, calculation with stationary state model; —, saturated solubility. (Reproduced with permission from *Can. J. Chem. Eng.* 81 (2003) 543–548.)

From the results during the initial period, the reaction rate of CHClF_2 , $-\Omega_{\text{HCFC-22}}$ was obtained (equation (21)):

$$-\Omega_{\text{HCFC-22}} = k_1 C_{\text{HCFC-22}} C_{\text{NaOH}}^2 \tag{21}$$

The value of k_1 was estimated to be $0.0823 \text{ L}^2 \text{ mol}^{-2}$.

The material balance for CHClF_2 is written as equation (22):

$$\frac{dC_{\text{HCFC-22}}}{dt} = K_L a (C_{\text{HCFC-22}}^S - C_{\text{HCFC-22}}) - k_1 C_{\text{HCFC-22}} C_{\text{NaOH}}^2 \tag{22}$$

It is interesting to note that the addition of NaCl decreases the mass transfer rate because it decreases solubility of HCFC-22, and conversely increases the reaction rate. Mathematically speaking, in the initial period, both the mass transfer and reaction rates affect each other, and finally reach a stationary state. Since the right-hand-side is zero at the stationary state, the value of $K_L a$ has been calculated as 0.0911 min^{-1} from the experimental data. Comparison of the experimental data with the back calculation was made. Fig. 19 shows the effects of NaOH concentrations on CHClF_2 concentrations in the solution. Fig. 20 shows the produced NaCl vs. time. The calculated results were in excellent agreement with the experimental data.

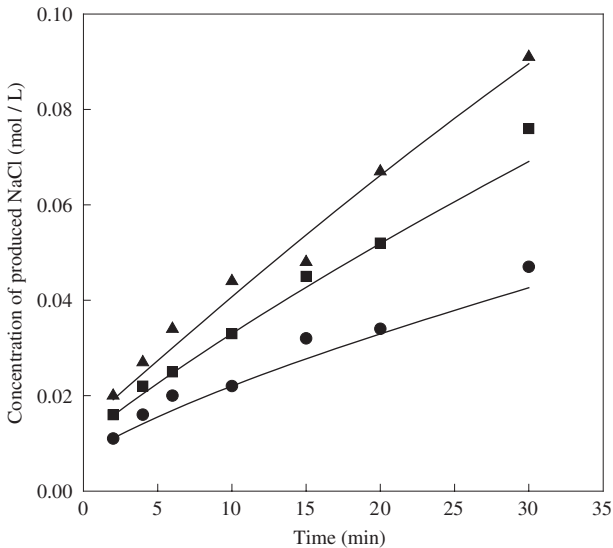


Fig. 20. Comparison between calculated NaCl concentration and experimental data at 303 K and 0.5 mol L^{-1} of NaOH in methanol solution. HCFC-22 partial pressures: ●, 5; ■, 10; ▲, 15 kPa; —, calculation with stationary state model. (Reproduced with permission from Can. J. Chem. Eng. 81 (2003) 543–548.).

6. CONCLUSION

Fluorocarbons of the first-generation refrigerants are easily and rapidly decomposed under UV irradiation in alcohol–NaOH or $-\text{CH}_3\text{ONa}$ solution at room temperature and atmospheric pressure. Moreover, the products are found to be mainly second- or third-generation refrigerants. There are great possibilities, therefore, to consider CFCs or HCFCs as chemical feedstock, instead of waste.

As the vapor pressure of 1,1-difluoromethyl ether CH_3OCHF_2 obtained from either CHC-12 or CHClF_2 was found to be similar to that of $\text{C}_2\text{H}_3\text{ClF}_2$, the ether has a good possibility for being used as an alternative refrigerant or a foaming agent in place of $\text{C}_2\text{H}_3\text{ClF}_2$.

Decomposition of C_2HF_5 under UV irradiation shows a chain reaction. Decomposition of CHClF_2 occurs rapidly even in the absence of UV irradiation. Increased bubbling seems to yield the same results. As the conversion reaction is fast, a stationary state is observed as a result of the competition between mass transfer and reaction.

REFERENCES

- [1] "Destruction Technologies of Substances That Deplete the Stratospheric Ozone Layer" edited by Japan Committee of Technologies for Destruction of Substances that Deplete the Stratospheric Ozone Layer, Industrial Conference for Ozone Layer Protection (JICOP) (1991).
- [2] S. Kondo, A. Miyazaki, Incineration and Thermal Decomposition Methods, *ibid.* (1991) 44–47.
- [3] K. Mizuno, T. Wakabayashi, H. Komaki, T. Amano, H. Ohuchi, Decomposition by an Inductively Coupled R.F. Plasma, *ibid.* (1991) 48–52.
- [4] A. Kanazawa, H. Sekiguchi, T. Honda, Decomposition of Chlorofluorocarbons using a Thermal Argon Plasma, *ibid.* (1991) 53–56.
- [5] K. Mizuno, Y. Fujii, M. Tajima, Catalytic Hydrolysis of Chlorofluorocarbons, *ibid.* (1991) 57–60.
- [6] S. Imamura, Catalytic Decomposition of Halogenated Organic Compounds, *ibid.* (1991) 61–67.
- [7] M. Ichikawa, R. Ohnishi, Catalytic Transformation of CFCs to Useful Raw Materials, *ibid.* (1991) 68–71.
- [8] A. Oku, Complete Destruction of CFCs by Reductive Dehalogenation, *ibid.* (1991) 72–80.
- [9] T. Hakuta, Supercritical Water Hydrolysis of CFC, *ibid.* (1991) 81–83.
- [10] K. Matsunaga, Superoxide-Induced Destruction of Chlorofluorocarbons (CFCs), Halon and Chlorocarbons (CCs) at Room Temperature, *ibid.* (1991) 84–86.
- [11] K. Tanaka, T. Hisanaga, Photochemical Degradation, *ibid.* (1991) 87–90.
- [12] H. Nishiumi, K. Sato, Dechlorination Process of Chlorofluorocarbons or Compounds Containing Chlorine With or Without UV Irradiation, *ibid.* (1991) 91–94.
- [13] M. Koyama, M. Suzuki, A. Okada, K. Suzuki, Decomposition of CFCs by UV-Irradiation, *ibid.* (1991) 95–99.
- [14] K. Toriyama, M. Okazaki, K. Numome, Conversion of Frons to Their Substitutes by Ionic Radiation, *ibid.* (1991) 100–102.

- [15] H. Nishiumi, K. Sato, Fluorocarbon Removal with Photodechlorination (Jpn), 55th Annual Meeting of Society of Chemical Engineers Japan, Nagoya, Japan (1990), p.79.
- [16] S. Kondo, K. Tokuhashi, Res. Disaster (Jpn) 23 (1992) 156.
- [17] S. Kondo, Report of Disaster Science Research (1995), p. 1.
- [18] K. Mizuno, Chemistry 45 (1990) 86.
- [19] K. Mizuno, Adv. Chem. (Jpn) 1990 (1990) 35.
- [20] K. Mizuno, Sep. Technol. 22 (1992) 273.
- [21] H. Nishiumi, Conversion of Waste CFCs and HCFCs into Resources, 6th World Congress of Chemical Engineering, Melbourne, Australia (2001), pp. 1–10.
- [22] H. Nishiumi, K. Sato, (Photo)-Decomposition Process for Compounds Containing Chlorine, Trans. Mat. Res. Soc. Jpn 18A (1993) 387–390.
- [23] K. Sato, H. Nishiumi, Photodechlorination of Fluorocarbons (Jpn), in Chemical Engineering Symposium Series 62, Chemical Reaction Engineering of Photo and Radical Species, Soc. Chem. Eng. Jpn (1998), 101–107.
- [24] Y. Takita, K. Yamada, T. Ishihara, Y. Mizuhara, Nihon-kagaku-kaishi 1990 (1990), 584.
- [25] K. Sato, H. Nishiumi, T. Kasatani, Vapor Pressure of CH_3OCHF_2 Synthesized from HCFC22, Fluid Phase Equilibria 144 (1998) 211–216.
- [26] R.C. Reid, J.M. Prausnitz, B.E. Polong, The Properties of Gases and Liquids, 4th Edn, McGraw-Hill, New York, 1987, pp. 14–15.
- [27] M. Takenouchi, R. Kato, H. Nishiumi, Henry's Law Constant Measurements of CCl_2F_2 , CHClF_2 , CH_2F_2 , C_2ClF_5 , C_2HF_5 , CH_2FCF_3 , and CH_3CHF_2 in Methanol, Ethanol, and 2-Propanol, J. Chem. Eng. Data 46 (2001) 746–749.
- [28] R. Kato, H. Nishiumi, Henry's Law Constant Measurements of CHClF_2 , CH_2F_2 , C_2ClF_5 , CH_2FCF_3 , and CH_3CHF_2 in Methanol, and Ethanol with Headspace Gas Chromatography, J. Chem. Eng. Data 47 (2002) 1140–1144.
- [29] H. Nishiumi, M. Narita, Decomposition Rate of HCFC22 under Room Temperature and Atmospheric Pressure, 34th Autumn Meeting of Society of Chemical Engineers Japan, Sapporo, Japan, 2001.
- [30] H. Nishiumi, R. Kato, Effect of NaCl Precipitation on Vapour-Liquid Dechlorination of CHClF_2 , J. Chem. Technol. Biotechnol. 78 (2003) 298–302.
- [31] J. Hine, J.J. Porter, Methylene Derivatives in Polar Reactions. VIII. Difluoromethylene in the Reaction of Chlorodifluoromethane with Sodium Methoxide, J. Am. Chem. Soc. 79 (1957) 5493–5496.
- [32] H. Aruga, H. Nishiumi, K. Sato, Photo-decomposition Mechanism of CFC115, Kagaku Kogaku Ronbunshu 25 (6) (1999) 837–841.
- [33] R. Kato, H. Nishiumi, Stationary State Model in Reforming HCFC22 (CHClF_2) to Difluoromethylether (CH_3OCHF_2), Can. J. Chem. Eng. 81 (2003) 543–548.
- [34] H. Nishiumi, K. Sato, Fluorocarbon Decomposition Methods Containing Chlorine with Bubble Column Reactor, ppm 1991 (1991) 64–69.
- [35] ASRAE, ASHRAE Thermodynamic Properties of Refrigerants, America Society of Heating, Refrigerating and Air Conditioning Engineers, 1987.
- [36] A. Ogata, H.H. Kim, S. Futamura, S. Kushiya, K. Mizuno, Effects of Catalysts and Additives on Fluorocarbon Removal with Surface Discharge Plasma, Appl. Catal. B-Environmental 53 (2004) 175–180.
- [37] J.L. Lin, Y. Yates, Thermal-Reactions of Fluorocarbon and Hydrofluorocarbon Species on $\text{Si}(100)-(2 \times 1)-\text{CF}_3$, CF_3CH_2 , and C_2F_4 , J. Vacuum Sci. Technol. A—Vacuum Surfaces and Films 13 (1995) 178–182.
- [38] Y. Oyumi, K. Nagayama, Combustion Behavior of Fluorocarbon Boron AP Propellant at High-Pressure, Propellants Explosives Pyrotechnics 20 (1995) 79–82.
- [39] D.R.F. Burgess, M.R. Zachariah, W. Tsang, P.R. Westmoreland, Key Species and Important Reactions in Fluorinated Hydrocarbon Flame Chemistry, Halon Replacements ACS Symposium Series 611 (1995) 22–340.

- [40] F.W. Breitbarth, D. Berg, K. Dumke, H.J. Tiller, Investigation of the Low-Pressure Plasma-Chemical Conversion of Fluorocarbon Waste Gases, *Plasma Chem. Plasma Process.* 17 (1997) 39–57.
- [41] Y. Sato, R. Hagiwara, Y. Ito, Thermal Decomposition of 1st Stage Fluorine–Graphite Intercalation Compounds, *J. Fluorine Chem.* 110 (2001) 31–36.
- [42] R.F. Howe, S. Thomson, Y.N. Yang, K. Lee, E.M. Kennedy, B.Z. Dlugogorski, Zeolite Catalysts for Halon Conversion, *J. Mol. Catal. A-Chemical* 181 (2002) 63–72.
- [43] M. Jasinski, J. Mizeraczyk, Z. Zakrzewski, J.S. Chang, Decomposition of C₂F₆ In Atmospheric-Pressure Nitrogen Microwave Torch Discharge, *Czechoslovak J. Phys.* 52 (Suppl. D) (2002) 743–749.
- [44] G. Angelino, C. Invernizzi, Experimental Investigation on the Thermal Stability of Some New Zero ODP Refrigerants, *Int. J. Refrig.-Revue Internationale Du Froid*, 26 (2003) 51–58.
- [45] N. Hayashi, K. Yamamoto, S. Ihara, M. Kamatani, S. Satoh, C. Yamabe, Treatment of Fluorocarbon using Nonthermal Plasma Produced by Atmospheric Discharge, *Jpn. J. Appl. Phys. Part 1-Regular Papers Short Notes & Review Papers* 41 (2002) pp. 5399–5403.
- [46] N. Hayashi, S. Satoh, Treatment of a Perfluorocarbon using Nonthermal Plasma Produced by Atmospheric Streamer Corona Discharge, *IEEE Trans. Plasma Sci.* 33 (Part 1) (2005) 274–275.
- [47] H. Ikeda, M. Urakami, K. Sasabe, N. Yamasaki, Dechlorination of PCBs in Transformer Oil By Alkaline Methanol, *Kagaku Kogaku Ronbunshu* 30 (2004) 211–216.
- [48] A. Matsuyama, Production of Fluoroether from HCFC22, Master thesis, Hosci Univ. (2002).

Volcanic Fluorine Emissions: Observations by Fourier Transform Infrared Spectroscopy

Georgina M. Sawyer* and Clive Oppenheimer

Department of Geography, University of Cambridge, Downing Place, Cambridge CB2 3EN, UK

Contents

1. Introduction	165
2. Fluorine geochemistry	167
3. Open-path Fourier transform infrared spectroscopy	169
4. Field observations of HF and SiF ₄	174
5. Emission rates	180
6. Future directions and challenges	180
Acknowledgments	182
References	182

Abstract

Volcanoes are an important natural source of fluorine to the environment. For several decades, fluorine emissions from volcanoes have been measured by laboratory analysis of samples collected *in situ*, and abundances compared with other gas species to infer magmatic and hydrothermal processes occurring at depth. More recently, open-path Fourier transform infrared (OP-FTIR) spectroscopy has been applied to field measurements of volcanic gas plumes, offering several advantages including the ability to detect and quantify simultaneously, and with high time resolution, many volcanic gas species. These include hydrogen fluoride (HF) and silicon tetrafluoride (SiF₄), and potentially other F-bearing gases. Such measurements yield valuable insights into the degassing of fluorine from magmas and contribute to our understanding of the environmental impacts of volcanic emissions.

1. INTRODUCTION

Volcanoes emit substantial quantities of gases and particles into the atmosphere both sporadically, when eruptions occur, and in a sustained manner during protracted episodes of magmatic or fumarolic degassing. The dominant elements in a volcanic plume are C, O, H, S, Cl and F and these combine to form the major

*Corresponding author.

E-mail: gms26@cam.ac.uk

species H_2O and CO_2 , along with lesser proportions of SO_2 , HCl , HF , CO , H_2S and H_2 , among others. Various oxidative processes also occur in volcanic plumes as they are transported in the atmosphere. Monitoring of volcanic gas geochemistry provides valuable insights into the evolution and dynamics of magmatic-hydrothermal systems (e.g., see Refs [1–4]). Temporal variations in the fluxes and relative abundances of fluorine, chlorine and sulphur, for instance, provide information on magma storage and transport, the dynamics of degassing, and interactions between magmatic gases and hydrothermal systems. Such information can have immediate application in forecasting volcanic activity and hazard assessment (e.g., see Refs [5–7]). In addition, assessing and monitoring emission rates of these species into the atmosphere is crucial to understanding and mitigation of their potential effects on local communities and ecosystems [8].

For more than a century, volcanic gas samples have been collected at fumarole vents or close to active lava bodies and analysed in the laboratory. There are several procedures used to collect gas samples in the field, the most common, employing ‘Giggenbach’ bottles or filter packs. The Giggenbach bottle consists of an evacuated flask partially filled with NaOH or other caustic solution and with a headspace under vacuum. It is connected *via* tubing to the volcanic vent to be sampled [9]. Gas is allowed to bubble through the solution so that acid species (e.g., SO_2 , HCl and HF) condense. The condensed phases are typically analysed in the laboratory by ion chromatography, while the incondensable species (e.g., helium and hydrogen), collected in the headspace, can be analysed by gas chromatography. Base-treated filters assembled in packs are also used to trap acid species, and can be deployed around crater rims and close to gas sources. Elements adsorbed on filters are eluted using distilled water sometimes with additional H_2O_2 and then analysed by ion chromatography (e.g., see Refs [5,10]).

These techniques, whilst capable of providing detailed analyses, are impractical or prohibitively dangerous at many volcanoes and may thus be unsuitable for routine or long-term monitoring. They can also lead to uncertainties in speciation of the original gas mixture due to post-collection reactions, and the inevitable delays in obtaining results limit their utility during volcanic crises. In addition, analysis by ion chromatography does not permit the distinction between F-bearing species. As a result, fluorine is often reported as HF in gas analyses by convention, with the possible presence of other gases, such as SiF_4 , being neglected [11]. Although it is possible to quantify amounts of silica in samples, it is difficult to determine whether this silica is from SiF_4 , from other Si-bearing species or simply from volatilisation of silica sampling tubes *via* reaction with HF [12].

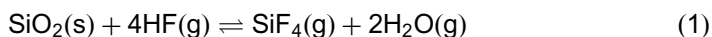
Infrared (IR) spectroscopy is well suited to investigations of volcanic gas emissions since many of the significant molecular species exhibit strong rotational–vibrational features in the ‘fingerprint’ region of the IR spectrum. In particular, both HF and SiF_4 can be observed. The past decade has witnessed the availability of compact and robust Fourier transform infrared (FTIR) spectrome-

ters that are suitable for field deployment. Volcanoes often present harsh environmental conditions but seldom mains power supplies, so instrumentation for field use needs generally to be portable, able to withstand knocks and acid gases, and run on car batteries, generators or solar cells. Equipment can be readily deployed in open-path (OP) configurations that permit flexible sensing strategies for working on active volcanoes. The primary aim of this chapter is to explain the application of FTIR spectroscopy, especially in open-path configurations (OP-FTIR), to volcanic gas geochemistry, and to provide an overview of the main results achieved to date that pertain to fluorine emissions. We begin with an outline of the behaviour of fluorine in magmas, and conclude with a discussion of future developments and challenges.

2. FLUORINE GEOCHEMISTRY

Compared with volatiles such as H₂O, CO₂, Cl and S, fluorine is highly soluble in silicate melts. Experimental work has shown that in some enriched melt compositions up to 10 wt.% F can be dissolved [13]. Analyses of melt inclusions from some metaluminous and peraluminous rhyolites indicate F contents of up to 5 wt.%, consistent with the high solubility of F. The affinity of fluorine for the melt can be understood in terms of its dipole moment, which is similar to that of water, which means that it readily ionises or induces ionisation, and its ability to fit within the silicate melt (or glass) structure. The ionic radius of F⁻ is very similar to that of O²⁻, such that fluoride ions can play a similar role to oxygen ions in bridging SiO₄ tetrahedra in melt or glass [14]. Where F is abundant in silicate melts, it can influence physical properties such as density and viscosity [15]. Very few studies indeed have been conducted on the degassing of F from magmas as a function of composition, decompression or cooling and crystallisation, and much of what we know in this regard has to be inferred from measurements of gas emissions from volcanoes. Certainly, some volcanoes, especially ‘open vent’ volcanoes, where magma degases directly to the atmosphere (e.g., from a lava lake or dome located at the top of the volcanic conduit), sustain high fluxes of F primarily in the form of HF. Certain mineral phases, such as apatite, micas and amphiboles, also readily abstract F from the melt [16,17].

Whilst the principal F-bearing component of volcanic gas is HF, other species including SiF₄, SiOF₂, ClSiF₃ and AlF₂O may also be present under certain conditions [12]. The relative proportions of HF and SiF₄ are thermodynamically controlled by the equilibrium:



Thermochemical modelling of this equilibrium has been explored by several authors including Rosenberg [11], White and Hochella [18], Symonds *et al.* [12],

Symonds and Reed [19] and De Hoog *et al.* [20]. Their results show that the equilibrium composition is strongly dependent on temperature, pressure and HF fugacity. At atmospheric pressure, SiF_4 is abundant only at high HF fugacity and low temperature. While low temperatures favour SiF_4 over HF, the stoichiometry in Reaction (1) indicates that decompression of magmatic gas will shift the equilibrium to the left. At high pressure, the proportion of HF to SiF_4 is again strongly dependent on HF fugacity, with a disproportionate increase in SiF_4 with increasing HF partial pressure (Fig. 1).

This model suggests that the abundance of SiF_4 as a primary magmatic gas is negligible but it may be formed at lower temperatures by reactions between vent wall rocks and HF [21] or as HF diffuses through a fresh lava flow or dome [18]. De Hoog *et al.* [20] have also considered reaction (1) as a potential means for precipitating silica in vesicles in lavas. Disruption and collapse of lava domes has been observed to release considerable quantities of fine ash, rich in cristobalite, which may pose a health hazard (e.g., see Ref. [22]). It has been suggested that reaction (1) could be responsible for this formation of crystalline silica. [Note of the Editor: see also in this series the chapter by K. Anazawa devoted to fluorine and volatiles in magmas and volcanic rocks.]

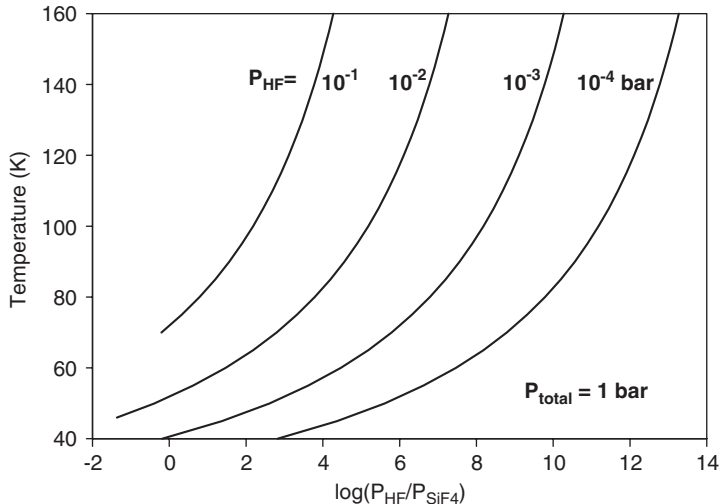


Fig. 1. An empirical relationship, calculated by de Hoog *et al.* [20], between HF/ SiF_4 ratios and temperature for different partial pressures of HF, and 1 bar total vapour pressure ($P_{\text{HF}} + P_{\text{SiF}_4} + P_{\text{H}_2\text{O}} = 1$). Uncertainties in heat of formation and enthalpy of SiO_2 , HF, H_2O and SiF_4 are equivalent to about 25 K and 0.2 log units on this plot. The relative importance of SiF_4 increases both with decreasing temperature and with total amount of F in the system (i.e., P_{HF}).

3. OPEN-PATH FOURIER TRANSFORM INFRARED SPECTROSCOPY

Infrared spectroscopy measures the absorption or emission of IR radiation arising from changes in the rotational and vibrational energy states of molecules. Since different molecular species have unique spectral 'fingerprints', it is possible to identify components of a gas mixture from a measured spectrum. Furthermore, the intensity of absorption or emission lines is related to the amount of gas present in the path by the Beer-Lambert law:

$$I_{1,\lambda}/I_{0,\lambda} = \exp(-\varepsilon_{\lambda}cl) \quad (2)$$

where $I_{0,\lambda}$ and $I_{1,\lambda}$ are the intensity of the source and transmitted radiation at wavelength λ , respectively, ε_{λ} is the absorption coefficient of the molecular species in question (related to its cross-section) and c and l are the sample concentration and path length, respectively. The quantity on the left-hand side of equation (2) is often termed the transmittance, and the logarithm (base 10) of the transmittance is referred to as the absorbance. Analysis of a measured spectrum, therefore, can yield information on the column amount as well as type of infrared-active gases present in the path between a source of IR radiation and the spectrometer. In the literature, gas column amounts integrated across a path length are reported in (ppm m) or (molecules cm^{-2}) with conversion between the two using the following relationship:

$$cl \left[\frac{\text{molec}}{\text{cm}^2} \right] = cl[\text{ppm m}] \times N_0 \times \left\{ \frac{T_0 P}{T P_0} \right\} \quad (3)$$

at any T , P -conditions where T_0 and P_0 are STP ($T_0 = 273.15$ K; $P_0 = 1013.25$ kPa) and N_0 is the Loschmidt number (equal to Avogadro's number/molar volume of an ideal gas at STP). Here we report column amounts in units of molecules cm^{-2} .

OP-FTIR spectroscopy (as opposed to closed path measurements which require gas to be drawn into a cell within the optical path of the instrument) is being increasingly used in volcanic gas studies since a number of compact FTIR instruments came on to the market in the 1990s (Fig. 2). For comprehensive reviews of FTIR spectroscopy principles and applications, see Refs [23,24]. The approach affords quantitative, high temporal resolution remote surveillance of a wide range of volcanic gases such as H_2O , CO_2 , CO , OCS , SO_2 , HCl , HF and SiF_4 , and potentially other molecular species [25]. A typical OP-FTIR spectrum is illustrated in Fig. 3. It takes as little as 1 s to acquire a wideband (e.g., 600–6000 cm^{-1}) spectrum at 0.5 cm^{-1} spectral resolution although several spectra are often co-added to increase the signal-to-noise ratio.

Several commercially available spectrometers are sufficiently field portable and robust to be used in harsh and remote volcanic environments. Depending on the



Fig. 2. MIDAC brand FTIR spectrometer (optically connected to a Newtonian telescope) being set up at the summit crater rim of Mt. Erebus, Antarctica. The detector dewar is being filled with liquid nitrogen. The volcano's active lava lake was used as an infrared source. The edge of the gas and aerosol plume emitted from the lake is visible at the right-hand edge of the photograph (photo C. Oppenheimer).

sensing geometry, measurements can be made at a degassing vent or several km or tens of km downwind using natural or artificial sources of IR radiation (Fig. 4). This versatility is a tremendous advantage for field measurements on active volcanoes allowing sensing strategy to take account of access, local topography, levels of activity, meteorological conditions and logistical considerations.

A variety of detectors can be used for OP-FTIR spectroscopic measurements although liquid nitrogen cooled indium antimonide (InSb) and mercury–cadmium–telluride (MCT) detectors, sensitive between approximately 1800–6000 and 600–5000 cm^{-1} , respectively, have been most commonly used for volcanological applications. Where liquid nitrogen is not readily available, Stirling-engine- or thermoelectrically cooled detectors are an attractive (but potentially more expensive) alternative [26].

InSb detectors provide a stronger and more linear response than MCT detectors. However, unlike MCT detectors, InSb detectors cannot reach the longer wavelengths where some important molecules have spectral lines. SiF_4 , for example, has a fundamental line centred at 1032 cm^{-1} (Fig. 5a). The strength of this feature means that the gas can be detected at column amounts $< 2.7 \times 10^{15}$ molecules cm^{-2} , when measuring with a spectral resolution of 0.5 cm^{-1} , over a path length of $\sim 2\text{m}$, using hot rock as an IR source) [21]. HF (Fig. 5b), on the

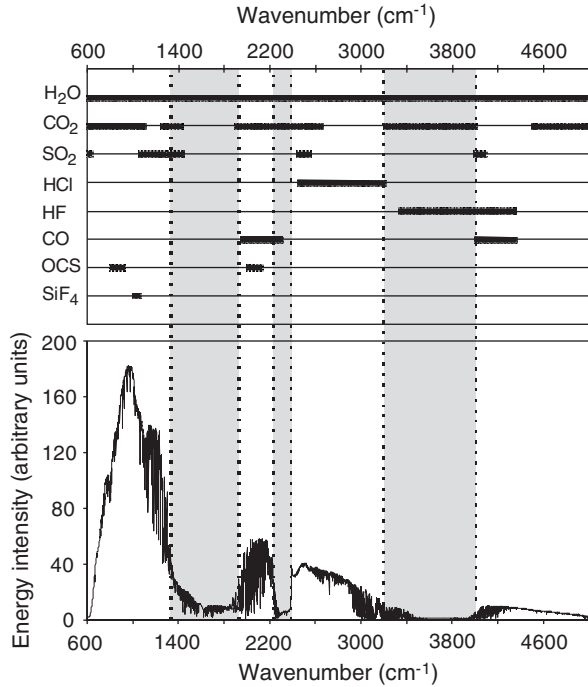


Fig. 3. Lower plot shows a typical OP-FTIR spectrum collected at Masaya volcano (Horrocks *et al.* [39]). Upper plot shows absorption regions for several volcanic gases. Grey shaded areas represent ‘blind’ regions of the spectrum where all IR radiation is absorbed, mainly by H₂O and CO₂ in the atmosphere. Units on the x-axis are in wavenumbers, which are equal to 10⁴ divided by wavelength in μm, i.e., 10 μm = 1000 cm⁻¹.

other hand, exhibits rotational–vibrational structure between 3540 and 4280 cm⁻¹ and thus can be measured using either the MCT or InSb detectors. In typical atmospheric conditions, the spectral lines within the *P*-branch are heavily contaminated by water vapour so only lines in the *R*-branch (3980–4280 cm⁻¹) are used for retrievals. However, the limited strength of spectral lines coupled with high levels of contamination by H₂O lines, even in this region, typically results in increased errors in HF retrievals. Based on measurements collected at Masaya volcano, at a spectral resolution of 0.5 cm⁻¹, over a 518 m path, using an IR lamp, it has been estimated that, within 10% error, HF has a detection limit of 3 × 10¹⁸ molecules cm⁻² and, within 20% error, the detection limit is 4 × 10¹⁷ molecules cm⁻² [27].

The underlying theory for gas retrievals is expressed by the Beer-Lambert law (equation (2)) but several options are available for determining column amounts of target molecules from field spectra. One method, used by e.g., Francis *et al.* [21,28] and Mori *et al.* [29,30], is to calculate absorbance spectra (as in Fig. 5)

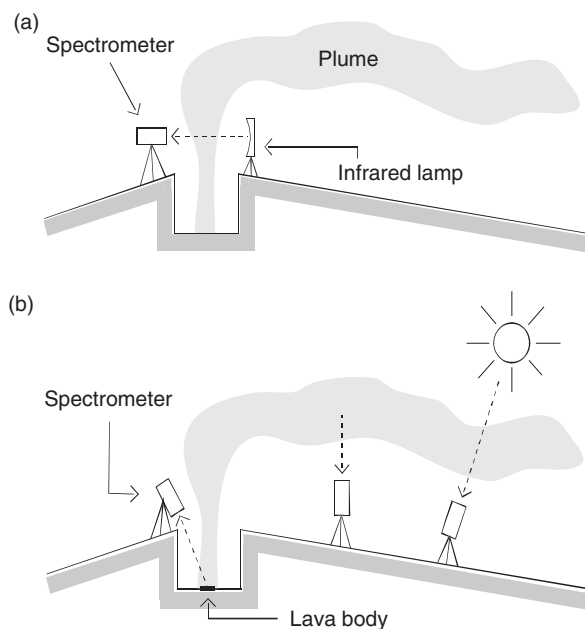


Fig. 4. Possible configurations for OP-FTIR spectroscopic measurements on volcanoes. (a) Active measurements using an artificial IR source across a vent or fumarole. (b) Passive measurements using the Sun, hot rock or the plume itself as a source.

from the logarithm of ratios of two transmittance spectra, one containing volcanic gas and the other containing minimal or no volcanic gas (collected with the same instrument set-up but when the wind is transporting the plume away from the optical path). A laboratory reference spectrum of the target species is then scaled to fit the field absorbance spectra. In this case, the product of the optimum scaling factor and the column amount represented by the reference spectrum gives the retrieved column amount. Alternatively, retrievals can be performed by simulating an OP spectrum in specified spectral ‘micro-windows’ using a radiative transfer model such as the Reference Forward Model [31] and line parameters from a high-resolution molecular absorption database such as HITRAN [32]. The simulated spectrum can be fitted to a measured spectrum via a least-squares fitting procedure, and the column amount of gas that produces the best fit to the measured data is returned. This method has been employed in numerous volcanological investigations (e.g., see Refs [33,34]).

In most cases relevant to volcanic gas observations, the atmospheric mixing ratio of a target gas species is not required, and indeed is usually variable along the viewing path due to variations in atmospheric transport of the plume or discontinuous emission from the vent. Column amounts of gas from one spectrum to

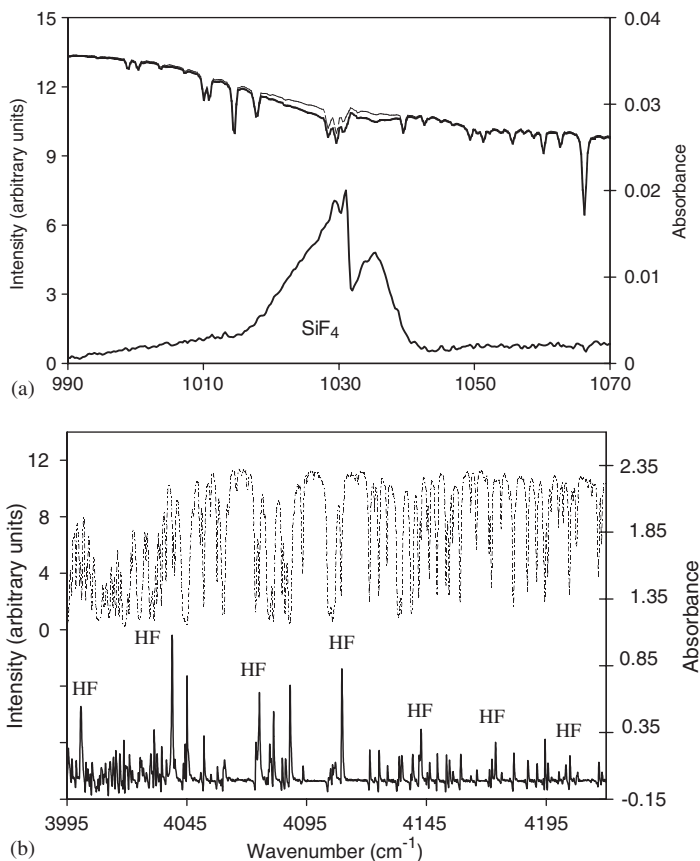


Fig. 5. Fluorine species detected by OP-FTIR spectroscopy. (a) SiF₄ observed at Vulcano, Italy by Francis *et al.* [21]. (b) HF observed at Masaya volcano by Horrocks *et al.* [39]. Upper traces in (a) and (b) represent two single-beam spectra with differing column amounts of volcanic gas, whose ratio is used to derive the absorbance spectra shown in the lower traces in (a) and (b).

the next may vary considerably (Fig. 6a) but the ratio of column amounts for two gas species should equal the ratio of their abundances in the atmosphere since emissions are typically well mixed. Gas ratios can therefore be derived from an individual spectrum or from a series of spectra (Fig. 6b) and hence used to infer changes in magmatic systems feeding volcanoes [35] or as indicators of eruptive activity [36] or of atmospheric chemistry (e.g., see Ref. [37]). It is not always clear whether the amount of scatter in plots similar to that shown in Fig. 6 arises from errors in measurement and retrieval procedures or represents real changes in gas composition. Plotting temporal variations of ratios and comparing with observations of volcanic activity can assist with interpretation of these data.

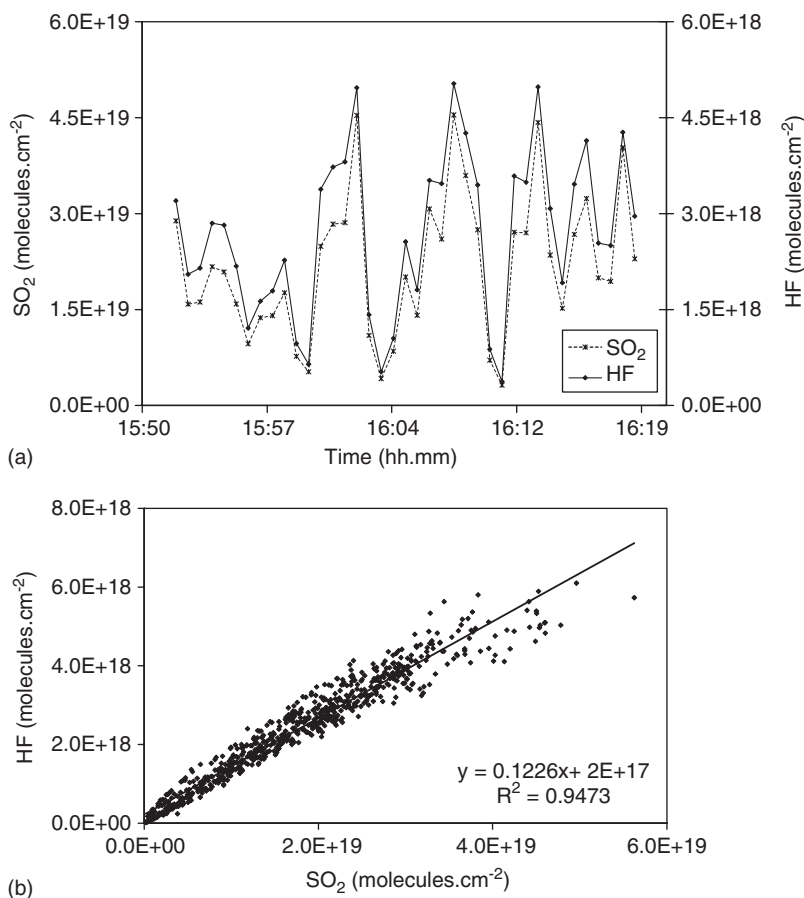


Fig. 6. (a) SO₂ and HF column amounts measured over a 27 min period at Masaya volcano. A clear correlation between column amounts of the two species is shown. (b) Retrieved HF vs. SO₂ column amounts. The gradient of the regression line (in this case ~ 0.12) represents the mean molar ratio between the two species. The regression line should pass very close to the origin since there is negligible SO₂ or HF present in the background atmosphere.

4. FIELD OBSERVATIONS OF HF AND SiF₄

HF and/or SiF₄ have been successfully detected using OP-FTIR spectroscopy at several volcanoes worldwide (Table 1). Francis *et al.* [21] observed low SiF₄ proportions on Mt. Etna, Sicily, but relatively high SiF₄ abundances in fumarole emissions on Vulcano, Eolian Islands (example spectra collected during this campaign are featured in Fig. 5a). Measurements of SiF₄ on Vulcano were made

Table 1. OP-FTIR measurements of volcanic HF and/or SiF₄ with corresponding fluxes (for error estimates, see relevant publications)

Volcano	Date	IR source and path length	SO ₂ /HF (mol mol ⁻¹)	SO ₂ /SiF ₄ (mol mol ⁻¹)	SiF ₄ /HF (mol mol ⁻¹)	Flux (kg s ⁻¹)	Reference
Aso, Japan	May and July 1996	unknown	–	> 3000	–	SiF ₄ < 0.0006	Mori <i>et al.</i> [30]; Ohta <i>et al.</i> [55]
Etna, Sicily	Sept./Oct. 1994	Artificial lamp/hot rock (up to 0.9 km)	–	~2700	–	–	Francis <i>et al.</i> [21,28]
	June 1997	Solar (12 km from summit)	14.8	–	–	HF = 1.30	Francis <i>et al.</i> [41]
	Oct. 1997	Solar (1 km from summit)	9.7	–	–	HF = 2.20	Francis <i>et al.</i> [41]
	14 June 2000	Lava fountain (990 m)	20 to 0.9 ^a	–	–	–	Allard <i>et al.</i> [34]
	1 May 2001	Lava flow (2 km)	2.51	–	–	–	Burton <i>et al.</i> [33]
	2 May 2001	Solar (1–3 km from summit)	9.12 ^b 4.91 ^c	–	–	HF = 0.60	Burton <i>et al.</i> [33]
	25 July 2001	Lava flow (path length unknown)	2.55 ^d	–	–	–	Burton <i>et al.</i> [33]
	28 July 2001	Solar (distance from summit unknown)	6.86	–	–	–	Burton <i>et al.</i> [33]
Masaya, Nicaragua	Feb./Mar. 1998	Artificial lamp (518 m)	7.05	–	–	HF = 0.90	Horrocks <i>et al.</i> [39] Delmelle <i>et al.</i> [8]
	Mar. 1999	Artificial lamp (518 m)	7.72	–	–	HF = 0.80	Horrocks <i>et al.</i> [39]; Delmelle <i>et al.</i> [8]
	Apr. 2000	Solar (from summit)	9.4	–	–	HF = 0.27 ^e	Duffell <i>et al.</i> [40]
	Apr./May 2001	Solar (from summit) and artificial lamp (518 m)	29.6	–	–	HF = 0.10	Duffell <i>et al.</i> [36]; Galle <i>et al.</i> [48]

Table 1. Continued

Volcano	Date	IR source and path length	SO ₂ /HF (mol mol ⁻¹)	SO ₂ /SiF ₄ (mol mol ⁻¹)	SiF ₄ /HF (mol mol ⁻¹)	Flux (kg s ⁻¹)	Reference
Popocatepetl, Mexico	21–24 Feb. 1997	Emission spectra with cold sky background (4–10 km from summit)	20.8	956 to 417 ^f	0.035	HF = 0.61; SiF ₄ = 0.073	Love <i>et al.</i> [38]
	26 Feb. 1997	Emission spectra with cold sky background (4–10 km from summit)	–	90 to 956 ^g	–	HF = 13.19 to 0.88; SiF ₄ = 12.50 to 0.08	Love <i>et al.</i> [38]; Goff <i>et al.</i> [6]
	27 Feb. 1997	Emission spectra with cold sky background (4–10 km from summit)	16.4	SiF ₄ below detection limits	SiF ₄ below detection limits	HF = 2.89	Goff <i>et al.</i> [6]
	Feb. 1998	Emission spectra using cold sky background (4–17 km from summit)	10.1	–	–	HF = 0.64	Goff <i>et al.</i> [56]
Satsuma-Iwojima, Japan	Oct. 1996	Hot rock (~250 m)	40	71	0.57	HF = 0.05 SiF ₄ = 0.15	Mori <i>et al.</i> [30]; Shinohara <i>et al.</i> [57]
La Soufrière, Guadeloupe	Between May 2003 and Sept. 2004	Artificial lamp (640 m, intersecting plume 140 m downwind)	–	6 to 12	–	–	Bernard <i>et al.</i> [58]
	9 Apr. 2004	Artificial lamp (690 m, intersecting plume 15 m downwind)	–	2.9	–	–	Bernard <i>et al.</i> [58]

Vulcano, Eolian Islands	Sept./Oct. 1994	Hot rock (few metres)	–	~170	~0.1 ^h	–	Francis <i>et al.</i> [21,28] Aiuppa <i>et al.</i> [59]
	May 2002	Artificial lamp (20 m)	6	–	–	–	

^a Measurements made during, and immediately after, a 40-min fountaining episode.

^b Molar ratio for the bulk plume.

^c Molar ratio for the Southeast crater plume.

^d Molar ratio for gas emitted from a hornito in the Valle del Leone.

^e SO₂ and HCl fluxes measured using a solar tracking OP-FTIR along a road 15 km downwind from the summit. HF/HCl ratios, measured from the summit, were used to calculate the HF flux.

^f Data collected prior to an explosive event.

^g Data collected immediately after the explosive event.

^h Calculated by combining measured HCl/SiF₄ ratios with conventional measurements of HCl/HF.

over path lengths of a few metres, using hot rock as a source of IR radiation. SO_2/SiF_4 molar ratios were found to be $\sim 1.7 \times 10^2$. Unfortunately, HF was not measured (due to insufficient short-wave radiation reaching the MCT detector) but a SiF_4/HF ratio of ~ 0.1 was inferred from HCl/SiF_4 ratios measured by the OP-FTIR spectrometer and HCl/HF ratios from conventional measurements. Francis *et al.* [21] concluded that the highly temperature-dependent nature of reaction (1) could be exploited in order to estimate the temperature of fumaroles.

Love *et al.* [38] observed both HF and SiF_4 in the plume emitted by Popocatepetl volcano, Mexico. These measurements were collected during an eruptive episode in February 1997 when direct sampling was impossible. SiF_4 was detected in long-wave IR spectra collected using only the thermal emission from the gases themselves, viewed against the cold sky. HF was visible in the short-wave IR spectra obtained using cloud-scattered sunlight. All measurements were made between 4 and 10 km from the volcano. During the 3 days prior to a series of moderate explosive ash eruptions, a steady decrease in SO_2/SiF_4 molar ratio (from 956 to 417) was observed, coupled with a decrease in SO_2 flux from 46 to 23 kg s^{-1} ($4000\text{--}2000 \text{ t d}^{-1}$). Immediately after the eruptions, a much lower SO_2/SiF_4 molar ratio (~ 90) was measured with a high SO_2 flux ($> 694 \text{ kg s}^{-1}$ or $60,000 \text{ t d}^{-1}$) but over the course of the following 3 hours both values returned to their pre-eruption levels. These observations of short-term compositional variations associated with an explosive eruption are a good illustration of the potential of high temporal resolution, remote surveillance of volcanic plumes to identify pre-eruptive changes in gas geochemistry, which may have an important bearing on hazard assessment.

Horrocks *et al.* [39] measured HF at Masaya volcano, Nicaragua, in 1998 and 1999 using an IR lamp over a distance of 518 m, across the active summit crater (example spectra from this campaign are featured in Fig. 5b). The composition of gas showed little variation on timescales of days, weeks and even between successive campaigns a year apart. The average SO_2/HF molar ratio was 7.05 in 1998 and 7.72 in 1999. Amounts of SiF_4 were not detectable in measured spectra. If we consider a similar thermodynamic modelling system to that presented by de Hoog *et al.* [20] where $P_{\text{HF}} + P_{\text{SiF}_4} + P_{\text{H}_2\text{O}}$ is equal to the total vapour pressure of 1 bar, and perform retrievals for water vapour and HF from this set of spectra, we calculate that $P_{\text{HF}} \sim 0.002$. Using the empirical formula derived by de Hoog *et al.* [20] we see that if column amounts are to be detectable ($> 2.7 \times 10^{15}$ molecules cm^{-2} ; see Ref. [21]) the gas mixture would have to equilibrate at a temperature less than $\sim 570 \text{ K}$. Observed intermittent glow from the vent during the measurement period suggested high temperature ($\sim 1300 \text{ K}$) degassing, however. The absence of SiF_4 can therefore be explained by the magmatic temperatures of the gas emission and rapid quenching that prevents re-equilibration to ambient air temperatures.

Subsequent campaigns at Masaya in 2000 and 2001, reported by Duffell *et al.* [36,40], showed variations in plume composition, suggesting a substantial change in degassing behaviour from previous years. An SO_2/HF molar ratio of 9.4 was observed in 2000 and an average ratio of 29.6 was observed in April–May 2001. This increase in SO_2/HF ratio, coupled with increases in SO_2/HCl and CO_2/SO_2 ratios, and a reduction in emission rates of all measured gas species, occurred prior to a minor explosion on 23 April 2003. After the explosion, the authors observed an increased variability in the daily gas ratios compared to previous campaigns. These phenomena were explained by increased influence of a hydrothermal system that abstracted the highly soluble species (i.e., HF and HCl) from the gas mixture prior to emission to the atmosphere. The explosion was phreatic or phreatomagmatic in character, indicating the interaction between magma and groundwater. Thus the increased hydrothermal activity is consistent with the explosion that occurred.

At Satsuma–Iwojima volcano, Japan, Mori *et al.* [30] reported high SiF_4/HF ratios from fumaroles in the Ohachi-oku region on Mt. Iwodake. Measurements of HCl/SiF_4 and HCl/HF were made with MCT and InSb detectors, respectively, and combined to yield a SiF_4/HF molar ratio of 0.57. Hot rock, at a distance of 250 m was used as an IR source. Thermodynamic calculations performed by Mori *et al.* [30] suggest that the observed SiF_4/HF ratio cannot be explained solely by high temperature fumarolic gas but requires a 40% contribution from F-rich low-temperature fumaroles.

On Mt. Etna, HF has been measured on several occasions (Francis *et al.* [41] and on a regular basis by the Istituto Nazionale di Geofisica e Vulcanologia (INGV) since 2000). In May 2001, Burton *et al.* [33] used OP-FTIR spectroscopic measurements of SO_2 , HCl and HF emitted from the four summit craters to constrain models of the shallow plumbing system of the volcano. Gases released from three of the craters had indistinguishable gas ratios ($\text{SO}_2/\text{HF} \sim 9.0$, $\text{SO}_2/\text{HCl} \sim 2.9$ all molar), suggesting that they were connected to a central conduit system that branched either at depth (>2 km) or, close to the surface ($<<1$ km) to supply each vent with gas of identical composition. Weaker emissions from a fourth crater were comparatively depleted in SO_2 ($\text{SO}_2/\text{HF} \sim 4.9$, $\text{SO}_2/\text{HCl} \sim 1.5$), implying that this crater was fed either by a separate conduit or by a branch of the central conduit whose geometry favoured solubility-controlled volatile fractionation. Allard *et al.* [34] collected OP-FTIR spectra during a phase of lava fountaining from the Southeast crater on Mt. Etna in June 2000. Spectra were collected using the active lava as a source of IR radiation from a distance of 990 m. In this instance, the observed changes in CO_2/SO_2 , SO_2/HCl and HCl/HF ratios during and after fountaining suggested that the activity was driven by separate ascent of a gas layer that had accumulated at moderate depth (~ 1.5 km) within the volcanic edifice. These measurements were the first field data to allow detailed and direct observations of the dynamics of a lava fountain.

5. EMISSION RATES

Emission of fluorine into the atmosphere has important implications for the environment and for human and animal health. Gaseous fluorine compounds, particularly HF, are phytotoxic and damage in the form of leaf injury, and a reduction in the number of plant communities has been observed close to active vents [42,43]. HF is readily scavenged from the atmosphere through dry and wet deposition, and adsorption on to, and reaction with, particulate material. Once on the ground, fluorine in the form of bio-available NaF and CaF₂ is highly toxic for grazing animals [42,44]. In humans, exposure to high concentrations of F increases the risk of dental and skeletal fluorosis [45,46]. [Note of the Editor: The effects of fluorine emissions on plants and organisms are presented in this series in the chapter by A. W. Davison and L. H. Weinstein.]

Direct evaluation of fluorine emission rates by FTIR spectroscopy in solar occultation traverses is difficult due to relatively low column amounts of F-bearing gases in ageing volcanic plumes and spectral contamination by water vapour [40]. Instead, X/SO₂ mass ratios (where X represents F bearing gas species) can be used in conjunction with the emission rate of SO₂, which is routinely measured at several volcanoes worldwide using a variety of ground- and satellite-based remote sensing techniques (e.g., see Refs [47–49]). Halmer *et al.* [50] extrapolated from a compilation of observations from 50 volcanoes, pertaining both to explosive and quiescent emissions, to estimate the annual global volcanic emission of SO₂. Then, using HF/SO₂ ratios reported for high temperature fumaroles from subduction zone-related, rift zone-related and ocean island-related volcanoes, they estimated a global annual HF emission of 0.7–8.6 Tg. The uncertainty here reflects a very real lack of knowledge about emissions from the global volcano population, and of variations in emissions in time and space.

Using OP-FTIR spectroscopic techniques to calculate X/SO₂ ratios offers many advantages over sampling from high temperature fumaroles. Many spectra can be collected rapidly, during both eruptive and non-eruptive activity, and the bulk plume composition is evaluated rather than single point measurements that may or may not be representative of overall emissions. In addition, fluxes of both HF and SiF₄ can be measured (Table 1).

6. FUTURE DIRECTIONS AND CHALLENGES

Since the first field deployment of an OP-FTIR spectrometer at Mt. Unzen volcano, Japan [51], there has been widespread recognition of the potential of the technique for volcano studies and monitoring. Accordingly, numerous innovations and refinements have been made to enable measurements on several different volcanoes, using a variety of natural and artificial IR sources, over path lengths

ranging from a few metres to several kilometres. Many important volcanic gas species, namely, H_2O , CO_2 , CO , OCS , SO_2 , HCl , HF and SiF_4 , have been detected and quantified and several other species remain a possibility.

However, reliable volcanological interpretation of OP-FTIR spectroscopic data requires a much deeper understanding of the degassing of magma, the interactions between gas, rock and hydrothermal fluids, and, in the case of distal measurements, an understanding of physical and chemical processes that occur in a plume as it ages. Data collected from locations near an active vent produce gas ratios that can be assumed to be similar to those equilibrated at depth whereas data collected several kilometres downwind may become significantly altered. Different gas species undergo different rates of scavenging by ash particles and aqueous aerosol and as a result, gas ratios may differ downwind from those at the vent [37,52,53]. HF , for example, is readily scavenged from the plume [50] so downwind concentrations may be disproportionately lower than those measured at the summit. Simultaneous measurements with two or more spectrometers, positioned at different distances from an active vent, would allow the evaluation of the chemical evolution of volcanic plumes and hence a more informed interpretation of observed ratios in terms of source degassing.

To date, relatively few OP-FTIR spectroscopic measurements of HF and/or SiF_4 have been made. It has been demonstrated, however, that HF/SiF_4 ratios can be used to estimate the temperature of fumaroles, and HF/SO_2 and SiF_4/SO_2 ratios can be used in combination with SO_2 flux data to calculate fluxes of these F-bearing gas species. In addition, ratios of S-, Cl- and F-bearing species can provide insights into gas sources, magma storage and dynamics and the geometry of magmatic plumbing systems. Measurements at further degassing volcanoes, representing different tectonic settings and eruptive regimes, will provide a broader understanding of fluorine degassing. To this end, we have recently carried out OP-FTIR measurements at three intraplate volcanoes: (1) Mt. Erebus, Antarctica, (2) Nyiragongo, Democratic Republic of Congo, and (3) Erta 'Ale, Ethiopia. In the future, longer-term, more continuous monitoring of F-bearing and other volcanic gas species by OP-FTIR spectroscopy and other spectroscopic techniques, such as automated ultraviolet spectrometer networks [54], will greatly enhance our ability to identify and interpret temporal trends in gas composition and flux. Several volcano observatories (including INGV-Sezione Catania, Montserrat Volcano Observatory, the Hawaiian Volcano Observatory, the Observatoire Volcanologique et Sismologique de Guadeloupe, and the Instituto Geofisico in Quito) have begun using these techniques for monitoring purposes, providing a further opportunity to compare and correlate geochemical, seismic and geodetic time series. Such multi-parameter surveillance, combined with a good understanding of magma dynamics and magma-hydrothermal processes, offers arguably the strongest basis for short- to medium-term forecasting of volcanic activity and hazard assessment.

Further developments in measuring volcanic fluorine emissions could come from the application of higher sensitivity spectroscopy. Several F-bearing species, besides HF and SiF₄, are infrared-active and may therefore be detectable using this technique, particularly when measuring over short path lengths so that contamination of spectra by atmospheric lines is minimised. Future efforts to understand and model the speciation and thermodynamics of F in magmas would benefit greatly from field observations of these trace species.

ACKNOWLEDGMENTS

G.M.S. gratefully acknowledges the States of Jersey Education Committee for their financial support. C.O. thanks the NSF Office of Polar Programs and the United States Antarctic Program. We thank Cees-Jan de Hoog for reviewing the original manuscript, and Alain Tressaud for editorial handling.

REFERENCES

- [1] A. Aiuppa, C. Federico, A. Paonita, G. Pecoraino, M. Valenza, S. Cl and F degassing as an indicator of volcanic dynamics: the 2001 eruption of Mount Etna, *Geophys. Res. Lett.* 29 (11) (2002) .
- [2] M. Pennisi, M.F. Le Cloarec, Variations of Cl, F, and S in Mount Etna's plume, Italy, between 1992 and 1995, *J. Geophys. Res.-Solid Earth* 103 (B3) (1998) 5061–5066.
- [3] P. Allard, J. Carboneille, N. Metrich, H. Loyer, P. Zettwoog, Sulphur output and magma degassing budget of Stromboli volcano, *Nature* 368 (6469) (1994) 326–330.
- [4] R.E. Stoiber, S.N. Williams, B. Huebert, Sulphur and halogen gases at Masaya caldera complex, Nicaragua: Total flux and variations with time, *J. Geophys. Res.* (91) (1986) 12215–12231.
- [5] A. Aiuppa, C. Federico, S. Giudice, A. Paonita, M. Valenza, Plume chemistry provides insights into mechanisms of sulfur and halogen degassing in basaltic volcanoes, *Earth Planet. Sci. Lett.* 222 (2) (2004) 469–483.
- [6] F. Goff, C.J. Janik, H. Delgado, C. Werner, D. Counce, J.A. Stimac, C. Siebe, S.P. Love, S.N. Williams, T. Fischer, L. Johnson, Geochemical surveillance of magmatic volatiles at Popocatepetl volcano, Mexico, *Geol. Soc. Am. Bull.* 110 (6) (1998) 695–710.
- [7] I.A. Menyailov, L.P. Nikitina, V.N. Shapar, Results of geochemical monitoring of the activity of Ebeko volcano (Kurile Islands) used for eruption prediction, *J. Geodyn.* 3 (3–4) (1985) 259–274.
- [8] P. Delmelle, P. Baxter, A. Beaulieu, M. Burton, P. Francis, J. Garcia-Alvarez, L. Horrocks, M. Navarro, C. Oppenheimer, D. Rothery, H. Rymer, K. St. Amand, J. Stix, W. Strauch, G. Williams-Jones, Origin, effects of Masaya volcano's continued unrest probed in Nicaragua, *EOS Trans. AGU* 80 (1999) 575–581.
- [9] W.F. Giggenbach, A simple method for the collection and analysis of volcanic gas samples, *Bull. Volcanol.* 39 (1975) 132–145.
- [10] A.G. Allen, P.J. Baxter, C.J. Ottley, Gas and particle emissions from Soufriere Hills volcano, Montserrat, West Indies: Characterization and health hazard assessment, *Bull. Volcanol.* 62 (1) (2000) 8–19.

- [11] P.E. Rosenberg, HF–SiF₄ ratios in volcanic and magmatic gases, *Geochim. Cosmochim. Acta* 37 (1) (1973) 109–112.
- [12] R.B. Symonds, M.H. Reed, W.I. Rose, Origin, speciation, and fluxes of trace-element gases at Augustine volcano, Alaska – Insights into magma degassing and fumarolic processes, *Geochim. et Cosmochim. Acta* 56 (2) (1992) 633–657.
- [13] J.D. Webster, Partitioning of F between H₂O and CO₂ fluids and topaz rhyolite melt: Implications for mineralizing magmatic-hydrothermal fluids in F-rich granitic systems, *Contrib. Mineral. Petrol.* 104 (1990) 424–438.
- [14] M.R. Carroll, J.D. Webster, Solubilities of sulphur, noble gases, nitrogen, chlorine, and fluorine in magmas. In: M.R. Carroll and J.R. Holloway (Eds.), *Reviews in Mineralogy, Volume 30: Volatiles in Magmas*. Mineralogical Society of America, Washington, DC, Ch. 7, 1994, pp. 231–279.
- [15] R.A. Lange, The effect of H₂O, CO₂ and F on the density and viscosity of silicate melts. In: M.R. Carroll J.R. Holloway (Eds.), *Reviews in Mineralogy, Volume 30: Volatiles in Magmas*. Mineralogical Society of America, Ch. 9, 1994, pp. 331–369.
- [16] J.V. Smith, J.S. Delaney, R.L. Hervig, J.B. Dawson, Storage of F and Cl in the upper mantle – geochemical implications, *Lithos* 14 (2) (1981) 133–147.
- [17] K. Aoki, S. Kanisawa, Fluorine contents of some hydrous minerals derived from upper mantle and lower crust, *Lithos* 12 (3) (1979) 167–171.
- [18] A.F. White, M.F. Hochella, Surface-chemistry associated with the cooling and sub-aerial weathering of recent basalt flows, *Geochim. Cosmochim. Acta* 56 (10) (1992) 3711–3721.
- [19] R.B. Symonds, M.H. Reed, Calculation of multicomponent chemical-equilibria in gas–solid–liquid systems – calculation methods, thermochemical data, and applications to studies of high-temperature volcanic gases with examples from Mount St-Helens, *Am. J. Sci.* 293 (8) (1993) 758–864.
- [20] J.C.M. de Hoog, M.J. van Bergen, M.H.G. Jacobs, Vapour phase crystallisation of silica from SiF₄-bearing volcanic gases, *Ann. Geophys.* 48 (2005) 775–785.
- [21] P. Francis, C. Chaffin, A. Maciejewski, C. Oppenheimer, Remote determination of SiF₄ in volcanic plumes: A new tool for volcano monitoring, *Geophys. Res. Lett.* 23 (3) (1996) 249–252.
- [22] C.J. Horwell, R.S.J. Sparks, T.S. Brewer, E.W. Llewellyn, B.J. Williamson, The characterisation of respirable volcanic ash from the Soufriere Hills Volcano, Montserrat, with implications for health hazard, *Bull. Volcanol.* 65 (2003) 346–362.
- [23] Z. Bacsik, J. Mink, G. Keresztury, FTIR spectroscopy of the atmosphere. I: Principles and methods, *Appl. Spectrosc. Rev.* 39 (2004) 295–363.
- [24] Z. Bacsik, J. Mink, G. Keresztury, FTIR spectroscopy of the atmosphere. II: Applications, *Appl. Spectrosc. Rev.* 40 (2005) 327–390.
- [25] C. Oppenheimer, P. Francis, M. Burton, A. Maciejewski, L. Boardman, Remote measurement of volcanic gases by Fourier transform infrared spectroscopy, *Appl. Phys. B* 67 (1998) 505–515.
- [26] K.A. McGee, T.M. Gerlach, Airborne volcanic plume measurements using a FTIR spectrometer, Kilauea volcano, Hawaii, *Geophys. Res. Lett.* 25 (5) (1998) 615–618.
- [27] L. Horrocks, Infrared spectroscopy of volcanic gases at Masaya, Nicaragua. Ph.D. thesis, University of Cambridge, 2001.
- [28] P. Francis, A. Maciejewski, C. Oppenheimer, C. Chaffin, T. Caltabiano, SO₂–HCl ratios in the plumes from Mt Etna and Vulcano determined by Fourier-transform spectroscopy, *Geophys. Res. Lett.* 22 (13) (1995) 1717–1720.
- [29] T. Mori, K. Notsu, Remote CO, COS, CO₂, SO₂, HCl detection and temperature estimation of volcanic gas, *Geophys. Res. Lett.* 24 (16) (1997) 2047–2050.
- [30] T. Mori, M. Sato, Y. Shimoike, K. Notsu, High SiF₄/HF ratio detected in Satsuma-Iwojima volcano's plume by remote FT-IR observation, *Earth Planets Space* 54 (3) (2002) 249–256.

- [31] D.J. Edwards, A. Dudhia, Reference forward: High level algorithms definition, ESA document PO-MA-OXF-GS-0004 (1996).
- [32] L.S. Rothman, D. Jacquemart, A. Barbe, D.C. Benner, M. Birk, L.R. Brown, M.R. Carleer, C. Chackerian, K. Chance, L.H. Coudert, V. Dana, V.M. Devi, J.M. Flaud, R.R. Gamache, A. Goldman, J.M. Hartmann, K.W. Jucks, A.G. Maki, J.Y. Mandin, S.T. Massie, J. Orphal, A. Perrin, C.P. Rinsland, M.A.H. Smith, J. Tennyson, R.N. Tolchenov, R.A. Toth, J. Vander Auwera, P. Varanasi, G. Wagner, The HITRAN 2004 molecular spectroscopic database, *J. Quant. Spectrosc. Radiat. Transfer* 96 (2) (2005) 139–204.
- [33] M. Burton, P. Allard, F. Mure, C. Oppenheimer, FTIR remote sensing of fractional magma degassing at Mount Etna, Sicily. In: C. Oppenheimer, D.M. Pyle, J. Barclay (Eds.), *Volcanic Degassing*. Edited by Geological Society, Special publication 213, 2003, pp. 281–293.
- [34] P. Allard, M. Burton, F. Mure, Spectroscopic evidence for a lava fountain driven by previously accumulated magmatic gas, *Nature* 433 (7024) (2005) 407–410.
- [35] R.B. Symonds, Y. Mizutani, P.H. Briggs, Long-term geochemical surveillance of fumaroles at Showa-Shinzan dome, Usu volcano, Jpn, *J. Volcanol. Geotherm. Res.* 73 (3–4) (1996) 177–211.
- [36] H. Duffell, C. Oppenheimer, D.M. Pyle, B. Galle, A.J.S. McGonigle, M. Burton, Changes in gas composition prior to a minor explosive eruption at Masaya volcano, Nicaragua, *J. Volcanol. Geotherm. Res.* 126 (3–4) (2003) 327–339.
- [37] L. Horrocks, C. Oppenheimer, M. Burton, H. Duffell, Compositional variation in tropospheric volcanic gas plumes: Evidence from ground-based remote sensing, In *Volcanic degassing*, Geological Society Special Publications 213 (2003) 349–369.
- [38] S.P. Love, F. Goff, D. Counce, C. Siebe, H. Delgado, Passive infrared spectroscopy of the eruption plume at Popocatepetl volcano, Mexico, *Nature* 396 (6711) (1998) 563–567.
- [39] L. Horrocks, M. Burton, P. Francis, Stable gas plume composition measured by OP-FTIR spectroscopy at Masaya Volcano, Nicaragua, 1998–1999, *Geophys. Res. Lett.* 26 (23) (1999) 3497–3500.
- [40] H. Duffell, C. Oppenheimer, M. Burton, Volcanic gas emission rates measured by solar occultation spectroscopy, *Geophys. Res. Lett.* 28 (16) (2001) 3131–3134.
- [41] P. Francis, M.R. Burton, C. Oppenheimer, Remote measurements of volcanic gas compositions by solar occultation spectroscopy, *Nature* 396 (6711) (1998) 567–570.
- [42] S. Thorarinsson, On the damage caused by volcanic eruptions with special reference to tephra and gases, In: P.D. Sheets, D.K. Grayson (Eds.), *Volcanic activity and Human Ecology*, Academic Press, New York, (1979), pp. 125–159.
- [43] P. Delmelle, J. Stix, P.J. Baxter, J. Garcia-Alvarez, J. Barquero, Atmospheric dispersion, environmental effects and potential health hazard associated with the low-altitude gas plume of Masaya volcano, Nicaragua, *Bull. Volcanol.* 64 (6) (2002) 423–434.
- [44] S.J. Cronin, V.E. Neall, J.A. Lecointre, M.J. Hedley, P. Loganathan, Environmental hazards of fluoride in volcanic ash: A case study from Ruapehu volcano, New Zealand, *J. Volcanol. Geotherm. Res.* 121 (2003) 271–291.
- [45] P.J. Baxter, R.E. Stoiber, S.N. Williams, Volcanic gases and health – Masaya volcano, Nicaragua, *Lancet* 2 (8290) (1982) 150–151.
- [46] A. Heikens, S. Sumarti, M. van Bergen, B. Widianarko, L. Fokkert, K. van Leeuwen, W. Seinen, The impact of the hyperacid Ijen Crater Lake: Risks of excess fluoride to human health, *Sci. Total Environ.* 346 (2005) 56–69.
- [47] T. Caltabiano, R. Romano, G. Budetta, SO₂ flux measurements at Mount Etna (Sicily), *J. Geophys. Res.* (99) D6 (1994) 12809–12819
- [48] B. Galle, C. Oppenheimer, A. Geyer, A.J.S. McGonigle, M. Edmonds, L. Horrocks, A miniaturised ultraviolet spectrometer for remote sensing of SO₂ fluxes: A new tool for volcano surveillance, *J. Volcanol. Geotherm. Res.* 119 (1–4) (2003) 241–254.

- [49] S.A. Carn, G.J.S. Bluth, Prodigious sulphur dioxide emissions from Nyamuragira volcano, D.R. Congo, *Geophys. Res. Lett.* 30 (23) (2003) 2211.
- [50] M.M. Halmer, H.-U. Schmincke, H.-F. Graf, The annual volcanic gas input into the atmosphere, in particular into the stratosphere: A global data set for the past 100 years, *J. Volcanol. Geotherm. Res.* 115 (3–4) (2002) 511–528.
- [51] T. Mori, K. Notsu, Y. Tohjima, H. Wakita, Remote detection of HCl and SO₂ in volcanic gas from Unzen volcano, Japan, *Geophys. Res. Lett.* 20 (13) (1993) 1355–1358.
- [52] C. Oppenheimer, P. Francis, J. Stix, Depletion rates of sulfur dioxide in tropospheric volcanic plumes, *Geophys. Res. Lett.* 25 (14) (1998) 2671–2674.
- [53] C. Oppenheimer, V.I. Tsanev, C.F. Braban, R.A. Cox, J.W. Adams, A. Aiuppa, N. Bobrowski, P. Delmelle, J. Barclay, A.J.S. McGonigle, BrO formation in volcanic plumes, *Geochim. Cosmochim. Acta* 2006 (in press).
- [54] M. Edmonds, R.A. Herd, B. Galle, C. Oppenheimer, Automated, high time-resolution measurements of SO₂ flux at Soufriere Hills Volcano, Montserrat, *Bull. Volcanol.* 65 (2003) 578–586.
- [55] K. Ohta, N. Matsuwo, H. Shimizu, R. Fukui, M. Kamada, T. Kagiya, Emission rates of sulphur-dioxide from some volcanoes in Japan, in *Proceedings of Kagoshima International Conference on Volcanoes*, pp. 420–423, National Inst. Res. Adv. and Kagoshima Prefectural Government, 1988.
- [56] F. Goff, S.P. Love, R.G. Warren, D. Counce, J. Obenholzner, C. Siebe, S.C. Schmidt, Passive infrared remote sensing evidence for large, intermittent CO₂ emissions at Popocatepetl volcano, Mexico, *Chem. Geol.* 177 (1–2) (2001) 133–156.
- [57] H. Shinohara, K. Kazahaya, G. Saito, N. Matsushima, Y. Kawanabe, Degassing activity from Iwodake rhyolitic cone, Satsuma-Iwojima volcano, Japan: Formation of a new degassing vent, 1990–1999, *Earth Planets Space* 54 (3) (2002) 175–185.
- [58] M.-L. Bernard, J. Molinie, R.-H. Petit, F. Beauducel, G. Hammouya, G. Marion, Remote and *in situ* plume measurements of acid gas release from La Soufrière volcano, Guadeloupe, *J. Volcanol. Geotherm. Res.* 150 (2006) 395–409.
- [59] A. Aiuppa, M. Burton, F. Mure, S. Inguaggiato, Intercomparison of volcanic gas monitoring methodologies performed on Vulcano Island, Italy, *Geophys. Res. Lett.* 31 (2) (2004) .

This page intentionally left blank

CHAPTER 6

Fluorine and Coexisting Volatiles in the Geosphere: The Role in Japanese Volcanic Rocks

Katsuro Anazawa*

Department of Earth and Environmental Sciences, Faculty of Science, Kagoshima University, 1-21-35 Korimoto, Kagoshima 890-0065, Japan

Contents

1. Introduction	188
2. Determination of fluorine in silicate rocks	189
2.1. Various approaches for the determination of fluorine in silicate rocks	189
2.2. Electrode method in combination with hexamethyldisilazane (HMDS) distillation	190
2.2.1. Fundamentals of the method	190
2.2.2. Experimental	191
2.2.3. Recommended procedures	193
2.2.4. Analysis of reference materials	194
2.3. Ion chromatographic method in combination with cation-exchange pretreatment	194
2.3.1. Fundamentals of the method	194
2.3.2. Experimental	195
2.3.3. Recommended procedures	196
2.3.4. Pretreatment by cation exchange	196
2.3.5. Analysis of reference materials	197
3. Fluorine and other volatile abundances in Japanese volcanic rocks	198
3.1. Geochemical studies on volatile elements in volcanic rocks	198
3.2. Samples and methods	199
3.2.1. Samples and chemical analysis	199
3.2.2. Statistical strategy	199
3.2.3. Data pretreatment	200
3.3. Results and discussion	201
3.3.1. Abundance of fluorine and other volatile contents in volcanic rocks	201
3.3.2. Statistical analysis of fluorine, chlorine, sulfur, and boron	202
3.3.3. Principal component analysis of major and volatile elements	204
3.3.4. Factor analysis of volatiles	205

*Corresponding author.

E-mail: anazawa@sci.kagoshima-u.ac.jp

3.4. Conclusions	211
Acknowledgments	211
Appendix 1. Volatile contents of Japanese volcanic rocks (113 samples)	212
Appendix 2. Composition of volcanic rocks in Japan (44 samples)	217
References	223

Abstract

Comprehensive knowledge of the volatile behavior in volcanic rocks is of great value to clarify the process of magma generation and differentiation. However, few studies on volatile elements, particularly the fluorine content in volcanic rocks, have been made because of the difficulties of the analytical technique. In the present research, two types of analytical techniques have been investigated. One is a progressed separation method of distillation with potentiometric determination and the other is a chromatographic method combined with cation-exchange pretreatment. Using the above techniques, fluorine was determined on the 113 volcanic rocks obtained from various parts of Japanese islands. In addition, the other volatile and major elements were also determined on 44 different samples. The analytical results were geochemically interpreted using multivariate analysis in the light of magma generation theory in the subduction zones. The geographical distribution of volatile elements showed that the chemical contents were more related to the source of the elements rather than the chemical property or ionic radius. The factor structure of volatile elements led to the following findings: (1) seawater components brought by subducting slab have a significant influence on the behavior of chlorine, bromine, boron, and arsenic; (2) fluorine and sulfur are mainly contributed by the mantle components.

1. INTRODUCTION

Volatile behavior in magmas bears on both the conditions of their formation and the chemical composition of the upper mantle. The volatile content in volcanic rocks is of great value to understand magma genesis and differentiation processes, particularly in subduction zones. However, systematic researches of volatiles in volcanic solids from island arcs have been disabled by the difficulty of analytical technique and the difficulty in estimating the original concentration in magmas. Specifically only a few studies on the fluorine content in volcanic rocks have been made because of the difficulty of the analytical technique. The concentration of fluorine in volcanic rocks is relatively high ($<20\text{--}2000\text{ mg/kg}$), but analytical data on geological reference samples from the Geological Survey of Japan (GSJ) are varied nonetheless, e.g., 780–1163 mg/kg for JR-1 sample, 81–144 mg/kg for JB-2 sample, and 165–295 mg/kg for JA-1 sample [1].

Consequently, in this chapter, two types of analytical techniques have been presented. One is a progressed separation method of distillation with potentiometric determination and the other is a chromatographic method combined with cation-exchange pretreatment. Using those techniques, fluorine was determined in the 113 volcanic rocks obtained from various parts of Japanese islands.

In addition, the other volatile and major elements were also determined. The analytical dataset was subjected to the multivariate analysis to seek the potential factors, which control fluorine and other volatile behaviors in volcanic rocks.

2. DETERMINATION OF FLUORINE IN SILICATE ROCKS

2.1. Various approaches for the determination of fluorine in silicate rocks

The analytical difficulty in the determination of fluorine is chiefly due to the high reactivity of this element. Specifically, the considerable difficulty associated with fluorine determination in silicate rocks is due to the affinity of silicon or aluminum, present in hundreds of times the equivalent of fluorine. The method used to separate fluoride from other constituents is an essential key for the fluorine analysis of silicates.

Various methods and modifications have been proposed for the liberation of fluoride from silicate rock samples as well as the subsequent determination of the separated fluoride. Most frequently, the separation is obtained by distillation or diffusion. The pyrohydrolysis technique is useful for some solid samples, but unsuitable for solutions.

Distillation was formerly the separation technique most commonly used in fluorine determination. The basic Willard and Winter steam distillation method [2] included the volatilization of hexafluorosilicic acid with vapor from perchloric or sulfuric acid at 135°C, in the presence of glass beads or powder. It is still widely used and is the method used to compare other methods for fluoride determination. This classical method is, however, tedious and time-consuming and moreover the distillate is so highly diluted by the steam condensate that the sensitivity of the total analysis is significantly lowered.

The chromatographic method has recently been introduced for the separation and determination of halogens in a large variety of samples. In comparison with other separation methods, this method is simple and saves time for the separation procedure. The ion-exchange technique has also been widely used for the chromatographic separation. This method is, however, problematic with regard to fluorine separation in silicate rocks due to the high fluorine affinity with major elements in the silicates. Fluorine precipitates with silica at a low pH, and at a high pH, fluorine forms a complex with aluminum. In either case, elemental fluorine or fluoride ions cannot be separated from the decomposed solution.

For non-destructive analysis, which does not require a separation procedure from the matrix, several analytical techniques have been proposed for the de-

termination of fluorine in silicate rocks. X-ray fluorescence spectrometry (XRF) [3], high-temperature mass spectrometry [4,5], and ion-beam analysis [6] may be applied directly to solids. The practical difficulties of these techniques are the need for special instruments and/or time-consuming processes.

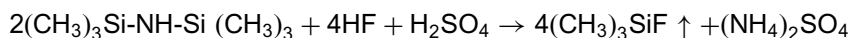
With the reliability and availability of instruments, precision, accuracy, rapidity, and simplicity in mind, two of the major analytical methods will be shown in the following section. One is a progressed separation method of distillation with potentiometric determination and the other involves chromatographic methods in combination with cation-exchange pretreatment.

2.2. Electrode method in combination with hexamethyldisilazane (HMDS) distillation

2.2.1. Fundamentals of the method

Distillation is one of the most common methods used to separate fluorine from matrix, but most conventional distillation methods are time-consuming and tedious. Taves [7–9] reported that silicones greatly accelerated the diffusion of fluorine because of the formation of volatile fluorosilanes. He succeeded in separating fluoride at room temperature by applying hexamethyldisiloxane (HMDSO) to form trimethylfluorosilane (TMFS). This method was ten times faster than the HF diffusion method. Although the method was applicable to various samples, HMDSO requires strong acid.

Tsuchiya *et al.* [10], developed a distillation method using HMDS instead of HMDSO. Under acidic conditions, fluoride in the sample reacts with HMDS to yield volatile TMFS, according to the following reaction:



TMFS diffuses from the aqueous phase into the air and is then trapped in the NaOH solution of the absorption vessel. Under basic conditions, the TMFS reacts with the hydroxyl ion to form trimethylsilanol and the free inorganic fluoride ion:



The released fluoride is monitored by a fluoride-selective electrode. The interference of trace aluminum and some other metal ions is eliminated by the addition of phosphoric acid. In addition to the improvement of the distillation apparatus, over 98% recovery can be achieved from reaction media at pH 0–1, and interference by silicate is prevented. Pyrophosphoric acid is used as the reaction medium because it has a stronger masking ability for aluminum than orthophosphoric acid.

The following basic procedure is given by Tsuchiya *et al.* [10], modified by Ohshima and Yoshida (personal communication). The proposed method is ap-

plicable to the analysis of geochemical materials with high contents of silica and aluminum, such as silicate rocks. Fluoride at a level of $1\ \mu\text{g/L}$ can be determined by distilling from 500-mL sample solutions.

2.2.2. Experimental

2.2.2.1. Apparatus

The distillation apparatus made of borosilicate glass is shown in Fig. 1. The reaction vessel for the ordinary distillation has an inner diameter of 25 mm and is 230 mm long (capacity 100 mL), while the absorption vessel has an inner diameter of 14 mm and is 150 mm long (capacity 20 mL). Sintered-glass filter balls, with pores $20\text{--}30\ \mu\text{m}$ in size, are fitted at the ends of the gas-inlet tubes of both the reaction and absorption tubes. All parts are connected by ground-glass joints, sealed by phosphoric acid, and fastened with springs to withstand inner pressures. The reaction vessel for the concentrating distillation has a capacity of 700 mL (46 mm i.d., 450 mm length). A suitably extended adapter and a longer gas-inlet tube are prepared. The potentiometric determination of fluoride was

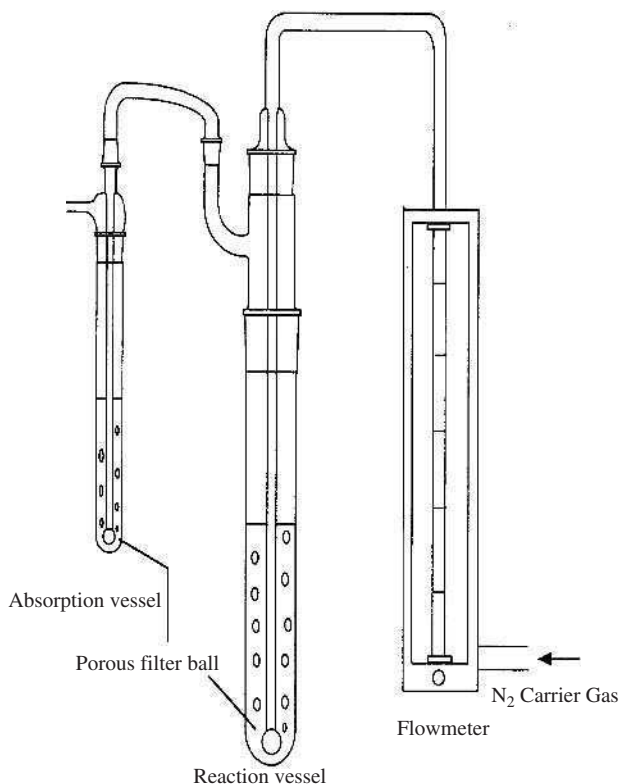


Fig. 1. Distillation apparatus.

done with a Toa-Denpa model IM-20E ion meter with an F-125 fluoride-selective electrode and an HS-305DP reference electrode, while pH was measured with a Toa-Denpa model HM-5ES pH.

2.2.2.2. Reagents

A standard fluoride solution (1000 mg/L) was prepared from sodium fluoride dried by heating in a platinum crucible at a low red heat; working standards were prepared by suitable dilution. HMDS was an extra-pure reagent (> 95% obtained by gas chromatography; Tokyo Kasei Kogyo Co.).

2.2.2.3. Modified total ionic strength adjustment buffers TISAB A for standard solution for calibration

The 57 mL of acetic acid, 102 g of sodium nitrate, and 117.6 g of trisodium citrate dihydrate were dissolved in *ca.* 400 mL of deionized-distilled water; the pH was adjusted to 5.4 with 5 mol/L sodium hydroxide and the solution was diluted to 1000 mL.

2.2.2.4. TISAB B for sample determination

The preparation was the same as for A, except that 59.4 g of sodium nitrate was used. The difference in the amount of sodium nitrate between A and B corresponds to the amount produced by neutralization of the absorbing solution with nitric acid.

2.2.2.5. Absorbing solution

About 0.1 mol/L sodium hydroxide was prepared and the volume needed to neutralize 2.0 mL of 0.50 ± 0.01 mol/L nitric acid was determined by titration to a methyl orange end-point. The nitric acid solution was prepared by diluting *ca.* 1 mol/L nitric acid, and the concentration was precisely determined by alkali titration (e.g., Na_2CO_3 standard solution).

2.2.2.6. Phosphoric acid solutions

Pyrophosphoric acid (*ca.* 75% P_2O_5 , chemically pure; Wako Co.) was diluted with the same volume of water in an ice-bath to avoid rapid hydrolysis; this solution was prepared daily and stored below 10°C. Purified orthophosphoric acid (*ca.* 10 mol /L) was prepared by diluting reagent-grade phosphoric acid (500 g) with the same volume of water, adding 5 mL of HMDS, and evaporating to about 450 mL on a boiling water bath with nitrogen bubbling.

All chemicals were of analytical grade and deionized-distilled water was used throughout.

2.2.3. Recommended procedures

2.2.3.1. Ordinary distillation

The outline of the analytical procedure is shown as a flow chart in Fig. 2. Place 10 mL of the absorbing solution in the absorption vessel. Connect the apparatus as shown in Fig. 1, except for the reaction vessel. Transfer up to 50 mL of the sample solution to the reaction vessel. Dilute to about 50 mL, if necessary, and add 6 mL of the pyrophosphoric acid solution, whereupon the concentration of the acid will become about 1 mol/L in terms of orthophosphoric acid with a pH of 0.5–1. Immediately after the addition of 55 μL of HMDS by microsyringe, connect the reaction vessel to the adapter. Introduce nitrogen gas at the rate of 60 mL min^{-1} for

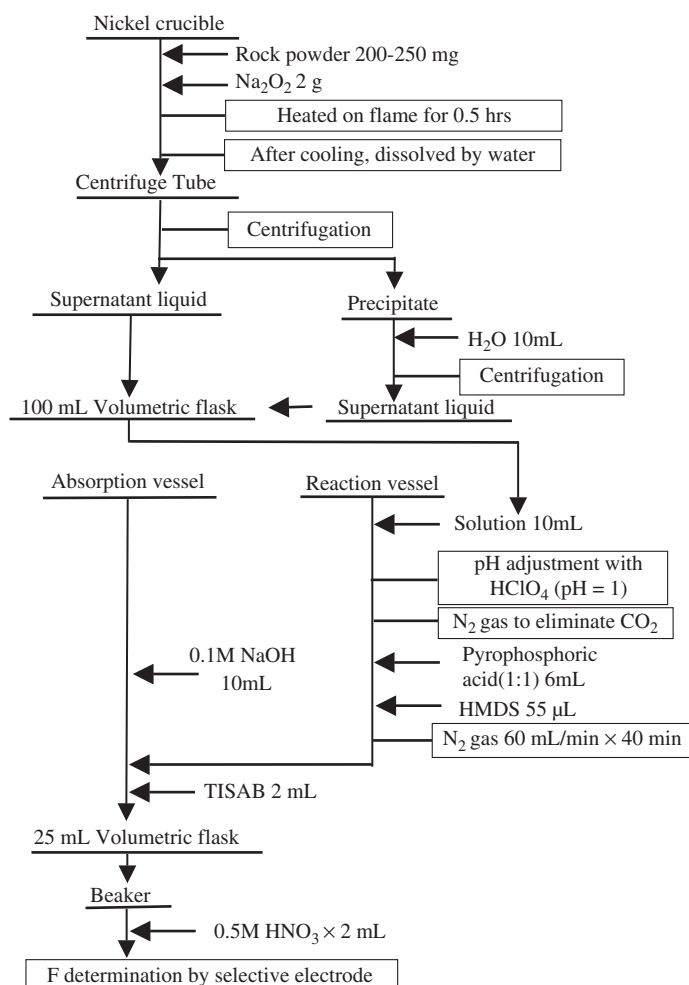


Fig. 2. Flow chart of the determination method by specific electrode.

30 min, and then remove the absorption vessel. Transfer this solution quantitatively with a 25-mL volumetric flask containing 2.0 mL of modified TISAB B and combine the washings of the absorption vessel. Dilute to the mark.

2.2.3.2. Concentrating distillation

Place up to 500 mL of sample solution in the 700-mL reaction vessel, distil in the manner described above, adding 30 mL of the purified orthophosphoric acid and 0.55 mL of HMDS.

2.2.3.3. Potentiometric measurement

Add 2.0 mL of the 0.50 mol/L nitric acid to the distillate prepared as given above in the 25-mL volumetric flask. Transfer this solution to a 50-mL beaker. Determine the concentration of fluoride with the calibrated ion meter, using the single-point method. The solutions used for calibration are prepared by adding 2.0 mL of modified TISAB A to 25 mL of standard fluoride solutions.

2.2.4. Analysis of reference materials

The proposed method was applied to the geochemical reference rock samples of the GSJ [1]. The reference samples include one rhyolite JR-1 (obsidian); two basalts JB-1a (alkali basalt) and JB-2 (tholeiitic basalt); two andesites JA-1 and JA-2; and one granitic rock JG-1a (granodiorite). In a nickel crucible, 100–300 mg of powdered sample was weighed and fused with an 8–10 fold amount of sodium peroxide (Na_2O_2). The cake was then dissolved in about 30 mL of water and centrifuged in a 50-mL tube, following which the supernatant liquid was transferred to a 100-mL volumetric flask. The residue was washed with a small amount of water and re-centrifuged. The washings were added to the flask and the solution was diluted to the mark. A 50-mL aliquot of the solution was transferred to the reaction vessel of the distillation apparatus. The pH was adjusted to approximately 1 by the addition of perchloric acid. Carbon dioxide was expelled by passing nitrogen through the solution. Fluoride was separated and determined as stated in the above distillation procedure. The results were highly reproducible and were in good agreement with the recommended values (Table 1).

2.3. Ion chromatographic method in combination with cation-exchange pretreatment

2.3.1. Fundamentals of the method

Although the above ion-selective electrode method gives satisfactorily accurate and precise results, it requires a rather complex preparation stage, e.g., TMFS distillation. In this section, ion chromatographic method is proposed to develop a

Table 1. Fluorine contents (in mg/kg) of GSJ reference materials

	Sample descriptions	Reference value [1]	Potentiometry ^a	IC [11]
JR-1	Rhyolite	991	1000	1061 ± 57
JB-1a	Basalt	357	390	384 ± 15
JB-2	Basalt	98.5	90	104 ± 7
JA-1	Andesite	161	160	153 ± 22
JA-2	Andesite	223 ^b	230	227 ± 20
JG-1a	Granodiorite	439	460	434 ± 40 ^c

^a The precision is ±10 mg/kg for the rock samples of <400 mg/kg and ±3% for the samples of >400 mg/kg.

^b Preferable values. Other reference values are recommended values.

^c The sample powder of JG-1a was prefused with ZnO in addition to Na₂O₂ + Ba(OH)₂·8H₂O to lower the melting point.

rapid and quantitative method to determine fluorine in rock samples. The merit of using this technique is that ion chromatography (IC) is commonly available in many laboratories and useful for sensitive and rapid anion determination. Moreover, the IC technique possibly enables us to perform simultaneous determination of the other halogens in addition to fluorine.

This technique requires rendering the samples into a non-acidic solution, and for this reason, alkali fusion would be the exclusive practical method for the rock decomposition. After the treatment, however, the sample solution contains considerable amounts of undesirable anions and cations, which prevents direct IC analysis. To eliminate those ions, a cation-exchange pretreatment technique is demonstrated in this section. The sample solution is decarbonated and dehydrated by this cation-exchange treatment in addition to the elimination of undesirable cations. The interference of dissolved aluminum from rocks, a major residual problem, is minimized by maintaining optimal pH conditions during the pretreatment [11].

2.3.2. Experimental

2.3.2.1. Apparatus

A Dionex Model QIC (Sunnyvale, CA, USA) ion chromatographic instrument was used with conductivity detection. Calibration was achieved in the range 0–20 ppm F by adding known aliquots of NaF standard solutions to representative blank solutions.

2.3.2.2. Reagents

The working standard solutions were prepared from analytical reagent-grade chemicals using deionized water obtained from a Millipore Milli-Q SP water-purification system.

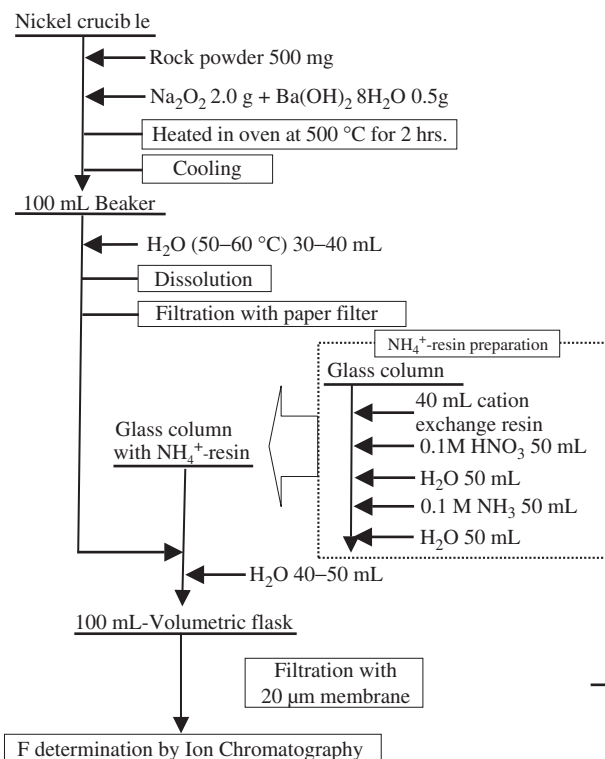


Fig. 3. Flow chart of the determination method by ion chromatography.

2.3.3. Recommended procedures

The outline of the analytical procedure is shown as a flow chart in Fig. 3. Rock powder (0.5 g) was fused with a mixture of 2.0 g Na_2O_2 + 0.5 g $\text{Ba}(\text{OH})_2 \cdot 8\text{H}_2\text{O}$ in an oven at 500°C for 2 h. The decomposition reagent was carefully pre-fused to release the water content. The “pancake” was then crushed and dissolved in 50–60 mL of hot water, followed by filtration.

Consequently, the sample solution was passed through a column of 40 mL NH_4^+ -based cation-exchange resin (SIGMA DOWEX-50W8-200; dry mesh size 100–200), collected in a 100-mL volumetric flask, and diluted to the mark with water.

The obtained solution was filtered with a disposal sample preparation cartridge (Advantec 25AS020AN) and injected into the above IC apparatus.

2.3.4. Pretreatment by cation exchange

The solution obtained from alkali fusion is unsuitable for direct analysis by IC because the high concentrations of carbonate and hydroxide in the solution could

act as eluents, thus modifying the retention times and causing a large analytical peak. The solution should therefore be pretreated by a cation-exchange resin, both to neutralize the solution and to lower the content of the solute (dissolved solids in the solution) that may cause IC column overloading.

In the cation-exchange treatment, unfavorable cation elements for the IC column and the majority of Na^+ are removed. At the same time, CO_3^- , HCO_3^- , and OH^- are removed as CO_2 and H_2O , respectively. The possible anions in the posttreatment solutions are F^- , Cl^- , SO_4^{2-} , and PO_4^{3-} . The cation-exchange pretreatment is expressed as



After the above pretreatment, however, the determination value of fluorine was significantly lower than the expected value. The possible reason for this analytical anomaly was suspected to be aluminum interference, which was released from rock powders during alkali fusion; it is well known that aluminum ion forms a complex and precipitates with F^- and OH^- . Formed aluminum hydroxide precipitates in the vicinity of pH 7, but under higher pH conditions, a large amount of OH^- would hinder the formation of aluminum fluoride complex. To avoid interference from aluminum, pH treatment was performed to maintain the solution within the desirable pH range, $\text{pH} > 8$, throughout the cation exchange procedure. At the same time, the pH condition should be less than *ca.* 10 to ensure the complete elimination of carbonate and hydroxide.

Consequentially, H^+ -, NH_4^+ -, and Na^+ -formed resins were investigated concerning aluminum interference. After this pretreatment, the pH values of the solutions were < 6 , ~ 8 , and > 12 , respectively. Whereas only 5–11% fluorine were recovered for a solution of the H^+ -formed resin treatment, an effective recovery of 83–97% was obtained for the NH_4^+ -formed resin treatment (Fig. 4). On the other hand, the solution obtained by the Na^+ -formed resin treatment did not provide the results for masking a large analytical peak. Spike recoveries or the other experimental results are found in our previous literature [11].

2.3.5. Analysis of reference materials

The analytical results of this method and the published values for reference materials are summarized in Table 1. A positive agreement has been obtained between the results of the present work and the recommended values by the GSJ. This result signifies that the recommended cation exchange procedure used in this study is reasonably accurate and precise. The applicability of this method for the simultaneous determination of other anions, such as chlorine, has also been certified by the comparison with recommended values of GSJ standard samples [11].

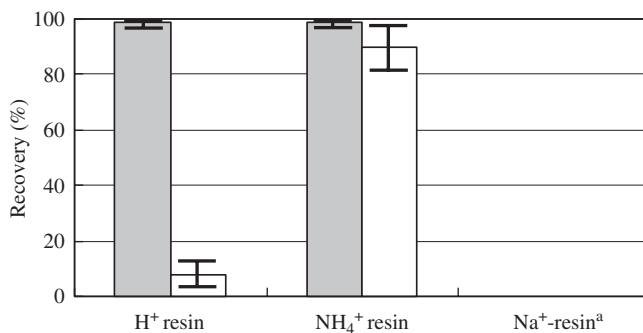


Fig. 4. Influence of aluminum on the IC method. The pretreatment solution contains 5 mg/kg of fluorine with 1 M of NaOH. ■, with no aluminum solution; □, with 100 mg/kg of aluminum solution; I, error bar; ^a, undetectable for a large OH⁻ peak.

3. FLUORINE AND OTHER VOLATILE ABUNDANCES IN JAPANESE VOLCANIC ROCKS

3.1. Geochemical studies on volatile elements in volcanic rocks

Since volatiles in volcanic bulk rocks have been assumed to be residual of degassing during the ascent of magmas, little attention has been paid to their concentration in bulk rocks. Studies of volatiles in volcanic rocks have mainly been performed on submarine volcanic glasses [12]. The studies on these kinds of glass samples have intensively been performed in ocean-ridge or hot spot regions, but less often in island arc regions [13,14]. Another approach to volatiles is attempted by the determination of melt or glass inclusions. Various studies have been reported [15–19], but the use of melt inclusions involves the following difficulties: (1) a paucity of fresh, glassy non-vesicular quenched at high pressure suitable for direct analysis; (2) an absence of indicative minerals in parental magmas; (3) complex mineral/liquid relations; (4) the possible high-pressure saturation of silicate liquid with a CO₂-rich gas; and also its tiny size for chemical analysis (100 μm in diameter).

Fluorine is generally thought to have considerable affinity to silicate melts as compared to fluid phases than the other volatile components, such as H₂O, Cl, or S [20,21]. Studies of fluorine in bulk rocks and glasses have shown that fluorine degassing is undetectable from the interior of lava flows [22,23], and instead, the fluorine in bulk rocks behaves as an incompatible element [12]. Experimental work shows that the fluorine degassing rate is much smaller than chlorine or other volatile components [24,25]. Thus, even bulk rocks may reveal meaningful information to evaluate the behavior of fluorine or presumably other volatile behavior in magmas.

In the present study, fluorine and other volatile elements in bulk rocks obtained from various parts of the islands of Japanese arc were investigated using multivariate analysis. The major purpose was (1) to evaluate the availability of volatile data in bulk rocks to investigate the magma genesis or differentiation process and (2) to find a potential factor to control the volatile elements.

3.2. Samples and methods

3.2.1. Samples and chemical analysis

Bulk rock samples of rhyolite, andesite, and basalt were collected mainly from the quaternary volcanoes of the Japanese islands (Fig. 5). Those samples cover most of the volcanic rock types in the Japanese islands. Samples had the altered part cut off, cleaned with deionized water, dried, and crushed to a fine powder.

Major elements were analyzed by XRF. Ferrous iron was determined by potentiometric titration. Approximately 0.5 g of the accurately weighed and finely powdered rock material was decomposed by a mixture of HF–H₂SO₄; the solution was poured onto saturated boric acid and titrated with a 0.02 M KMnO₄ standard solution. Water on the grains of the sample, conventionally noted H₂O(–), was determined by the loss in weight when heated at 110°C for 12 h. The determination of total water was made based on the loss on ignition with the correction of ferrous iron oxidation. A powdered sample was heated at 1050°C by an electric furnace for 3 h; the sample was then weighed, and the residual ferrous iron content was determined by KMnO₄ titration. The ignition loss was corrected for the amount of the oxidized ferrous iron. Bound water, conventionally noted H₂O(+), was obtained by the difference between total water and H₂O(–). Fluorine determination was performed by the distillation method shown in Chapter 1. The analytical data of the major elements was reported in our previous chapter [26]. Part of the volatile quantitative data was included in the following literature; fluorine, chlorine, bromine, iodine [27] (Yoshida unpublished), sulfur [28,29], boron [30], and arsenic (Tanaka unpublished).

3.2.2. Statistical strategy

Regarding multivariate analysis, particularly, factor analysis (FA) is a widely known statistical technique, which enables us to extract the underlying common factors that control behavioral patterns. In the present work, this technique was applied to extract and understand both the source information and variation of each chemical solute in the natural water samples. The co-variances among chemical components were statistically analyzed and categorized by principal component analysis (PCA). Under these procedures, the potential factors of chemical variation were extracted using FA method.

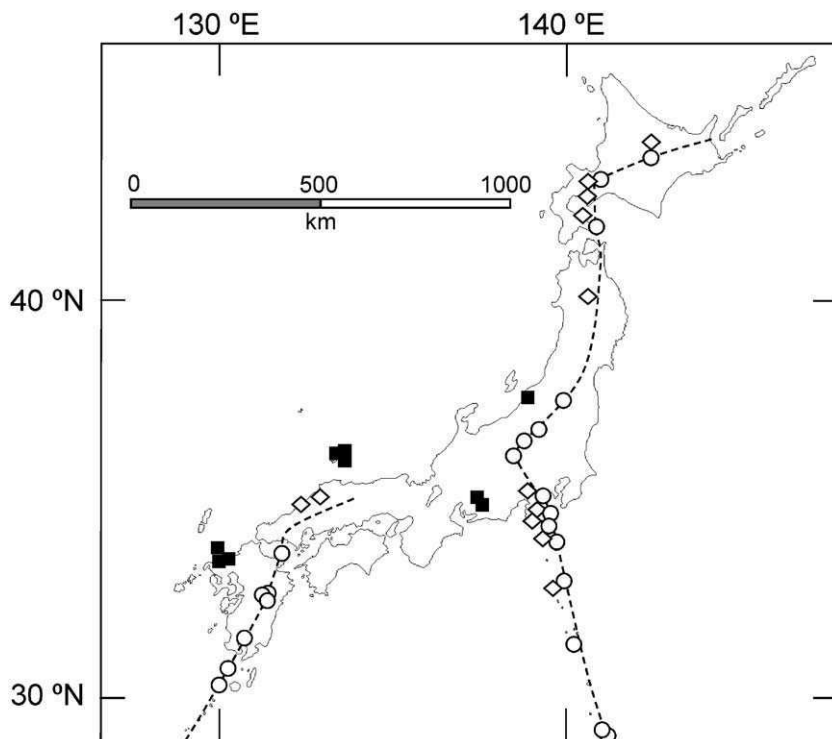


Fig. 5. Map of sampling points with the volcanic front (dashed lines). Symbols: open circle (○); volcanoes within 20 km from the volcanic front (VF), open lozenge (◇); volcanoes 20–50 km from VF, solid square (■); volcanoes over 50 km from VF.

3.2.3. Data pretreatment

In general, volcanic rocks contain a small quantity of water-soluble volatiles. Some samples, however, show a large amount of water-soluble Cl and Br. Rock samples with considerable amounts of water-soluble Cl and Br were mostly obtained from a seaside area, where the volcanic rocks were highly prone to secondary contamination by seawater. Hence, the data of water-insoluble Cl and Br were used for the following statistical analysis.

The employed statistical techniques are applicable on datasets of normal distribution. Major elements generally show approximately normal distribution, but trace elements tend to take log-normal distribution [31]. In practical terms, the volatile data of this study is distributed almost log-normally (Fig. 6), and logarithmic transformations were made for volatile data before statistical analyses. To treat each chemical component equally, the chemical data was standardized,

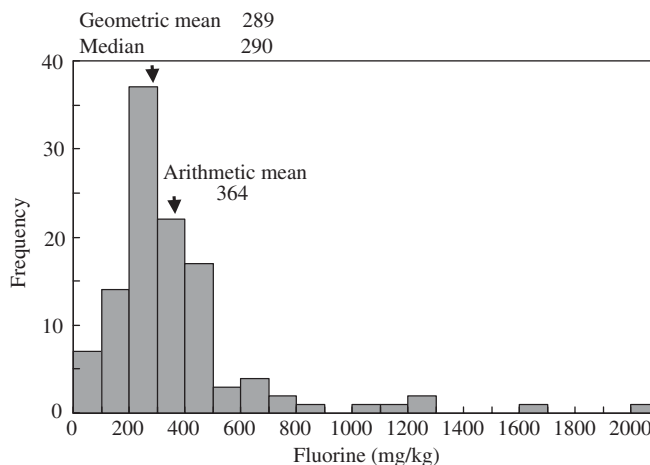


Fig. 6. Frequency distribution of the fluorine dataset illustrated by the histogram.

whereby the mean value is 0 and the variance is 1. Multivariate methods were also applied under the observation of literature [32,33].

3.3. Results and discussion

3.3.1. Abundance of fluorine and other volatile contents in volcanic rocks

The sample descriptions and analytical results are listed in Appendix 1. The other volatile and major element contents of regional representative samples are also listed in Appendix 2 after our previous study [26]. As shown in Fig. 6, the fluorine content takes log-normal distribution, and the other volatiles are also dispersed log-normally. The geometrical or arithmetic mean values of the fluorine content in the rock samples are 289 mg/kg and 364 mg/kg respectively, whereas the continental crustal average is 525 mg/kg (Tables 2 and 3). The analytical value of this study is slightly smaller than the crustal average, although the value remains within the same order of magnitude. Those of the other volatiles also fall within values similar to those of the crustal average.

The relation between fluorine and other volatiles is rather unclear (Fig. 7 (a)–(g)). On the other hand, geographical distribution of volatile elements is prominent in relation to the distance from the volcanic front. Although sulfur, arsenic, and iodine are uniformly dispersed, samples on the volcanic front (VF) show low levels of fluorine and $\text{H}_2\text{O}(+)$, and high chlorine, bromine, and boron, whereas back-arc samples over 50 km away from the VF show relatively high levels of F and $\text{H}_2\text{O}(+)$, and low Cl, Br, and B.

Table 2. Summary statistics of volatile abundances in volcanic rocks (mg/kg); H₂O(+) in wt%

	F	Cl	Br	I	S	B	As	H ₂ O(+)
Number of samples	113	113	44	44	113	113	44	44
Arithmetic mean	364	232	0.78	0.09	106.1	18.6	2.56	1.04
Geometric mean	289	122	0.52	0.07	20.9	12.9	1.76	0.71
Median	290	145	0.50	0.07	20	14	2.04	0.56
Standard deviation	295	233	0.66	0.07	515	20	2.35	1.02
Minimum	20	5	0.09	0.01	0.1	0.5	0.21	0.14
Maximum	2000	950	2.6	0.32	5390	169	10.71	5.42

Table 3. Average chemical composition and ratios (mg/kg)

	(1) Crustal average [40]	(2) Sea water [41]	(3) Shales [41]	(4) Primitive mantle [42]	(5) (2)/(1)	(6) (3)/(1)	(7) (4)/(1)
Si	288,000	3	275,000	210,000	0.00	0.95	0.73
Ti	4010	0.001	4600	1205	0.00	1.15	0.30
Al	79,600	0.001	88,000	23,500	0.00	1.11	0.30
Fe	43,200	0.007	48,000	62,600	0.00	1.11	1.45
Mn	716	0.003	850	1045	0.00	1.19	1.46
Mg	22,000	1270	16,000	228,000	0.06	0.73	10.36
Ca	38,500	400	16,000	25,300	0.01	0.42	0.66
Na	23,600	10,560	59,000	2670	0.45	2.50	0.11
K	21,400	380	24,500	240	0.02	1.14	0.01
P	757	0.068	700	90	0.00	0.92	0.12
F	525	1.3	800	25	0.00	1.52	0.05
Cl	472	18,980	160	17	40.21	0.34	0.04
Br	1	65	24	0.05	65.00	24.00	0.05
I	0.8	0.05	2.2	0.01	0.06	2.75	0.01
S	697	884	2400	250	1.27	3.44	0.36
B	11	4.8	130	0.3	0.44	11.82	0.03
As	1.7	0.024	13	0.05	0.01	7.65	0.03

3.3.2. Statistical analysis of fluorine, chlorine, sulfur, and boron

The correlation matrix of fluorine, chlorine, sulfur, and boron for 113 samples is shown in Table 4. A significantly high correlation is only found between Cl and B, where the correlation coefficient is +0.51; and moderate correlation is found between F and S (+0.27). Correlation coefficients have levels of significance exceeding 0.01.

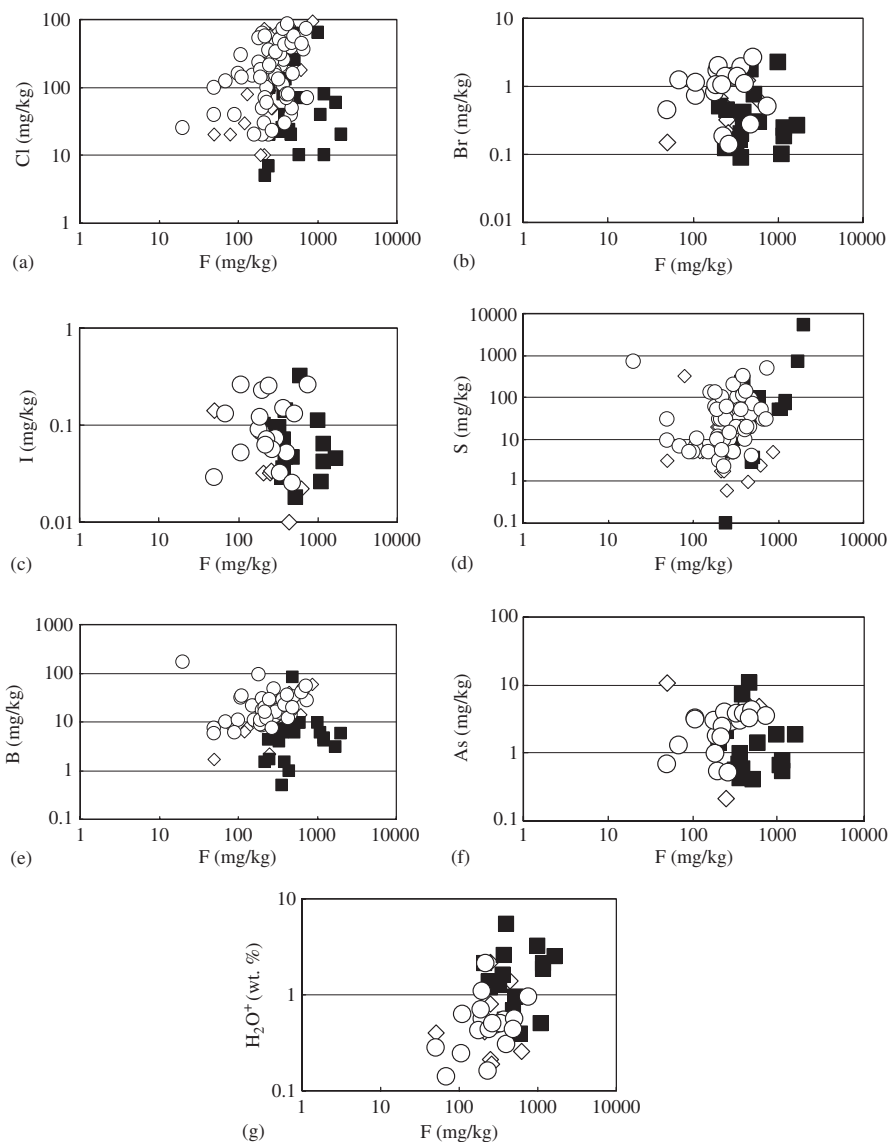


Fig. 7. Correlation between fluorine and other volatiles. (a) F and Cl on 113 samples; (b) F and Br on 44 samples; (c) F and I on 44 samples; (d) F and S on 113 samples; (e) F and B on 113 samples; (f) F and As on 44 samples; and (g) F and H_2O^+ on 44 samples. [Symbols are the same as in Fig. 5.]

Based on this correlation matrix, a PCA calculation was performed to summarize the correlation among volatiles, clearly reflecting the above correlation feature (Table 5). Chlorine and boron are correlated to the first principal component (P1) with a proportionate contribution of 38%, while fluorine and sulfur are on the

Table 4. Correlation matrix of fluorine, chlorine, sulfur, and boron on 113 volcanic rock samples

	log(F)	log(Cl)	log(S)	log(B)
log(F)	1.00			
log(Cl)	0.13	1.00		
log(S)	0.27	-0.12	1.00	
log(B)	-0.04	0.51	0.14	1.00

Table 5. Eigenvectors and eigenvalues of the correlation matrix of fluorine, chlorine, sulfur, and boron ($n = 113$)

	P1	P2	P3	P4
log(F)	0.18	0.66	0.65	-0.33
log(Cl)	0.69	-0.19	0.31	0.62
log(S)	0.11	0.72	-0.57	0.39
log(B)	0.69	-0.10	-0.39	-0.60
Eigenvalue	1.52	1.26	0.85	0.37
Proportion	0.38	0.31	0.21	0.09
Cumulative proportion	0.38	0.70	0.91	1.00

second component (P2) with a proportion of 31%. The scatter plot of the PCA scores is drawn in Fig. 8. The samples on the VF (open circle or open lozenge) take high P1 scores and low P2 scores, respectively, whereas back-arc samples (solid square) are widely dispersed with relatively low P1 and high P2 scores.

The above geographical distribution of volatiles is consistent with other works on Japanese volcanic rocks [27,34]; the fluorine contents in volcanic rocks increase from the trench side to the back-arc side of the Japanese islands, whereas chlorine shows the opposite tendency.

3.3.3. Principal component analysis of major and volatile elements

In addition to the above four elements, bromine, iodine, arsenic, and major elements were intensively analyzed using the representative samples of each region (Appendix 2). The correlation matrix is shown in Table 6. Although a high degree of correlation is clearly observed among major elements with a correlation coefficient range between 0.7 and 0.9, moderate or low correlation occurs among volatile elements, except for a high correlation between Cl and Br. Exclusively poor correlation was found between volatiles and major elements, while incompatible elements, such as K_2O and P_2O_5 , showed little correlation with fluorine or other volatiles.

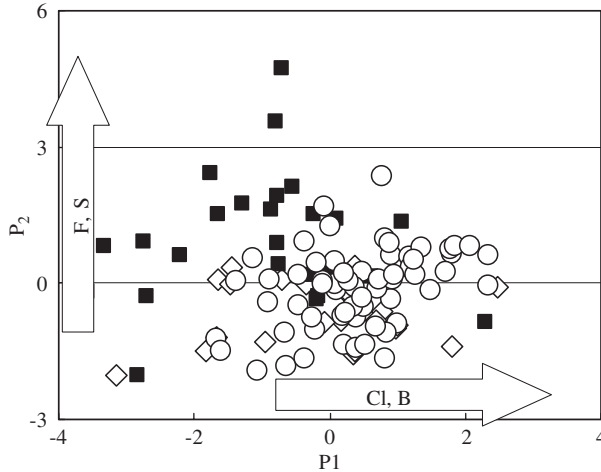


Fig. 8. Scattered plot of principal component analysis on the first and second components (P1 and P2) for fluorine, chlorine, sulfur, and boron on the 113 samples. The symbols are the same as in Fig. 5.

The PCA result shows that the first 5 components account for about 80% of the variance in the dataset (Table 7). The first component, responsible for 36% of the covariance, heavily weights the contributions of major elements, but has no such effect for volatile elements. The second or other principal components load on the volatile elements. The PCA structure shows that most of the major and volatile elements do not correlate with each other, and the volatile elements take the correlation groups as chlorine and bromine group; fluorine, sulfur, phosphate, H₂O group; arsenic and boron group; and iodine.

3.3.4. Factor analysis of volatiles

In this section, FA was applied to the volatiles on the 44 representative samples, to extract the potential factors responsible for the volatile behavior. The principal factor method with various rotation methods was applied to the volatile elements, and these calculations revealed an identical factor structure. Table 8 shows the representative result obtained by quartimax rotation. Factor 1 shows high values for Cl, Br, B, and As, whereas factor 2 is associated with H₂O(+), F, and S. Those results are consistent with the 4 volatile correlations on 113 samples.

Factor 1 shows a high contribution to Cl, Br, B, and As. The contents of Cl and Br in seawater are significantly higher than those in the mantle or crust, and even B and S show moderately high values in seawater, compared with other components (Table 3). Moreover, B and As tend to concentrate in marine sediments

Table 6. Correlation matrix of major and volatile elements ($n = 44$)

	SiO ₂	TiO ₂	Al ₂ O ₃	Fe ₂ O ₃	FeO	MnO	MgO	CaO	Na ₂ O	K ₂ O	P ₂ O ₅	log(H ₂ O ⁺)	log(F)	log(Cl)	log(Br)	log(I)	log(S)	log(B)	log(As)
SiO ₂	1.00	-0.82	-0.35	-0.72	-0.90	-0.77	-0.86	-0.91	0.42	0.52	-0.59	-0.17	0.03	0.22	0.13	-0.08	-0.26	0.44	0.44
TiO ₂	-0.82	1.00	0.10	0.70	0.72	0.64	0.65	0.68	-0.22	-0.39	0.71	0.37	0.23	-0.32	-0.27	0.01	0.47	-0.42	-0.37
Al ₂ O ₃	-0.35	0.10	1.00	0.27	0.23	0.13	0.15	0.31	-0.11	-0.31	-0.20	-0.18	-0.22	-0.16	-0.06	0.20	-0.07	-0.09	-0.27
Fe ₂ O ₃	-0.72	0.70	0.27	1.00	0.53	0.66	0.43	0.56	-0.12	-0.20	0.57	0.02	0.04	-0.49	-0.31	0.22	0.25	-0.38	-0.37
FeO	-0.90	0.72	0.23	0.53	1.00	0.80	0.82	0.92	-0.51	-0.69	0.38	0.05	-0.22	0.01	0.07	0.06	0.18	-0.20	-0.27
MnO	-0.77	0.64	0.13	0.66	0.80	1.00	0.60	0.75	-0.16	-0.59	0.56	0.00	-0.02	-0.14	-0.03	0.11	0.20	-0.13	-0.11
MgO	-0.86	0.65	0.15	0.43	0.82	0.60	1.00	0.86	-0.53	-0.55	0.45	0.06	-0.10	-0.03	0.01	-0.09	0.08	-0.42	-0.48
CaO	-0.91	0.68	0.31	0.56	0.92	0.75	0.86	1.00	-0.58	-0.73	0.48	-0.02	-0.22	0.00	0.07	0.05	0.20	-0.2	-0.34
Na ₂ O	0.42	-0.22	-0.11	-0.12	-0.51	-0.16	-0.53	-0.58	1.00	0.16	-0.03	0.16	0.55	-0.19	-0.22	0.00	0.09	0.16	0.03
K ₂ O	0.52	-0.39	-0.31	-0.20	-0.69	-0.59	-0.55	-0.73	0.16	1.00	-0.12	0.14	0.17	-0.23	-0.25	-0.01	-0.10	-0.17	0.22
P ₂ O ₅	-0.59	0.71	-0.20	0.57	0.38	0.56	0.45	0.48	-0.03	-0.12	1.00	0.38	0.52	-0.29	-0.27	-0.10	0.46	-0.37	-0.19
log(H ₂ O ⁺)	-0.17	0.37	-0.18	0.02	0.05	0.00	0.06	-0.02	0.16	0.14	0.38	1.00	0.44	-0.02	-0.06	0.10	0.32	-0.25	-0.14
log(F)	0.03	0.23	-0.22	0.04	-0.22	-0.02	-0.10	-0.22	0.55	0.17	0.52	0.44	1.00	-0.07	-0.14	-0.21	0.42	-0.07	-0.11
log(Cl)	0.22	-0.32	-0.16	-0.49	0.01	-0.14	-0.03	0.00	-0.19	-0.23	-0.29	-0.02	-0.07	1.00	0.89	0.04	-0.09	0.64	0.35
log(Br)	0.13	-0.27	-0.06	-0.31	0.07	-0.03	0.01	0.07	-0.22	-0.25	-0.27	-0.06	-0.14	0.89	1.00	0.22	-0.07	0.61	0.38
log(I)	-0.08	0.01	0.20	0.22	0.06	0.11	-0.09	0.05	0.00	-0.01	-0.10	0.10	-0.21	0.04	0.22	1.00	0.30	0.08	0.11
log(S)	-0.26	0.47	-0.07	0.25	0.18	0.20	0.08	0.20	0.09	-0.10	0.46	0.32	0.42	-0.09	-0.07	0.30	1.00	-0.04	-0.02
log(B)	0.44	-0.42	-0.09	-0.38	-0.20	-0.13	-0.42	-0.23	0.16	-0.17	-0.37	-0.25	-0.07	0.64	0.61	0.08	-0.04	1.00	0.59
log(As)	0.44	-0.37	-0.27	-0.37	-0.27	-0.11	-0.48	-0.34	0.03	0.22	-0.19	-0.14	-0.11	0.35	0.38	0.11	-0.02	0.59	1.00

Note: **Bold**; 0.01 level of significance.

Table 7. Eigenvectors and eigenvalues of the correlation matrix of major and volatile elements ($n = 44$)

	P1	P2	P3	P4	P5
SiO ₂	-0.37	-0.03	0.01	-0.01	0.04
TiO ₂	0.33	-0.13	0.14	-0.01	-0.04
Al ₂ O ₃	0.11	0.11	-0.29	0.39	0.21
Fe ₂ O ₃	0.28	-0.12	-0.06	0.29	0.02
FeO	0.34	0.20	0.03	-0.04	0.00
MnO	0.30	0.08	0.12	0.12	0.21
MgO	0.32	0.12	-0.04	-0.26	-0.06
CaO	0.35	0.20	0.00	-0.05	0.01
Na ₂ O	-0.15	-0.28	0.17	0.22	0.51
K ₂ O	-0.22	-0.28	-0.08	-0.02	-0.43
P ₂ O ₅	0.25	-0.24	0.28	-0.13	-0.01
log H ₂ O(+)	0.06	-0.23	0.32	-0.09	-0.33
log(F)	0.00	-0.34	0.39	-0.11	0.27
log(Cl)	-0.11	0.39	0.33	-0.18	-0.04
log(Br)	-0.08	0.41	0.31	-0.02	-0.10
log(I)	0.02	0.08	0.09	0.66	-0.39
log(S)	0.12	-0.15	0.39	0.28	-0.13
log(B)	-0.18	0.30	0.29	0.15	0.29
log(As)	-0.18	0.17	0.25	0.13	-0.11
Eigenvalue	6.93	3.36	2.23	1.46	1.15
Proportion	0.36	0.18	0.12	0.08	0.06
Cumulative proportion	0.36	0.54	0.66	0.74	0.80

and the altered oceanic crust [35]. When seawater contributes to the generation of magma, volcanic rocks are enriched in those components.

The geochemical behavior of Br and Cl resemble each other in comparison with other halogens [27,36], and the Br/Cl ratio is considered to be conservative in the chemical processes. A linear regression calculation between Br and Cl yields a Br/Cl ratio of 0.0034 ± 0.00050 . This value is identical to the Br/Cl ratio of seawater (0.0034), which is higher than the mantle value (0.0020), and significantly lower than the shale value (0.15). The Br/Cl ratio shows positive correlation to the interpretation that F1 indicates a seawater influence on magma.

According to a generalized model of magma genesis in subduction zones, the seawater which is brought into the upper mantle with the sinking oceanic crust plays an important role in the partial melting of the mantle wedge [37]. The present results reflect this concept. However, sulfur, present in high concentrations in seawater, shows no correlation with factor 1; this result can be explained by the formation of insoluble sulfate salts at high temperature.

Table 8. Factor loadings of volatile elements ($n = 44$)

	F1	F2	F3
log H ₂ O(+)	-0.11	0.55	0.06
log(F)	-0.07	0.82	-0.29
log (Cl)	0.89	0.01	-0.07
log (Br)	0.89	-0.03	0.10
log (I)	0.13	0.10	0.96
log (S)	-0.05	0.57	0.25
log (B)	0.77	-0.09	-0.01
log (As)	0.50	-0.09	0.06

Sulfur exists in the form of a sulfate ion in seawater. Only limited amount of sulfur in the marine sediments forms sulfide salts but it is mainly made by the bacterial reduction of sulfate, only under anoxic environments [38], and a significant amount of sulfur is found in marine sediments as sulfate. The solubility of CaSO₄ and MgSO₄ decreases with increasing temperature [39]. The amount of Ca and Mg concentrations in seawater or marine sediments is sufficient to consume all S in those sources to form insoluble sulfate salts. Subsequently, sulfur which is carried into the mantle by subducting plate forms insoluble salts with Ca and Mg when exposed to the high temperature of the mantle. When the volatiles in seawater are carried into the mantle with the subducting plate, Cl, Br, B, and As are released from the plate with H₂O by the heat of the mantle and absorbed in the overlying mantle wedge. Sulfur, however, is fixed in the form of insoluble sulfur compounds and remains in the subducting plates at this stage.

Factor 2 is highly correlated with H₂O(+), F, and S. This factor is interpreted as the effect of the mantle material on the magma genesis and/or process. Table 3 shows that sulfur is highly concentrated in the mantle in the same order as the seawater. In consideration of the mass balance and calcium sulfate water insolubility, it is reasonable to assume the mantle as a potential major source of sulfur. Part of the sulfur may be supplied from the deep boundary region between the subducted lithosphere and the overlying mantle wedge. In the deep region, however, it is possible that at the phlogopite decomposed point [37], the plate boundary circumstance is less hydrated than the shallower part, and the oxygen fugacity is lower. Here, the seawater-derived insoluble sulfate salt is reduced by mantle materials subject to high pressure and temperature. The reduced sulfur forms sulfide and is released into the overlying mantle wedge. In this case, since the sulfide is generated by interaction with the mantle material, this sulfur is essentially regarded in the same light as the mantle-derived sulfur.

On the contrary, fluorine shows a rather low concentration rate. It has a high affinity with silicate to break the silicate bond structure and thus tends to be

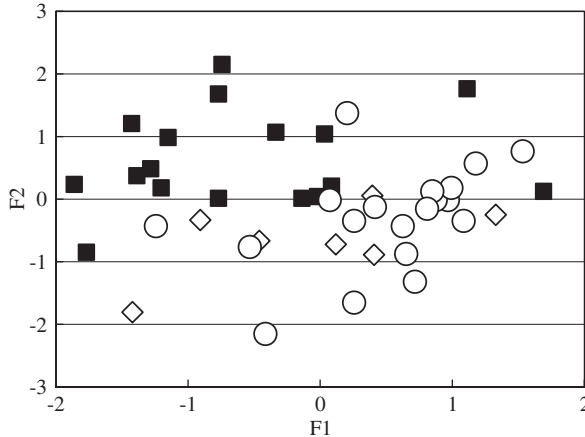


Fig. 9. Scattered plot of factor scores on the first and second factors (F1 and F2) for volatiles on the 44 samples. F1 is highly associated with Cl, Br, and moderately with B and As; F2 is associated with F, H₂O(+), and S. The symbols are the same as in Fig. 5.

concentrated in the liquid phase (magma) rather than the solid phases. In consideration of the mass balance for each source, the contribution of mantle materials to magma genesis is of greater significance than other sources, as mentioned above. Therefore, factor 2 would correspond to the contribution of the mantle component.

Factor 3 is exclusively correlated with iodine, revealing the unique behavior of this element as compared to other volatiles. The provisional interpretation of this factor was shown in our previous work [26].

The geographical distribution of factor scores supports the above interpretation of F1 and F2 (Fig. 9). Samples of the VF region take high F1 scores and low F2 scores, whereas back-arc side samples take low F1 scores and high F2 scores, respectively. Those factors presumably reflect the variation of magma genesis across the arc. The above evidences also introduced the fact that F1 reflects the contribution of seawater-derived volatiles to magma genesis, and that F2 corresponds to the contribution of the mantle component. The factor interpretation of F1 and F2 is summarized in Fig. 10 in the form of a schematic diagram.

The factor structure is consistent with the behavior in submarine glasses [13]; that is, chlorine, bromine, and possibly boron and arsenic are rich in the trench side area, since those elements are inherited from the subduction slab, on the contrary, fluorine and sulfur are varied in the vertical direction of the VF, since those elements originate potentially from an enriched subarc mantle wedge. Volatile data in the bulk rocks possibly give useful information to discuss the magma differentiation or its chemical processes.

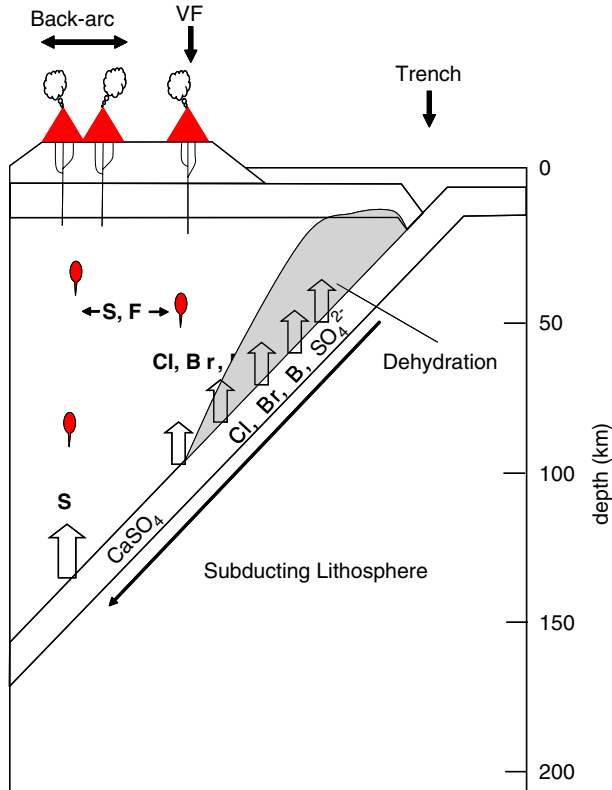


Fig. 10. Schematic diagram of the volatile distribution in the shallow subduction zone. Large amounts of Cl and Br, and presumably B and As are supplied from subducted marine crust. Contributions of fluorine and sulfur come from the components of the mantle wedge.

The concentrations of volatiles in magmas probably change before final solidification as a result of crystallization differentiation and degassing during the magma ascent. If the volatile contents in bulk rocks only reflected the rate of degassing, the uni-factor of the “degassing rate” would have been obtained with high loading for each volatile. On the contrary, if the volatiles were exclusively controlled by crystallization differentiation, volatiles would have formed a “crystallization differentiation” factor with other incompatible elements, such as K_2O . The present result, however, shows no such factors. Besides, the obtained factors are reasonably interpreted by the original source of each volatile. Moreover, the factor features of volatiles are in accordance with the other volatile studies of submarine glasses. Volatile contents in bulk rocks would possibly reveal meaningful information about the volatile behaviors in magmas.

3.4. Conclusions

In this chapter, the correlation between fluorine and other volatile elements in volcanic bulk rocks was investigated by applying multivariate analysis. The results based on the PCA showed considerable correlation among most of the major elements to form one group, though the volatiles show various dispersions. The factor structure of volatile elements led to the following findings: (1) Seawater components brought by subducting slab have a significant influence on the behavior of chlorine, bromine, boron, and arsenic. (2) Fluorine and sulfur are mainly contributed by the mantle components. Those volatile correlations are basically consistent with volatile studies of submarine glass samples. Even bulk rock composition would give meaningful information to understand the volatile behavior in magma processes.

ACKNOWLEDGMENTS

The author greatly appreciates the help of Dr Minoru Yoshida, and Messrs Mineharu Ohshima and Kentaro Tsuchiya for the instruction in potentiometric analytical procedure and the provision of their data.

**APPENDIX 1. VOLATILE CONTENTS OF JAPANESE VOLCANIC ROCKS (113 samples in mg/kg.
Cl abundances are water-insoluble data)**

Sample descriptions	F	Cl	S	B
J-1 Basalt; lava of 1950, Mihara-yama, O-shima, Tokyo Metr.	108	298	6.95	31
J-2 Basalt; Okata, O-shima, Tokyo Metr.	50	100	9.52	7.4
J-3 Basalt; lava of 1962, Miyake-jima, Tokyo Metr.	197	586	11.7	19
J-4 Basalt; Western foot of Higashi-yama, Hachijo-jima, Tokyo Metr.	50	40	30	5.8
J-5 Basalt; Southeastern foot of Nishi-yama, Hachijo-jima, Tokyo Metr.	70	125	6.98	10
J-6 Basalt; Sakasagawa, Ito, Shizuoka Pref.	250	90	0.59	2.2
J-7 Basalt; lava of 864, Aokiga-hara, Fuji-san, Yamanashi Pref. No. 1	210	200	1.69	20
J-8 Basalt; lava of 864, Aokiga-hara, Fuji-san, Yamanashi Pref. No. 2	270	260	5	22
J-9 Basalt; Kenmarubi lava, Fuji-yoshida, Fuji-san, Yamanashi Pref.	230	220	1.69	19
J-10 Basalt; Maku-iwa, Fuji-san, Shizuoka Pref.	190	200	10	14
J-13 Basalt; Shirogane Lava, Tokachi-dake, Hokkaido	300	420	14.2	18
J-14 Basalt; Orimoto-toge, Shidara, Aichi Pref.	250	100	37.3	10
J-15 Basalt; Okuwa, Shidara, Aichi Pref.	400	130	238	10
J-16 Basalt; intrusive sheet, Yuto, Shidara, Aichi Pref.	210	145	71.5	11
J-17 Basalt; Kakuda-yama, Nigata Pref.	300	380	10	4.8
J-18 Basalt; Nishimura, Nakamura, Dogo, Oki, Shimane Pref.	580	10	90	9.6
J-19 Basalt; Kuniga, Nishino-shima, Oki, Shimane Pref.	1200	10	70	4.2
J-20 Basalt; Imazu, Saigo, Dogo, Oki, Shimane Pref.	520	260	3.54	5.9
J-21 Basalt; Iwano, Karatsu, Saga Pref. No. 1	360	25	20.8	0.5
J-22 Basalt; Iwano, Karatsu, Saga Pref. No. 2	440	24	20	1
J-23 Basalt; Taka-shima, Karatsu, Saga Pref.	390	40	17.8	1.5
J-24 Basalt; Hinodematsu, Karatsu, Saga Pref.	250	20	5	1.7
J-26 Trachyandesitic Basalt; intrusive sheet, South of Okuwa, Shidara, Aichi Pref.	370	25	240	9.5

J-27	Nepheline basalt; Nagahama, Hamada, Shimane Pref.	1690	60	730	3
J-28	Dolerite; Kawai, Shidara, Aichi Pref.	330	22	190	4
J-29	Dolerite; South of Kawai, Shidara, Aichi Pref.	470	20	30	14
J-31	Basaltic andesite; Dyke, Sukumo-gawa, Hakone, Kanagawa Pref.	100	160	5	11
J-32	Chilled margin of dyke, Sukumo-gawa, Hakone, Kanagawa Pref.	200	220	5	8.5
J-33	Andesite; Kami-futago-yama, Hakone, Kanagawa Pref.	180	230	60	22
J-34	Andesite; Shimo-futago-yama, Hakone, Kanagawa Pref.	150	150	5	21
J-35	Andesite; Nagao-toge, Hakone, Kanagawa Pref.	90	40	5	6
J-37	Andesite; Jukkoku-toge, Shizuoka Pref.	130	80	5	7.5
J-38	Andesite; Southeast of Okimura, Haha-jima, Bonin Islands, Tokyo Metr.	200	620	3.17	9.3
J-39	Andesite; bomb ejected in 1962, Tokachi-dake, Hokkaido	370	610	47.2	14
J-40	Andesite; Kitamuki-kako lava, Tokachi-dake, Hokkaido	330	500	100	13
J-41	Andesite; Kami-horokametokku-kabu lava, Tokachi-dake, Hokkaido	470	40	40	14
J-42	Andesite; Kumano-sawa-shita, Tokachi-dake, Hokkaido	410	430	60	20
J-43	Andesite; lava of parasitic crater (Minami-kako), Yotei-zan, Hokkaido	620	180	2.36	14
J-44	Andesite; somma lava, Usu, Hokkaido	120	30	5	6.2
J-45	Andesite; dome lava, Tarumai-yama, Hokkaido	240	20	30	26
J-46	Andesite; bomb, Tarumai-yama, Hokkaido	200	50	30	30
J-47	Andesite; Eniwa-dake, Hokkaido	200	20	10	17
J-48	Andesite; Kenga-mine, Komaga-take, Hokkaido	210	10	20	10
J-49	Andesite; around the crater, Komaga-take, Hokkaido	250	160	20	16
J-50	Andesite; block in a mud flow, Komaga-take, Hokkaido	270	50	20	10
J-51	Andesite; lava of Yake-yama, Tamagawa Spa, Akita Pref.	408	84	24.7	24
J-52	Andesite; Iwaya, Kakuda-yama, Nigata Pref.	430	710	20	7.4
J-53	Andesite; ejecta of Meiji eruption, Azuma-issaikyo-yama, Fukushima Pref.	280	290	30	47

Appendix 1. Continued

	Sample descriptions	F	Cl	S	B
J-54	Andesite; lava of 1783, Asama-yama, Gumma Pref.	240	350	60	20
J-55	Andesite; Sessho-gawara, Kusatsu-shirane-san, Gumma Pref.	110	140	10.3	34
J-56	Andesite; Dyke, Kuniga, Nishino-shima, Oki, Shimane Pref.	1200	80	80	4.7
J-57	Andesite; Imi, Fuse, Dogo, Oki, Shimane Pref.	2000	20	5390	5.7
J-58	Andesite; Yunoo, Karatsu, Saga Pref.	220	5	5	1.5
J-59	Andesite; Yakataga-udo, Neko-dake, Aso, Kumamoto Pref.	300	300	5	13
J-61	Andesite; Dyke, Oshoji-iwa, Yamaguchi-dani, Neko-dake, Aso, Kumamoto Pref.	210	30	30	12
J-62	Andesite; chilled margin of dyke, Tengu-iwa, Neko-dake, Aso, Kumamoto Pref.	160	20	130	11
J-65	Andesite; the 5th valley of Western slope of Neko-dake, Aso, Kumamoto Pref.	260	150	10	24
J-68	Andesite; scoria lava of 1958, Naka-dake, Aso, Kumamoto Pref.	350	340	50	26
J-69	Andesite; Northern slope of Ogi-yama, Aso, Kumamoto Pref.	370	110	20	17
J-70	Andesite; Sensui-yane, Taka-dake, Aso, Kumamoto Pref.	350	210	30	15
J-71	Andesite; Northern slope of Narao-dake, Aso, Kumamoto Pref.	380	260	20	18
J-72	Andesite; Southern slope of Naka-dake, Aso, Kumamoto Pref.	290	170	5	15
J-73	Andesite; the top of Ogi-yama, Aso, Kumamoto Pref.	270	240	10	14
J-74	Andesite; Southeastern slope of Naka-dake, Aso, Kumamoto Pref.	230	100	10	9.6
J-75	Andesite; Southwestern valley of Naka-dake, Aso, Kumamoto Pref.	290	140	20	13
J-76	Andesite; the top of Taka-dake, Aso, Kumamoto Pref.	480	50	90	18
J-77	Andesite; Eastern slope of Okamado-yama, Aso, Kumamoto Pref.	410	70	10	16
J-78	Andesite; Southern slope of Naka-dake, Aso, Kumamoto Pref.	670	360	30	45

J-79	Andesite; road cutting near the Akamizu station, Aso, Kumamoto Pref.	470	390	20	25
J-80	Andesite; Kometsuka, Aso, Kumamoto Pref.	300	150	5	17
J-81	Andesite; bomb, Eastern slope of Ojo-dake, Aso, Kumamoto Pref.	240	200	30	15
J-82	Andesite; crater wall of Ojo-dake, Aso, Kumamoto Pref.	220	70	100	20
J-83	Andesite; under the bridge on the Kuro-kawa, Aso, Kumamoto Pref.	320	130	20	17
J-84	Andesite; lava of 1946, Sakura-jima, Kagoshima Pref.	340	313	190	15
J-85	Andesite; lava of 1914, Sakura-jima, Kagoshima Pref.	300	330	200	16
J-86	Andesite; Anei lava, Sakura-jima, Kagoshima Pref.	390	420	110	24
J-87	Andesite; Bummei lava, Sakura-jima, Kagoshima Pref.	480	460	40	20
J-88	Rhyolite; Iwo-dake, Satsuma-Iwo-jima, Kagoshima Pref.	407	79	16.4	21
J-89	Andesite; Inamura-dake, Satsuma-Iwo-jima, Kagoshima Pref.	190	180	9.96	8.7
J-90	Andesite; Yahazu-dake lava, Sakamoto, Satsuma-Iwo-jima, Kagoshima Pref.	190	140	50	11
J-91	Andesite; the uppermost lava of Shin-dake, Kuchino-erabu-shima, Kagoshima Pref.	250	210	60	29
J-92	Glassy andesite; Southern slope of E-san, Hokkaido	180	530	130	94
J-93	Glassy rhyolite; Showa-Iwo-jima, Satsuma-Iwo-jima, Kagoshima Pref.	504	560	70	33
J-94	Glassy rhyolite; Showa-Iwo-jima, Satsuma-Iwo-jima, Kagoshima Pref. (Pumiceous part)	363	739	50	29
J-95	Dacitic andesite; lava of young somma, Sukumo-gawa, Hakone, Kanagawa Pref.	230	60	2.29	12
J-96	Dacitic andesite; Sanbe-yama, Shimane Pref.	250	140	4.29	13
J-97	Trachyandesite; Suribachi-yama, Iwo-jima, Sulfur Islands, Tokyo Metr.	750	70	500	28
J-98	Trachyte; Funakoshi, Nishino-shima, Oki, Shimane Pref.	370	80	22.4	6

Appendix 1. Continued

	Sample descriptions	F	Cl	S	B
J-99	Phonolitic trachyte; Tokage-iwa, Tsuzurao-yama, Dogo, Oki, Shimane Pref.	240	7	0.1	4.3
J-100	Dacite; dome lava, Showa-shinzan, Usu, Hokkaido	80	20	320	8.5
J-101	Dacite; dome lava, Ousu-dake, Usu, Hokkaido	260	50	19.9	16
J-102	Dacite; dome lava (red colored part), Ousu-dake, Usu, Hokkaido	190	10	20	13
J-103	Dacite; lava of somma, Akagi-yama, Gumma Pref.	266	23	14.1	7.5
J-104	Dacite; Eboshi-dake, Aso, Kumamoto Pref.	390	30	320	22
J-105	Dacite; Koeboshi-dake, Aso, Kumamoto Pref.	430	80	20	12
J-106	Dacite; Eboshi-dake lava, Northeast of Tarutama Spa, Aso, Kumamoto Pref.	630	440	50	41
J-108	Rhyodacite; Eastern slope of Otogase (Senriga-hama volcano), Aso, Kumamoto Pref.	720	720	30	54
J-109	Liparite; Tenjo-san, Koze-shima, Tokyo Metr.	250	630	5.89	17
J-110	Liparite; Southeastern foot of Tenjo-san, Koze-shima, Tokyo Metr.	300	630	5	14
J-111	Liparite; South of Naga-hama, Koze-shima, Tokyo Metr.	200	620	20	13
J-112	Liparite; Takodo-yama, Koze-shima, Tokyo Metr.	210	730	10	16
J-113	Liparite; Koze-shima, Tokyo Metr.	247	590	7.77	12
J-117	Liparite; Southeastern coast of Shikine-jima, Tokyo Metr.	220	570	5.65	16
J-118	Rhyolitic rock; Nishida, Saigo, Dogo, Oki, Shimane Pref.	1100	40	50	6
J-119	Potash Liparite; Manzo-yama, Shimoda, Shizuoka Pref.	50	20	3.03	1.7
J-120	Alkali rhyolite; Madara-jima, Saga Pref.	600	70	100	9.5
J-121	Obsidian; Shirataki, Hokkaido	437	794	0.97	41
J-127	Obsidian; Wada-toge, Nagano Pref. (pale part)	870	950	5	60
J-130	Obsidian; Koshi-dake, Imari, Saga Pref.	483	613	2.81	82
J-131	Obsidian; Hime-shima, Oita Pref. No. 1	485	157	4.08	20

J-134	Obsidian; in a welded tuff of Aso volcano (so-called Aso lava), Kumamoto Pref.	20	25	720	169
J-135	Obsidian; in a deposit of ejecta of Kikai Caldera, Satsuma-Iwojima, Kagoshima Pref.	420	850	140	36
J-138	Glassy rock; Igo, Nakamura, Dogo, Oki, Shimane Pref.	1000	650	51.6	9.7

APPENDIX 2. COMPOSITION OF VOLCANIC ROCKS IN JAPAN (44 SAMPLES)

	J-1	J-2	J-3	J-5	J-6	J-7	J-13	J-14
Abundances in wt%								
SiO ₂	52.83	47.87	53.99	49.92	49.05	50.67	51.3	52.39
TiO ₂	1.17	0.63	1.35	1.23	0.95	1.46	1.13	1.83
Al ₂ O ₃	14.54	17.04	14.24	17.58	17.16	17.05	17.64	17.02
Fe ₂ O ₃	2.37	1.79	2.92	4.19	2.21	2.98	3.13	2.43
FeO	10.62	9.03	9.9	8	7.79	7.91	6.77	7.12
MnO	0.2	0.18	0.22	0.18	0.16	0.16	0.17	0.16
MgO	4.43	7.07	3.68	3.77	7.51	4.87	5.02	4.07
CaO	9.95	13.24	8.21	11.18	9.73	9.81	9.31	7.75
Na ₂ O	2	1.24	2.91	2.22	2.42	2.73	2.57	4.14
K ₂ O	0.45	0.15	0.62	0.27	0.33	0.78	1.21	0.84
P ₂ O ₅	0.1	0.03	0.16	0.11	0.2	0.29	0.16	0.3
H ₂ O(+)	0.24	0.28	0.56	0.14	0.8	0.41	0.48	1.18
H ₂ O(-)	0.05	0.08	0.11	0.05	0.22	0.06	0.12	0.07
Abundances in mg/kg								
F	108	50	197	70	250	210	300	250

Appendix 2. Continued

	J-1	J-2	J-3	J-5	J-6	J-7	J-13	J-14
Cl	298	100	586	125	90	200	420	100
Br	0.73	0.44	1.66	1.24	0.32	0.68	1.38	0.45
I	0.052	0.029	0.086	0.13	0.084	0.032	0.072	0.095
S	6.95	9.52	11.7	6.98	0.59	1.69	14.2	37.3
B	31	7.4	19	10	2.2	20	18	10
As	3.21	0.68	1.75	1.27	0.21	2	2.83	2.08
	J-15	J-16	J-19	J-20	J-21	J-23	J-26	J-27
Abundances in wt%								
SiO ₂	54.27	52.13	51.82	46.75	48.23	49.28	53.12	36.8
TiO ₂	1.54	1.55	2.27	1.81	1.78	1.82	2.37	2.57
Al ₂ O ₃	16.73	17.18	16.96	14.15	15.21	15.4	14.47	10.63
Fe ₂ O ₃	0.76	1.47	4.4	2.07	2.37	2.72	3.97	4.72
FeO	7.47	6.63	4.18	7.92	7.72	7.15	6.94	9.12
MnO	0.13	0.14	0.15	0.15	0.16	0.15	0.17	0.29
MgO	2.13	4.59	3.05	10.96	7.74	7.83	2.85	8.01
CaO	7.39	8.45	5.96	9.29	8.85	8.33	6.52	15.1
Na ₂ O	3.57	3.77	3.75	2.62	3.07	3.44	4.36	3.46
K ₂ O	0.55	0.83	3.79	1.53	1.81	1.81	1.62	1.67
P ₂ O ₅	0.33	0.24	0.87	0.47	0.45	0.5	0.38	2.23
H ₂ O(+)	5.42	2.12	1.83	0.94	1.6	0.54	2.54	2.52
H ₂ O(-)	0.11	0.28	0.7	0.22	0.32	0.12	0.25	0.28
Abundances in mg/kg								
F	400	210	1200	520	360	390	370	1690
Cl	130	145	10	260	25	40	25	60

	J-28	J-33	J-38	J-39	J-43	J-54	J-55	J-56
Br	0.41	0.5	0.24	0.75	0.16	0.27	0.09	0.26
I	0.14	0.1	0.042	0.02	0.029	0.046	0.070	0.045
S	238	71.5	70	3.54	20.8	17.8	240	730
B	10	11	4.2	5.9	0.5	1.5	9.5	3
As	7.17	1.41	0.54	0.41	0.68	0.59	0.97	1.88
<hr/>								
	J-28	J-33	J-38	J-39	J-43	J-54	J-55	J-56
<hr/>								
Abundances in wt%								
SiO ₂	51.2	56.3	58.21	52.59	63.31	60.01	59.88	50.33
TiO ₂	2.64	0.74	0.76	1.11	0.85	0.71	0.66	2.13
Al ₂ O ₃	14.85	16.7	16.28	17.79	16.27	15.83	16.11	18.71
Fe ₂ O ₃	3.97	2.66	2.84	2.85	1.69	1.92	2.12	3.43
FeO	7.25	5.1	4.6	6.65	4.19	4.82	5	4.23
MnO	0.17	0.13	0.13	0.18	0.18	0.11	0.12	0.13
MgO	3.71	4.03	3.79	4.44	1.48	4.17	3.6	2.88
CaO	7.83	8.49	7.61	8.87	4.32	6.87	6.78	6.77
Na ₂ O	3.88	2.76	3.2	2.69	4.86	3.07	2.9	3.59
K ₂ O	1.16	0.55	0.92	1.23	1.57	1.21	1.73	3.68
P ₂ O ₅	0.5	0.08	0.15	0.19	0.3	0.12	0.14	0.95
H ₂ O(+)	1.26	0.42	1.1	0.54	0.26	0.44	0.63	2.13
H ₂ O(-)	0.5	0.07	0.1	0.06	0.08	0.1	0.12	0.58
Abundances in mg/kg								
F	330	180	200	370	620	240	110	1200
Cl	22	230	620	610	180	350	140	80
Br	0.15	0.83	2.02	1.89	0.6	1.4	1.12	0.18
I	0.096	0.091	0.23	0.15	0.022	0.25	0.26	0.064
S	190	60	3.17	47.2	2.36	60	10.3	80
B	4	22	9.3	14	14	20	34	4.7
As	0.56	3	0.54	3	4.86	3.89	3.06	0.77

Appendix 2. Continued

	J-1	J-2	J-3	J-5	J-6	J-7	J-13	J-14
	J-84	J-88	J-89	J-93	J-95	J-96	J-97	J-98
Abundances in wt%								
SiO ₂	60.73	71.5	54.17	68.89	66.26	64.74	58.87	67.78
TiO ₂	0.81	0.63	0.7	0.66	0.75	0.34	0.9	0.25
Al ₂ O ₃	16.5	13.97	18.89	14.29	15.12	17.22	16.09	16.28
Fe ₂ O ₃	1.89	1.39	2.05	1.66	1.95	2.03	3.21	1.77
FeO	4.95	1.7	5.78	2.52	3.35	1.62	3.81	0.37
MnO	0.14	0.1	0.14	0.11	0.15	0.09	0.22	0.01
MgO	2.57	0.76	3.69	1.13	1.35	1.62	1.44	0.15
CaO	6.17	2.54	9.81	3.41	4.48	4.84	2.99	0.44
Na ₂ O	3.51	4.39	2.82	4.19	4.52	4.3	5.74	5.06
K ₂ O	1.65	2.43	0.67	2.18	0.87	1.69	4.15	5.9
P ₂ O ₅	0.18	0.12	0.14	0.16	0.18	0.17	0.46	0.03
H ₂ O(+)	0.5	0.3	0.7	0.56	0.16	0.21	0.95	0.52
H ₂ O(-)	0.16	0.03	0.1	0.04	0.03	0.05	0.33	0.34
Abundances in mg/kg								
F	340	407	190	504	230	250	750	370
Cl	313	79	180	560	60	140	70	80
Br	1.4	1.08	1.03	2.6	0.18	0.48	0.5	0.2
I	0.032	0.052	0.12	0.13	0.070	0.032	0.26	0.036
S	190	16.4	9.96	70	2.29	4.29	500	22.4
B	15	21	8.7	33	12	13	28	6
As	3.8	3.86	0.99	4.33	2.41	2.49	3.47	0.42
	J-99	J-101	J-103	J-113	J-117	J-118	J-119	J-120

Abundances in wt%								
SiO ₂	60.43	70.22	63.8	75.29	75.84	70.6	70.11	69.98
TiO ₂	0.24	0.39	0.53	0.17	0.12	0.28	0.31	0.11
Al ₂ O ₃	17.4	15.02	17.49	12.81	12.75	14.94	13.77	14.53
Fe ₂ O ₃	3.68	1.6	2.53	0.55	0.53	1.36	2.23	1.95
FeO	2.33	2.2	2.41	0.64	0.3	0.08	0.11	0.67
MnO	0.17	0.16	0.12	0.08	0.06	0.01	0.05	0.09
MgO	0.12	0.86	1.77	0.24	0.11	0.07	0.03	0.08
CaO	0.91	3.49	5.81	1.08	0.7	0.58	0.02	0.17
Na ₂ O	6.81	4.71	3.65	4.36	4.41	4.59	0.18	6.49
K ₂ O	5.37	1	1.27	2.95	3.16	5.94	11.81	4.44
P ₂ O ₅	0.02	0.13	0.16	0.04	0.02	0.04	0.04	0.01
H ₂ O(+)	1.35	0.19	0.5	2.16	2.14	0.5	0.4	0.39
H ₂ O(-)	0.27	0.05	0.15	0.05	0.2	0.1	0.05	0.05
Abundances in mg/kg								
F	240	260	266	247	220	1100	50	600
Cl	7	50	23	590	570	40	20	70
Br	0.12	0.21	0.14	1.42	1.05	0.1	0.15	0.3
I	0.080	0.034	0.056	0.063	0.062	0.026	0.14	0.32
S	0.1	19.9	14.1	7.77	5.65	50	3.03	100
B	4.3	16	7.5	12	16	6	1.7	9.5
As	2.19	2.73	0.52	2.77	1.71	0.65	10.59	1.42
		J-121		J-130		J-131		J-138
Abundances in wt%								
SiO ₂		75.62		75.68		74.53		67.7

Appendix 2. Continued

	J-121	J-130	J-131	J-138
TiO ₂	0.03	0.04	0.01	0.33
Al ₂ O ₃	12.96	13.19	14.85	14.55
Fe ₂ O ₃	0.38	0.26	0.22	0.84
FeO	0.77	0.88	0.94	1.75
MnO	0.06	0.05	0.1	0.06
MgO	0	0.05	0.1	0.24
CaO	0.41	0.59	0.47	0.83
Na ₂ O	3.96	3.88	4.35	4.07
K ₂ O	4.5	4.46	3.66	5.97
P ₂ O ₅	0.02	0.02	0.12	0.04
H ₂ O(+)	1.39	0.68	0.44	3.2
H ₂ O(-)	0.22	0.05	0.05	0.16
Abundances in mg/kg				
F	437	483	485	1000
Cl	794	613	157	650
Br	1.2	1.74	0.27	2.28
I	0.010	0.047	0.025	0.11
S	0.97	2.81	4.08	51.6
B	41	82	20	9.7
As	5.34	10.71	3.18	1.82

REFERENCES

- [1] N. Imai, S. Terashima, S. Itoh, A. Ando, 1994 compilation values for GSJ reference samples, "igneous rock series", *Geochem. J.* 29 (1995) 91–95.
- [2] H.H. Willard, O.B. Winter, Volumetric method for determination of fluorine, *Ind. Eng. Chem. Anal. Ed.* 5 (1933) 7–10.
- [3] B. Buhn, A.H. Rankin, Composition of natural, volatile-rich Na-Ca-REE-Sr carbonatitic fluids trapped in fluid inclusions, *Geochimica et Cosmochimica Acta* 63 (1999) 3781–3797.
- [4] K.E. Aggrey, D.W. Muenow, J.M. Sinton, Volatile abundances in submarine glasses from the North Fiji and Lau back-arc basins, *Geochim. Cosmochim. Acta* 52 (1988) 2501–2506.
- [5] D.W. Muenow, M.R. Perfit, K.E. Aggrey, Abundances of volatiles and genetic relationships among submarine basalts from the Woodlark Basin, southwest Pacific, *Geochim. Cosmochim. Acta* 55 (1991) 2231–2239.
- [6] G.E. Coote, Ion beam analysis of fluorine: its principles and applications, *Nucl. Instr. Meth. B* 66 (1992) 191–204.
- [7] D.R. Taves, Separation of fluoride by rapid diffusion using hexamethyldisiloxane, *Talanta* 15 (1968) 969–974.
- [8] D.R. Taves, Determination of submicromolar concentrations of fluoride in biological samples, *Talanta* 15 (1968) 1015–1023.
- [9] D.R. Taves, Effect of silicone grease on diffusion of fluoride, *Anal. Chem.* 40 (1968) 204–206.
- [10] K. Tsuchiya, T. Imagawa, K. Yamaya, M. Yoshida, Separation of microamounts of fluoride coexisting with large amounts of aluminum and silica by improved trimethylsilylating distillation, *Anal. Chim. Acta* 176 (1985) 151–159.
- [11] K. Anazawa, T. Tomiyasu, H. Sakamoto, Simultaneous determination of fluorine and chlorine in rocks by ion chromatography in combination with alkali fusion and cation-exchange pretreatment, *Anal. Sci.* 17 (2001) 217–219.
- [12] O. Stecher, Fluorine geochemistry in volcanic rock series: examples from Iceland and Jan Mayen, *Geochim. Cosmochim. Acta* 62 (1998) 3117–3130.
- [13] S.M. Straub, G.D. Layne, The systematics of chlorine, fluorine, and water in Izu arc front volcanic rocks: implications for volatile recycling in subduction zones, *Geochim. Cosmochim. Acta* 67 (2003) 4179–4203.
- [14] S.M. Straub, G.D. Layne, C.H. Langmuir, Volcanic Glasses at the Izu Arc Volcanic Front: New Perspectives on Fluid and Sediment Melt Recycling in Subduction Zones. *Geochem. Geophys. Geosyst* 5 (2004) Q01007.
- [15] V.V. Yarmolyuk, V.I. Kovalenko, V.B. Naumov, Geodynamics, flows of volatile components, and their exchange between the mantle and the earth's upper shells, *Geotectonics* 39 (2005) 39–55.
- [16] F. Li, J. Zhu, B. Rao, L. Zhang, Z. Jin, Origin of Li-F-rich granite: evidence from high P-T experiments, *Sci. China, Ser. D: Earth Sci.* 47 (2004) 639–650.
- [17] L.X. Gu, X.Q. Gou, Z.Z. Zhang, C.Z. Wu, J.J. Liao, H. Yang, L. Yin, M.Z. Min, Geochemistry and petrogenesis of a multi-zoned high Rb and F granite in eastern Tianshan, *Acta Petrol. Sinica* 19 (2003) 585–600.
- [18] J. Stix, G.D. Layne, S.N. Williams, Mechanisms of degassing at Nevado del Ruiz volcano, Colombia, *J. Geol. Soc.* 160 (2003) 507–521.
- [19] I.D. Ryabchikov, I.P. Solovova, T. Ntaflou, A. Büchl, P.I. Tikhonenkov, Subalkaline picobasalts and plateau basalts from the Putorana plateau (Siberian continental flood basalt province): II. Melt inclusion chemistry, composition of "primary" magmas and P-T regime at the base of the superplume, *Geochem. Int.* 39 (2001) 432–446.
- [20] D.A.C. Manning, D.L. Hamilton, C.M.B. Henderson, M.J. Dempsey, The probable occurrence of interstitial Al in hydrous, F-bearing and F-free aluminosilicate melts, *Contrib. Mineral Petrol.* 75 (1980) 257–262.

- [21] J.D. Webster, Partitioning of F between H₂O and CO₂ fluids and topaz rhyolite melt: implications for mineralizing magmatic-hydrothermal fluids in F-rich granitic systems, *Contrib. Mineral Petrol.* 104 (1990) 424–438.
- [22] J. Barclay, M.R. Carroll, B.F. Houghton, C.J.N. Wilson, Pre-eruptive volatile content and degassing history of an evolving peralkaline volcano, *J. Volcanol. Geotherm. Res.* 74 (1996) 75–87.
- [23] A.A. Gurenko, H.-U. Schmincke, Geochemistry of sideromelane and felsic glass shards in Pleistocene ash layers at Sites 953, 954, and 956, *Proc. ODP, Sci. Results* 157 (1998) 421–428.
- [24] M. Yoshida, The volatilization of chlorine and fluorine compounds from igneous rocks on heating, *Bull. Chem. Soc. Jpn.* 36 (1963) 773–782.
- [25] M. Yoshida, I. Makino, N. Yonehara, I. Iwasaki, The fractionation of halogen compounds through the process of the volatilization and the sublimation from volcanic rocks on heating, *Bull. Chem. Soc. Jpn.* 38 (1965) 1436–1443.
- [26] K. Anazawa, M. Yoshida, Multivariate analysis of Japanese volcanic rocks: volatile and major elements, *Geochem. J.* 30 (1996) 355–372.
- [27] M. Yoshida, K. Takahashi, N. Yonehara, T. Ozawa, I. Iwasaki, The fluorine, chlorine, bromine, and iodine contents of volcanic rocks in Japan, *Bull. Chem. Soc. Jpn.* 44 (1971) 1844–1850.
- [28] Y. Arikawa, Sulfur contents of volcanic rocks in Japan, *Bull. Chem. Soc. Jpn.* 60 (1987) 885–890.
- [29] Y. Hong, Determination of Ultramicro Amounts of Sulfur in Igneous Rocks, Tokyo Institute of Technology, Tokyo, 1988.
- [30] A. Isozaki, M. Yoshida, S. Utsumi, I. Iwasaki, The boron content of volcanic rocks in Japan, *Nippon Kagaku Kaishi* 1973 (1973) 1896–1904.
- [31] L.H. Ahrens, The lognormal distribution of the elements, *Geochim. Cosmochim. Acta* 5 (1954) 49–73.
- [32] J.C. Davis, *Statistics and Data Analysis in Geology*, Wiley, New York, 1986, pp. 468–574.
- [33] B. Flury, H. Riedwyl, *Multivariate Statistics: A Practical Approach*, Chapman & Hall, London, 1988.
- [34] K. Ishikawa, S. Kanisawa, K. Aoki, Content and behavior of fluorine in Japanese quaternary volcanic rocks and petrogenetic application, *J. Volcanol. Geotherm. Res.* 8 (1980) 161–175.
- [35] C.-F. You, D.A. Butterfield, A.J. Spivack, J.M. Gieskes, T. Gamo, A.J. Campbell, Boron and halide systematics in submarine hydrothermal systems: effects of phase separation and sedimentary contributions, *Earth Planet. Sci. Lett.* 123 (1994) 227–238.
- [36] J.-G. Schilling, M.B. Bergeron, R. Evans, Halogens in the mantle beneath the North Atlantic, *Phil. Trans. R Soc. Lond. A* 297 (1980) 147–178.
- [37] Y. Tatsumi, Migration of fluid phases and genesis of basalt magmas in subduction zones, *J. Geophys. Res.* 94 (1989) 4697–4707.
- [38] N.B. Price, Chemical Diagenesis in Sediments, in: J.P. Riley, (Ed.), *Chemical Oceanography*, Vol. 6, Academic Press, London, 1976, pp. 1–58.
- [39] A.J. Ellis, W.A.J. Mahon, *Geochemistry of the Hydrosphere. Chemistry and Geothermal systems*, Academic Press, Orlando, FL, 1977, p. 137.
- [40] K.H. Wedepohl, The composition of the continental crust, *Geochim. Cosmochim. Acta* 59 (1995) 1217–1232.
- [41] K.H. Wedepohl, Chemical fractionation in the sedimentary environment, In: L.H. Ahrens (Ed.), *Origin and distribution of the elements*, Pergamon Press, Oxford, England, 1968, pp. 1011–1013.
- [42] W.F. McDonough, S.-S. Sun, The composition of the Earth, *Chem. Geol.* 120 (1995) 223–253.

CHAPTER 7

Fluorine Compounds in Gaseous Emissions from Industrial Sources: The Case of Ceramic Industries

Giuliana Bonvicini, Alberto Fregni* and Carlo Palmonari

*Italian Ceramic Centre, Faculty of Engineering, University of Bologna, Via Martelli, 26/A,
40138 Bologna, Italy*

Contents

1. Introduction	226
1.1. Tile production technology	227
1.1.1. Raw material preparation	227
1.1.2. Shaping and drying	228
1.1.3. Traditional firing	228
1.1.4. Glazing and decorating	229
1.1.5. Fast firing	229
2. Environmental impact of the ceramic industry	229
2.1. Fluoride as a pollutant in raw materials for bodies	230
2.2. Firing reactions	231
3. Pollutant abatement	234
3.1. Characteristics of gas stream	235
3.2. Techniques for cleaning fluorine emissions arising in ceramic tile firing stage	236
3.2.1. Dry kiln gas cleaning systems	236
3.2.2. Wet cleaning systems of kiln exhaust gases	238
3.3. Control emission efficiency data	239
4. Methods for emission sampling and analysis of fluorine	240
4.1. Fluorine clay content analysis	240
4.2. Fluorine emission sampling	242
4.3. Fluorine determination	243
4.3.1. Volumetric methods	243
4.3.2. Colorimetric methods	243
4.3.3. The fluoride-specific ion electrode	244
4.3.4. Ion chromatography	244
5. Phytotoxic effects of fluorides	245
References	246

*Corresponding author.

E-mail: fregni@cencerbo.it

Abstract

This chapter assesses fluorine emissions as an atmospheric pollutant that originated from the clay-based raw material used in ceramic industries. After a short review on the production technology of ceramic products, the main features of fluorine emission in firing processes are outlined. It is demonstrated that the emission rate of fluorine increases with the increasing fluorine content in the raw material and the firing temperature. A roundup of methods has been reported for emission sampling and analysis of fluorine content both in gaseous emission and in clay raw materials. The fluorine content of clays on an average is much the same as the one typically found in the Earth's crust, as shown by different studies reported in this work; hence, clays cannot be considered as a major source of fluoride. However, due to the large amount of clays used, the total emission needs to be under control: a detailed review of principal abatement techniques usually used in the ceramic sector is described, in order to underline the different abatement efficiency. A very brief summary of diseases caused in animals and plants by an excess of fluoride in water and atmosphere is also presented.

1. INTRODUCTION

Air pollution can be defined as a result of the introduction of any substance into air in such a way that they modify the salubrity of the atmosphere and cause damage to public health and to private or public property [1]. Air pollution, in its complexity, may be described according to the origin of the emissions, which makes it either a natural phenomenon (volcanoes, forest fires, organic material decomposition from oceans and soil) or an anthropogenic phenomenon (domestic activities, industrial processes, vehicle traffic) [2].

In the recent years, industries have been the subject of many environmental studies on the origin of pollutants. This paper would provide a review of informations concerning fluoride emissions into the atmosphere caused by industrial plants. In nature, fluorine appears only in the combined state in the form of a variety of minerals. Fluorine can hardly be classed as a minor element. Currently, it is placed 13th in order of abundance and it estimated that it comprises 0.065% by weight of the Earth's crust. It is present as a natural component of soil, rocks and minerals such as apatite, cryolite, topaz, micas and hornblendes [3]. On the contrary, F is one of the most aggressive chemical elements of non-metallic character. In the presence of water, it forms hydrofluoric acid which attacks all metallic and non-metallic compounds, and even glass. Only polymers such as Teflon, to some extent, are immune.

The major sources of fluorine compounds in the atmosphere are well-known. The most involved industries and processes are as follows:

1. Primary aluminium production
2. Iron and steel production
3. Clay firing industries
4. Glass industries [4]

This review will underline the role of ceramic industry regarding this problem. The categories involved are tile and brickworks, refractory, pottery and sanitary ware, and cement works.

Even the glass industry is worth mentioning, because it produces glazed and frits used in coating and decoration of some ceramic products. It must be underlined that even if the fluorine pollution is related to the ceramic production in general, in the following chapter the report will pay more attention to the tile industry.

1.1. Tile production technology

The production process of glazed articles [5] is mainly organised according to the following steps: raw material preparation (for glaze and for body), pressing, drying, biscuit firing (double firing), glazing and single firing. The traditional technology is that of double firing (almost into disuse); in the recent years a glazed product has been produced using a simplified process without the biscuit firing as this takes place simultaneously with the glost firing. This technology is that of single firing (Fig. 1).

1.1.1. Raw material preparation

Raw materials are crushed using dry or wet mills. Then in the case of dry grinding, a quantity of finely milled fireclay grog (precalcined clay) and water is added to give the clay workability. In this preparation stage, the process is varied depending on the type of product being made. If a single raw material is used, dry grinding may be sufficient, but for hard and soft body earthenware, many materials are present and wet grinding is necessary. In this case each material has different hardness and crushability, so the hard materials (quartz, feldspar, limestone) are usually ground separately, while the softer materials (clay) are disintegrated in vessels provided with agitators. The two fractions are then put together in a single mixer from which they are pumped into a suitable drier. The latter operation is necessary to reduce the moisture content to suitably low levels for pressing the body in the form of a fine powder. There are two methods for removing the water used in grinding and mixing: filter pressing and spray drying. If a filter press is used, the resulting cakes of materials, still wet, are crumbled, dried and milled to give a powder, which is then remoistened. If a spray dry is used, the clay suspension is introduced in droplet form into a drying tower, dried within seconds and collected at a suitable grain size and moisture content ready for pressing. Fritting of glaze components is carried out in crucible or rotary kilns from which the fused material runs down and is wet ground in suitable porcelain ball mills.

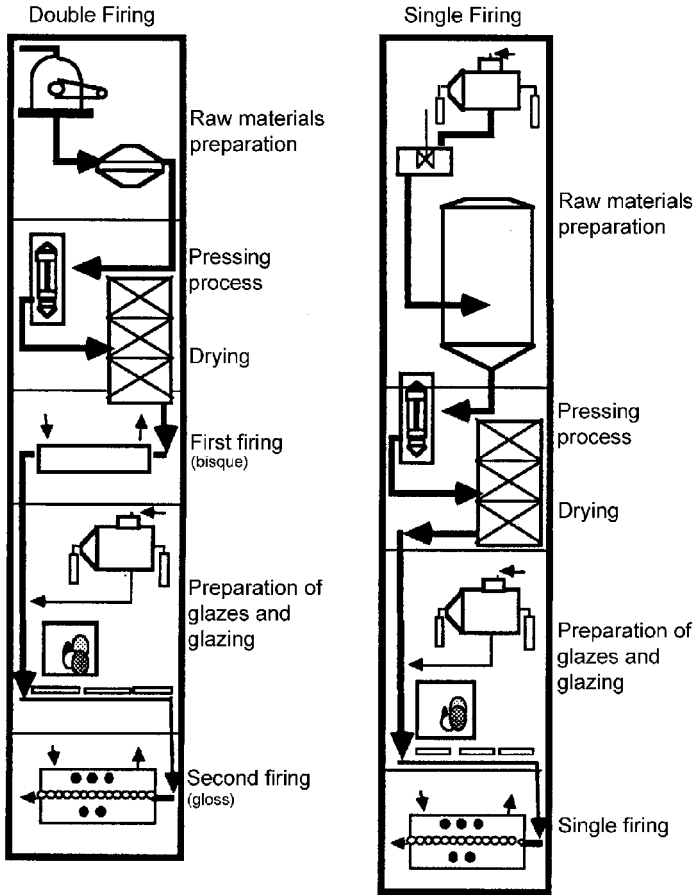


Fig. 1. Schematic diagram of ceramic tile production processes.

1.1.2. Shaping and drying

Shaping is by means of fly wheel or hydraulic presses, the former type being more widely used. A sorting operation is necessary between pressing and drying of the tile (also between biscuit and glost firing and after glost firing). The drying is generally carried out by tunnel dryers, partially or completely supplied by recycled heat from the biscuit kilns.

1.1.3. Traditional firing

Firing is by means of tunnel kilns. The ceramic article achieves its intended consistency through a series of physical and chemical reactions during this stage.

1.1.4. *Glazing and decorating*

Glazing machines with screen-printing equipment and other accessories are used for this process. A second glaze firing serves to fix the glaze and decoration. Tunnel kilns with muffles, roller-hearth kilns are the usual types employed.

1.1.5. *Fast firing*

Fast firing is done in monolayer kilns where the material to be fired is spread out in a single layer rather than stacked as is done with traditional kilns. Fast firing monolayer kilns have considerable technical, economical and operative advantages (better uniformity of firing, flexibility of operation and type of products which can be produced, lower energy consumption); in addition, the air pollution resulting from the use of these kilns is less than that from traditional kilns.

2. ENVIRONMENTAL IMPACT OF THE CERAMIC INDUSTRY

Like all industries involved in the transformation and processing of raw materials, the ceramic industry inevitably has an effect on the surrounding environment. It should be pointed out that a ceramic production plant has less polluting potential than factories in many other industries in that a considerable proportion of pollutants, especially solid particles, can be efficiently filtered at a relatively low cost to avoid their release into the atmosphere. It also recycles a considerable amount of its scraps and de-watered sludge and much of the wastewater. Moreover, because of the changes, which take place during firing, solid residue and sludge are generally rendered inert.

Nevertheless, the problem should certainly not be underestimated, especially where industrialisation leads to a concentration of factories within a given area, inhibiting the effective dispersion of pollutants, an indispensable requisite for partial self-cleaning of the environment. To illustrate just how the tile manufacturing industry has developed, it should be underlined that Italy has the world's highest concentration of ceramic plants and machinery manufactures. In Italy alone 190 such companies employ 7,200 workers and generate total sales of around 1.6 billion Euro/year with 632 millions of m²/year (2000) [6]. The Ceramic District of Sassuolo (provinces of Modena and Reggio Emilia, Italy), where in an area of around 60 km² there are about 250 ceramic factories which produce around 85% of the Italian tile production and about 1/4 of the world's production of ceramic floor and wall tile, is a case in point, and has provided the industry with valuable experience as regards the pollution problems associated with the manufacture of ceramic tiles resulting in enormously improved environmental protection measures.

A ceramic production plant is an “open” system which draws from the environment its supply of raw materials, water, fuels and electricity, and introduces the following back into it: finished products, gaseous emissions, solid and slurry waste, wastewaters, heat energy and noise [7]. In particular, the gaseous effluents emitted into the atmosphere contain various quantities of pollutants, mainly dust particles, lead and fluorine, in addition to other substances (oxides of sulphur, nitrogen, and carbon; boron, zinc, and calcium compounds) in minor negligible quantities of little qualitative importance as regards the contamination of the environment.

The emission can be classified according to temperature and the pollutants contained:

- cold emissions are those which result from the processes of grinding the raw materials, pressing and glazing. They consist of the air aspirated from plants and working areas to limit the diffusion of dust in the work environment. These emissions are at room temperature and contain only particulate matter.
- hot emissions are those which result from drying and firing processes. They are at a temperature, in general, above 70–100°C and also contain gaseous pollutants, especially fluorine compounds that are under investigation in this work: hydrofluoric acid, fluorosilicic acid and silicon tetrafluoride (see following sections).

2.1. Fluoride as a pollutant in raw materials for bodies

Raw materials for ceramic tile production are natural, apart from some used in glazes and colours. They are of two kinds: clay and non-clay raw material. The principal mineral constituents of clays are kaolinite, illite, chlorite and montmorillonite. The mineral compounds of non-clay materials are mainly quartz, feldspar, calcite and dolomite. As far as clay raw materials are concerned, a great variety of types and composition exists. According to the product required, clays may be used singularly if the working properties are adequate, or mixed together. In Italy, much use is made of clays containing carbonates and iron compounds (for porous and coloured products) and clays containing no carbonates (for low-porosity materials: stoneware, clinker). In other cases, mixture of pure kaolinic clays, mainly from abroad, is used (for white body products: soft and hard body earthenware). The non-clay is mixed with clay materials when the clay materials themselves have no natural, non-clay content. The non-clay materials flux to form a ceramic matrix within the body hence altering the compactness. The fluoride content of clays on an average is much the same as the one typically found in the Earth's crust, and hence clays cannot be considered as a source of fluoride in the same way as other fluoride-rich minerals can.

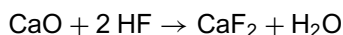
However, due to the large amount of clay used in these industries the total emission needs to be under control, even if prevention-oriented public health policies and technological innovation deserve much of the credit that pollutant emissions have been reduced significantly.

Fluorine may be present in clays as anion F^- within the crystal lattice by replacing the hydroxyl anion OH^- at $Al(OH)_6$ octahedron vertices [8]. This behaviour is linked to the fact that F^- and OH^- are vicariant or isomorphic. It is obvious that the replacement of an ion with another one is influenced in particular by steric bulk: OH^- and F^- have almost the same ionic radius (1.33 vs. 1.36 \AA) [9].

2.2. Firing reactions

The most important release of fluorine in the ceramic process occurs during the firing step because the high temperature causes the collapse of clay mineral structure. On the contrary, due to the low process temperatures involved, emission of gaseous fluorine compounds from the dryer is unlikely. As the heated air used in the dryer is typically drawn from the cooling zone of a tunnel kiln, a possibility exists that fluorides emitted in the kiln-firing zone could be drawn into the dryers, if airflows are balanced incorrectly. Emission tests conducted on a number of brick dryers in Victoria (Australia) have indicated low-fluorine compound emission rates, representing approximately 0.5% of the total fluoride released during the brick-manufacturing process.

Fluorine contained in the crystal lattice of clay (phyllosilicates) is released during firing at around 500°C depending on the kind of minerals and firing process. This phenomenon is catalysed by water vapour which helps in the formation of HF, and can be released along with the exhausted gas or can react with calcium from raw materials according to the following reaction [10]:



CaF_2 at temperature higher than 800°C reacts with water vapour released by the clay body, and the reaction described above changes direction and forms HF again that combines itself with SiO_2 . This last compound reacts with NH_3 produced by the decomposition of organic compounds in forming ammonium fluorosilicate. Later acid gaseous emissions released by combustion products within the kiln react with it followed by the production of HF and SiF_4 [11].

According to this the only emission of fluoride is in the form of gaseous HF and SiF_4 . Other combustion products such as SO_2 , SO_3 , H_2O , CO and CO_2 may be present depending on the type of fuelling, but they are not under investigation in this review. Because of the same considerations, glass is made from fusion

Table 1. List of the principal raw materials with their fluorine content and emission after firing

Raw material	F (%)	Loss of F (%) after firing at 1000°C
Brick clays	0.050–0.066	57–82
Flogopite	1.60	25
Biotite	0.34	23
Muscovite	0.27	68
Apatite	0.58	51.7
Talc	0.25	24
Kaolin	0.026	76.9

of various minerals at around 1500°C, the principal ones being sand, sodium carbonate or sulphate and limestone. Fluorides, present either as impurities in the raw materials or as additives for the production of special glasses, will be emitted at these high temperatures both in gaseous (HF, SiF₄, F₂, BF₃, H₂SiF₆) and in particulate forms (CaF₂, NaF, Na₂SiF₆, PbF₂). The following table makes a list of the principal raw materials with their fluorine content and emission after firing (Table 1):

In quartz and feldspars, fluorine is present in quantities of 0.0002–0.042% [12], up to 0.3% in clays (0.05–0.125% in Italy, 0.04–0.07 in Germany [13,14], 0.05–0.17% in the Ceramic District [15]) and up to 2% and more of micaceous materials; the amount of fluctuations depends on their geological history [16,17]. Fluorine-bearing clays are illitic (0.1–0.33% [18]) and montmorillonite (0.10–0.14% [19])-containing materials, such as mica, muscovite (0–0.4% fluorine) and biotite (1.9–2.3% fluorine) [20]. On the contrary, chaolinitic raw materials contains less fluorine than micaceous clays [21] (0.02–0.05% [22]). However, it should be noted that not all the fluorine contained in the raw materials is released as a result of the firing operation; some of it remains bound in the fired product.

A study about F⁻ release during firing has been carried out on a set of brick raw materials [23]. The content of fluorine has been evaluated both in dried and in attendant fired products. The fluorine release during firing varies from 0 to 83% even if in most of the specimen the value is lower than 40% of the original content. An equation that links fluorine content of clays and fluorine emissions during firing process has not been verified because some factors, such as firing temperature, technical kiln parameter and fluorine retention by kiln refractory framework, have a strong influence on the emission itself. Fluorine emissions also depend on the following factors: the initial F content in the raw material, the particle size distribution, the calcite content, the firing temperature, the time and the heating rate.

Significant differences in fluorine emissions were found as a function of the type of ceramic produced. They were influenced more by the differences in the firing temperatures (higher in the products with low porosity and in those with light-coloured bodies) rather than by the fluorine content of the respective raw materials.

It has been shown that the higher the firing temperature (above the 800°C [24]), the higher is the fluorine release from the clay lattice [25]. The rate of fluoride release from the clay body is maximum between 800 and 1050°C [26,27] on the upward section of the firing cycle, while the body is still open for gas diffusion. As vitrification and shrinkage occur the rate of release diminishes. Dense solid clay product releases less fluoride than perforated shapes, or shapes with a higher surface area. Therefore, bricks with perforations or voids release more fluoride than solid extruded products. Pavers and roof tiles release more fluoride per tonne of product than bricks.

High content in alkaline metals (due to the presence of calcite and dolomite) lowers the fluorine emission because of the reaction between F and Ca. If CaF_2 has time to crystallise regularly, some of the fluoride will remain in this form in the fired body [28]; however, if it is less well crystallised it will dissociate at higher temperatures releasing some of the fluoride. It has been studied that SO_x gases (SO_2 and SO_3) in the kiln atmosphere make the release of F easier because they are chemically stronger and they move F out of its compounds.

Increase in air combustion [29] also helps in the fluorine emission during the firing step (even if at the same time it decreases fluorine concentration in the fumes because of the dilution effect).

Especially significant for fluorine emissions is the influence of firing time [30]. Emissions of fluorine were considerably reduced in going from traditional kilns (with 20–30 h firing cycles for single firing and biscuit firing and 10–15 h for the second firing) to monolayer kilns (with 1–2 h firing cycles for single firing and 0.5–1 h cycles for the second firing).

The longer the firing time, the higher is the fluorine emission (Table 2) [31].

Variations in the concentration of fluorine in the uncontrolled emissions of ceramic floor and wall tile-manufacturing processes are reported in Table 3.

Table 2. Fluorine emission according to the duration of firing

Kiln	Firing time	Tile production m^2/day	F emission g/m^2
Single firing	27 h 12 min	700	7.4
Fast single firing	3 h 55 min	1250	1.9
Glazed firing	8 h	830	3.33
Fast glazed firing	35 min	1910	1.30

Table 3. F concentrations in uncontrolled emissions for different production phases

Production phase	F (mg/Nm ³) Nm ³ : volume at 273,15 K and 1013 hPa
Biscuit firing: combustion gases stack	10–50
Biscuit firing: degassing stack	0–600
Biscuit firing: cooling air stack	0–15
Glost firing: combustion gases stack	8–30
Glost firing: degassing stack	0–80
Single firing: combustion gases stack	10–50
Single firing: degassing stack	0–80
Fritting	0–200

These data are the result of thousands of measurements carried out over 7 years by the Italian Ceramic Centre.

According to the emission of fluorine per each ceramic production step linked to the total ceramic production in the Sassuolo District, the Italian Ceramic Centre estimated the global emission of fluorine in the atmosphere without pollutant control plant as 727 t/year (1978). Usually real emission values are much lower than the estimated values, but they are higher than the limits indicated in the TA Luft – Germany (1986: 5 mg/Nm³ HF), BOE (Atmospheric Protection Normative) – Spain (1975: 2 mg/Nm³ HF) [32] or D.M. rules – Italy (1999: 10 or 5 mg/Nm³ specific for Sassuolo District) [33].

It has been estimated that the global emission purified of fluorine could be around 73 t/year (according to the 90% of emission reduction with purification plants). These results clearly explain the necessity to use purification plants.

3. POLLUTANT ABATEMENT

The environmental impact factors, fluorine emission in particular, from ceramic tile production units, have been studied in Italy since the early 1970s, in the framework of research programmes carried out in close co-operation, over the last three decades, by Centro Ceramico Bologna, the regional environmental protection agency (ARPA) and the ceramic tile industries (and their association, Assopiastrelle, as well).

Facing an environmental legislation developed with the main purpose of achieving the compliance with the existing Environmental Quality Standards (EQS), the Italian ceramic tile industry, due to its quite outstanding dimensional and productive characteristics, was the first and, for a rather long period, the only

Table 4. Fluorine emission upstream the purification plant

Fluorine emission	No purification	CET value	Emilia-Romagna emission standard
mg/Nm ³	15–40	10	5

ceramic tile industry in Europe to develop and adopt techniques for the reduction of environmental impact. Beneficial effects of this policy are documented, at local scale, in the Ceramic District of Sassuolo, where, as already seen, around 85% of the Italian tile production is concentrated in a relatively small area.

The prevention/reduction of air pollution has been pursued, in the ceramic tile sector, through the development and use of pollutant control system and less-polluting processes and technologies (e.g., concerning the firing technology, through the evolution from double firing to single firing, and from slow firing in tunnel kilns to fast firing in single layer roller kiln). In Italy, where since 1980 the ceramic tile factories are subjected to very restrictive regulations, which include limits on pollutant emissions, these new technologies were not sufficient to avoid the adoption of purification technologies for gaseous emissions. Table 4 reports the fluorine emission upstream the purification plant, the emission limit recommended by CET (European Federation of the ceramic tile manufactures) and the emission limit established in the Emilia-Romagna rules [34].

3.1. Characteristics of gas stream

As already said, firing ceramic tile usually takes place in single-deck roller kilns. These kilns exhibit two potential pollutant emission foci; the flue exhaust gas stack and the cooling air intake stack.

The gases arising in the tile heating zone exit through the exhaust stack. These emissions mainly consist of gases produced during the combustion of natural gas as well as gases released during the chemical decomposition that occurs in the body during heat treatment. The hot gases produced in cooling the tiles from peak temperature down to kiln exit temperature leave via the cooling stack. As no chemical reaction takes place during cooling, the stream arising in this stack consists of hot air and no cleaning treatment is required.

The data, reported in Table 5 [35], on the nature and concentrations of the substances present as well as stream characteristics, only refer to the exhaust stack emissions in which pollutants may need to be cleaned. The parameters that were determined to characterise the gas stream, and which are needed for designing a suitable cleaning system, are flow rate (Q), temperature (T) and moisture content (H). Table 6 sets out their variation ranges.

Table 5. Concentration of substances in the exhaust stack

Substance	Variation range	Substance	Variation range
PM (mg/Nm ³)	5–50	Pb (mg/Nm ³)	<0.15
F (mg/Nm ³)	5–40	NO _x (ppm)	15–60
B (mg/Nm ³)	<0.5	SO ₂ (mg/Nm ³)	<10
Cl (mg/Nm ³)	20–90	CO (ppm)	1–15
		CO ₂ (%)	1.5–4

PM, airborne particulate matter.

Table 6. Characteristics of the stream exiting the kiln

Parameter	Variation range	Parameter	Variation range
Q _{dry} (Nm ³ /h)	5000–15,000	H (m ³ water/m ³ total)	0.05–0.10
T (°C)	130–300		

The stream of gases exiting the kiln via the exhaust stack as a result of the firing process is a stream with a low flow rate. The temperature values measured were variable and mainly depended on the type of product being fired and firing curve design in each case. The moisture content of the gases came mainly from the water that formed during combustion, and from the moisture removed from the body and the glaze in the first stage of the firing process.

3.2. Techniques for cleaning fluorine emissions arising in ceramic tile firing stage

The cleaning system to be implemented in a tile firing kiln needs to fulfil a double task: capturing the fluorine in the gas phase and separating the particulate matter suspended in the gases, thus cleaning the gases. Taking into account the data set out in the foregoing sections, the most suitable cleaning systems for cutting back concentrations in firing stage emissions are bag filters, electrostatic precipitators and wet filters. This section describes the specific technical characteristics required by each of these types of cleaning systems to allow using them in this stage.

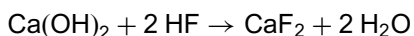
3.2.1. Dry kiln gas cleaning systems

In these systems, the fluorine present in the gas phase is made to react with a solid reagent and the reaction product is separated from the gas stream by a system that separates suspended particulates.

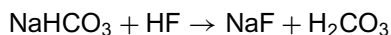
The efficiency of the different reagents used for capturing fluorine in the gas stream depends on many factors, of which the following are particularly to be highlighted:

- Starting fluorine concentration in the gas stream
- Contact time between gases and reagent
- Gas temperature
- Specific surface area of the reagent used
- Level of turbulence reached in the reaction region, etc.

The reagents normally used to capture fluorine are calcium hydroxide ($\text{Ca}(\text{OH})_2$) and sodium bicarbonate (NaHCO_3), which form calcium and sodium fluoride, respectively. If calcium hydroxide is used as a reagent to retain fluorine, the following chemical reaction arises:



According to the literature [36], for an HF concentration in the gas stream of a single-deck roller kiln ($4\text{--}40 \text{ mg/Nm}^3$), the quantity of calcium hydroxide to be used is $6.48 \text{ g Ca}(\text{OH})_2/\text{g HF}$. If sodium bicarbonate is used to retain fluorine, the following chemical reaction arises:



The product that really reacts with HF is sodium carbonate, which forms when sodium bicarbonate loses a water molecule at above 180°C [37]. The sodium carbonate that is thus formed has a high specific surface area and therefore high efficiency in fluorine retention. The quantity of substance that is ultimately produced is the sum of the excess sodium bicarbonate and the sodium fluoride that forms, therefore being $4.20 \text{ g NaHCO}_3/\text{g HF}$ [38].

3.2.1.1. Bag filters

Bag filter design for this emission source must especially take into account the high temperatures of the gases to be treated. The fact will mainly affect bag filter operation and the type of bag to be used. The flue gases from the single-deck roller kiln are drawn to the bag filter. When the flue gases travel to the bag filter, the solid reagent ($\text{Ca}(\text{OH})_2$ or NaHCO_3) is injected into the stream to retain fluorine by a pneumatic spraying system. It is important to add the reagent as far away as possible from the bag filter, to obtain the longest contact time between the gas phase and the solid phase. The bag filter is designed to work at a given temperature, normally below kiln gas exiting temperature. If necessary, these hot gases need to be cooled by bleeding in air at ambient temperature or by using an

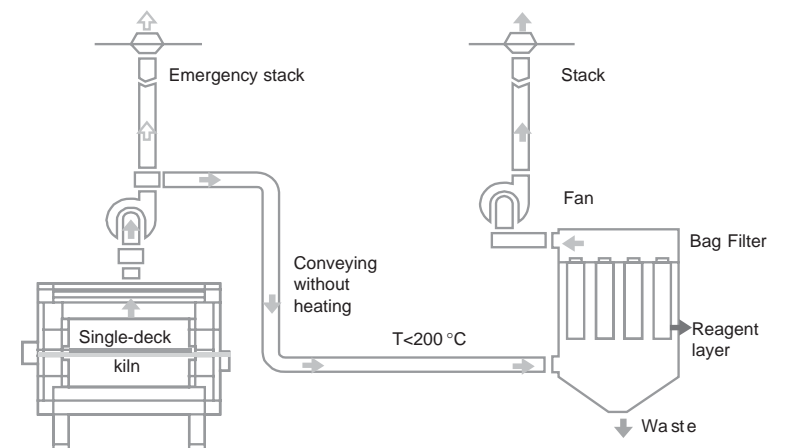


Fig. 2. Scheme of the kiln exhaust gas cleaning system with a bag filter.

air–air heat exchanger. The bag fabric is defined by the temperature of the gases to be treated, and may be of polytetrafluoride ethylene (Teflon or gorotex), aromatic polyamide (tefloned nomex), polyester (dracon), acrylic (dralon T) or polyamide material. A bag filter facility allows achieving fluorine concentrations in the treated stream of less than 5 mg/Nm^3 and suspended dust concentrations of less than 20 mg/Nm^3 . The cleaning efficiency of these systems is estimated at 99% for retention of suspended particulates and 90% for fluorine retention [7,39] (see Fig. 2).

3.2.1.2. Electrostatic precipitator

The flue gases from the single-deck roller kiln are drawn to the electrostatic precipitator. All the aspects relating to the reagents and their use are the same as in cleaning with bag filters.

This cleaning system has the advantage of being able to run at high temperatures, easily exceeding 400°C , so that no cooling of the exhaust flue gases is required prior to cleaning and energy recovery from the clean gases is facilitated [38] (see Fig. 3).

3.2.2. Wet cleaning systems of kiln exhaust gases

In a wet gas scrubbing facility the following points should be taken into consideration:

- The need to work at temperatures of $70\text{--}80^\circ\text{C}$ can determine whether to use heat exchangers, as the gases exit the stack at temperatures of around 200°C .

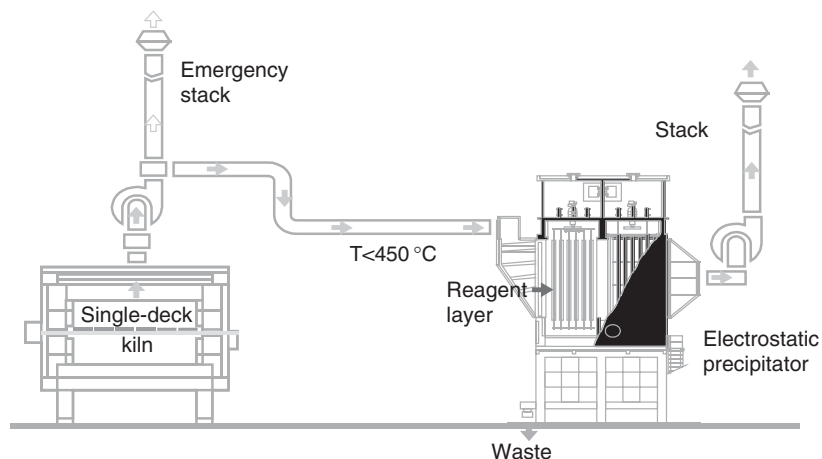


Fig. 3. Scheme of the kiln exhaust gas cleaning system with an electrostatic precipitator.

- The equipment needs to be built with materials and systems that are corrosion-proof, as the gas pollutants on entering the liquid phase usually form a corrosive medium. To counteract this effect, in some systems pH of water is monitored and reagents are added to neutralise and/or enhance the scrubber's yield for specific pollutants.

In particulate removal, to obtain suitable yields high-speed Venturi systems should be implemented.

As in dry gas cleaning, the system used depends on the reagent employed to capture fluorine, i.e., whether the substances in the water are sodium or calcium compounds. In this case, sodium hydroxide and sodium carbonate are employed as sodium compounds, although sodium compounds of a deflocculating nature could be used for the body slip, such as sodium metasilicate and sodium tripolyphosphate (see Fig. 4).

3.3. Control emission efficiency data

Since the early 1980s in Italy only bag filter facilities are used for fluorine pollution control; therefore, in this paragraph data about this technique are reported. The following table reports the emission factors (E.F.) for the F compounds relative to the various manufacturing operations, with and without control. They are reported in terms of 1 m² of ceramic tile produced with the exception of the data relative to the production of frit, where the data are referred to 1 kg of frit produced. The emission factor (see Table 7) defines the amount of pollutant

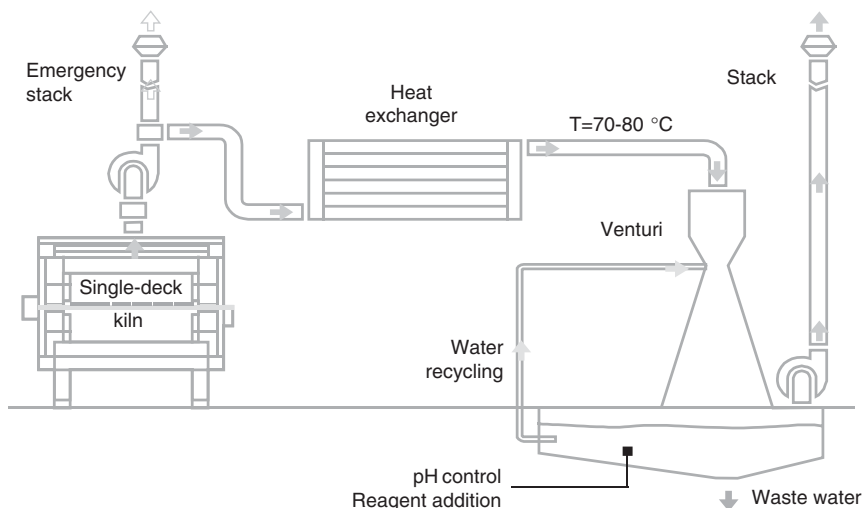


Fig. 4. Scheme of the kiln exhaust gas cleaning system with a wet scrubbing Venturi-type facility.

that generally is emitted into the atmosphere from a specific production process [40]. Generally, the emission factor is expressed in terms of weight of the pollutant emitted with respect to the weight of the product or raw material employed, or other similar parameters suitably representative of the production sector involved.

Overall emission factors for the various types of production are given in Table 8; these values are the sum of the emission factors for the individual manufacturing operations.

In comparison with other industries the ceramic floor and wall tile industry is relatively clean. However, it must not be forgotten that before control systems were generally adopted, quite serious environmental problems were found. This was especially true in areas with a high concentration of ceramic factories such as the ceramic district around Sassuolo.

4. METHODS FOR EMISSION SAMPLING AND ANALYSIS OF FLUORINE

4.1. Fluorine clay content analysis

Different methods of analysis exist. Usually the most appreciated technique for evaluating the fluorine contents in clayey and in ceramic products was based on sample alkaline fusion, followed by distillation in steam flow [41]. A small amount of sample was fused with a mix of Na_2CO_3 and K_2CO_3 , cooled and distilled at

Table 7. Emission factor (E.F.) data for different firing processes

Production phase	Specific flow rate (Nm ³ /m ²)	E.F. uncontrolled (g/m ²)	E.F. controlled (g/m ²)
Biscuit firing: high-porosity ware	200	1.4	0.2
Biscuit firing: medium-porosity ware	200	2.6	0.3
Biscuit firing: coloured low-porosity ware	200	3.2	0.4
Biscuit firing: light colour low-porosity ware	200	8.5	0.7
Glost firing: slow	290	1.0	0.2
Glost firing: fast	100	0.6	0.1
Single firing: coloured low-porosity ware	290	3.2	0.4
Single firing: light-coloured low-porosity ware	290	8.5	0.7
Single firing: coloured low-porosity ware	290	1.0	0.2
Single firing: light-coloured low-porosity ware	290	2.5	0.3
Fritting (refers to 1 kg of frit)	9	0.8	0.03

Table 8. Total emission factors, uncontrolled and controlled, for different production technologies

Production technology	Total E.F. (g/m ²) uncontrolled	Total E.F. (g/m ²) controlled
Double firing	2.4–9.5	0.4–0.9
Traditional single firing	3.2–8.5	0.4–0.7
Fast single firing	1.0–2.5	0.2–0.3

160°C with water and H₂SO₄. The collected solution was analysed with the specific ion electrode (S.I.E., see Section 4.3.3 below).

Since the late 1990s new techniques were introduced to improve the velocity of fluorine determination. X-ray emission spectra induced by an electron beam

(electron probe microanalysis, EPMA), X-ray (X-ray fluorescence spectroscopy, XRF or X-ray photoelectron spectroscopy, XPS [42]) or ion beam (particle-induced X-ray emission, PIXE) have been applied to qualitative and quantitative analyses for solid samples [43]. It is based on the emission of electromagnetic radiations from the inner electron levels of the atoms which are characteristic per each element. Usually these techniques are preferred to ion-selective electrodes because the former provides faster and more reliable F measurement. X-ray diffraction or XRD [44,45] is used as well. This analysis is not destructive and is carried out directly on a powder sample, but the content of fluorine is evaluated usually by Retveld and the error is quite considerable.

In any case, the fusion of the sample followed by distillation is still the best available technique for determining the fluorine content in raw materials.

4.2. Fluorine emission sampling

Fluorine sampling is done with the sucked emission bubbling in a water solution of KOH [46,47]. The typical sampling apparatus [48,49] utilises a probe, two bubbling tubes in line, pump, flow-meter, thermometer and counter. The apparatus is simplified for the ceramic plants because no filter is needed: fluorine emission in the ceramic chimneys is for the most part just in the gaseous form. Furthermore, no heating system is required because in ceramic plants the emissions under analysis are already hot. Each bubbling tube contains around 150 cm³ of a 0.05 N KOH water solution. The ideal gas flow, according to a study carried out by Centro Ceramico, has been estimated within an interval of 1.5–2.1 per min. This value, which is quite low, guarantees an optimal contact between gas and absorbing solution. The total collected volume is around 100 L [50–52]. As said above, the main problem about collecting fluorine emission is due to the extremely reactivity of this element and of its compounds. For this reason, it is necessary to use fluorine attack-resistant materials or devices that are able to capture all the fluorine content without leaving an amount of fluorine itself to be stuck in the system framework.

It has to be underlined that fluorine can be in fumes as gas or in the particulate form; consequently, a sampling under isocinetic conditions could be appropriate. However, the results have shown that in the most part of situations there are no significative differences between isocinetic and non-isocinetic data. To set up the sampler the aspects described above have to be considered. The probe has to be built with Teflon or quartz: Teflon does not react with fluorine compounds; on the contrary, quartz, if reacts with fluorine, gives SiF_6^{2-} and SiF_4 , gaseous compounds that are sampled by adsorbing solution without any losses. It is quite easy to realise isocinetic probes with Teflon, but they cannot be used above

200–220°C. On the contrary, quartz has no problems with high temperature, but it is a fragile, hardly workable and expensive material, so it is not used in building this kind of probes.

As a consequence of these considerations Centro Ceramico uses Teflon probes under 220°C and quartz probe and non-isocinetetic conditions in all other cases. Furthermore, Centro Ceramico carried out a study on the bubbling framework. It showed that bubbling tubes work better if a plate or a porous septum is put at the bottom because they permit to smash the gas flow and to improve the contact efficiency between gas and adsorbing solution [12].

4.3. Fluorine determination

After sampling, the adsorbing solution is quantitatively moved into a polyethylene bottle, mixing the content of both bubbling tubes and the washing water collected by the probe tube [53]. The principal methods used for fluoride determination on samples such as these involve volumetric or colorimetric determinations or the use of fluoride-specific ion electrode [54]. Since 2000 Italian rules introduced a new technique [55]: ion chromatography.

4.3.1. Volumetric methods

The most commonly used titrants were the thorium and lanthanum nitrates, and the endpoints were usually determined from the colour change of an indicator dye such as alizarin red-S [56], used for a wide range of concentration (0.005–10.0 mg), or Erichrome cyanine R [57], though other methods of detecting the end point, such as fluoride ion electrode, fluorescing indicators and conductometry and spectrophotometry, have been used. Interferences could occur with ions such as phosphate, sulphates, oxalates, nitrates and peroxides, sulphides and metals such as aluminium or silicon. In the presence of a significant amount of these species a double distillation might be required.

4.3.2. Colorimetric methods

These include the aluminium–Erichrome cyanine R method, the thorium–thoran method [58], the lanthanum–alizarin method [59,60] and the zirconium–SPADNS method [61]. The typical range of this latter procedure is 0.1–1.4 µg/ml of fluoride [62], so some prior knowledge of the concentration range to be expected was needed to use the correct number of dilutions on the sample. This method was one of the two procedures recommended by EPA: Method 13 [63,64], the other was S.I.E. which will be discussed in the next section.

4.3.3. *The fluoride-specific ion electrode*

The combination fluoride electrode measures free fluoride ions in aqueous solutions [65].

The electrode consists of a sensing element bonded into an epoxy body. When the sensing element is in contact with a solution containing fluoride ions, an electrode potential develops across the sensing element. This potential, which depends on the level of fluoride ions in solution according to the Nerst equation, is measured against a constant reference potential with a digital pH /mV meter or specific ion meter.

This electrode was capable of selectively measuring fluoride activity in solution over a wide range of fluoride concentrations that can be measured in any convenient concentration unit. To measure a large number of samples a calibration curve has to be performed with a series of standards (sample with known fluorine concentration). The concentration of the samples is determined by comparison to the standards. ISA is added to all solutions to ensure that samples and standards have similar ionic strength. TISAB (total ionic strength adjuster buffer) is added to samples and standards as well, so the background ionic strength is high, fluoride is decomplexed, and the pH of the solution is adjusted and hydroxyl ion interferences are eliminated. Moreover, ISEs are highly sensitive to sample composition (particularly to the calcium content) and require a stable solution, which is difficult to obtain.

4.3.4. *Ion chromatography*

The term chromatography is the general name for a wide range of physico-chemical separation processes in which the components to be separated are distributed between a stationary and a mobile phase [66,67]. To analyse F⁻ (anion) in a solution, the ion liquid (both stationary and mobile phase are liquid) chromatography is used. The separations occur by ion exchange on stationary phase that for every ion is characterised by corresponding ion exchange equilibrium. The various ionic components of a sample can thus be separated on the basis of their different affinities for the stationary phase of the ion exchanger (generally made with organic materials based on synthetic resins). The chromatogram (the elution curve that gives signal versus time) is the result of the whole chromatographic system. From that it is possible to figure out the retention time (time needed by an injected substance until its concentration maximum appears at the end of the separation system) and other chromatographic parameters, such as the peak area, that is directly proportional to the amount of substance. The peak area of an unknown sample is compared to those of standard solutions plotted in a calibration curve to calculate the ion concentration.

5. PHYTOTOXIC EFFECTS OF FLUORIDES

Fluorine and many fluorides are considered extremely harmful for both people and plants. These effects will be presented in detail in this volume in Chapter 7 by A.W. Davison and L.H. Weinstein. Gaseous compounds such as hydrogen fluoride and silicon tetrafluoride probably are mainly responsible for fluoride injury to vegetation. Even many soluble salts, that is sodium and/or potassium fluorides, are extremely poisonous; on the contrary, particulate materials such as calcium fluoride and cryolite dust are deposited on leaf surfaces where they have little effect on the plant and are easily washed off by rain. It has to be underlined that large sensitivity of various species among the species of the various cultivars is frequently reported [68–70]. Different plant species differ greatly in their sensitivity or susceptibility to fluoride. Extremely sensitive plants, such as apricot, peach, tulip, young pine needle and certain varieties of gladiolus, may be marked by exposure to hydrogen fluoride concentration below 0.1 ppb, while most species will show no effects from several times as much fluoride [71], such as tomato, celery, cucumber, cauliflower and old pine needles. Fluoride pollutants have effects both via root uptake and/or via direct foliar absorption [72–74]. There are a lot of parameters that may influence the sensitivity of the plant to fluoride injury: the concentration and duration of exposure, the time of the year when plants were exposed, the soil moisture regime, the form of fluoride present, the nutrition status of the plant, age of tissues, the general plant vigour and genetic sensitivity. The characteristic symptoms are visible in the leaf, showing tip (“tip burn”) and marginal necrosis, separated from the healthy, unaffected tissues by a very sharply marked reddish-brown line [75]. In general, it may be excluded that the absorbed fluorine does not migrate into other parts of the plant, such as flowers, roots and fruits [76], but some exceptions exist in peach, apricot, apple and grape plants.

On the contrary, fluorine amount absorbed from the atmosphere by cattle is generally negligible (less than 1% of fluorine present) in comparison with gastroenteric absorption [77]. It is clear that fluorine injuries on livestock and human beings are related to the fluorine ingested during nutrition; consequently, the most important fluorine emission in food chain is due to forage first and then water. Chronic ingestion of fluoride-rich fodder and water in endemic areas leads to the development of musculoskeletal disease [78], from dental lesions to pathological changes of bones, a chronic disease known as fluorosis [79]. Studies on livestock reported lesion in the teeth and skeleton, stiffness and inflamed leg joints, dental fluorosis and bone deformation. The degree to which inorganic fluoride can induce skeletal changes varies considerably among the various animal species. Cattle are the most sensitive to skeletal fluorosis, followed by sheep, horses, pigs, rabbits, rats and turkeys [80]. The sensitivity of cattle is attributed to their negative calcium balance, which is particularly noticeable in lactating cattle after

calving; another contributing factor is the length of time for which the bolus remains in the stomach of ruminants. Since almost the total amount of fluoride is concentrated in the skeleton it seems that the concentration in meat and milk are not influenced by animal diet.

As with animals, mottling of the teeth is the first sign of exposure to fluoride [81]. The phases of human skeletal fluorosis are quite similar to those mentioned above: sporadic pain, stiffness of joints and osteosclerosis of pelvis and vertebral column representing the first stage. These are followed by chronic joint pain, arthritic symptom and slight calcification of ligaments, increased osteosclerosis bones with/without osteoporosis of long bones. The last stage is characterised by the limitation of joint movement, calcification of ligament/neck and vertebral column, crippling deformity of spine and major joints, muscle wasting and neurological defects/compression of spinal cord.

Although approximately 50% of ingested fluoride is cleared by the kidneys, it is estimated that fluorosis occurs after 10–20 years of daily exposure of 10–25 mg/day [82]. More information on the effect of fluoride on the environment can be obtained from Refs. [83,84].

REFERENCES

- [1] D.Lg.vo 13 Luglio 1966, no. 615; G.U.no. 201 13 August 1966, Provvedimento contro l'inquinamento atmosferico, art. 1 (Italian rule).
- [2] P. Mazzali, *Inquinamento atmosferico-origine, prevenzione, controllo*, Pitagora Editrice Bologna, 1989.
- [3] E. Haselhoff, G. Bredemann, W. Haselhoff, *Entstehung and Beurteilung von Rauchshäden*, Verlagsbuchhandlung Gebulder Berntreger, Berlin, 1932.
- [4] K. Macken, M. Reilly, "Critical study of measurement methods for fluoride emissions to the atmosphere used in the main fluoride emitting industries". A study made for commission of the European Communities: Environment and Consumer Protection Service-Final report, Ireland, July 1980.
- [5] C. Palmonari, G. Timellini, Pollutant emission factors for the ceramic floor and wall tile industry, *APCA* 32 (10) (1982) 1095–1100.
- [6] *Applied Ceramic Technology*, Volume II- Sacmi (2002).
- [7] G. Busani, C. Palmonari, G. Timellini, *Piastrelle ceramiche e Ambiente*, Edicer, 1995.
- [8] *Interventi contro l'inquinamento atmosferico da industrie ceramiche*, no. 18, Dip. Ambiente Territorio e Trasporti Regione Emilia Romagna, 1980.
- [9] G. Carobbi, "Trattato di mineralogia" Primo volume. UTET Sansoni Edizioni Scientifiche spa, Firenze, 1971.
- [10] S.G. Bayer, C. Wong, R.T. Yang, Kinetics of the reaction between HF and CaO for fluoride emission control, *Environ. Sci. Technol.* 17 (1983) 84–88.
- [11] Problems of lead and fluorine air pollution from industrial sources, Proceedings of the international seminar, January 1978.
- [12] C. Palmonari, *Inquinamento atmosferico da industrie ceramiche. Studio di un comprensorio: Sassuolo. Capitolo 2: Materie Prime*, pp. 16–21. Centro Ceramico Bologna, 1978.
- [13] G. Garuti, Il contenuto in Fluoro di alcune argille di uso ceramico della provincia di Mo e RE, *Ceramurgia* IV 3 (1974) 170–175.

- [14] F. Keil, F. Gille F., Zerstörung eines ringofen schornsteins durch fluorhaltige rauchgase, TIZ (Ton Industrie Zeitung) 17/18, 226 (1950).
- [15] E. Schmidt, Verminderung luftunreinigender fluor-emissionen durch kalkhydratpulver, Ziegelindustrie 3 (1972) 120.
- [16] P. Hermann, Zur chemischen analyse geringer fluorgehalte in festoffen und bei emissions-messungen, Ziegelindustrie 4 (1975) 142.
- [17] G. Routschka, A. Majidic, Fluoride emission in the kiln firing of refractory clays to chamotte (grog), Ziegelindustrie Int. 1 (1978) 6.
- [18] G. Routschka, Ch. Buttgerit, U. Berger, Der gehalt an fluor in feuerfesten tonen und schamotte und die beeinflussung der fluorabgabe beim brand der schamotteerzeugnisse, Sprechsaal 103 (1970) 901.
- [19] K. Bergman, F. Trojer, Ursachen der fluoremissionen bei tunnelöfen in ziegeleien und die möglichkeit ihrer unterbindung, Ziegelindustrie 5 (1972) 234.
- [20] W. Strohenger, Zur Fluorproblematik in der Ziegelindustrie, Ziegelindustrie Int 2 (1983) 67–72.
- [21] R. Gratz, Möglichkeiten zur beeinflussung der fluor.emissionen und erkenntnisse aus kontinuierlichen fluor-messungen im rauchgas, Ziegelindustrie 4 (1975) 130.
- [22] F. Fröhlich, Bestimmung kleiner fluorgehalte in tonen, D.K.G. Ber. 10 (1963) 567.
- [23] B. Fabbri, M. Dondi, Caratteristiche e difetti del laterizio, Faenza Editrice, 1995.
- [24] H. Wilson, L.D. Johnson, Characterization of air pollutants emitted from brick plant kilns. Am. Cer. Soc. Bull. 54 (1975) 990.
- [25] G. Troll, A. Farzaneh, Fluorine loss in production of bricks and comparison with the loss in fluorine-bearing materials, Interceram 4 (1978) 400.
- [26] Environmental guidelines for the fired clay building products industry, State Government of Victoria, 1998.
- [27] P. Mazzali, G. Fogliani, L. Orlandi, G. Busani, Effetto della temperatura e del contenuto di calcio sulla cessione di fluoro nella cottura di piastrelle ceramiche, 4 Simposio Internazionale della Ceramica, Modena, October 1978.
- [28] G. De Negri, Emissione di fluoro da argille del Comprensorio di Sassuolo durante un processo industriale di cottura. Atti Sem. Int. "problemi da inquinamento per piombo e fluoro," Ed. Centro Ceramico Bologna, 1978.
- [29] E. Schmidt, Erfahrungen mit Massnahmen zur Verminderung der emission luftunreinigender stoffe, Ziegelindustrie 9 (1973) 325.
- [30] W.H. Holmes, The effect of fluorine on pottery bodies, Trans. J. Brit. Ceram. Soc. 72 (1) (1973) 25.
- [31] C. Palmonari, Inquinamento atmosferico da industrie ceramiche. Studio di un comprensorio: Sassuolo, Capitolo 3: Ciclo tecnologico dei prodotti ceramici, pp. 27–33. Centro Ceramico Bologna, 1978.
- [32] E. Galán, I. González, B. Fabbri, Estimation of fluorine and chlorine emissions from Spanish structural ceramic industries. The case study of the Bailén area, Southern Spain. Atmos. Environ. 36 (2002) 5289–5298.
- [33] D.m. 12 luglio 1990; G.U. no. 176, General series, part 1, supplement 051 30 July 1990, "Linea guida per il contenimento delle emissioni inquinanti degli impianti industriali e la fissazione dei valori minimi di emissione" (Italian rule).
- [34] C. Palmonari, G. Timellini, Impatto ambientale dell'industria delle piastrelle ceramiche. Nuova modalità di gestione in Europa, Ceramicaacta 12 (4) (2000) 16–35.
- [35] J.E. Enrique Navarro, Integrated pollution prevention and control in the ceramic tile industry. Best available techniques (BAT), V World congress on ceramic tiles quality. Qualicer'98 proceeding, pp. 89–117.
- [36] P. Mazzali, G. Fogliani, L. Orlandi, G. Busani, Effetto della temperatura e del contenuto di calcio e magnesio sulla cessione di fluoro nella cottura delle piastrelle ceramiche, La Ceramica 33 (2) (1980) 1.
- [37] NEUTREC Process. E.P. (European Patent) 0603218 (29/1/97): Global solution to fluegascleaning with sodiumcarbonate, Solvay.

- [38] R. Vicent, J. Aranguren, E. Monfort, Acid emission cleaning system with sodium bicarbonate for ceramic tile kilns. V. World Congress on Ceramic Tile Quality. Qualicer, Castellón, March 1998.
- [39] A. Blasco, A. Escardino, G. Butani, E. Monfort, Tratamiento de emsiones gaseosas, efluentes líquidos and residuos de la industria cerámica. Ed. AICE-ITC. ISBN:84-604-1114-1. Castellón, Spain, 1992.
- [40] P. Mazzali, La rilevazione di inquinanti non tradizionali nelle emissioni gassose dei processi di cottura di piastrelle ceramiche, *Cer. Acta* 6 (6) (1994) 6–15.
- [41] H. Ackermann, Fluorine determination in minerals, rocks and raw materials, *Inter-ceram* 4 (1978) 404.
- [42] K. Cheng, S. Zhang, W. Weng, The F content in sol-gel derived FHA coatings: an XPS study, *Surface Coatings Technol.* 198 (2005) 237–241.
- [43] S. Nishibu, S. Yonezawa, M. Takashima, Chemical state analysis of fluorine in various compounds using X-ray fluorescence spectra, *J. Fluorine Chem.* 126 (2005) 1048–1053.
- [44] S.M. Barinov, L.I. Shvorneva, D. Ferro, I.V. Fadeeva, S.V. Tumanov, Solid solution formation at the sintering of hydroxyapatite-fluorapatite ceramics, *Sci. Technol. Adv. Mater.* 5 (2005) 537–541.
- [45] K.T. Stanton, R.G. Hill, Crystallisation in apatite-mullite glass-ceramics as a function of fluorine content, *J. Crystal Growth* 275 (2005) 2061–2068.
- [46] European Aluminum Association, Guidelines for a method for the determination of fluoride emission values, 1974.
- [47] R.A. Powell, M.C. Stokes, A method for the continuous on-site measurement of fluorides in stack gases and emissions for period of up to five hours, *Atm. Env.* 7 (1973) 169–176.
- [48] G.H. Farrah *et al.*, Source sampling for fluoride Emissions from Aluminum, Steel and Phosphate production plants: a state of the art report, *Health Lab. Sci.* 11 (1974) 354–359.
- [49] O. Bjørseth, A reference method for measuring fluoride emission from Aluminum smelters, Sintef Report no. STF21 A73055, 1974.
- [50] Manuale Unichim no. 122, Misura alle emissioni, Parte II, Ed. Unichim (Italian Standard Institute), Milano, 1989.
- [51] Metodo Unichim no. 588, Determinazione dei fluoruri gassosi e dei fluoruri particellari, Metodo potenziometrico (EM/14) Ed. Unichim, Milano, 1989.
- [52] Metodo Unichim no. 620, Determinazione contemporanea dei fluoruri gassosi e dei fluoruri particellari, Metodo potenziometrico (EM/15) Ed. Unichim, Milano, 1989.
- [53] F.N. Howell, Standard methods of chemical analysis. Volume one – the Element, D. Van Nostrand Company, Inc., 1962.
- [54] F.M. Robinson, G.I. Gruber, W.O. Lusk, M.J. Santy, Engineering and cost effectiveness study of fluoride emission control. EPA (U.S. Environmental protection Agency) Report no. SN 16893.00, January 1972.
- [55] D.M. 25 Agosto 2000, Supplemento G.U. 23 Settembre 2000, no. 223. Aggiornamento dei metodi di campionamento, analisi e valutazione degli inquinanti (Italian rule).
- [56] ASTM (American Society for Testing Materials), Method for inorganic fluoride in the atmosphere. D1606-60, 447-457, Part 23, Book of ASTM Standards, 1968.
- [57] H.H. Willard, C.A. Horton, Indicators for tritration of fluoride with thorium, *Anal. Chem.* 22 (1950) 1190.
- [58] A.D. Little, Inc. Development of methods for sampling and analysis of particulate and gaseous fluorides from stationary sources, Report for EPA, 1972.
- [59] VDI (Association of German engineers)-Kommission reinhaltung der Luft, Gaseous emission measurement. Measurement of gaseous fluorine compounds. Adsorption method, VDI (Association of german engineers) 2470, October 1975.

- [60] VDI (Association of German engineers)-Kommission Reinhaltung der Luft, Auswurfbegrenzung, aluminium oxide winnung und aluminium schmelzflußelektronlyse, VDI 2286, March 1974.
- [61] W.H. Wharton, *Anal. Chem.* 34 (1962) 1296–1298.
- [62] R.S. Danchik, R.C. Obbink, G.F. Lenz, *Light Met. (New York)* 2 (1977) 381–397.
- [63] EPA, Standards of performance for new stationary sources (Primary Aluminium Reduction Plants), *Federal Register* 41 (26 January) (1976) .
- [64] EPA, Standards of performance for new stationary sources (Primary Fertilizer Plants), *Federal Register* 40 (6 August) (1975) .
- [65] ASTM, Standard Test Method for fluoride ion in water, D 1179-72:Test method B: Ion Selective Electrode. *Book of ASTM Standards*, 2004.
- [66] H. Schäfer, M. Läubli, R. Dörig, *Ion Chromatography*, Metrohm monography, 2003.
- [67] D.C. Harris, *Chimica analitica quantitativa*, Ed. Zanichelli, 1994.
- [68] R. Baroni Fornasiero, *Phytotoxic effects of fluorides*, *Plant Science* 161 (2001) 979–985.
- [69] A.C. Posthumus, Higher plants as indicators and accumulators of gaseous air pollution, *Env. Monit. Assess.* 3 (1982) 263–272.
- [70] G. Scholl, Grundlagen des verfahrens der standardisierten graskultur zur messung der wirkdosis von luftverunreinigungen, *VDI-Berichte* 609 (1987) 287–299.
- [71] M. Treshow, M.R. Pack, *Recognition of air pollution injury to vegetation: a pictorial atlas*, Air Pollution Control Association, Pittsburgh, PA, 1970.
- [72] W.H. MacIntire, S.H. Winterberg, J.G. Thompson, B.H. Hatcher, Fluoride content of plants, *Ind. Eng. Chem.* 34 (1942) 1469–1479.
- [73] M.D. Thomas, R.H. Hendricks, Effects of air pollution on plants, in: P.L. Magil, F.R. Holden, C. Ackley (Eds.), *Air Pollution Handbook Section 9*, McGraw-Hill, New York, 1956, pp. 9-1–9-44.
- [74] D.F. Adams, H.G. Applegate, J.W. Hendrix, Relationship among exposure periods, foliar burn and fluorine content of plants exposed to hydrogen fluoride, *J. Agri. Food Chem.* 5 (1957) 108–116.
- [75] L.H. Weinstein, R. Halscher-Herman, Physiological responses of plants to fluorine in: *Effects of gaseous air pollutants in agriculture and horticulture*, Butterworths, London, 1982, pp. 139–167.
- [76] L. De Cormis, J. Bonte, J. Cantuel, Sur les teneurs en fluor de la vigne et du raisin au voisinage d'une usine de production d'aluminium, *Pollution Atmosph.* 77 (1978) 1–16.
- [77] A. Canuti, I riflessi dell'inquinamento da fluoro sulla catena alimentare, *Industria Alimentari* 99 (1973) .
- [78] O.M. Radostitis, D.C. Blood, C.C. Gay, *Veterinary medicine – A text book of disease of cattle, sheep, pigs, goats and horses*, Bailliere Tindall/ELBS, London, 1994, pp. 1489–1493.
- [79] J.W. Suatie, Effects of inorganic fluorides on animals, *J. Air Pollut. Control Ass.* 14 (1964) 461–464.
- [80] K. Bronsch, N. Grieser, *Berliner und Muenchener tieraertliche Wochenschrift* 20 (1964) 401.
- [81] R. Wood, Fluorine as pollutant, *Trans. J. Br. Cerm. Soc.* 4 (72) (1973) 35–37.
- [82] <http://www.fluoridation.com>, Human skeletal fluorosis.
- [83] L.H. Weinstein, A.W. Davison, *Fluorides in the Environment: Effects on Plants and Animals*, CABI, Wallingford, UK, 2002.
- [84] A.W. Davison, L.H. Weinstein, this volume, Chapter 7, Some problems relating to fluorides in the environment: effects on plants and animals.

This page intentionally left blank

CHAPTER 8

Some Problems Relating to Fluorides in the Environment: Effects on Plants and Animals

Alan W. Davison^{1,*} and Leonard H. Weinstein²

¹*School of Biology, King George VI Building, University of Newcastle, Newcastle upon Tyne, NE1 7RU England*

²*Boyce Thompson Institute, Cornell University, Tower Road, Ithaca, New York 14850, USA*

Contents

1. Introduction	251
2. Questions relating to inorganic fluoride in soil	252
3. Is fluoride lost from plants?	258
4. Problems classifying plant species sensitivity	264
5. Problems estimating effects of fluoride on plant growth and yield	268
6. How significant are pollutant interactions?	276
7. How important are effects of HF on fertilization and seed set?	281
8. What do we know about fluoride and insects?	283
9. The increasing importance of organofluorine compounds to animals	286
References	291

Abstract

Several aspects of fluorides in the environment have been researched for decades so there is a great deal of published information. However, the authors consider that there are several important areas where information is lacking, data are contradictory, mechanisms of action have not been explored, or the environmental effects of particular compounds are not known. Therefore, this chapter reviews a selection of such topics: inorganic fluorides in soil; the loss of fluorides from plants; classifying species sensitivity to HF; estimating effects of fluorides on growth and yield; the significance of pollutant interactions; effects of HF on fertilization and seed set; fluorides and insects; and old and new problems associated with organofluorides in the environment.

1. INTRODUCTION

In Weinstein and Davison [1] we reviewed knowledge of all the major aspects of fluorides in the environment. During our research and writing the review it

*Corresponding author. Tel.: +44-1670-519-545;
E-mail: a.w.davison@ncl.ac.uk

became clear that although many topics are well known and thoroughly researched, there are several important areas where information is lacking, data are contradictory, mechanisms of action have not been explored, or the environmental effects of particular compounds are not known. Therefore in this chapter we present a discussion of a selection of such topics in the hope that it will generate further interest: inorganic fluorides in soil; the loss of fluorides from plants; classifying species sensitivity to HF; estimating effects of fluorides on growth and yield; the significance of pollutant interactions; effects of HF on fertilization and seed set; fluorides and insects; and old and new problems associated with organofluorides in the environment.

2. QUESTIONS RELATING TO INORGANIC FLUORIDE IN SOIL

Soil is a source of fluoride for plants and animals, and it acts as a sink for atmospheric deposition so it plays a central role in the biogeochemical cycling of the element. Fluorine was first detected in minerals in the late 18th century and measured in a variety of rocks in the 19th century [1]. More detailed research on soil fluoride started in the 1930s and 1940s because of concerns about the increasing use of fluoride-containing phosphate fertilizers and inorganic pesticides. It was thought that their use might increase the fluoride content of forage or crops to unacceptable levels. The result of the research is that there is a great deal known about the mineralogy of soil fluoride, concentrations in different soil types worldwide, and the chemical species present. However, there are still important gaps in our knowledge such as the bioavailability of fluoride to plants and the chemistry and mobility of fluoride in organic horizons.

In the mineral horizons of soils, the fluoride concentration ranges from under 100 to several thousand mg kg^{-1} dry wt. [2,3]. In many regions the average is from about 100 to 600 mg kg^{-1} . Because soil fluoride is associated with clay-sized minerals, heavier soils tend to have substantially higher concentrations than do sandy soils. Table 1 shows some comparisons between sandy and clay soils. Concentrations higher than a few hundred mg kg^{-1} are found where there are deposits of high-fluoride minerals such as fluorspar and, in old mining areas, they

Table 1. Examples of the fluoride content of mineral soils in relation to sand and clay content

Author [Ref.]	Country	Sandy soils	Clay soils
Gemmell [9]	New Zealand	68	540
Nommik [10]	Sweden	43–198	248–657
Piotrowska and Wiacek [11]	Poland	20–150	250–750

may reach as high as 12–17% of the dry weight [4,5]. In humid climates there is usually a measurable increase in the fluoride content with depth due to leaching, provided the soil is not plowed and there is no significant deposition to the surface from the air or from fertilizers [6–8]. In situations where fluoride is added as aerial deposition or in fertilizer, there may be higher concentrations in the surface layers.

The leaves of plants growing on mineral soils that have a few hundred mg F kg^{-1} contain less than about 20 mg F kg^{-1} , and usually, under 10 mg F kg^{-1} [12,13]. This is because the bioavailability in most soils is low and because of the nature of plant roots. At soil pH above about 5.5, fluoride exists principally in the anionic F^- form [14] and when it diffuses passively into roots it is mostly confined to the extracellular region, the apoplast. This is probably because cell walls have fixed charges that promote exclusion of negatively charged F^- ions [15] and it limits the amount that is held at sites where it can pass the endodermis and into the conducting system. The endodermis around the conducting system has very low permeability to F^- so it acts as a barrier. Davison, Takmaz-Nisancioglu, and Bailey [16] and Takmaz-Nisancioglu and Davison [15] proposed that most of the fluoride that reaches the leaves leaks past the endodermal barrier at the root tips where it is poorly developed, and where lateral roots emerge. If this is correct, it suggests that the background fluoride content of leaves is related to water use so fluoride uptake may be higher in species with a high rate of water use. A highly branched root system may also promote greater uptake but this has not been investigated. This theory also explains why it is that when roots are exposed to concentrations of fluoride ions that are higher than normally occur in the soil solution, uptake is proportionately greater. Some data of Bar-Yosef and Rosenberg [17] support the idea that greater water use leads to higher fluoride uptake (Table 2). They grew corn (*Zea mays*) and tomato (*Solanum esculentum*) in hydroponic culture and measured the effects of increasing fluoride on growth,

Table 2. The rate of water use and fluoride content of corn and tomato exposed to different concentrations of fluoride in hydroponic culture (data from Bar-Yosef and Rosenberg [17])

Fluoride in solution (mg L^{-1})	Rate of water use (ml g^{-1} root day^{-1})		Fluoride content of shoots (mg kg^{-1})	
	Corn	Tomato	Corn	Tomato
0	8.9	13.7	7	5
1	7.9	13	8.1	7.2
5	7.4	13.1	8.4	11.2
10	7.9	12.9	12.4	28
50	7.4	12.4	54.5	126

water use, and fluoride content. As Table 2 shows, tomato used almost twice as much water as corn, and the fluoride content of the leaves was about twice as high at the elevated fluoride concentrations. Using hydroponic culture, leaf concentrations can reach a few thousand mg kg^{-1} and similarly, where soils are heavily contaminated with fluoride, such as mine wastes, leaf fluorides may be very high. For example, Cooke *et al.* [4] reported concentrations from 280 to over 4000 mg kg^{-1} in a range of grass and legume species growing on fluorspar waste in England.

The bioavailability of soil fluoride depends on the concentration in the solution and on the chemical species of fluoride present. This is an area of research in which considerable progress has been made in recent years, mostly by a group in Australia [14,18]. The minimum solubility occurs at pH values between about 5.5 and 6.5 [14,19]. This is the pH range of many of the most productive agricultural soils so the potential for significant fluoride uptake in those soils is minimal. However, the solubility and chemical speciation of fluoride change with pH. Research in Australia has shown that in soil, fluoride may exist as the free F^- ion or form soluble complexes such as SiF_6^{2-} , AlF^{2+} , AlF_2^+ , AlF_3^0 , AlF_4^- , BF_4^- , and HF [18]. Above about pH 6 the anion F^- predominates but the various complexes predominate at lower pHs. The significance of this difference is, as Stevens *et al.* [14] remarked, that the species of fluoride that are most readily taken up by plants, HF, and some of the aluminum complexes, exist at the pH values where it is most soluble. The permeability of cell membranes to HF and some of the aluminum complexes is much greater so they are more readily taken up than the anion F^- . Bioavailability increases steeply with a decrease in pH so plants growing on acid soils would be expected to have higher foliar fluoride concentrations than plants on neutral soils (Fig. 1). This should be most evident where there is contamination from aerial deposition, mine waste, or fertilizer. However, there is a further complication because acid soils usually have a significant organic content and that also affects fluoride bioavailability.

The fluorine chemistry and bioavailability of fluoride in humus or soil horizons with a high organic content have not been subjected to anything like the scrutiny of mineral soils. It is important to know more about this subject because of the ecological importance of decomposition processes and because a significant fraction of root systems may be in the organic layers. Also, many emission sources such as aluminum smelters are located in regions with well-developed organic horizons. The sources of fluorine in organic matter are plant residues, atmospheric deposition, and soil minerals. As indicated earlier, the background level of fluoride in vegetation is usually under 10 mg kg^{-1} so humus with no soil minerals incorporated into it and in an area with no atmospheric deposition would be expected to have a concentration similar to the vegetation, minus losses due to leaching. Deposition of dust on the surface or the incorporation of minerals by soil processes will increase the fluoride, so the concentration should, theoretically, be related to

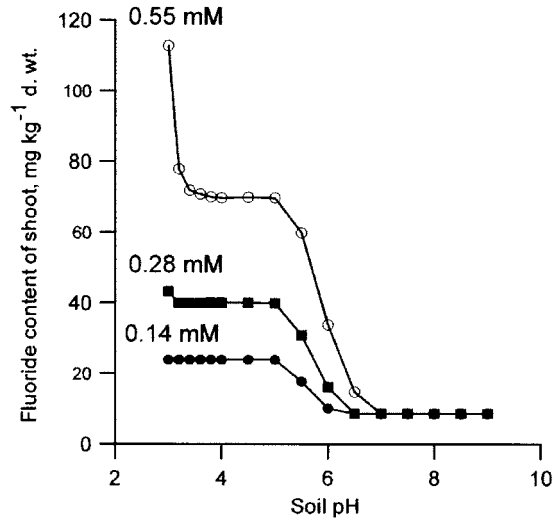


Fig. 1. Predicted shoot fluoride concentrations (mg F kg^{-1} day wt) in relation to soil pH and different concentrations of fluoride in solution: 0.14, 0.28, and 0.55 mM (2.65, 5.27, and $10.54 \text{ mg F L}^{-1}$, respectively). Drawn using data supplied by Stevens (personal communication) from a model described in Stevens *et al.* [14].

the mineral content. However, it is difficult to find published estimates of the total fluoride content of organic layers, especially in unpolluted regions. Thompson, Sidhu, and Roberts [20] reported $8\text{--}14 \text{ mg kg}^{-1}$ fluoride in humus in an unpolluted area in Newfoundland while Omueti and Jones [7] found an average concentration of around 9 mg kg^{-1} in the organic matter from the surface layers of three Illinois sandy loams.

In situations where humus or other organic materials have a low mineral content the fluoride would be expected to be mobile because of the lack of fixation sites. This idea is supported by Pickering [21] who found that commercial humic acid retained only very low amounts of fluoride and even that was probably due to clay-like impurities rather than the humic acid itself. The low retention capacity of organic matter raises the question of what happens when the fluoride input is increased by atmospheric deposition. However, there are only a few studies that provide useful information, notably Thompson, Sidhu, and Roberts [20], Sidhu [22], and Polonski, Flühler, and Blaser [23]. The first two authors investigated the effects of atmospheric deposition from a phosphate factory. Sidhu [22] reported on the fluoride content of the litter of ten species growing at different distances from the factory, while Thompson, Sidhu, and Roberts [20] analyzed the humus in the same locations. Some of their data are given in Table 3. The litter data were collected in a different year from the rest so these have to be interpreted with

Table 3. The fluoride content (mg F kg^{-1} dry wt) in leaves, litter and humus of balsam fir (*Abies balsamea*) and the calcium content of the humus (data from Thompson, Sidhu, and Roberts [20] and Sidhu [22])

Zone in relation to F source	Average F content of foliage	Average F content of leaf litter	Average F content of humus	"Available" (= TISAB buffer extracted) F in humus	Calcium content of humus
I: 80–95% trees dead	281	892	908	58	14,800
II: 40–60% dead	141	272	205	27	7593
III: 20–30% dead	91	163	36	15	5810
IV: no dead trees, some light tip burn	44	75	16	3.8	2762
Control area	7	18	10	2.4	2150

caution but some points are still clear. Where there was high fluoride in the air, such as zone 1, the fluoride content of the litter was much higher than in the control area and this was reflected in the concentration in the humus. At first sight the data seem to suggest significant retention in the humus but there may be a special reason for this because there was a high rate of deposition of particulate materials containing calcium at this particular location (Table 3). However, the fluoride did not appear to be immobilized to the same extent as in mineral soils because Thompson, Sidhu, and Roberts [20] recorded that the humus fluoride decreased significantly during 1973–1974 even though emissions were 75% higher in 1974. They stated that this was due to "more efficient leaching ... by groundwater." Clearly, further studies of fluoride retention and mobility in organic matter are warranted, particularly in areas where there is little calcium being deposited.

From a biological perspective it is important to be able to measure the fraction of soil fluoride that is available for uptake by plant roots. There have been many attempts to do this using a variety of techniques. Early studies mostly used a 1:1 soil–water extract to measure the "water–soluble" fluoride but others have used a saturated paste extract and many an electrolyte solution, acids, buffers, or complexing agents [24]. Larsen and Widdowson [19] used an anion exchange resin to extract the "labile" fluoride. Each of these extracts a different fraction to different extents and it is self-evident that a complexing buffer will extract different amounts than deionized water or an anion exchange resin. Many authors report their data as being the "available" fraction but the crucial test of an extraction

procedure is whether the results correlate with uptake by plants [25]. However, the degree of correlation varies greatly because Stevens *et al.* [26] found that published correlations give r^2 values ranging from 0 to 0.78. The reasons for this variability are discussed in Weinstein and Davison [1] but one of the most important results is that the amount available to roots depends on the fraction that is readily desorbed as the soil solution is depleted by the roots [19]. Also, the soil–solution ratio, the electrolytic composition, and the equilibration time all affect the amount of fluoride extracted from a soil. So, for example, if deionized water is used, the electrolyte concentration will vary with soil properties so it would be misleading to use this extractant to compare availability in organic and mineral horizons or leached sands with clays. Because soil pH affects solubility and speciation, if all of the soils examined have pH values above 5.5–6, the soluble fraction will tend to be universally low because of the dominating effects of pH over the total present. In that situation there is unlikely to be a correlation with plant uptake. Bioavailability and extraction procedures need to be re-examined to see if a more universally acceptable extraction procedure can be found that shows a high correlation with plant uptake over a wide range of soil pH and mineral/organic content.

It is generally concluded that in situations where plants are growing in the vicinity of a source of atmospheric fluoride, foliar fluoride concentrations will be dominated by direct uptake from the air and the contribution from the soil will be minimal [27]. However, there is very little evidence to confirm this in field situations where the total or “available” soil fluoride has been significantly increased by deposition. There are many reports of increased soil fluoride near atmospheric sources but in most cases it is impossible to tell if uptake from the soil is significant. However, three cases provide interesting data [28–30]. A comprehensive report on fluoride in relation to the Norwegian aluminum industry [28] contains an account of experiments in which plants were grown in fluoride-contaminated soil in areas where there was no atmospheric source. St John’s wort (*Hypericum perforatum*) had only low levels of fluoride on the contaminated soils ($< 10 \text{ mg kg}^{-1}$) but willow (*Salix* sp.) grown on a contaminated soil with $69 \text{ mg water-soluble F kg}^{-1}$ accumulated 18 mg kg^{-1} in the leaves. Plants on a control soil had only 1.5 mg kg^{-1} . This suggests a small amount of uptake but it also indicates a difference between species, a complication that has not been considered to any extent. Unfortunately, the report does not say whether the soil profiles were intact or whether plants were grown on material from only one horizon, but if whole profiles were used that might explain the differences between species provided they had different rooting behavior. In contrast, Sidhu [29] and Horntvedt [30] found no evidence of significant uptake from contaminated soil. Table 3 shows that at the site that Sidhu [22] investigated, the total fluoride in the humus and in what he called the “available” (i.e., TISAB buffer soluble) fraction were significantly higher than background. In 1975 the factory ceased emissions between

Table 4. The fluoride content (mg F kg^{-1} dry wt) in leaves of balsam fir (*Abies balsamea*) and black spruce (*Picea mariana*) growing in the vicinity of a phosphorus factory in 1974 and 1975 (data from Sidhu [29])

Species	Zone I		Zone II		Zone III		Zone IV		Outside Zone IV	
	1974	1975	1974	1975	1974	1975	1974	1975	1974	1975
Balsam fir	251	24.7	54.1	7.6	19.3	7.4	10.4	3.7	7.2	5.2
Black spruce	370	8.1	34.3	8.7	14.3	6.5	7.1	3.9	5.2	3.7

May and October so Sidhu examined leaf injury, growth, and the fluoride content of the leaves of four species. There was no visible injury that year and there was an increase in growth compared with the previous year and, most importantly, foliar fluoride concentrations fell dramatically to background levels (Table 4). Sidhu [29] concluded that the very low leaf concentrations in 1975 indicated little translocation from the soil or from older to younger foliage. Using a different approach, Horntvedt [30] analyzed the relationship between emission rates from an aluminum smelter and the fluoride content of pine (*Pinus sylvestris*) needles growing in the vicinity, between 1967 and 1992. The smelter started operation in 1954 and there was concern about the possibility of long-term effects due to build up of fluoride in the soil [25]. The emissions varied from <20 to about 60 kg F h^{-1} over the 25-year period between 1967 and 1992. Needle fluoride concentrations ranged from about 30 to 60 mg kg^{-1} and correlated very well with the emission rates. Because of this, Horntvedt [30] concluded that there were no apparent long-term effects on needle fluoride from fluoride in the soil. As the soils were acidic in these three cases, the data appear to contradict the predictions made by Stevens *et al.* [14] from their model (Fig. 1). However, the discrepancy may be explained if the fluoride in the organic layers of both Sidhu and Horntvedt's soils was very mobile and leached out readily when atmospheric concentrations changed. Another possibility is that the trees had most of their roots in the mineral horizons where fluoride concentrations were not so elevated. Future investigations would benefit from an examination of rooting depths, the mobility of fluoride in the organic horizons, and the fluoride profile with depth.

3. IS FLUORIDE LOST FROM PLANTS?

The fluoride content of plants is very important for providing a basis for monitoring emissions and for preventing harmful effects on crops and fluorosis in grazing animals. In many countries, the amount of fluoride in vegetation is used as a regulatory tool to try to prevent these deleterious environmental effects. Although not as common, there are some jurisdictions that also regulate the amount of

fluoride in native vegetation and ornamental plants with the purpose of preventing damage to those species. There are probably tens of thousands of plant fluoride concentrations published in the literature and several useful studies of fluoride uptake, but given the importance of understanding the dynamics of plant fluoride, there are some surprising gaps in our knowledge. For example, it is a common observation that two species growing side-by-side may have very different fluoride concentrations in their leaves. This disparity may be due to differences in the rate of uptake, leaf age, or leaf area/weight ratio [1]. Rates of deposition (surface deposition plus uptake) can be estimated using standard methods, so if the concentration of fluoride in the air is known, and there is information about stomatal conductance and specific leaf weight, it is possible to predict the total fluoride uptake over short periods of time with a reasonable degree of accuracy. But there are some still unknown factors that make longer-term estimates less reliable or impossible and there have been few attempts to produce a model that can be used to predict the fluoride content of leaves of different species under a range of conditions. An examination and comparison of some data on changes in fluoride content of leaves over time will highlight one of the main problems that arises in any attempt to predict the fluoride content of leaves; fluoride is not only taken up by leaves from the air but also, the concentration may fall, often over short periods of time. The mechanisms underlying rapid decreases in concentrations are still not clear, more than 20 years after the problem was first raised [31]. Figs. 2–4 show data for changes over time in willow (*Salix caprea*), rowan

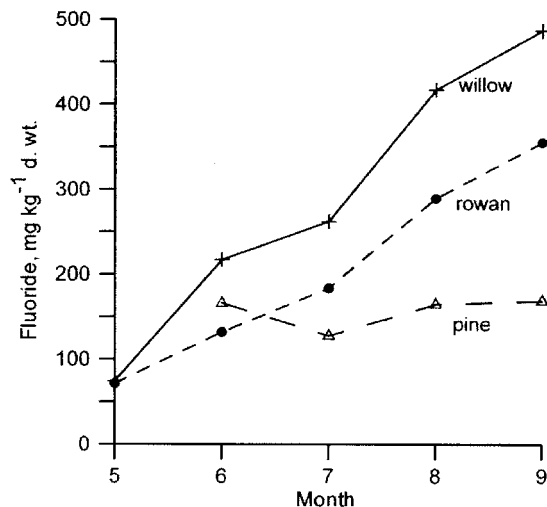


Fig. 2. The change in fluoride content in willow (*Salix caprea*), rowan (*Sorbus aucuparia*), and pine (*Pinus sylvestris*) growing close to each other in the vicinity of a Norwegian aluminum smelter between May and September. Re-drawn from Vike and Håbjørg [32].

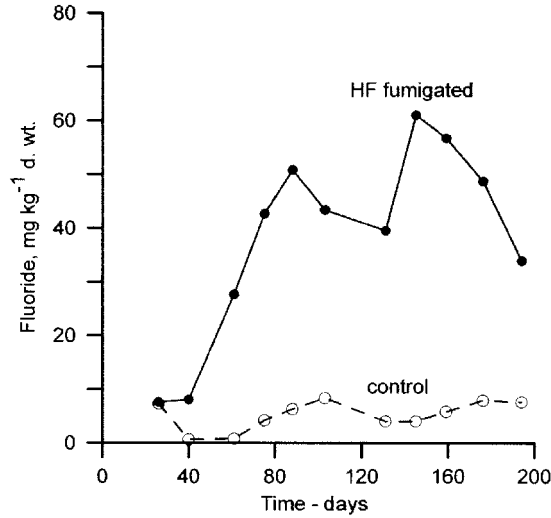


Fig. 3. The change in fluoride content in Shiraz grape leaves exposed in open-top chambers to a continuous mean concentration of 0.27 $\mu\text{g m}^{-3}$ F. Re-drawn from Murray [33].

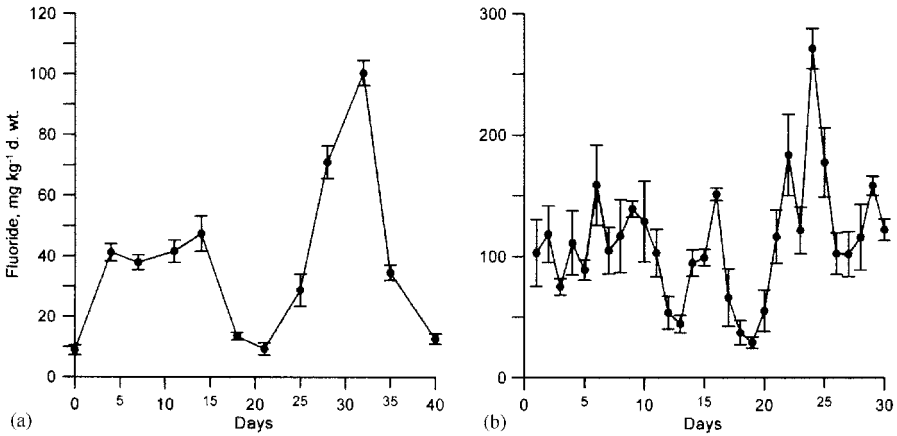


Fig. 4. Variation in the mean fluoride content (mg F kg⁻¹ and standard error) of pasture grass at two locations: a) near a brickworks in the Netherlands (van der Eerden, 1981) and b) near an aluminium smelter in England (Blakemore, 1978). Both data sets were collected in the autumn when there was no growth. Re-drawn from Blakemore [34] and van der Eerden [35].

(*Sorbus aucuparia*), pine (*Pinus sylvestris*) [32], grape (*Vitis vinifera*) [33], and grass swards [34,35]. All of the work was in the field ([33] was in open-top chambers) in a range of climates.

Fig. 2 shows the change in fluoride content of three tree species growing close to each other in the vicinity of a Norwegian aluminum smelter between May and September. Although there undoubtedly were changes in the fluoride concentration in the air, the mean concentration in the leaves of two species showed a reasonably steady increase in fluoride over time. The second-year pine needles showed little change, probably because stomatal conductance was very low and there may have even been some occlusion of the stomatal pores by waxes or dust, limiting further uptake. The increase in the two deciduous species is typical of trees and it gives the impression of steady accumulation of fluoride over the season. There is no indication of any decrease or loss from the leaves. Murray's [33] data (Fig. 3) are for Shiraz grape exposed in open-top chambers to a continuous mean concentration of $0.27 \mu\text{g m}^{-3}$ F (standard deviation 0.13). This is a low concentration but there was still significant accumulation in the leaves as the season progressed. However, after about 60–70 days there was an apparent fall, followed by an increase and a second fall. Some of the decrease may have been just sampling errors but it appears that grape is different in its fluoride dynamics from birch and rowan. Grass fluoride concentrations are typically even more dynamic, at least in the northern temperate parts of Europe where they have been most studied. Fig. 4 shows data on the fluoride content of grass swards growing near fluoride sources. In both cases, there were statistically significant falls in fluoride content over periods ranging from 1 to 10 days. Data published by Davison *et al.* [36] showed a loss of fluoride in a grass sward from 508 to 188 mg kg^{-1} in a week. Why did these trees, grape, and grasses behave so differently and why did the concentrations decrease so rapidly?

A summary of published reports of rapid decreases in fluoride concentrations is given in Table 5. Note that some of the examples occurred after plants were exposed to HF and then placed in a clean atmosphere; the others occurred while the plants were still exposed to HF in the field. Several possible mechanisms were discussed by Davison [31] and Weinstein and Davison [1]. These were as follows: growth dilution; leaching by rain; leaf death; shedding of surface waxes; guttation; translocation to the stem and root; and volatilization.

The idea of growth dilution, the plant producing dry matter faster than it takes up fluoride, has been around for decades but Davison and Weinstein [1] concluded that it is only likely to happen when the rate of uptake is very low and the growth rate is very high. Also, it cannot account for many of the reported decreases (Table 5), because they occurred in tissues or situations where there was no growth, such as mature spruce needles and grass swards in the late autumn.

Table 5. Reported examples of rapid decreases in the fluoride content of plants (after Davison [31], with additions)

Author	Observation
Zimmerman and Hitchcock [37]	First report in literature in English. No amount of loss given.
Weinstein [38]	Large losses of F from bean and tomato leaves 3, 6, and 9 days after cessation of exposure.
Hitchcock <i>et al.</i> [39]	Up to 46–70% loss from maize leaves one week or more after exposure
Guderian <i>et al.</i> [40]	F decreased from 310 to 105 $\mu\text{g g}^{-1}$ in old rape plants, and from 465 to 62 $\mu\text{g g}^{-1}$ in young rape plants in 11 days.
Knabe [41]	Loss of up to 340 $\mu\text{g g}^{-1}$ from spruce needles; up to 200 $\mu\text{g g}^{-1}$ in washed needles after 5 months post fumigation.
Hitchcock <i>et al.</i> [42]	Loss of 50% in alfalfa after 8–22 days postfumigation.
Georgsson and Petersson [43]	Grass contaminated with volcanic ash fell from 4300 to 30 $\mu\text{g g}^{-1}$ after 30 days.
Davison and Blakemore [44]	Loss of up to 27 $\mu\text{g g}^{-1}$ from washed grass in 1 day, in the field, continuous exposure.
Ghiasseddin <i>et al.</i> [45]	Decrease of up to 180 $\mu\text{g g}^{-1}$ in 7 days.
Davison <i>et al.</i> [36]	Many examples of decreases in forage of over 50 $\mu\text{g g}^{-1}$ in 1 day in the field with continuous exposure.
Bunce (personal communication)	Loss of 40 $\mu\text{g g}^{-1}$ in 7 days in hemlock.
Van der Eerden [35]	Losses of up to 70 $\mu\text{g g}^{-1}$ in 10 days in grass in the field with continuous exposure.

Intuitively, the idea that rain leaches fluoride from leaf surfaces or the interior seems feasible and there are several reports of inverse correlations between leaf fluoride and rainfall that appear to support this concept [summarized in Ref. 1]. However, the situation is complex because rain scrubs the atmosphere, reducing the fluoride concentration (which reduces uptake), but it increases the dissolved or suspended fluoride that can be deposited on the surfaces. Furthermore, the rate of deposition of fluoride on a wet leaf surface is greater than on a dry one so there are conflicting forces at work. The inverse correlation between rain volume and plant fluoride content may be simply due to the lower fluoride content in the atmosphere. Furthermore, experimental application of rain does not support the

idea of leaching and in contrast, Less *et al.* [46] found that artificial precipitation resulted in an increase in grass fluoride concentration of about twofold. The answer to this puzzle may be that the effect of precipitation may depend on how heavy and frequent the showers are. Less *et al.* [46] concluded that, "frequent rather than heavy rainfall would lead to greater absorption." The problem of the effects of rain remains unresolved.

Leaf death, shedding of surface waxes, and translocation to the stem and root were all considered to be minor or insignificant sources of change by Weinstein and Davison [1] because of the magnitude and speed of the reported changes. Grass leaves die and cuticular waxes are shed but not at such a speed as to cause changes within a day. Transport of fluoride from leaves to stems and roots (and perhaps loss from roots to the surrounding soil) is also unlikely because most of the evidence indicates that fluoride absorbed from the atmosphere is translocated to the leaf tips and not to any degree downward to stems or roots. For example, Ledbetter *et al.* [47] exposed tomato plants to ^{18}F and showed that the accumulation of fluoride was mainly in the leaves and glandular hairs of the petioles and stem, with little movement to the roots. But, Kronberger and Halbwachs [48] and Kronberger *et al.* [49] reported downward movement of fluoride in conductive tissues of spruce and accumulation in bark. However, some of the experimental data are equivocal [50] so this mechanism is not considered to be significant. Guttation is the expression of water droplets from the margins of leaves that occurs under certain conditions of temperature and humidity. It is common in grasses, and fluoride is detectable in guttation droplets, but Takmaz-Nisancioglu [51] thought that guttation could not account for the observed rates of decrease in grass swards. That leaves only one remaining mechanism, volatilization.

Volatilization has been invoked as an explanation of losses by plants, and it can be easily demonstrated, in principle, using artificial surfaces. For example, Takmaz-Nisancioglu [51] made 4 cm \times 4 cm filter paper squares impregnated with citrate-phosphate buffers to control pH over the range from 2.2 to 7.0. A sodium fluoride solution was then applied to the papers to give 60 μg F per paper (= 32 cm^2 , both surfaces). Papers were hung in fluoride-free air, sampled at intervals, and analyzed. Fig. 5 shows the rate of loss of F in $\mu\text{g m}^{-2} \text{day}^{-1}$ plotted against the pH of the paper. The shape of the curve reflects the fact that HF predominates over F^- with decreasing pH and that HF is volatile. A grass leaf weighs about 20 g m^{-2} so if the rate of loss is divided by 20 it gives an idea of the potential rate of loss from a leaf in $\mu\text{g g}^{-1} \text{day}^{-1}$. This is shown on the right-hand y-axis of the graph and it can be seen that under the conditions in the experiment, at pH values between 5 and 6, loss would be around 10–30 $\mu\text{g g}^{-1}$. Wind speed, the initial concentration on the paper, the shape of the model, and temperature all affected the rate of loss, but the experiment demonstrates that at moderately acidic pH, the rate of loss can be similar to that observed in the field

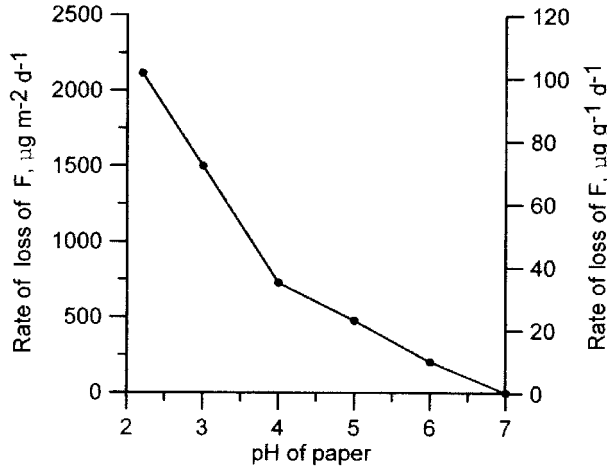


Fig. 5. The rate of loss of fluoride ($\mu\text{g}^{-2}\text{day}^{-1}$) plotted against the pH of 4 cm \times 4 cm filter paper squares suspended in a well-ventilated space. The graph also shows the hypothetical rate of loss ($\mu\text{g g}^{-1}\text{day}^{-1}$) from a grass leaf. Redrawn from Takmaz-Nisancioglu [51].

for grass swards. The rate would be substantially less for thicker or more sclerified leaves so if this mechanism occurs it is probably of significance only for grasses.

If volatilization from leaf surfaces can occur, then theoretically it can also occur from inside leaves via the stomatal pores, provided the pH of the fluid in the cell walls is low enough ($< \text{pH } 6$) to form HF and there is a difference in partial pressure between the inside and outside of the leaf. Surprisingly, there is experimental evidence that this can occur. Garrec and Chopin [52] attempted to confirm volatilization loss by analyzing the air blown over small fir (*Abies*) trees that were fed ammonium fluoride through the roots. They passed clean air over the trees, then filtered and analyzed it at the exit from the chamber. The rate of loss was measurable but low, which seems to confirm the possibility of volatilization from the interior of leaves. The low rate of loss may have been partly caused by the slow airflow in the exposure system and the low stomatal conductance of fir. Whatever the explanation is, this intriguing experiment needs to be repeated as part of a concerted study of the mechanisms by which the fluoride content of leaves can decrease so rapidly.

4. PROBLEMS CLASSIFYING PLANT SPECIES SENSITIVITY

The sensitivity or tolerance of plants to fluoride is almost universally based on the tendency of species to produce visible symptoms of injury. Once inside a leaf,

fluoride ions are carried with the transpiration stream of water from the vein ends through cell walls to the margins and tip, this causes accumulation of fluoride in the margins and this concentration mechanism is one of the main reasons for its extreme toxicity. If the concentration is high enough locally, cell membranes are damaged, the contents leak, and cells die. When the area dries, the necrotic patches turn tan, brown, or black, depending on the species (Plate 1, upper left) The dead tissue may drop off, leaving a distorted shape. At lower concentrations the fluoride may disrupt the extension of cell walls, more so at the margins, so the leaf becomes cupped or buckled (Plate 1, upper right). If sufficient fluoride diffuses into the chloroplasts it is thought to complex with magnesium and disrupt the chlorophyll molecules. This leads to chlorotic (yellow) areas between the veins (Plate 1, lower left). Species differ in their sensitivity by at least 2 orders of

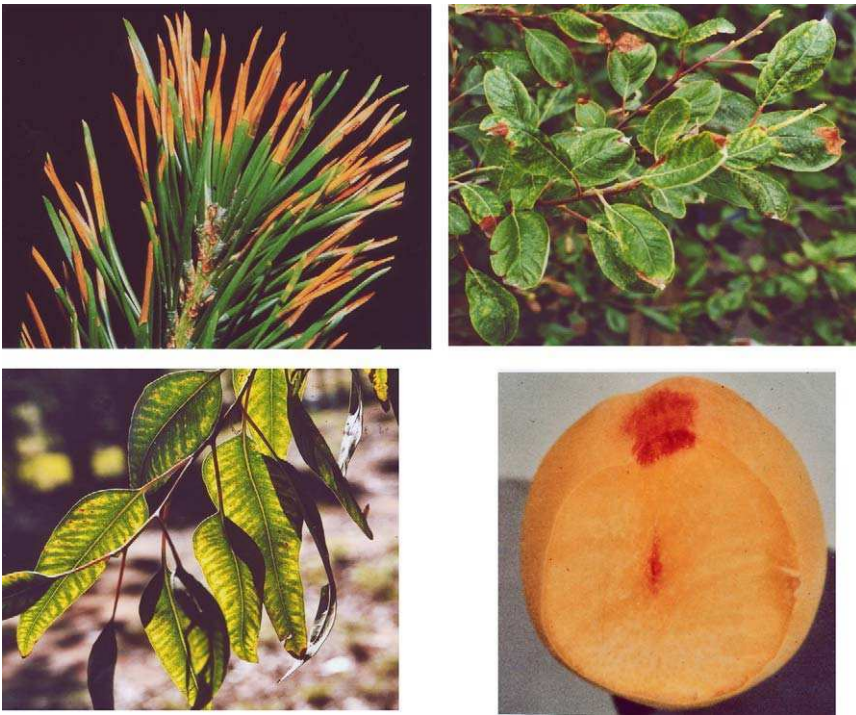


Plate 1. (*upper left*). Necrosis of the tips of the current year's needles of lodgepole pine (*Pinus contorta*) (photo LHW); (*upper right*). Tip necrosis, distortion, and interveinal chlorosis in willow (*Salix* sp.) (photo AWD); (*lower left*). Interveinal chlorosis viewed by transmitted light in *Eucalyptus grandis*. There are also faint spots due to red pigmentation (photo LHW); (*lower right*). Suture red spot in Elberta peach. Note the reddening and soft tissue in the region of the suture (photo LHW).

magnitude, the most sensitive being visibly injured by exposure to ca. $0.3 \mu\text{g m}^{-3}$ for prolonged periods.

Visible symptoms can be recognized by trained observers, but using such symptoms for classifying plants into categories of sensitivity or tolerance is fraught with many problems. One of these is that a species in one location may be sensitive while in another location, it may appear to be more tolerant. One example is *Eucalyptus globulus*, a species that is classed as of intermediate sensitivity in its native Australia [53], while in western Europe, where it is grown for pulp and timber, it appears to be more sensitive. This, of course, can be due to many factors, including the greater amount of precipitation in Europe, resulting in higher stomatal conductance [1]; but not to be ignored are differences in soil types, nutrition, and the genetic makeup of the population. Very little is known about the relative importance of these factors.

Over the years, many authors have published classifications of plants using the occurrence of visible symptoms near fluoride sources or occasionally in controlled experiments. The various classifications were discussed by Weinstein and Davison [1,54], but comprehensive lists have been offered by Weinstein [12], Guderian *et al.* [40], Doley [53], Borsdorf [55], Bossavy [56], Bolay and Bovay [57], Treshow and Pack [58], Dässler [59], Weinstein *et al.* [60], Weinstein and Hansen [61], and others. Although widely used, they are of limited accuracy for several reasons. First, a comparison of rankings is difficult because there are a limited number of species common to most lists. Second, sensitivity classes are subjective to the author and based on different criteria. Borsdorf [55] provides a good example. He divided species into four classes: *hochemfindlich* (highly sensitive), *empfindlich* (sensitive), *wenig empfindlich* (slightly sensitive), and *unempfindlich* (nonsensitive). The degree of sensitivity was based upon the degree of injury to a given species according to the distance from a single fluoride source in Central Germany. Thus, species that showed injury at the farthest distance from the source were the most sensitive, while those that exhibited little or no injury close to the source were tolerant. One assumes that the two other classes were intermediate in distance from the source but they were not defined by the author. An even simpler system was used by Bossavy [56] who divided species into only two classes: *sensibles* (sensitive) and *résistantes* (resistant). This was based upon observations in the French Alps in June, over several years, of the presence or absence of injury. The lack of consistency between the methods resulted in two different classifications of sensitivity for German iris (*Iris germanica*) by Borsdorf (*hochemfindlich*) and Bossavy (*sensibles*). Even more misleading is the classification of hawthorn (*Crataegus monogyna*) by Borsdorf as *wenig empfindlich* and by Bossavy as *résistante*. We have found that in the field all *Crataegus* species appear to be tolerant, unless exposed to a very high concentration of gaseous fluoride. Guderian *et al.* [40] used three categories to

describe injury: *sehr empfindlich* (very sensitive), *empfindlich* (sensitive), and *wenger empfindlich* (less sensitive). One might interpret the lack of a resistant category as meaning that all species exhibit some sensitivity to levels of fluoride found in the ambient air, but this is true only where there are unusually high concentrations or where high exposures are frequent. However, Borsdorf [55] also stated that many species are not injured even at the highest ambient concentrations. We have found that a very tolerant species such as *Juniperus virginiana* may gradually deteriorate after long-term relatively high concentrations. Even species that seem to be “untouchable” in most situations, such as camellia (*Camellia japonica*), rubber plant (*Ficus elastica*), privet (*Ligustrum ovalifolium*), or oleander (*Nerium oleander*), have been injured in areas immediately downwind of sources of high concentrations of HF. To add to this disorder, some authors have classified narrow groups of species, such as legumes, grasses, or grains according to their relative susceptibilities [40]. What these authors identify as the most susceptible species may be more commonly classified as moderately tolerant or tolerant on broader lists. So these different means of identifying the degree of a plant’s susceptibility or tolerance have resulted in what appear to be anomalies in the classifications of some species.

An examination of the lists cited above reveals that many were based on fumigations carried out in closed chambers, usually with little or no control over temperature, humidity, light intensity, and often with rudimentary controls over HF concentration. The extensive list published by Weinstein and Davison [1], however, depends to a large degree upon field observations near fluoride-emitting sources but, unfortunately, in most cases, there were no corresponding measurements of atmospheric fluoride concentrations to give greater credence to the classification.

How can a consistent system of sensitivity classification be constructed? Certainly one requirement would be to use a common, objective basis for the classification. Ideally, atmospheric fluoride concentration should be used as the baseline for comparison. The most sensitive category would include those species that respond to the lowest concentrations known to cause injury (ca. $0.2\text{--}0.3\ \mu\text{g m}^{-3}$), while the most resistant would be those that tolerate the highest concentrations that commonly occur. If the range of concentrations is too narrow, however, this approach can be misleading. For example, Guderian *et al.* [40] exposed a number of plant species in Mylar greenhouses to $0.85\ \mu\text{g HF m}^{-3}$ for 16 days or to $1.1\ \mu\text{g HF m}^{-3}$ for 49 days, concentrations that are 3–4 times higher than the minimum concentration required to induce injury in some very sensitive species. In their study, both exposures resulted in “very slight chlorosis” in white clover (*Trifolium repens*), yet it was placed in the same sensitive class as *Gladolus*, a classic bioindicator species that is injured at concentrations as low as $0.25\text{--}0.30\ \mu\text{g m}^{-3}$. In contrast, white clover was found to be insensitive by

Bossavy [56], a conclusion with which the present authors agree. There is little probability today that there will ever be sufficient funds, or adequate monitoring instrumentation, to conduct controlled studies where time, concentrations, effects of weather, nutrition, and response can be determined, even for a limited number of species.

Where does this leave us? Clearly, the numerous lists that have been published, notwithstanding the contradictions inherent between them, have value mostly as a aid to identification of symptoms observed in the field; if fluoride is the cause of symptoms then there should be much greater injury seen on sensitive species and less on more tolerant species. Furthermore, the degree of foliar injury can be used to map the “footprint” of emissions from a source, identifying areas where more investigation is needed. Annual surveys can be used to make comparisons from year to year in relation to changing emission rates or differences in the weather. Some plants are extremely valuable for diagnosing the presence of fluoride at concentrations that are so low that they are near the detection limits of automated measuring instruments. There are several species that have been used for mapping areas where fluoride injury occurs and they are termed as bioindicators. A bioindicator has been defined as “a sensitive species that responds in a characteristic and predictable manner to the conditions that occur in a particular region or habitat” [62]. This includes “changes in leaves, flowers or fruits, and include formation of chlorotic (yellow) or necrotic lesions, other pigment changes, such as the production of red pigments (anthocyanosis), numerous kinds of leaf distortions, fruit deformities, reduced growth, alteration in plant form and other effects” [1]. The most sensitive bioindicators are often termed as *sentinel* species, defined as “the most sensitive organisms to fluoride in each plant or animal category.” Some of the more useful species have been selected from the long list cited by Weinstein and Davison [1] and are shown in Table 6.

5. PROBLEMS ESTIMATING EFFECTS OF FLUORIDE ON PLANT GROWTH AND YIELD

Visible injury can be recognized in the field and it provides readily accessible evidence that fluoride concentrations have reached toxic levels but there is an obvious requirement to be able to assess the effects on the growth and yield of crops, trees, and other vegetation. Researching these effects is much more challenging than investigating visible injury so an obvious question is: whether there is a relationship between visible injury and effects on growth? If there is, it would assist assessment of the effects of fluoride sources. Logically, it would seem reasonable for there to be a relationship, especially if photosynthetic tissue is killed or leaves are lost. However, research on the growth of plants exposed to

Table 6. Relative sensitivities of selected higher plants to atmospheric fluorides classification on the basis of occurrence of foliar symptoms (data based on Weinstein and Davison [1])

Latin binomial	Common name	Response
<i>Abies balsamea</i>	Balsam fir	S
<i>Acacia aulacocarpa</i> , <i>A. fimbriata</i> , <i>A. pulchella</i>	Hickory wattle, Brisbane wattle, prickly moses	S
<i>Acer negundo</i>	Manitoba maple, box elder	S
<i>Amelanchier canadensis</i>	Service berry, Saskatoon berry	I
<i>Avena sativa</i>	Oat (young)	S
<i>Avena sativa</i>	Oat (mature)	T
<i>Berberis vulgaris</i> ^a	Common barberry	S
<i>Betula lutea</i> , <i>B. nigra</i> , <i>B. papyrifera</i> , <i>B. pendula</i> , <i>B. populifolia</i>	Yellow, black, white, European and gray birch	T
<i>Cercis canadensis</i>	Red bud	S
<i>Chamaecyparis spp.</i>	False cypress	T
<i>Convallaria majalis</i>	Lily of the valley	S
<i>Cornus canadensis</i> , <i>C. florida</i>	Bunchberry and flowering dogwood	T
<i>Corymbia citriodora</i> , <i>C. intermedia</i>	Lemon-scented gum, pink bloodwood	S
<i>Epilobium angustifolium</i>	Fireweed	I
<i>Eucalyptus globulus</i> , <i>E. grandis</i> , <i>E. punctata</i> , <i>C. nudis</i> , <i>C. saligna</i>	Tasmania blue gum, flooded gum, gray gum, western Australia flooded gum, Sydney bluegum	S
<i>Ficus benjamina</i> , <i>F. elastica</i>	Weeping fig, rubber plant	T
<i>Fraxinus americana</i>	White ash	S
<i>Hosta spp.</i>	Plantain lily	S
<i>Gladiolus hortus</i> ^a	Gladiolus, sword lily	S
<i>Hypericum perforatum</i> ^a	St John's wort, goatweed	S
<i>Juglans cinerea</i> , <i>J. nigra</i> , <i>J. regia</i>	Butternut, black, English walnut	I
<i>Juniperus spp.</i>	Juniper	T
<i>Larix occidentalis</i>	Western larch	S
<i>Liquidambar styraciflua</i>	Sweet gum	I
<i>Maianthemum canadense</i> , <i>M. bifolium</i>	False lily of-the-valley	S
<i>Malus domestica</i>	Apple	T

Table 6. Continued

Latin binomial	Common name	Response
<i>Medicago sativa</i>	Lucerne, alfalfa	T
<i>Nerium oleander</i>	Oleander	T
<i>Picea glauca</i> , <i>P. pungens</i>	White, Colorado spruce	I
<i>Pinus strobus</i> ^a , <i>P. mugo</i> , <i>P. contorta</i> , <i>P. taeda</i> , <i>P. ponderosa</i> , <i>P. sylvestris</i>	White, mugo, lodgepole, loblolly, ponderosa, scotch pine (young needles)	S
<i>Platanus acerifolia</i> , <i>P. occidentalis</i>	London plane tree, sycamore	I
<i>Populus deltoides</i>	Cottonwood	I-T
<i>Populus tremuloides</i>	Trembling aspen	S
<i>Prunus avium</i>	Sweet cherry	I
<i>Prunus persica</i>	Peach (leaves)	I
<i>Prunus persica</i>	Peach (fruit)	S
<i>Pseudotsuga menziesii</i>	Douglas-fir	S
<i>Quercus alba</i> , <i>Q. palustris</i> , <i>Q. velutina</i> , <i>Q. virginiana</i>	White, pin, black, live oak	T
<i>Robinia pseudoacacia</i>	Black locust	T
<i>Sorbus aucuparia</i>	European mountain ash, rowan	I
<i>Thuja occidentalis</i>	Arborvitae	T
<i>Tsuga canadensis</i>	Canadian hemlock	T
<i>Tulipa sp.</i>	Tulip	S
<i>Ulmus alata</i> , <i>U. americana</i> , <i>U. parvifolia</i> , <i>U. pumila</i>	Winged, American, Chinese, Siberian elm	T
<i>Vaccinium spp.</i>	Blueberry	S
<i>Vitis vinifera</i>	European grape	S
<i>Xanthorrhoea spp.</i>	Grass tree	S
<i>Zea mays</i>	Sweet corn (many cvs.), maize	S
<i>Zea mays</i>	Field corn, maize	I

^a Commonly used bioindicators.

other air pollutants such as ozone, sulfur dioxide, and nitrogen oxides informs us that the relationship between foliar symptoms and yield is usually, at best, tenuous. One reason is that these pollutants are metabolized after contacting plant tissues, and sulfur and nitrogen are essential plant nutrients. Fluoride, however, is a special case; it is not an essential element and normally it occurs in plants in only trace amounts as a contaminant from the soil, water, or atmosphere so a better relationship might be expected. Unfortunately, this is not the case; the relationship with growth and yield has rarely been shown to be significant. This is

important because most, if not all, fluoride air quality standards are based on the occurrence of visible effects on plants, whether as foliar lesions or other markings. These markings are adequate for establishing that the plant aesthetic has been degraded in residential landscapes and parks, and they can be used to protect certain soft fruit, but they do not guarantee that there are no effects on growth or yield. Therefore, this section reviews what is known about the effects of fluorides on growth and yield, drawing attention to the significant findings, shortcomings, and needs.

The quality and usefulness of all air pollution studies depend on the techniques that are available. A few studies have used tree rings to study the effects of fluoride on growth in the natural environment but most research on this subject, over more than six decades, has used controlled environments. This began with the use of glasshouses and other enclosed chambers to produce controlled concentrations of hydrogen fluoride or particulate materials. Although these closed chambers produced some informative data (e.g. Refs. [63–65]), lighting was often poor, temperatures too high, and inadequate air movement reduced pollutant uptake very significantly [1]. Their shortcomings were recognized in the 1960s and that led to the introduction of open-top chambers in which ambient air is blown into large transparent cylinders placed over vegetation in the field [66,67]. Rates of air movement are high to keep the temperature near ambient and the open-top chamber was designed to allow ingress of rain and insects, etc. They were thought to produce conditions that are a much closer simulation of the field environment and, hence they were considered to provide reliable data on yield. They became the workhorse of most air pollution studies, and current air quality standards for several pollutants are based on research using them. However, eventually it was realized that they too have certain limitations because they increase air and soil temperatures, reduce humidity, and alter the light environment by small but important amounts. The increased turbulence inside chambers usually results in greater uptake and deposition of the pollutant making it more difficult to quantify the relationship between the exposure and yield. In the last decade or so, there has been more use made of exposure systems in which plants grown in the field are not enclosed at all; so-called free-air systems [68–71]. These allow plants ranging from annual crops to mature trees to be exposed under real-life field conditions for long periods and they are currently the essential technique in investigations of the effects of elevated CO₂ and ozone. The significance of these changes in technology is that few of the studies of fluoride using enclosed chambers can be relied upon to provide useful data on growth or yield, while work using open-top chambers needs to be interpreted with caution. Unfortunately there have been no reported studies of fluoride using free-air systems, which may be due to the need for, and lack of, a fast-response, real-time analyzer that will work at sub- $\mu\text{g F m}^{-3}$ concentrations.

Table 7. Yield of field-grown wheat after exposure to HF for 4 days at two stages of development (after MacLean and Schneider [72])

HF ($\mu\text{g m}^{-3}$ for 4 day)	Yield per plant (g)	Spikes per plant	Weight per spike (g)
Exposed at boot stage			
0	1.29a	3.46b	0.364a
0.9	1.03b	3.45b	0.306b
2.9	1.21a	4.65a	0.254c
Exposed at anthesis			
0	1.57a	3.55a	0.488a
0.9	1.07b	3.26ab	0.333b
2.9	0.93b	2.99b	0.326b

Note: Means within a column followed by the same letter were not significantly different ($p = 0.05$).

There have been relatively few open-top chamber studies that have investigated fluoride but they all used realistic concentrations of HF and they have produced valuable data. We will discuss four studies as examples. The first is a study by MacLean and Schneider [72] in which wheat plants were grown in the field under background conditions of fluoride. When the spikes first emerged (the "boot" stage), plots were enclosed in open-top chambers and provided with air filtered through calcium carbonate and charcoal, or to 0.9 and 2.9 $\mu\text{g F m}^{-3}$ for 4 days. This experiment was repeated when another set of plants had reached anthesis (i.e. when the anthers are released). The short duration of the experiments reduced much of the effects induced by enclosure. Both exposure regimes resulted in significant effects (Table 7).

Grain yield was reduced in plants exposed at the boot stage by 0.9 $\mu\text{g m}^{-3}$ because the spikes were smaller. Oddly, the 2.9 $\mu\text{g m}^{-3}$ treatment did not affect yield because the smaller spikes were offset by a greater number of spikes per plant. At anthesis, the yield reduction was due to smaller and fewer spikes. This demonstrated that short-term exposures can have important effects on seed production and that the timing of flowering and fertilization is critical in determining effects on grain yield. Furthermore, there were no symptoms of injury on the wheat plants. Some of the effects on grain yield may have been due to direct effects of fluoride on the fertilization process, which we discuss in detail later. Also, the authors found that there was no movement of fluoride from the foliage to the grains, which is in agreement with field observations that grain fluoride is usually low. Studies with grapes in open-top chambers have also demonstrated

the lack of movement to the berry [73]. This is significant because, as emphasized by Weinstein and Davison [1], there is no risk to the consumer from ingesting grains or berries from fluoride-exposed plants.

The results of MacLean and Schneider [72] also demonstrate the lack of relationship between sensitivity assessments based on visible injury and yield loss. In most classifications, young wheat plants are listed as being sensitive and mature plants as tolerant. But MacLean and Schneider's [72] data, using low concentrations of HF for only 4 days would suggest that wheat in the boot and anthesis stages are sensitive. The authors recommended that plants be classified on different bases depending on their use – prevention of aesthetic loss or crop yield – is logical but, unfortunately, there are too few data that can be used to assemble such lists.

The second example is on the effects of long-duration exposure to HF by MacLean *et al.* [74]. They exposed bean (*Phaseolus vulgaris*) and tomato (*Solanum esculentum*) to $0.6 \mu\text{g F m}^{-3}$ for 43 and 95 days, respectively (Table 8). Bean, which is classed as tolerant in terms of visible injury, exhibited normal growth and no foliar lesions, but had much reduced fruit mass and numbers. Although open-top chambers tend to increase the effects of pollutants, after allowing for this, we consider that the concentration and duration were representative of the exposures that still occur near many HF sources. There was no effect on the growth or fruiting of tomato (results not shown here), which is generally classified as intermediate in tolerance so the authors proposed that the effects of fluoride on fruiting and foliar injury are each independent of the other.

The third example involved exposing wheat and sorghum plants to three successive 3-day exposures at 1.6 or $3.3 \mu\text{g F m}^{-3}$, which provides eight permutations of the concentrations plus a control [75]. The authors found that the yield of

Table 8. Effect of continuous exposure to $0.6 \mu\text{g HF m}^{-3}$ on the yield of bean plants (*Phaseolus vulgaris* cv. "Tendergreen") (MacLean *et al.* [74])

	Control	HF fumigated
Dry weight tops (g)	80.9	81.8
Dry weight leaves (g)	41.5	44.3
Dry weight stems (g)	39.4	37.5
No. of pods harvested	88.4	77.3*
No. of marketable pods	70.4	56.5
No. of unmarketable pods	18	20.8
Fresh weight pods (g)	424	337**
Fresh weight marketable pods (g)	391	298**
Fresh weight unmarketable pods (g)	34.3	40.5

* Significantly different from control, $p = 0.05$.

** Significantly different from control, $p = 0.01$.

wheat was not related to the mean concentration over all exposure periods, but to a weighted contrast between the first and the subsequent periods; yield of one hybrid of sorghum was related to a weighted mean of the second and third exposures. Anthesis was again shown to be the most sensitive period with respect to effects on yield. The important conclusion was that exposures of the same duration that result in the same mean concentration do not necessarily result in equivalent effects. This raises many problems in the design of appropriate experiments; the number of combinations of treatments, concentrations, crops, and varieties is immense, too many to contemplate a comprehensive study. They also suggested two reasons for this. First, sensitivity of the plant may be partially determined by the effects of preceding exposures, as indicated by Zahn [76] for SO₂, in which he suggested that one exposure might desensitize the plant to a subsequent exposure or potentiate the effects of a preceding exposure. Whether this is true for fluoride is not known. Second, when exposures occur over an extended period of time, the sensitivity of the plant can be altered by changes in the environment and the phenological stage of development.

The final example involves the production of a disorder called “suture red spot” of peaches [77]. In this unusual disorder, one or both sides of the suture ripens prematurely, expressed by a red area that extends into the flesh, and is usually located at the styler end of the fruit (Plate 1, lower right). In Elberta peach trees enclosed in open-top chambers, four overlapping exposure periods of 30

Table 9. Development of suture red spot in Elberta peach fruits exposed to overlapping 30-day exposures to 2 µg HF m⁻³. The first indication of pit hardening was on the 15th of June. The percentages are based on 150 fruits per treatment (data from MacLean *et al.* [77])

Dates of exposure	Fruits in each severity class (%)				Concentration of F in fruits at harvest maturity (mg kg ⁻¹)	
	With SRS	Slight	Moderate	Severe	Exocarp	Mesocarp
15 June–15 July	6.1	6.1	0	0	6.7	<1.0
30 June–30 July	71.9	50.0	18.0	3.9	5.3	1.0
15 July–14 August	97.8	52.7	37.1	7.8	6.6	<1.0
30 July–29 August	90.3	22.1	40.3	27.3	17.9*	9.2*
Control	<1.0	<1.0	0	0	3.1**	1.2

* Significantly greater than all other values in the respective columns ($p = 0.05$).

** Significantly lower than all other values in the respective columns ($p = 0.05$).

days to $2 \mu\text{g HF m}^{-3}$ resulted in a high proportion of abnormal fruit. The induction of suture red spot was associated with the period after pit-hardening when up to 98% of the fruits were affected (Table 9). Continuous exposure for 105 days at a concentration as low as $0.3 \mu\text{g HF m}^{-3}$ resulted in 95% afflicted fruit. It is believed that the symptoms are caused by the fluoride complexing with calcium in the suture region and altering cellular development. This example illustrates that a very low concentration of fluoride, $0.3 \mu\text{g HF m}^{-3}$, can have a serious effect on crop quality and therefore the marketable yield. Even if there was no reduction in yield, the red spot destroys the sale value of the crop. It is also worth noting that $0.3 \mu\text{g HF m}^{-3}$ is the concentration cited in several air quality standards designed to protect crops and other vegetation.

The analysis of tree rings to establish a historical record and quantify the effects of fluoride exposure has been used occasionally for more than 50 years. Collecting an adequate number of samples for tree ring analysis is time consuming and analysis of the data is challenging because of the natural variability, environmental differences with site and over time, and the co-occurrence of stresses other than fluoride. First-class statistical analysis is essential. During the so-called "pine blight" period near Spokane, USA, Lynch [78] showed by tree ring analysis that growth of ponderosa pine trees was depressed by fluoride emissions from a nearby aluminum smelter. Ring analysis was also used in determining the validity of claims of diminished forest tree growth in Mosjøen, Norway, between 1964 and 1973 [79]. Tree cores from 147 plots, a total of 1332 samples, mainly of Norway spruce (*Picea abies*) were analyzed independently by two statisticians. The cores covered 13 years before and 13 years after the smelter started operation giving a "before" and "after" comparison. There was broad agreement between the two statisticians and it was concluded that growth was reduced by about 20% up to about 4 km downwind but there was no effect beyond 8 km. However, the more interesting facts were that there was no clear functional relationship between foliar fluoride content and growth reduction, and that there was great variability between trees within plots and in adjacent plots. The presence of SO_2 was a complication but its influence on tree growth was not investigated. This illustrates that although tree ring analysis is potentially useful, it is important, if not essential, to have data on all of the potentially important environmental variables for each plot of trees. However, if there are several pollutants present and there is spatial variability in nutrients and other environmental stresses, it makes the statistical analysis more demanding.

Similar, but even more ambiguous results were obtained as a result of another study in Washington, USA [80]. In this case, there was a clear relationship between foliar leaf fluoride and reduction in ring growth of Douglas-fir (*Pseudotsuga menziesii*) but the authors drew attention to the presence of SO_2 as a complicating factor and suggested that fluoride and SO_2 interacted. They implied that this was the reason for large growth reductions in areas where the fluoride

Table 10. Estimated atmospheric fluoride concentrations and effects on western hemlock (*Tsuga heterophylla*) over two time periods (data from Bunce [82])

Period	Zone	Estimated HF ($\mu\text{g m}^{-3}$)	[F] in foliage (mg kg^{-1})	Change in basal area (%)	Change in wood volume (m^3)
1954–1973	Inner	3.42	271	–28.1	–12,703
	Outer	2.05	163	–19	–41,098
	Surround	1.3	104	–2.2	–4,212
1974–1979	Inner	109	87	–45.3	–3087
	Outer	0.34	29	2.8	+1192
	Surround	0.25	22	13.6	+4616

content of needles was relatively low. Because the SO_2 concentration was never measured, it was impossible to distinguish between effects of the two pollutants alone or in combination [80].

One of the most remarkable fluoride problems occurred in Kitimat, British Columbia, Canada, between 1956 (when a new aluminum smelter opened) and 1979. As a result of fluoride emissions (or one or more of many other factors present), there was an enormous outbreak of destructive insects in the area from 1961 until about 1969. Bunce [81] showed that growth reductions were evident until 1973 (after factoring out insect effects). They were estimated in three zones (termed “inner,” “outer,” and “surround”) as 28.1, 19.0, and 2.2%, respectively, and were associated with calculated atmospheric concentrations of 3.4, 2.1, and $1.3 \mu\text{g F m}^{-3}$. Astonishingly, when measured over a later period of greatly reduced emissions, Bunce [82] found that in the “outer” and “surround” zones, where the concentration was calculated to be 0.34 and $0.26 \mu\text{g F m}^{-3}$, growth appeared to be increased by 2.8 and 13.6%, respectively (Table 10). The apparent stimulation of growth by low concentrations of fluoride has been reported many times (see Ref. [12]) and this type of response from many toxic substances has been termed “hormesis.” However, the mechanism of this effect of fluoride is not known.

6. HOW SIGNIFICANT ARE POLLUTANT INTERACTIONS?

Perhaps the poorest understood area of air pollution, in general, is the joint action of two or more pollutants in combination, either sequentially or concurrently. Although the mechanisms of interaction at the metabolic level are not known, the mechanism by which one pollutant can alter the uptake of another pollutant, in the case of SO_2 , NO_2 , and O_3 , has been attributed to effects on diffusive conductance

of leaves [83]. The highly phytotoxic HF probably falls in the same category. Much is known about the effects of the common pollutants on stomatal conductance [84], but the complication is that SO₂, NO₂, and O₃ may both increase and decrease conductance, depending on the environment and the pollutant concentrations. So, for example, increased fluoride uptake might occur when it is present with low SO₂ and decreased uptake in high SO₂. In the case of joint action with NO₂, there is evidence that stomatal closure in the presence of NO₂ is offset by the effects of HF, which results in a greater fluoride accumulation [85]. Ozone has been reported [84] to reduce and increase stomatal conductance under different circumstances, but in general, reduction is more frequently reported so it would be expected to reduce fluoride uptake during episodes. Such episodes usually occur during warm, dry weather so leaves are often also water stressed to some degree and that also decreases stomatal conductance.

Each plant species appears to have its own distinct spectrum of responses to air pollutants, and for unknown reasons, it is not common for a species to be equally sensitive to two different pollutants. Giant ragweed (*Ambrosia trifida*) and lucerne (or alfalfa – *Medicago sativa*), for example, are very sensitive to SO₂, but are relatively tolerant to HF, while *Gladiolus* and Italian prune (*Prunus domestica* var. *italica*) are very sensitive to HF and relatively tolerant to SO₂. The developing needles of many pines (e.g., *P. sylvestris*), however, are sensitive to both pollutants. For a response to be understood of course, it must be studied experimentally, and the paucity of research is mostly responsible for our poor knowledge. On the other hand, those involved in studying interactions soon realize that the subject is very complex, for a number of reasons. The first problem is deciding on what concentrations of each pollutant should be used and what is to be measured: foliar lesions, growth, yield, or reproduction? The decisions affect the feasibility, design, and cost of the experiment. Two of the most important limitations are the lack of data on co-occurring pollutants in industrial atmospheres and the complex combinations of exposures that can occur when two or more pollutants occur sequentially. However, the most important problem, and it applies to all air pollutants, is a logistical one of how to devise a system for investigating the myriad of combinations of pollutants for anything other than two pollutants. Even three pollutants given at a single concentration involves eight combinations. Add to that the need for a minimum of three replicates, the expense of long-term exposures, and the costs become astronomical. This is an important problem because it is rare for there to be only a single pollutant in most atmospheres. For example, in atmospheres near aluminum smelters, HF is accompanied by variable concentrations of SO₂, O₃, and NO_x not to mention cryolite (Na₃AlF₆), several other fluoride-containing particles and considerable amounts of chlorine, chlorides, and hydrocarbons. A final problem is that the response to two pollutants, say, HF and SO₂, is different according to species, and probably variety. It is impossible to test all the combinations so we do not

know what happens for even one species when two or three pollutants are applied sequentially or concurrently, with the concentrations varying with time and meteorology.

So what is known about this difficult subject? Although there have been relatively few published accounts of the joint action of HF and other gaseous air pollutants, most of them consist of qualitative observations where the authors examined symptom expression, effects on growth, reproduction, and relative susceptibility of trees, crops, or ornamentals [86]. Continuous quantitative monitoring of the atmosphere was generally not available. There have been only a few experimental investigations of the joint action of HF with other gases, but they comprise such a paltry catalog as to limit what characterizes these joint actions.

Some pollutants are accumulated and metabolically transformed by plants, such as sulfur (from SO_2) and nitrogen (from NO_x), but others are broken down on entry to the leaf, such as ozone. Fluoride and sulfur are accumulated by plants as a nonessential and an essential element, respectively, but both are potentially toxic. Therefore, the accumulation of either element in combination is of importance, not only to the plant, but also, in the case of fluoride, to herbivores. If the accumulation is greater than additive, it constitutes an extra hazard to the consumers of these plants and they are exposed to an additional risk. If the accumulation is less than additive there would, of course, be reduced risk. The most consistent interactive effect reported has been a reduction in fluoride concentration by the presence of SO_2 (Table 11). In *Medicago sativa* (Mandl *et al.*, unpublished) the presence of SO_2 reduced the fluoride content, and the presence of HF reduced the sulfur content. In all cultivars of lucerne, the diffusive conductance to gas exchange was decreased by SO_2 as was the leaf temperature, which explains the interaction. Reduced fluoride accumulation in the presence of SO_2 has also been reported for citrus [87] and for maize by Mandl *et al.* [88]. Nitrogen dioxide, a relatively nonphytotoxic gas, was also found to reduce fluoride accumulation in maize when applied with $0.5 \mu\text{g HF m}^{-3}$, but not with $1.5 \mu\text{g HF m}^{-3}$ [85]. As O_3 commonly reduces gas exchange rates, a reduction in fluoride accumulation would be expected but it was unaffected in *Phleum pratense* and *Dactylis glomerata*, but was lower in perennial ryegrass (McCune, unpublished).

It is reasonable to expect that if a gaseous pollutant reduces the accumulation of fluoride, it should also reduce the incidence and severity of foliar lesions but there is little evidence to confirm this idea. In a controlled environment study, Mandl *et al.* [89] reported the occurrence of bifacial elliptical foliar lesions on maize in the presence of $400\text{--}790 \mu\text{g m}^{-3}$ of SO_2 , but when about $0.5 \mu\text{g m}^{-3}$ of HF was included, the number of lesions increased severalfold. These lesions occurred on a cultivar of maize that is more sensitive to HF than to SO_2 . When the experiments were repeated under field conditions [88], the same lesions

Table 11. Data on the joint action of pollutant gases on the fluoride content of plants. ↑, increase in concentration; ↓, decrease in concentration (modified from Weinstein and Davison [1])

Species	Effect	Authors [Ref.]
<i>Citrus</i>	↓ F accumulation	Matsushima & Brewer [87]
Sweet corn (<i>Zea mays</i>)	↓ F accumulation by ca. 30%	Mandl <i>et al.</i> [88]
	↓ F accumulation by ca. 40%	Mandl <i>et al.</i> [89]
Lucerne (<i>Medicago sativa</i>)	↓ F accumulation by ca. 30%	Brandt [90]
	↓ S accumulation by ca. 18%	
Millet (<i>Setaria italica</i>)	↓ F accumulation by ca. 20%	
Italian ryegrass (<i>Lolium multiflorum</i>)	↓ F accumulation	
<i>Gladiolus</i>	↓ F accumulation by ca. 34%	McCune [91]
<i>Lolium</i>	↓ F accumulation by ca. 24%	
Maize (<i>Zea mays</i>)	No effect	
Lucerne (<i>Medicago sativa</i>)	↓ F accumulation by ca. 24%	Mandl, cited by McCune [91]
	↓ S accumulation by ca. 18%	
Wheat (<i>Triticum aestivum</i>)	No striking effect on F accumulation, but	Murray and Wilson [92–94]; Davieson <i>et al.</i> [95]
Barley (<i>Hordeum vulgare</i>)	SO ₂ offset some of the effects of HF	
Soybean (<i>Glycine max</i>)		
Maize (<i>Zea mays</i>)		
Peanut (<i>Arachis hypogea</i>)	Concentrations of F low	
Bean (<i>Phaseolus vulgaris</i>)		
<i>Eucalyptus</i> spp (4)	↓ F accumulation in two species ↑ F accumulation in one species	
HF + NO ₂		

Table 11. Continued

Species	Effect	Authors [Ref.]
Maize, sweet corn (<i>Zea mays</i>)	↓ F accumulation with low [HF], no effect at higher	Amundson <i>et al.</i> [96]
Timothy grass (<i>Phleum pratense</i>)	↑ F accumulation	
Orchard grass (<i>Dactylis glomerata</i>)	↑ F accumulation	
HF + O ₃		
Timothy grass (<i>Phleum pratense</i>)	No effect	McCune (unpublished)
Orchard grass (<i>Dactylis glomerata</i>)	No effect	
Rye grass (<i>Lolium perenne</i>)	↓ F accumulation	
Radish (<i>Raphanus sativus</i>)	↑ F accumulation	
Maize, sweet corn (<i>Zea mays</i>)	↓ F accumulation	

were identified, but they were also observed on untreated plants. So, when a foliar symptom that occurs in an atmosphere containing HF + SO₂ can also occur from some unknown environmental variable, it raises the question if the joint action of the two pollutants is to sensitize the plant to a hitherto passive environmental factor. But in the experiments of Amundson *et al.* [96] using the same cultivar of maize, the elliptical lesions were not seen and typical fluoride-induced foliar injury was the result of exposure to 1.5 μg HF m⁻³. In other species, the predominant foliar symptoms were identical to HF injury, not to the other associated gas.

The joint action of HF with other pollutants is largely limited to the results shown in Table 11 because there has been very little work on growth or yield. In the environmental chamber studies of Mandl *et al.* [89] using HF and SO₂, there were no interactive effects on fresh or dry weight yields of maize. In comparable field experiments, however, there was a significant decrease in fresh and dry weights of stalks, and the effects were no greater than additive [88]. Research on these joint actions was terminated in the early 1980s for lack of funding and it is unlikely that it will be re-started because of the decline in fluoride and sulfur emissions.

7. HOW IMPORTANT ARE EFFECTS OF HF ON FERTILIZATION AND SEED SET?

One of the intriguing areas of research that remains relatively unexamined concerns the effects of fluoride on the fertilization process. When pollen is deposited on a receptive stigma surface, it hydrates, germinates, and pollen tubes grow down the style to fertilize the ovules. The process of tube growth is complex [97] but a key feature is that it is dependent on calcium gradients in the stigma and pollen tubes, and this makes the process susceptible to interference by fluoride. The effects of HF on fertilization and seed set were first described by two groups: Pack and his co-workers in the 1960s and 1970s [98–102] and by Facticeau [103,104]. After growing tomato plants at two levels of calcium (40 and 200 mg L⁻¹) and exposing them to 6.4 μg HF m⁻³ for 22 weeks, Pack [98] found that fruit size was related to both calcium and fluoride levels, the smallest fruit being in the low calcium + HF treatment, and that HF increased seedlessness. He concluded that calcium played an essential role in fertilization and that fluoride interfered with it. Pack [100] showed that exposure to HF as low as 0.55 μg m⁻³ caused a small increase in strawberry fruit deformation that was brought about by lack of development of seeds and associated receptacle tissue (the swollen, edible part of the fruit). This happened because normal receptacle growth takes place only if fertilization and normal embryo development occur. Work by Sulzbach and Pack [101] showed that fluoride affected pollen tube growth and fruit set in tomato, whereas Facticeau, Wang, and Rowe [103] reported fluoride interference with pollen growth in cherry. Further confirmation of the effects of fluoride on pollen was produced by Facticeau and Rowe's [104] work on Tilton apricot. Pollen germination *in vitro* was unaffected by sodium fluoride but in fumigated, pollinated flowers tube lengths and the percentage of styles in which the tubes reached the base were reduced by HF. The effect was greater for high concentrations given for short times than for the converse, lower concentrations for longer periods. They also commented that although Tilton apricot and Napoleon cherry were both classified as being of intermediate sensitivity on the basis of leaf injury, Tilton apricot is more sensitive in terms of pollen tube growth. A direct connection between HF, pollen tube growth, and calcium was made by Bonte *et al.* [105,106] when they examined the effects of HF on strawberry fruit development. Fruit deformity occurred much more frequently when carpels were exposed to HF than the pollen-producing anthers (Table 12). When carpels were exposed, 74% of the fruit were deformed but only 11% when the anthers were fumigated. They concluded that the stigmatic surface was altered by exposure to HF, affecting pollen tube growth and subsequent fertilization. Using an electron microprobe, they were able to show that there was a significant accumulation of fluoride on and just inside the stigmatic surface and that the fluoride disrupted the calcium gradient in the stigma and style [107].

Table 12. Effects of periods of fumigation with $5.4 \mu\text{g HF m}^{-3}$ on the % of malformed fruit and wt. per fruit of strawberry (after Bonte [106])

Combination of treatments	Period of treatment			Results	
	Before anthesis	Flowering/ fertilization	Maturation	Malformation (%)	Mean wt per fruit (g)
1	HF	HF	HF	57	3.47 a
2	HF	HF	CA	58	4.49 b
3	HF	CA	CA	1.3	5.58 c
4	CA	CA	CA	2.7	5.71 c
5	CA	CA	HF	5.4	5.56 c
6	CA	HF	HF	42	5.45 c

Note: Plants were fumigated at different times during development to give six combinations of treatment: 'HF' indicates stages when plants were fumigated and 'CA' indicates when they were in clean air. Means within a column followed by the same letter were not significantly different ($p = 0.05$).

Table 13. Differences in the fluoride content of leaves and fruit, and in the flowering, fruit set and seed production in blueberry growing in a transect from a phosphate fertilizer factory (data from Staniforth and Sidhu [108])

	Sites					
	A2	Td	A4	A5	A6	9B
Distance from factory (km)	1.4	4.6	5.8	8.6	10.3	18.7
Estimated mean [HF] in air ($\mu\text{g m}^{-3}$)	11.38	5.9	2.3	1.9	0.9	0.1
[F] in leaves (mg kg^{-1})	216	92	57	43	30	9
[F] in fruit (mg kg^{-1})	51	22	26	10	3	2
Leaf injured (%)	22	22	7.5	0	0	0
Flowers per plant	12.6a	15.2ab	14.8ab	16.4b	15.1ab	17.2b
Fruit set (%)	11	16	45	74	83	73
Seeds/fruit	17.6a	18.3a	28.8b	29.4b	33.0bc	41.8c

Note: The atmospheric concentrations of HF were estimated from deposition on alkali plates. Means followed by a different letter were significantly different ($p = 0.05$).

This graphic use of a microprobe demonstrates the potential of the technique in fluoride research but unfortunately it has been little used.

There is no reason to suppose that crops such as strawberry are unique in their reaction to fluoride but there appears to be only one study of fruiting and fruit/seed set in wild plants. It concerned conifers, raspberry, and blueberry [108,109]. The authors recorded reproductive performance in a transect downwind of a

phosphate fertilizer factory that emitted fluorides. Within a few kilometers of the factory the conifers were so badly damaged that it was impossible to tell if the effects on cones and seeds of conifers were indirect and due to massive growth loss, or direct and due to interference with the fertilization process. However, the data were clearer for blueberry (Table 13). In this species, leaves were injured within about 6 km of the factory but it was not very severe at that distance. Leaf fluoride contents were elevated all the way along the transect up to 10 km but fruit concentrations were relatively low. This is normal and it happens because of limited uptake by the fruit and the very low surface-volume ratio of the fruit [1]. However, the interesting data are the number of flowers per plant, the percentage of fruit set and number of seeds per fruit. Although it is impossible to conclude with certainty that differences were due to an effect of HF on the fertilization process, the fact that the number of flowers per plant was very little affected but fruit set and seed numbers were, are consistent with the idea. They indicate that there should be more studies of this type. With the appropriate examination of pollen tube growth in the plants in the field, it should be possible to confirm effects and to estimate the critical exposure that affects fertilization. Biologists might ask if there are subtle effects of HF on the seed set of wild species that are being missed because they are not so obvious. Which species are most sensitive to disruption of pollen tube growth? Are wind-pollinated species sensitive because they have huge stigmatic surfaces that are fully exposed to the air? They would certainly be good candidates for future research. If there are effects of HF on pollen tube growth, we must consider whether there is a potential effect on natural selection. Pollen tubes growing down a stigma compete in the race to fertilize ovules; the fastest growing grain fertilizes the ovule, so its genetic material will be passed on to the next generation. So if pistils or pollen differ in their sensitivity to HF, this may present a rapid method for natural selection to occur. The intriguing question that this raises is the genetic makeup of the selected adult. What adult characters might be inherited with the DNA from a fluoride resistant pollen grain?

8. WHAT DO WE KNOW ABOUT FLUORIDE AND INSECTS?

Insects are vitally important components of ecosystems, pollinating flowers, acting as food for other animals and playing vital roles in decomposition and nutrient cycling. Many are serious pests, yet little is known concerning the effects of atmospheric fluoride on insects, and their interaction with plants. How does fluoride affect the susceptibility of plants to insects and what are the effects of fluoride on the plants and the population of insects that it supports? There are three kinds of evidence for effects on insects that we can examine: correlations and observations, partially controlled experiments, and controlled experiments.

Together they show that there are some important effects but they also reveal apparent conflicts and highlight the importance of the need for further research on bioavailability to, and mode of action of fluoride on, insects.

There have been numerous published observations of insect populations (and other invertebrates) in the vicinity of fluoride sources and, as one might expect, many of them reported increased fluoride concentrations at various trophic levels [1]. Many conclude that they have observed decreases while others have reported increases in insect populations in relation to fluoride. However, few have provided information on either the composition of the atmosphere or of the other environmental conditions under which the effects occurred. A weakness of all these field observations is that it is not possible to separate the effects of fluoride from all the other possible environmental factors that can affect insect populations. We consider that observations and correlations like these are best used as starting points for research so in this discussion we focus on the next step, semi-controlled and controlled experiments.

Davies *et al.* [110] and Port *et al.* [111] worked with pine sawfly (*Diprion pini*) larvae collected in the field and a laboratory strain of the large white butterfly, *Pieris brassicae* respectively. Pine sawfly larvae were collected from the vicinity of an aluminum smelter and then reared in the laboratory on pine needles. Davies *et al.* [110] found that although the fluoride content of the needles was up to 170 mg kg^{-1} , and whole larvae initially contained up to 219 mg kg^{-1} , pupae contained no detectable fluoride. Also, there was no relationship between the fluoride content of the diet and pupal weight. A mass balance showed that 46% of the fluoride in the larvae was in transit in the digestive system and 23% was surface deposit. The larvae of *P. brassicae* showed a similar low rate of fluoride retention and there was no effect of up to 500 mg F kg^{-1} on growth or development [111]. These data indicate that in these species fluoride had no detectable effect because retention was very low. This in turn was probably because the high pH of herbivorous insect digestive systems produces the anion F^- , which has minimal bioavailability.

In contrast, there are several semi-controlled and controlled studies that have shown significant effects of fluoride. One of the first attempts at a controlled experimental study was on the growth and fecundity of the Mexican bean beetle (*Epilachna varivestis*) feeding on HF-fumigated bean plants over several generations [112]. Three major components of the plant-insect system, growth, development, and reproduction were each affected detrimentally. Growth of larvae was reduced by about half in each of the five successive generations and for unknown reasons, adult males were affected less than adult females. Although leaves of bean plants were not washed before their introduction to the beetles, one can presume that most of the fluoride ingested was from internal not external fluoride. So severe effects were found on growth, development, and reproduction in each of the five generations.

Table 14. Pupal weight of *Trichoplusia ni* after feeding larvae on noncabbage and cabbage diets containing fluoride (modified from Hughes *et al.* [113])

Treatment	[F] in diet	Mean pupal weight (mg)			
		Noncabbage diets		Cabbage diets	
		Male	Female	Male	Female
Control	10	232.7	215.5	238.9	217.5
NaF	60	219.9	208.5	236.8	216.5
NaF	210	186.8	178.5	218.8	212.5

Experiments with cabbage looper (*Trichoplusia ni*) larvae demonstrated effects of fluoride but also resulted in unanswered questions [113]. Larvae were cultured on two kinds of medium. When the larvae were raised on an artificial diet with sodium fluoride added, the results were as expected; a reduction in growth, survival, and pupal weight. However, addition of cabbage leaves reduced toxicity (Table 14). Fluoride added as HF-fumigated cabbage had no effect, even when the concentration in the diet was as high as 438 mg F kg^{-1} . Both treatments reduced the concentration of fluoride retained by the insects which was probably due to fluoride complexing with components of the leaf tissue and reducing availability.

One of the most examined cases, using field observations, semi-controlled, and controlled experiments involves the silkworm, *Bombyx mori*. The toxicity of fluoride-contaminated mulberry leaves to silkworm larvae has been recognized for decades and fluoride pollution has been a challenge to commercial silk production in China, Japan, and India. Several field studies have shown correlations between fluoride and changes in silkworms [114–118] while experimental feeding studies indicate that silkworm larvae are extremely sensitive to fluoride. It alters feeding rates, softens the cuticle, and reduces growth rate or may even cause death (see Ref. [1] for details). Metabolic studies in general indicate that fluoride affects not only larval metabolism [119], but also the nutritional quality of the larval food, the mulberry leaf. Food conversion efficiency may also be affected [120]. Wang and Bian [121] found that the toxicity threshold concentration in mulberry leaves is about 30 mg kg^{-1} dry wt), and the lethal dose is between 120 and 200 mg kg^{-1} . No mortality occurred up to 30 mg kg^{-1} , but between 30 and 50 mg kg^{-1} , the mortality was more than 30%. These studies provide a convincing example of fluoride toxicity to insects.

Overall, research on the effects of fluoride on insects has thrown up evidence that some species may be affected but others not, and there are some puzzling, unexplained results. In some species such as pine sawfly absorption of fluoride appears to be minimal so that it is extremely tolerant, yet cabbage looper larvae show a difference between fluoride presented in an artificial diet and presented in

cabbage. Silkworm larvae are intolerant to leaf fluoride contents higher than 30 mg kg^{-1} so these differences need to be explained. For this it is essential to investigate the bioavailability of fluoride to different species and, in particular, the mechanisms underlying toxicity and tolerance. Some recent work in China offers a possible system for making progress in both of these fields. Chen *et al.* [122] and Xu *et al.* [123] have investigated the fluoride tolerance of silkworms and have reported differences in tolerance between strains. This is probably the first research to demonstrate that there are within-species differences in fluoride tolerance in insects. The phenomenon is well known for plants, but not for animals. The same authors have also identified a molecular marker of fluoride tolerance and plan to use it to assist breeding programs. This not only offers the possibility of producing fluoride tolerant strains but also demonstrates that molecular methods could provide excellent tools for investigating bioavailability and the toxic mechanisms of fluoride in insects.

9. THE INCREASING IMPORTANCE OF ORGANOFLUORINE COMPOUNDS TO ANIMALS

There are about 30 organofluorine compounds of natural origin [124] but over a million have been manufactured by chemists, and the number continues to rise [125,126]. Natural organofluorine compounds are the result of geological and biological processes while the production of the huge number of manufactured compounds is due to the fact that fluorination produces properties that are invaluable to medicine, agriculture, and industry. Although most natural organofluorides are restricted in their distribution, almost everyone has contact with a range of manufactured compounds. Some have appeared in remote regions of the biosphere such as Antarctica.

The first naturally occurring organofluoride to be identified was monofluoroacetate [127]. This was the result of many years of investigation into the toxic principle of poisonous African plants of the genus *Dichapetalum*. Later, other species were found to contain the same compound and a few were also found to contain ω -fluorinated fatty acids. All of these compounds are highly toxic to mammals but they have been reported as occurring in only a few genera in South Africa, Australia, and South America (Table 15). Nevertheless, their effects on livestock health and human social history have been profound [1]. In Australia, for example, monofluoroacetate played a major part in controlling European settlement of western regions and they continue to kill large numbers of sheep and cattle.

An obvious feature of the list in Table 15 is that the species are in several families that are separated both geographically and in the evolutionary sense. There are many species of *Gastrolobium* and a number of *Dichapetalum* species that produce organofluorides but *Acacia georginae* and *Palicourea marcgravii* are

Table 15. Species known to contain toxic organofluorides, mostly in the form of monofluoroacetate (data from Weinstein and Davison [1] with additions)

Genus/species	Family	Region/country
<i>Gastrolobium</i> , <i>Oxylobium</i> , <i>Nemcia</i> (the latter two genera are now included in <i>Gastrolobium</i>)	Fabaceae	Australia
<i>Acacia georginae</i>	Mimosaceae	Australia
<i>Cyamopsis</i> <i>tetragonolobus</i>	Fabaceae	India, Pakistan, grown as a crop in many countries
<i>Dichapetalum</i>	Dichapetalaceae	Tropics: Africa, Borneo, China, Philippines, Brazil, Mexico
<i>Palicourea marcgravii</i>	Rubiaceae	Brazil
<i>Arrabidaea bilibiata</i>	Bignoniaceae	Brazil
<i>Spondianthus preussii</i>	Anacardiaceae	Cameroon, Niger, Ivory Coast

the only members of large genera that are known to produce these compounds. *Cyamopsis tetragonolobus* is unusual in that it is widely cultivated as a crop and used as cattle fodder. A product, guar gum, is used in dairy products such as ice cream and as a stabilizer in cheese and cold-meat processing. The fluoroacetate content [128] is reported as being very low (0.07–1.42 µg fluoroacetic acid g⁻¹), much lower than most of the species in Table 15 apart from *Palicourea marcgravii*. Vartiainen and Gynther [128] state that ‘the low concentrations of fluoroacetate ... dispel any considerations about possible health risks associated with fluoroacetate during the prolonged use of guar gum.’

The fact that unrelated species have the capacity to synthesize fluorinated organic compounds indicates that it has evolved independently several times. Research in Australia suggests that accumulation of fluoroacetate evolved as a defense mechanism against herbivores and that, in common with other plant defense systems, some animals have evolved tolerance [129–133]. The circumstances that lead to one species in a genus evolving the capacity to manufacture and tolerate monofluoroacetate while related species living in the same region do not, are not known. The fact that the capacity to synthesize organofluorides has evolved several times may also mean that there are differences in the metabolic pathways between species but the pathway or pathways are still not clearly defined. The problem in investigating the biochemistry of these compounds in

plants is that some of the species are difficult to cultivate, are slow growing, and the concentrations of organofluorides are very low. *Cyamopsis tetragonolobus* is a fast growing annual but the concentrations are very low, which may limit its use for investigations. Until recently the analytical detection and quantification of organofluorides was also difficult. Furthermore, the half-life of fluorine isotopes is too short to be of much use in tracing biochemical pathways.

Organofluorine accumulation by plants is known because of the toxicity of monofluoroacetate to livestock and humans so attention has focused on those species. However, it is possible that organofluorides also occur in other species, particularly those that are not eaten by livestock or, as in the case of *Cyamopsis tetragonolobus*, in concentrations that are too low to be toxic. In Australia, symptoms of toxicity are well known so it is unlikely that there are any new families or genera that wait to be discovered there. Similarly, in Africa *Dichapetalum* has been investigated but it is a large genus that is found across the warmer latitudes, including places as far apart as Borneo and Mexico. There are no reports of members of this genus being toxic outside of Africa (Prance personal communication) but there have been no systematic searches for the compounds in other countries. In South America, fluoroacetate has been identified in two unrelated species but again, there has not been a thorough search for others in the same genera or families. *Palicourea marcgravii*, the better known of the two, is a member of a large genus and some are used medicinally so there may be other species that also contain fluoroacetate. Bearing in mind the species richness of South America and tropical Asia, it would seem to be unlikely that there are not other species of organofluoride accumulators in those regions.

There are three known organofluorine compounds of microbial origin: the antibiotic nucleocidin (4'-fluoro-5'-O-sulfoamoyl-adenosine), 4-fluorothreonin, and monofluoroacetate. All were discovered accidentally during research on antibiotics. Nucleocidin was isolated in 1957 from *Streptomyces calvus* that was obtained from an Indian soil sample but it was not until much later that it was realized that it contained a fluorine atom. The metabolite has not been re-isolated from cultures so it is impossible to elucidate the fluorination mechanism [134]. This is unfortunate because O'Hagan and Harper [134] have suggested that, because of the location of the fluorine atom on the ribose moiety, the fluorination process in this organism may be different from that in other organisms. Clearly, efforts to re-isolate the organism from soil are needed but it may never be available again for laboratory study [134]. The other two microbial compounds, 4-fluorothreonin and fluoroacetate, were discovered in *Streptomyces cattleya* [135]. This isolate is still available and it has provided a useful system for the investigation of organofluorine synthesis in microorganisms. However, in relation to our present concern, fluorides in the environment, it is not known if either *S. calvus* or *S. cattleya* produces organofluorine compounds in nature or if they have any environmental significance.

Organofluorides produced by geological processes are mostly of more recent discovery. They have been reported as occurring in minerals such as fluorite and in emissions from volcanic gas and thermal springs [124]. At present, over 20 have been identified, including a number of fluoroalkanes with climate forcing potential such as perfluoromethane, CF_4 (CFC-14). There are still questions about the quantities of some of the geological compounds that are emitted and analytical problems such as ways of extracting them without altering their chemical composition and preventing contamination of samples. However, readers are recommended to consult Gribble [124] who summarized the unresolved issues relating to these compounds, notably questions on the origin of the carbon and the mechanisms of their formation.

Manufactured organofluorides include pharmaceuticals, insecticides, pesticides, fluoropolymer fabrics, surfactants, refrigerants, aerosol propellants, non-stick surfaces for cookware, and chemical resistant tubing [1]. Some of these, such as inhalation anesthetics and insecticides are released directly into the atmosphere but many are solid and end up in land fill or incinerators. Agrochemicals in particular find their way into the soil and in some cases water bodies. For many years there was no great concern about the environmental fate or effects of manufactured organofluorides but the well-known case of chlorofluorocarbons (CFCs) changed that position. They had an enormously beneficial effect on the lives of millions of people but they were eventually shown to persist in the stratosphere, have serious effects on the ozone layer and to contribute to climate forcing (see Ref. [1] for a historical account). This highlighted the persistence of some organofluorides and demonstrated the need for greater vigilance and risk assessment in relation to the environment.

The chemical transformations and fate of manufactured organofluorides in the environment vary greatly but they can be considered as falling into two categories: (1) those that are readily defluorinated and biodegradable and (2) those that are resistant to defluorination and biodegradation. Based on research on mono-fluoroacetate and on the breakdown products of fluorinated inhalation anesthetics and hydrochlorofluorocarbons [136] the evidence suggests that mono- and di-fluoro methyl groups are readily defluorinated by biological means. For example, the old anesthetic methoxyflurane ($\text{CHCl}_2\text{-CF}_2\text{-O-CH}_3$) breaks down in the body to produce oxalic acid and inorganic fluoride, while extensive studies in New Zealand and Australia have shown that when monofluoroacetate is used as a rodenticide, it rapidly breaks down in soil [137–140]. This rapid defluorination means that in general compounds in which the fluorine is present in mono- and di-fluoro methyl groups do not accumulate and probably have little environmental impact. In contrast, many agrochemicals and pharmaceuticals contain tri-fluoro methyl groups while solids such as fabrics, insulation, tubing, and cookware linings are fluoropolymers. These are resistant to defluorination in the environment and have limited, if any, biodegradability. This was brought home by

research into the breakdown of hydrochlorofluorocarbons (HCFCs), the replacements for CFCs [136]. The HCFC risk assessment identified one of the important breakdown products as being trifluoroacetic acid (TFA). The risk assessment [128] also showed that although TFA has low animal and plant toxicity, it is not defluorinated in soils or water so it accumulates in the aquatic environment [141]. By the mid-1990s it was clear that TFA was detectable in the air, rain, fresh water, and oceans in most parts of the world. There are two other known sources of this compound, the breakdown of some inhalation anesthetics and the combustion of fluoropolymers but calculations showed that the concentrations and the total amount in the biosphere were far higher than could be accounted for by all the known industrial sources [136]. Frank *et al.* [141] concluded that the source of the massive reservoir of TFA in the oceans is ancient and that it pre-dates industry. They consider that the oceans are a final sink for a natural source whose nature is unknown and that the TFA in the other compartment is mostly of anthropogenic origin.

The research on HCFCs and TFA happened because of the effects of CFCs and the concern that they generated but there has not been comparable interest in the many thousands of other persistent organofluorides. The first indication that organofluorides can be transferred from the immediate area of their use started with a report by Taves [142] of the occurrence of an organofluorine component in human serum. The analytical procedure available at the time was not specific but the observation was later confirmed and in 1976 the use of NMR

Table 16. Examples of the concentrations of perfluoro-octane sulphonate (PFOS, $C_8F_{17}SO_3$) found in various animal tissues (data from Geisy and Kannan [144])

Group	Species	Location	Tissue	<i>N</i>	Range of concentrations (ng g ⁻¹ wt tissue)
Birds	Polar skua	Antarctica	Plasma	2	< 1–14
	Black-tailed gull	Hokkaido, Japan	Plasma	24	2–12
	Cormorant	Italy	Liver	12	33–740
	Bald eagle	Mid-west USA	Plasma	26	1–2570
Fish	Yellow-fin tuna	North Pacific	Liver	12	< 7
	Blue-fin tuna	Mediterranean	Liver	8	21–87
	Chinook salmon	Michigan, USA	Liver	6	22–170

suggested that the compound might be perfluoro-octanoic acid, which is used in the manufacture of fluoropolymers [143]. More recent work using better analytical techniques has revealed that a number of perfluoro compounds occur in the serum of the general population and in animal tissues collected in regions that are remote from industry and human habitation (Table 16). This work, principally by Geisy and Kannan and colleagues [144–150] demonstrated that compounds that we might think of as being restricted to industrial and urban situations, do in fact find their way into most parts of the biosphere. The pathways and rates of movement are not known and much more information is needed on the animal toxicity. Geisy and Kannan [145] concluded that “*knowledge of the critical mechanisms of toxic effects is needed to select appropriate endpoints and biomarkers of functional exposure and to assess complex PFC (perfluoro chemical) mixtures and their relationship to one another and to other environmental residues.*” The same can be said for other groups of fluorinated compounds such as the residues from herbicides, pesticides, and pharmaceuticals so we finish by supporting Key, Howell, and Criddle [151] who concluded that “*Research is needed to assess the fate and effects of non-volatile fluorinated organics, the fluorinated impurities in commercial formulations....*”

REFERENCES

- [1] L.H. Weinstein, A.W. Davison, Fluorides in the Environment: Effects on Plants and Animals, CABI, Wallingford, UK, 2002.
- [2] National Academy of Sciences, Effects of Fluorides in Animals. A Report Prepared by the Committee on Animals Nutrition, National Academy of Sciences, Washington, DC, 1974.
- [3] A. Kabata-Pendias, Trace Elements in Soils and Plants, 3rd ed, CRC Press, New York, 2001.
- [4] J. Cooke, M. Johnson, A. Davison, A. Bradshaw, Fluoride in plants colonising fluorspar mine waste in the Peak District and Weardale, Environ. Pollut. 11 (1976) 9–23.
- [5] N.A. Geeson, P.W. Abrahams, M.P. Murphy, I. Thornton, Fluorine and metal enrichment of soils and pasture herbage in the old mining areas of Derbyshire, UK, Agriculture, Ecosystems Environ. 58 (1998) 217–231.
- [6] W.O. Robinson, G. Edgington, Fluorine in soils, Soil Sci. 61 (1946) 341–353.
- [7] J.A.I. Omueti, R.L. Jones, Fluorine distribution with depth in relation to profile development in Illinois, J. Soil Sci. Soc. Am. 44 (1980) 247–249.
- [8] P. Loganathan, G.C. Hedley, G.C. Wallace, A.H.C. Roberts, Fluoride accumulation in pasture forages and soils following long-term application of phosphorus fertilisers, Environ. Pollut. 115 (2001) 275–282.
- [9] G.D. Gemmell, Fluorine in New Zealand soils, New Zealand J. Sci. Technol. 27 (1946) 302–306.
- [10] H. Nommik, Fluorine in Swedish agricultural products, soils and drinking water, Acta Polytech. 12 (1953) 1–121.
- [11] M. Piotrowska, K. Wiacek, Fluorine content in some Polish soils, Roczniki Nauk Rolniczych 101A (1975) 93.
- [12] L.H. Weinstein, Fluoride and plant life, J. Occup. Med. 19 (1977) 49–78.

- [13] A.W. Davison, in: J.L. Shupe, H.B. Peterson, N.C. Leone (Eds.), *Fluorides: Effects on Vegetation, Animals and Humans*, Paragon Press, Salt Lake City, 1983, pp. 62–82.
- [14] D.P. Stevens, M.J. McLaughlin, P.J. Randall, G. Keerthisinghe, Effect of fluoride supply on fluoride concentrations in five pasture species: Levels required to reach phytotoxic or potentially zootoxic concentrations in plant tissue, *Plant Soil* 227 (2000) 223–233.
- [15] S. Takmaz-Nisancioglu, A.W. Davison, Effects of aluminium on fluoride uptake by plants, *New Phytol.* 109 (1988) 149–155.
- [16] A.W. Davison, S. Takmaz-Nisancioglu, I.F. Bailey, in: A.K. Susheela, (Ed.), *Fluoride Toxicity*, ISFR, New Dehli, 1985, pp. 30–46.
- [17] B. Bar-Yosef, R. Rosenberg, Response of corn and tomato to fluorine concentration in solution culture, *Agronomy J.* 80 (1988) 173–177.
- [18] D.P. Stevens, M.J. McLaughlin, A.M. Alston, Phytotoxicity of hydrogen fluoride and fluoroborate and their uptake from solution culture by *Lycopersicon esculentum* and *Avena sativa*, *Plant Soil.* 200 (1998) 175–184.
- [19] S. Larsen, A. Widdowson, Soil fluorine, *J. Soil Sci.* 22 (1971) 210–221.
- [20] L.K. Thompson, S.S. Sidhu, B.A. Roberts, Fluoride accumulation in soils and vegetation in the vicinity of a phosphate plant, *Environ. Pollut.* 18 (1979) 221–234.
- [21] W.F. Pickering, The mobility of soluble fluoride in soils, *Environ. Pollut. (Series B)* 9 (1985) 281–308.
- [22] S.S. Sidhu, Fluoride deposition through precipitation and leaf litter in a boreal forest in the vicinity of a phosphorus plant, *Sci. Total Environ.* 123 (1982) 205–214.
- [23] J. Polomski, H. Flühler, P. Blaser, In Proceedings of a Symposium on Effects of Air Pollutants on Mediterranean and Temperate Forest Ecosystems. General Technical Report PSW-43, Pacific Southwest Forest and Range Experiment Station, Forest Service, U.S. Department of Agriculture, Berkeley, CA, 1980, p. 246.
- [24] L. Bégin, J. Fortin, Evaluation of an acid ammonium oxalate extraction to determine fluoride resident concentrations in soils, *J. Environ. Quality* 32 (2003) 662–673.
- [25] A.K.M. Arnesen, Effect of fluoride pollution on pH and solubility of Al, Fe, Ca, Mg, K and organic matter in soil from Årdal (Western Norway), *Water, Air Soil Pollut.* 103 (1998) 375–388.
- [26] D.P. Stevens, M.J. McLaughlin, A.M. Alston, Phytotoxicity of aluminium–fluoride complexes and their uptake from solution culture by *Avena sativa* and *Lycopersicon esculentum*, *Plant Soil* 192 (1997) 81–93.
- [27] S.N. Braen, L.H. Weinstein, Uptake of fluoride and aluminum by plants grown in contaminated soils, *Water, Air Soil Pollut.* 24 (1985) 215–223.
- [28] Anonymous, *The Norwegian Aluminium Industry and the Local Environment*, Aluminiumindustri Miljøsekretariat, Oslo, 1994.
- [29] S.S. Sidhu, A summer of vegetation recovery near a phosphorus plant, Long Harbour, Newfoundland, *Bimonthly Res. Notes* 32 (1976) 16–17.
- [30] R. Hornvedt, Fluoride uptake in conifers related to emissions from aluminium smelters in Norway, *Sci. Total Environ.* 163 (1995) 35–37.
- [31] A.W. Davison, in: M.H. Unsworth, D.P. Ormrod (Eds.), *Effects of Gaseous Air Pollution in Agriculture and Horticulture*, Butterworths, London, 1982, pp. 267–292.
- [32] F. Vike, A. Håbjørg, Variation in fluoride content and leaf injury on plants associated with aluminum smelters in Norway, *Sci. Total Environ.* 163 (1995) 25–34.
- [33] F. Murray, Effects of long-term exposure to hydrogen fluoride on grapevines, *Environ. Pollut.* 36 (1984) 337–349.
- [34] J. Blakemore, Fluoride deposition to grass swards under field conditions. PhD Thesis, University of Newcastle, Newcastle upon Tyne, England, 1978.
- [35] L.J. Van der Eerden, Fluoride-accumulatie in gras: voorgangsverlag, no 1. Report no. R256, Research Institute for Plant Protection, Wageningen, The Netherlands, 1981.

- [36] A.W. Davison, J. Blakemore, C. Craggs, The fluoride content of forage as an environmental quality standard for the protection of livestock, *Environ. Pollut.* 20 (1979) 279–296.
- [37] P.W. Zimmerman, A.E. Hitchcock, Fluorine compounds given off by plants, *Am. J. Bot.* 33 (1946) 233.
- [38] L.H. Weinstein, Effects of atmospheric fluorides on metabolic constituents of tomato and bean leaves, *Contrib Boyce Thompson Inst.* 21 (1961) 215–231.
- [39] A.E. Hitchcock, L.H. Weinstein, D.C. McCune, J.S. Jacobson, Effects of fluorine compounds on vegetation, with special reference to sweet corn, *J. Air Pollut. Control Assoc.* 14 (1964) 503–508.
- [40] R. Guderian, H. van Haut, H. Stratmann, Experimentelle Untersuchungen über Pflanzenschädigende Fluorwasserstoff-Konzentrationen, *Fortschritte der Landesanstalt Nordrhein-Westfalen* 2017 (1969) 54.
- [41] W. Knabe, Natural loss of fluorine from leaves of Norway spruce (*Picea abies* Karst.), *Staub-Reinhaltung der Luft* 30 (1970) 29–32.
- [42] A.E. Hitchcock, D.C. McCune, L.H. Weinstein, D.C. MacLean, J.S. Jacobson, R.H. Mandl, Effects of hydrogen fluoride fumigation on alfalfa and orchard grass: A summary of experiments from 1952 through 1965, *Contrib. Boyce Thompson Inst.* 24 (1971) 363–386.
- [43] G. Georgsson, G. Petursson, Fluorosis of sheep caused by the Hekla eruption in 1970, *Fluoride* 5 (1972) 58–66.
- [44] A.W. Davison, J. Blakemore, in: T.A. Mansfield, (Ed.), *Effects of Air Pollutants on Plants*, Cambridge University Press, Cambridge, 1972, pp. 17–30.
- [45] M. Ghiasseddin, J.M. Hughes, J.E. Diem, J.W. Mason, Accumulation of fluoride by the soybean (*Glycine max* L. Merrill var Dare): II. Accumulation in leaves, fruit, and seeds, *J. Plant Nutr.* 3 (1981) 441–456.
- [46] L.N. Less, A. McGregor, L.H.P. Jones, D.W. Cowling, E.L. Leafe, Fluoride uptake by gas from aluminium smelter fume, *Internat. J. Environ. Studies* 7 (1975) 153–160.
- [47] M.D. Ledbetter, R. Mavrodineanu, A.J. Weiss, Distribution studies of radioactive fluorine-18 and stable fluorine-19 in tomato plants, *Contrib. Boyce Thompson Inst.* 20 (1960) 331–348.
- [48] W. Kronberger, G. Halbwachs, Distribution of fluoride in *Zea mays* grown near an aluminum plant, *Fluoride* 12 (1978) 129–135.
- [49] W. Kronberger, G. Halbwachs, H. Richter, Fluoride translocation in *Picea abies* Karsten, *Angewante Botanik* 52 (1978) 149–154.
- [50] L.H. Weinstein, R. Alscher-Herman, Physiological responses of plants to fluorine, in: M.H. Unsworth, D.P. Ormrod (Eds.), *Effects of Gaseous Air Pollution in Agriculture and Horticulture*, Butterworths, London, 1982, pp. 139–167.
- [51] S. Takmaz-Nisancioglu, Dynamics of fluoride uptake, movement and loss in higher plants. PhD Thesis, University of Newcastle upon Tyne, England, 1983.
- [52] J.P. Garrec, S. Chopin, Mise en evidence d'un dégagement de fluor gazeux par les végétaux soumis à une pollution fluorée, *Environ. Pollut. Series A* 30 (1983) 201–210.
- [53] D. Doley, *Plant-Fluoride Relationships. An Analysis with Particular Reference to Australian Vegetation*, Inkata Press, Melbourne, 1986.
- [54] L.H. Weinstein, A.W. Davison, Native plant species suitable as bioindicators and biomonitors for airborne fluoride, *Environ. Pollut.* 125 (2003) 3–11.
- [55] W. Borsdorf, Beiträge zur Fluorschädendiagnostik. 1. Fluorschäden-Weiserpflanzen in der Wildflora, *Phytopathologische Zeitschrift* 38 (1960) 309–315.
- [56] J. Bossavy, Échelons de sensibilité au fluor, *Revue Forestière Française* 17 (1965) 205–211.
- [57] A. Bolay, E. Bovay, Observations sur la sensibilité aux gazes fluorés de quelques espèces végétales du Valais, *Phytopathologie Zeitschrift* 53 (1965) 289–298.

- [58] M. Treshow, M. Pack, Fluoride, In Recognition of Air Pollution Injury to Vegetation: A Pictorial Atlas, Informative Report 1, TR-7 Agricultural Committee Air Pollution Control Association, Pittsburgh, PA, 1970, pp. D1–D77.
- [59] H.G. Dässler, H. Raft, H.K. Rein, Zur Widerstandsfähigkeit von Geholzen gegenüber Fluorbidungen und Schwefeldioxid, *Flora (Jena)* 161 (1972) 289–302.
- [60] L.H. Weinstein, A.W. Davison, U. Arndt, Fluoride, in: R.B. Flagler, (Ed.), Recognition of Air Pollution Injury to Vegetation. A Pictorial Atlas(2nd edition), Air and Waste Management Association, Pittsburgh, PA, 1998, pp. 4-1–4-27.
- [61] L.H. Weinstein, K.S. Hansen, Relative susceptibility of Brazilian vegetation to airborne fluoride, *Pesquisa Agropecuaria Brasileira* 23 (1988) 1125–1137.
- [62] K. Mellanby, *Ecological Indicators for the Nation*, National Academy Press, Washington, DC, 2000.
- [63] A.E. Hitchcock, P.W. Zimmerman, R.R. Coe, Results of ten years' work (1951–1960) on the effect of fluorides on gladiolus, *Contrib. Boyce Thompson Inst.* 21 (1962) 303–344.
- [64] A.E. Hitchcock, P.W. Zimmerman, R.R. Coe, The effect of fluorides on milo maize (*Sorghum* sp.), *Contrib. Boyce Thompson Inst.* 22 (1963) 175–206.
- [65] D.C. McCune, A.E. Hitchcock, J.S. Jacobson, L.H. Weinstein, Fluoride accumulation and growth of plants exposed to particulate cryolite in the atmosphere, *Contrib. Boyce Thompson Inst.* 23 (1965) 1–12.
- [66] R.H. Mandl, L.H. Weinstein, M. Keveny, A cylindrical open top chamber for the exposure of plants to air pollutants in the field, *J. Environ. Qual.* 2 (1973) 371–376.
- [67] A.S. Heagle, D.E. Body, W.W. Heck, An open top chamber to assess the impact of air pollution on plants, *J. Environ. Qual.* 2 (1973) 365–368.
- [68] A.R. McLeod, K. Alexander, P. Hatcher, Open-air fumigation of field crops: Criteria and design for a new experimental system, *Atmos. Environ.* 19 (1985) 1639–1649.
- [69] A.R. McLeod, C.K. Baker, in: W.W. Heck, O.C. Taylor, D.T. Tingey (Eds.), *Assessment of Crop Loss from Air Pollutants*, Elsevier, UK, 1988, pp. 181–210.
- [70] L.H. Allen Jr., Free air CO₂ enrichment experiments: An historical overview, *Crit. Revs. Plant Sci.* 11 (1992) 121–134.
- [71] R.J. Norby, K. Kobayashi, B.A. Kimball, Commentary: Rising: CO₂ – future ecosystems, *New Phytol.* 150 (2001) 215–221.
- [72] D.C. MacLean, R.E. Schneider, Effects of gaseous hydrogen fluoride on the yield of field-grown wheat, *Environ. Pollut.* 24 (1981) 39–44.
- [73] F. Murray, Response of grapevines to fluoride under field conditions, *J. Am. Soc. Hort. Sci.* 108 (1983) 526–529.
- [74] D.C. MacLean, R.E. Schneider, D.C. McCune, Effects of chronic exposure to gaseous fluoride on field-grown bean and tomato plants, *J. Am. Soc. Hort. Sci.* 102 (1977) 297–299.
- [75] D.C. MacLean, D.C. McCune, R.H. Schneider, Growth and yield of wheat and sorghum after sequential exposures to hydrogen fluoride, *Environ. Pollut.* 36 (1984) 351–365.
- [76] R. Zahn, Wirkungen von Schwefeldioxid auf die Vegetation, Ergebnisse aus Begasungsversuchen, *Staub-Reinhalt. Luft* 21 (1961) 56–60.
- [77] D.C. MacLean, L.H. Weinstein, D.C. McCune, R.E. Schneider, Fluoride-induced suture red spot in 'Elberta' peach, *Environ. Exp. Bot.* 24 (1984) 353–367.
- [78] D.W. Lynch, Diameter growth of *Ponderosa* pine in relation to the Spokane-blight problem, *Northwest Sci.* 5 (1951) 157–163.
- [79] B. Høgdahl, R. Karstensen, E. Virik, Solution of an indemnity case for damage to vegetation around an aluminium smelter. Paper A 77–84, Meeting of the Metallurgical Society of the American Institute of Mining, Metallurgical and Petroleum Engineers, Atlanta, Georgia, USA, 1977.

- [80] R.J. Taylor, F.A. Basabe, Patterns of fluoride accumulation and growth reduction exhibited by Douglas fir in the vicinity of an aluminium reduction plant, *Environ. Pollut. Series A* 33 (1984) 221–235.
- [81] H.W.F. Bunce, Fluoride emissions and forest growth, *J. Air Pollut. Control Assoc.* 29 (1979) 642–643.
- [82] H.W.F. Bunce, Apparent stimulation of tree growth by low ambient levels of fluoride in the atmosphere, *J. Air Pollut. Control Assoc.* 35 (1985) 46–48.
- [83] T.A. Mansfield, P.H. Freer-Smith, in: M.H. Unsworth, D.P. Ormrod (Eds.), *Effects of Gaseous Air Pollution in Agriculture and Horticulture*, Butterworths, London, 1982, pp. 131–146.
- [84] N.M. Darrall, The effect of air pollutants on physiological processes in plants, *Plant Cell Environ* 12 (1989) 1–30.
- [85] R.G. Amundson, L.H. Weinstein, P. van Leuken, L.J. Colavito, Joint action of HF and NO₂ on growth, fluorine accumulation, and leaf resistance in marcross sweet corn, *Environ. Exper. Bot.* 22 (1982) 49–55.
- [86] D.C. McCune, in: A. Legge, S. Krupa (Eds.), *Air Pollutants and Their Effects on the Terrestrial Ecosystem*, Wiley-Interscience, , 1986, pp. 305–324.
- [87] J. Matsushima, R.J. Brewer, Influence of sulfur dioxide and hydrogen fluoride as a mix or reciprocal exposure on citrus growth and development, *J. Air Pollut. Control Assoc.* 22 (1972) 710–713.
- [88] R.H. Mandl, L.H. Weinstein, M. Dean, M. Wheeler, The response of sweet corn to HF and SO₂ under field conditions, *Environ. Exper. Bot.* 20 (1980) 359–365.
- [89] R.H. Mandl, L.H. Weinstein, M. Keveny, Effects of hydrogen fluoride and sulphur dioxide alone and in combination on several species of plants, *Environ. Pollut.* 9 (1975) 133–143.
- [90] C.J. Brandt, Wirkungen von Fluorwasserstoff auf *Lolium multiflorum*, Landesanstalt für Immissions- und Bodennutzungsschutz der Landes Nordrhein-Westfalen Berichte 14 (1981) 140.
- [91] D.C. McCune, in: J.L. Shupe, H.B. Peterson, N.C. Leone (Eds.), *Fluorides: Effects on Vegetation, Animals and Humans*, Paragon Press, Salt Lake City, 1983, pp. 121–126.
- [92] F. Murray, S. Wilson, Effects of sulphur dioxide, hydrogen fluoride and their combination on three *Eucalyptus* species, *Environ. Pollut.* 52 (1998) 265–279.
- [93] F. Murray, S. Wilson, Joint action of sulfur dioxide and hydrogen fluoride on growth of *Eucalyptus tereticornis*, *Environ. Exper. Bot.* 28 (1998) 343–349.
- [94] F. Murray, S. Wilson, Yield responses of soybean, maize, peanut and navy bean exposed to SO₂, HF and their combination, *Environ. Exper. Bot.* 30 (1990) 215–223.
- [95] G. Davieson, F. Murray, S. Wilson, Effects of sulphur dioxide, hydrogen, fluoride, singly and in combination, on growth and yield of wheat in open-top chambers, *Agr. Ecosys. Environ.* 30 (1990) 317–325.
- [96] R.G. Amundson, L.H. Weinstein, In: *Proceedings. Symposium on Effects of Air Pollutants on Mediterranean and Temperate Forest Ecosystems*, Pacific Southwest Range and Forest Experiment Station, Berkeley, CA, 1980.
- [97] V.E. Franklin-Tong, The difficult question of sex: The mating game, *Curr. Opin. Plant Biol.* 5 (2002) 14–18.
- [98] M.R. Pack, Response of tomato fruiting to hydrogen fluoride as influenced by calcium nutrition, *J. Air Pollut. Control Assoc.* 16 (1966) 541–544.
- [99] M.R. Pack, Effects of hydrogen fluoride on bean reproduction, *J. Air Pollut. Control Assoc.* 21 (1971) 133–137.
- [100] M.R. Pack, Response of strawberry fruiting to hydrogen fluoride fumigation, *J. Air Pollut. Control Assoc.* 22 (1972) 714–717.
- [101] C.W. Sulzbach, M.R. Pack, Effects of fluoride on pollen germination, pollen tube growth and fruit development of tomato and cucumber, *Phytopathology* 62 (1972) 1247–1253.

- [102] M.R. Pack, C.W. Sulzbach, Response of plant fruiting to hydrogen fluoride fumigation, *Atmos. Environ.* 26 (1976) 714–717.
- [103] T.J. Facticeau, S.Y. Wang, R.E. Rowe, The effect of hydrogen fluoride on pollen germination and pollen tube growth in *Prunus avium* L. cv. 'Royal Ann', *J. Am. Soc. Hort. Sci.* 98 (1973) 234–236.
- [104] T.J. Facticeau, R.E. Rowe, Effect of hydrogen fluoride and hydrogen chloride on pollen tube growth and sodium fluoride on pollen germination in 'Tilton' apricot, *J. Am. Soc. Hort. Sci.* 102 (1977) 95–96.
- [105] J. Bonte, C. Bonte, L. de Cormis, Les composés fluorés atmosphériques et la fructification. Approche des mécanismes d'action sur le développement des akènes et du réceptacle de la fraise, *Comptes Rendus Academie Agriculture de France*, Séance de 16 Janvier 16 (1980) 80–89.
- [106] J. Bonte, in: M.H. Unsworth, D.P. Ormrod (Eds.), *Effects of Gaseous Air Pollution in Agriculture and Horticulture*, Butterworths, London, 1982, pp. 207–223.
- [107] J. Bonte, J.P. Garrec, Pollution de l'atmosphère par les composés fluorés et fructification chez *Fragaria* L.: Mise en évidence par analyse directe à la microsonde électronique d'une forte accumulation de fluor à la surface des stigmates, *Comptes Rendus Hebdomadaires des Séances de l'Académie des Sciences, Series D: Nat. Sci.* 290 (1980) 815–818.
- [108] R.J. Staniforth, S.S. Sidhu, Effects of atmospheric fluorides on foliage, flower, fruit and seed production in wild raspberry and blueberry, *Can. J. Bot.* 62 (1984) 2827–2834.
- [109] S.S. Sidhu, R.J. Staniforth, Effects of atmospheric fluoride on foliage, and cone and seed production in balsam fir, black spruce and larch, *Can. J. Bot.* 64 (1986) 923–931.
- [110] M.T. Davies, A.W. Davison, G.R. Port, Fluoride loading of pine sawfly from a polluted site, *J. Appl. Ecol.* 29 (1992) 63–69.
- [111] G.R. Port, M.T. Davies, A.W. Davison, Fluoride loading of a lepidopteran larva (*Pieris brassica*) fed on treated diets, *Environ. Pollut.* 99 (1998) 233–239.
- [112] L.H. Weinstein, D.C. McCune, J.F. Mancini, P. van Leuken, In *Proceedings of the Third International Clean Air Congress*, VDI Verlag GmbH, Dusseldorf, 1973, pp. A150–A153.
- [113] P.R. Hughes, L.H. Weinstein, L.M. Johnson, A.R. Braun, Fluoride transfer in the environment: Accumulation and effects on cabbage looper *Trichoplusia ni* of fluoride from water soluble salts and hydrogen fluoride-fumigated leaves, *Environ. Pollut. Series A* 37 (1985) 175–192.
- [114] M. Colombini, C. Mauri, R. Olivo, G. Vivoli, Observations on fluorine pollution due to emissions from an aluminum plant in Trentino, *Fluoride* 2 (1969) 40–48.
- [115] S. Kuribayashi, Environmental pollution effects on sericulture and its countermeasures, *Sericult. Sci. Technol.* 10 (1971) 48–49.
- [116] S. Kuribayashi, Influence of air pollution with fluoride on sericulture, *J. Sericult. Soc. Jpn.* 41 (1972) 316–322.
- [117] S. Kuribayashi, Effect of atmospheric pollution by hydrogen fluoride on mulberry trees and silkworms, *J. Sericult. Soc. Jpn.* 46 (1977) 536–544.
- [118] Y. Yoshida, Experimental study on mulberry leaf poisoning by air pollution due to factories' exhaust, *Shiga Prefecture Exp. Sta. Proc.* 32 (1975) 93–97.
- [119] Z.-W. Chen, Some physiological and biochemical changes of fluorosis in silkworm, *Bombyx mori* L., *Chin. J. Sericult* 13 (1987) 164–168.
- [120] C.A. Aftab Ahmed, M.V. Chandrakala, Effect of oral administration of sodium fluoride on food and water utilisation in silkworm, *Bombyx mori* L., *Insect Scientific Appl.* 19 (1999) 193–198.
- [121] J.X. Wang, Y.M. Bian, Fluoride effects on the mulberry-silkworm system, *Environ. Pollut.* 51 (1988) 11–18.

- [122] K.P. Chen, C. Lu, Z.H. Xiang, Q. Yao, C.Q. Lin, M.W. Li, C.X. Hou, Y. Zhao, Cloning and sequencing the RAPD markers of enduring fluoride in silkworm (*Bombyx mori*), *J. Agric. Biotech.* 9 (2001) 136–138.
- [123] Q.G. Xu, K.P. Chen, Q. Yao, X.Y. Liu, Screening and cloning of RAPD marker of fluoride tolerance gene in silkworm, *Bombyx mori.*, *Zool. Res.* 25 (2004) 69–72.
- [124] G.W. Gribble, In: *The Handbook of Environmental Chemistry. Anthropogenic Compounds, Part N, Organofluorines*, Springer, Berlin, 2003, pp. 121–136.
- [125] H. Schofield, Fluorine chemistry statistics: numbers of organofluorine compounds and publications associated with fluorine chemistry, *J. Fluorine Chem.* 100 (1999) 7–11.
- [126] SynQuest Laboratory Research Catalog, 2000.
- [127] J.S.C. Marais, The isolation of the toxic principle “potassium cymonate” from “Gifblaar”, *Dichapetalum cymosum* (Hook) Engl., *Onderstepoort J. Vet. Sci.* 18 (1943) 203–206.
- [128] T. Vartiainen, J. Gynther, Fluoroacetic acid in guar gum, *Food Chem. Toxicol.* 22 (1984) 307–308.
- [129] R.J. Mead, A.J. Oliver, D.R. King, Metabolism and defluorination of fluoroacetate by the brush-tailed possum (*Trichosurus vulpecula*), *Aust. J. Biol. Sci.* 32 (1979) 15–26.
- [130] R.J. Mead, A.J. Oliver, D.R. King, P.H. Hubach, The coevolutionary role of fluoroacetate in plant–animal interactions in Australia, *Oikos* 44 (1985) 55–60.
- [131] R.J. Mead, L.E. Twigg, D.R. King, A.J. Oliver, The tolerance to fluoroacetate of geographically separated population of the quokka (*Setonix brachyurus*), *Aust. Zool.* 21 (1985) 503–511.
- [132] L.E. Twigg, R.J. Mead, Comparative metabolism of and sensitivity to fluoroacetate in geographically separated populations of *Tiliqua rugosa* Gray, Scincidae, *Aust. J. Zool.* 37 (1990) 617–626.
- [133] L.E. Twigg, D.R. King, The impact of fluoroacetate-bearing vegetation on native Australian fauna: A review, *Oikos* 61 (1991) 412–430.
- [134] D. O’Hagan, D.B. Harper, Fluorine-containing natural products, *J. Fluorine Chem.* 100 (1999) 127–133.
- [135] M. Sanada, T. Miyano, S. Iwadare, J.M. Williamson, B.H. Arison, J.L. Smith, A.W. Douglas, J.M. Liesch, E. Inamine, Biosynthesis of fluorothreonine and fluoroacetic acid by the thienamycin producer, *Streptomyces cattleya*, *J. Antibiot.* 39 (1986) 259–265.
- [136] J.C. Boutonnet, P. Bingham, D. Calamari, C. de Rooij, J. Franklin, T. Kawano, J-M. Libre, A. McCulloch, G. Malinverno, J.M. Odom, G.M. Rusch, K. Smythe, I. Sobolev, R. Thompson, J. Tiedje, Environmental risk assessment of trifluoroacetic acid, *Hum. Ecol. Risk Assess.* 5 (1999) 59–124.
- [137] A.A. Seawright, C.T. Eason, *Proceedings of the Science Workshop on 1080. The Royal Society of New Zealand Miscellaneous Series 28*, SIR Publishing, Wellington, 1994.
- [138] R. Bowman, Fate of sodium monofluoroacetate (1080) following disposal of pest bait to landfill, *New Zealand J. Ecol.* 23 (1999) 193–197.
- [139] C.T. Eason, M. Wickstrom, P. Turck, G.R.G. Wright, A review of recent regulatory and environmental toxicology studies on 1080: Results and implications, *New Zealand J. Ecol.* 23 (1999) 129–137.
- [140] L.E. Twigg, L.V. Socha, Physical versus chemical defense mechanisms in toxic *Gastrolobium*, *Ecology* 108 (1996) 21–28.
- [141] H. Frank, E.H. Christoph, O. Holm-Hansen, J. Bullister, Trifluoroacetate in ocean waters, *Environ. Sci. Technol.* 3 (2002) 12–15.
- [142] D.R. Taves, Evidence that there are two forms of fluoride in human serum, *Nature* 217 (1968) 1050–1051.
- [143] W.S. Guy, D.R. Taves, W.S. Brey, *Biochemistry Involving Carbon–Fluorine Bonds*, R. Filler (Ed.), *Am. Chem. Soc. Symp. Series 1976, No. 28*, pp. 117–134.

- [144] J.P. Geisy, K. Kannan, Global distribution of perfluorooctane sulfonate in wildlife, *Environ. Sci. Technol.* 35 (2001) 1339–1342.
- [145] J.P. Geisy, K. Kannan, Perfluorochemical surfactants in the environment, *Environ. Sci. Technol.* 36 (2002) 147A–152A.
- [146] J.P. Geisy, K. Kannan, P.D. Jones, Global monitoring of perfluorinated organics, *The Scientific World* 1 (2001) 627–629.
- [147] K. Kannan, J.C. Franson, W.W. Bowerman, K.J. Hansen, P.D. Jones, P.J. Geisy, Perfluorooctane sulfonate in fish-eating water birds including bald eagles and albatrosses, *Environ. Sci. Technol.* 35 (2001) 3065–3070.
- [148] K. Kannan, J. Koistinen, K. Beckmen, T. Evans, J.F. Gorzelany, K.F. Hansen, P.D. Jones, E. Helle, M. Nyman, J.P. Geisy, Accumulation of perfluorooctane sulfonate in marine mammals, *Environ. Sci. Technol.* 35 (2001) 1593–1598.
- [149] K. Kannan, S. Corsolini, J. Falandysz, G. Oehme, S. Focardi, J.P. Geisy, Perfluorooctane sulfonate and related fluorinated hydrocarbons in marine mammals, fishes, and birds from coasts of the Baltic and Mediterranean Seas, *Environ. Sci. Technol.* 36 (2002) 3210–3216.
- [150] K. Kannan, J.L. Newsted, R.S. Hallbrook, J.P. Geisy, Perfluorooctane sulfonate and related fluorinated hydrocarbons in mink and river otters from the United States, *Environ. Sci. Technol.* 36 (2002) 2566–2571.
- [151] B.D. Key, R.D. Howell, C.S. Criddle, Fluorinated organics in the biosphere, *Environ. Sci. Technol.* 31 (1997) 2445–2454.

SUBJECT INDEX

- Aerosols, 38
- Alternatives (to CFCs, HCFCs), 33–34, 39, 41, 45, 47, 49, 51, 59, 67, 70–71, 74, 79–82
- Atmospheric chemistry, xv–xvi, 8–22, 91–100
- Atmospheric lifetime, 34, 39, 41, 43, 53, 59–60, 67–68, 70–71, 75, 81, 114, 122–124
- Bioavailability, 305–307
- Bromine stratospheric, 18–19
- Ceramic industries, 225–226, 231–233
- Chlorine stratospheric, 14–18
- Chlorofluorocarbons (CFCs), 1–8, 10, 21–22, 24, 26–29, 33–36, 39, 41, 44–45, 47–49, 51, 53, 59–62, 67–68, 71, 74, 79, 81–82, 131–133, 137–138, 141–143, 162
- Dechlorination, 136–164
- Decomposition, 131, 141, 144, 148–149, 156
- Electron attachment, 90, 97, 114–117, 121–122, 124
- Environmental assessment, 34, 51, 229–230
- Fire extinguishers, 36, 71
- Flammability, 34, 40–41, 43, 71–72
- Fluoride-selective electrode, 190, 192, 196–200
- Fluoride effects on animals, 252, 258, 338–343
- Fluoride effects on insects, 335–338
- Fluorine analysis, 196–200, 226, 240–246
- Fluorine emissions, 165, 167, 169, 171, 173, 175, 177, 179–183, 185, 225–227, 230–245
- Fluorine in plants, 310–320
- FTIR, 166–167, 169–170, 180
- Gas purification, 234–235
- Gaseous emission, 225–226, 230–231, 235
- Geochemistry fluorine, 169–170, 204–210
- Global environment, xv–xvi, 37–42
- Global-warming potential, 20–23, 34, 41, 65–66
- Greenhouse gas, 1, 3, 20–21, 89–91, 94–97, 110, 122–124
- Greenhouse gas potential, 132–133
- Halons, 1–6, 22, 28–29
- Halogen sinks, 3, 4
- Halogen sources, 4–7
- HCFCs, 1, 3–8, 22, 24, 26, 28, 131–133, 138, 142, 162
- Hydrofluorocarbons (HFCs), 38–39, 41, 49, 51, 53, 59–60, 71–72, 75, 78–82
- Hydrogen fluoride effects, 13, 332–335
- Ion chromatography, 194, 201–204
- Kyoto protocol, 2–3, 21
- Lifetimes, 3–4, 29, 125–128
- Lyman- α radiation, 123
- Mass transfer, 132–133, 146, 156–159, 161–162
- Mesospheric reactions, 123
- Monitoring emissions, 24, 26, 39, 244–245
- Montreal protocol, 2, 5–6, 28
- Multivariate analysis, 188–189, 199, 211

- Open-path configuration, 167
Ozone depleting substances, 6, 27, 29
Ozone depletion, 19–21, 34–36, 63
- Perfluorocarbons (PFCs), 1, 3, 22, 38–39
Phase out (CFCs), 2, 3, 37–42
Photochemical decomposition, 131, 137–138
Photodissociation, 1
Photoelectron–photoion coincidence, 100
Photoionisation, 89, 93, 98, 112
Phytotoxic effects, 246–247
Plant reproduction, 277, 278, 284
Pollutant abatement, 236–241
Pollutant interactions, 230, 251–252, 276, 328–330
- Reaction mechanism, 131–133, 146, 150–151, 156
Reaction rate, 131–133, 142, 146, 149–151, 153–154, 156–157, 159, 161
Reductive dehalogenation, 136–137
Refrigerants, 135
Relative sensitivity, 269–270
- SF₅CF₃, 89–94, 97–100, 102–112, 114–117, 120–124
Soil fluoride, 252, 254, 256–257
Spectroscopies, 94–96, 101–113, 171–181
Stratosphere, 1–2, 6–9, 11, 13–14, 16, 27, 29
Stratospheric chemistry, 7–17
Supercritical water, 131, 137
Sustainable, 43, 80, 85
Synchrotron radiation, 102
- Total warming predictions, 43, 76, 77
Troposphere, 5, 13, 21, 27
- Useful fluorocarbon wastes, 141–146
- Volatiles, 167–168, 211–216
Volcanic gas geochemistry, 166–167
Volcanic plume, 165–166, 178, 180–181
Volcanic rocks, 187–189, 198–201, 204, 207
Volcanoes, 165–167, 170, 172–174, 180–181, 218–221
- Wastes (fluorocarbons), 136–164